NOVA SCHOOL OF
SCIENCE & TECHNOLOGY

DEPARTAMENT OF
MATERIALS SCIENCE

SMART HYDROGEL-BASED INJECTABLE SYSTEMS FOR BREAST CANCER THERANOSTICS

HENRIQUE NUNO CURADO CARRÊLO

Master in Materials Engineering

PhD IN SCIENCE AND MATERIALS ENGINEERING

DEPARTAMENT OF
MATERIALS SCIENCE

SMART HYDROGEL-BASED INJECTABLE SYSTEMS FOR BREAST CANCER THERANOSTICS

Henrique Nuno Curado Carrêlo

Master in Materials Science and Engineering

Advisers: Maria Teresa Varanda Cidade
Associate Professor with Habilitation, NOVA University Lisbon
João Paulo Miranda Ribeiro Borges
Full Professor, NOVA University Lisbon

Co-adviser: Paula Isabel Pereira Soares
Principal Researcher, NOVA University Lisbon

Examination Committee:

Chair: Rodrigo Ferrão de Paiva Martins,
Full Professor, NOVA University Lisbon

Rapporteurs: Maria Violante de Paz Báñez,
Full Professor, Universidad de Sevilla

Maria Ascensão Ferreira Silva Lopes,
Full Professor, Faculty of Engineering of the University of Porto

Adviser: Paula Isabel Pereira Soares,
Principal Researcher, NOVA University Lisbon

Members: António João Pina da Costa Feliciano Abreu,
Coordinator Professor ISEL, Instituto Superior de Engenharia de Lisboa

Loic Hugues Gilles Hilliou,
Principal Researcher, University of Minho

Rodrigo Ferrão de Paiva Martins,
Full Professor, NOVA University Lisbon

PhD in Science and Materials Engineering

NOVA University Lisbon
October, 2023

Smart hydrogel-based Injectable systems for breast cancer theranostics

To those who know.

ACKNOWLEDGMENTS

I write the following section in my native language, Portuguese.

Agradeço ao CENIMAT/i3N, ao Departamento de Ciências de Materiais e à Faculdade de Ciências e Tecnologia da Universidade Nova de Lisboa. Agradeço à Fundação para a Ciência e Tecnologia pelo financiamento (SFRH/BD/144986/2019).

Queria agradecer aos meus orientadores por me terem aceitado e guiado durante este percurso. Agradeço à Professora Teresa Cidade, ao Professor João Paulo Borges e à Professora Paula Soares por tudo.

Agradeço em especial à Professora Teresa Cidade que não pôde ver esta parte final da tese devido à sua partida. No entanto, quero dizer um profundo obrigado por todo o apoio e orientação que tive enquanto trabalhei com a Professora. Graças a si aprendi e evoluí muito e levarei todas as suas lições comigo. Estarei sempre grato por ter me proporcionado esta oportunidade, e de me treinar na Reologia e na Academia. Espero que esteja bem onde estiver.

Quero agradecer ao Professor João Paulo e Professora Paula por terem continuado a orientar-me após a partida da Professora Teresa, obrigado por todo o apoio e paciência que tiveram comigo.

Agradezco en castellano, al Profesor Alberto Romero Garcia, al Departamento de Química de la Universidad de Sevilla, y a todos como Mercedes, Víctor, Antonio, Emre y Johar, por mi estadía en la capital andaluza y por todo el estupendo apoyo que me han dado.

Agradeço a todos os do laboratório que me apoiaram e deram-me forças durante este percurso, Rafa, Marci, Catarina, Adriana, César, Dona Augusta, Tânia, Diogo, Ricardo, Susete e Professora Helena.

À família e amigos, aqueles que sabem, sabem. Em vez de deixar escrito, prefiro agradecer pessoalmente, e criar memórias enquanto cá estamos. Mesmo que me arrependa mais tarde de não ter escrito aqui, digo que vida sem arrependimentos é vida mal vivida.

Obrigado a todos!

"Tudo vale a pena quando a alma não é pequena." (Mensagem, Fernando Pessoa).

ABSTRACT

Breast cancer is the most common cancer in women. Current cancer treatments present severe side effects, decreasing the quality of life of patients. Thus, a critical challenge is to develop innovative drug delivery systems that are capable of delivering drugs/bioactive agents without causing toxic side effects. This Ph.D. thesis endeavors to meet this challenge by the development of an *in situ* injectable thermoresponsive drug delivery system tailored for cancer treatment. This system integrates polymeric magnetic microparticles within a thermoresponsive hydrogel, enabling localized drug delivery. The hydrogel performs a multifaceted role: transports the microparticles, and controls the drug release rate, thereby prolonging treatment effectiveness.

The production of microparticles composed of Gellan Gum and Alginate was optimized using a coaxial air-flow method. These microparticles were engineered to include superparamagnetic iron oxide nanoparticles and methylene blue as a model drug, which served the dual purpose of enabling magnetic hyperthermia and controlled drug release.

Microparticles were embedded within thermoresponsive systems, particularly Pluronic gels (F127 and F68 in varying ratios) and a chitosan hydrogel with β-Glycerophosphate. Notably, a Pluronic gel ratio of 17:3 (F127:F68) with 2 and 5 w/w% of microparticles demonstrated the ability to instantaneously shift from a sol state, at room temperature, to a gel state at body temperature. On the other hand, the chitosan hydrogel with microparticles exhibited a more prolonged transition from to the gel state at 37°C while demonstrating non-cytotoxicity to Vero cell lines, more rigid structure than the Pluronic hydrogel, and was able retard the drug release from the microparticles.

In conclusion, the designed microparticle/hydrogel systems showed potential as drug delivery systems for future cancer therapies. Their development represents a significant stride towards more targeted and less harmful cancer treatments, with promising applications in other diseases as well.

Keywords: Hydrogels; Microparticles; Magnetic nanoparticles; Breast cancer; Rheology

RESUMO

O cancro da mama é o cancro mais comum nas mulheres. Os actuais tratamentos de cancro apresentam graves danos secundários, reduzindo a qualidade de vida destes. Um desafio crítico é desenvolver sistemas de transporte de fármacos capazes de administrar medicação sem causarem efeitos secundários tóxicos. Esta tese de doutoramento procura enfrentar este desafio desenvolvendo um sistema de transporte de fármacos termoresponsivo e injectável *in situ* feito para o tratamento de cancro. Este sistema integra micropartículas poliméricas dentro de hidrogéis termorresponsivos capazes de tranporte de fármacos. O hidrogel fará um papel multifacetado: transporte e salvaguarda das micropartículas, e controlo da libertação do fármaco, assim prolongando a eficácia do tratamento.

A produção das micropartículas feitas de goma gelana e alginato foram optimizadas usando o método de fluxo de ar coaxial. Estas micropartículas foram desenvolvidas para incluir nanopartículas superparamagneticas de óxido de ferro e azul metileno, para o duo propósito de permitir hipertermia magnética e controlo da libertação de fármaco.

Estas micropartículas foram depois integradas em sistemas termorresponsíveis, nomeadamente, géis de Pluronic (F127 e F68 com diferentes rácios) e um hidrogel de quitosano com *β*-glicerofosfato. Notavelmente, um rácio de 17:3 (F127:F68) com 2 e 5 w/w% de micropartículas demonstrou a habilidade de instantaneamente alterar de estado sol, à temperatura ambiente, para o estado gel à temperatura corporal. Por outro lado, o hidrogel de quitosano com as micropartículas exibiu uma transição mais prolongada para o estado gel a 37ºC, demonstrando nenhuma citotoxicidade a células da linha VERO, uma estrutura mais rígida que o gel de Pluronic, e foi capaz de retardar a libertação de medicação das micropartículas.

Em suma, o sistema micropartícula/hidrogel desenvolvido demonstrou potencial como um sistema de libertação de fármacos que poderão ser usados no tratamento de cancro. O seu desenvolvimento representa um passo para tratamentos de cancro mais localizados e menos tóxicos, com possíveis aplicações em outras doenças.

Palavras chave: Hidrogéis; Micropartículas; Nanopartículas magnéticas; Cancro da mama; Reologia.

CONTENTS

LIST OF FIGURES

LIST OF TABLES

ACRONYMS

abs	Absorbance
AC%	Absorption Capacity
AE%	Absorption Efficiency
Alg	Alginate
APTES	(3 -Aminopropyl)Triethoxysilane
ATCC	American Type Culture Collection
BRCA	Breast cancer gene
CA4	Combretastatin A
Ch	Chitosan
Ch/β	Chitosan/β-GP hydrogel
conc	Concentration
COV	Coefficient of Variation
DDS	Drug Delivery Systems
DEX	Dexamethasone
DLS	Dynamic light scattering
DMEM	Dulbecco's modified Eagle's medium
DMSA	Dimercaptosuccinic acid
DMSO	Dimethyl sulfoxide
DOE	Design of Experiments

DOX	Doxorubicin
DSC	Differential Scanning Calorimetry
DTX	Docetaxel
ECM	Extracellular matrix
EDX	Energy dispersive X-ray
EE%	Encapsulation Efficiency
EGFR	Epidermal growth factor receptors
ESTRG	Estrogen
FBS	Fetal Bovine Serum
FDA	Food and Drug Administration
FTIR	Fourier
GG	Gellan Gum
GG:Alg	Gellan Gum Alginate microparticles
GlcN D	Glucosamine
GlcNAc N	Acetyl- D - glucosamine
HER2	Human epidermal growth factor receptor 2
HPMC	Hydroxypropylmethylcellulose
ICB	Immune Checkpoint Blockade
ISO	International Organization for Standardization
KP	Korsmeyer
LC%	Loading Capacity
LCST	Lower Critical Solution Temperature
MB	Methylene Blue
MCF-7	Michigan Cancer Foundation -7
MDR	Multidrug resistance
MF	Magnetic field
mNPs	Magnetic nanoparticles
MRI	Magnetic resonance imaging
o/w	Oil in water

OA	Oleic Acid
PBS	Phosphate
PCL	poly(caprolactone)
PEG	poly(ethylene glycol)
PEO	poly(ethylene oxide)
PLGA	poly(lactic
PLLA	poly(Lacticacid)
PNIPAAm	poly(N-isopropylacrylamide)
PP	Plate Plate
PPO	poly(propylene oxide)
PRGTRS	Progesterone
PS	Peppas - Sahlin
SAOS	Small Angle Oscillatory Shear
SAR	Specific absorption rate
SEM	Scanning electron microscope
siRNA	Small interfering RNA
SPIAPTs	Superparamagnetic Iron Oxide Nanoparticles with APTES
SPIONs	Superparamagnetic Iron Oxide Nanoparticles
THR	Thermoresponsive hydrogels
TGA	Thermal gravimetric analysis
UCST	Upper Critical Solution Temperature
UK	United Kingdom
USA	United States of America
UV	Ultraviolet
VEGF	Vascular endothelial growth factor
VERO cells	Kidney tissue cells derived from a adult African green monkey.
w/o	Water in oil
W/O/W	Water/Oil/Water
w/v%	Weight/volume percentage

w/w%	Weight/weight percentage
XRD	X-ray diffraction

SYMBOLS

C_{NP}	Specific heat of Fe_3O_4
Cl	Specific heat of the liquid
$(dT/dt)_{max}$	Maximum derivative of the temperature ramp
c	Microparticle concentration
d	Percentile
g	Grams
G′	Elastic modulus
G′′	Viscous modulus
h	Hours
m	Slope
M	Molar
Mw	Molecular weight
$m_{encap.MB}$	Mass of encapsulated MB
$m_{GG:alg}$	Mass of the particles
mL	Mililiters
m_{mNP}	Mass of adsorbed nanoparticles
ms_0	Mass of MB in the initial solution
msf	Mass after the swelling of the particles
m_{sn0}	Mass of nanoparticles in the initial suspension
m_{snf}	Mass of nanoparticles in suspension
mV	Millivolts
nm	Nanometers
R^2	Adjusted error (adjusted R^2)
t	Time
T	Temperature
T_{lag}	Lag time prior to drug release
T_i	Initial temlperature
T_p	Plateau temperature
W	Weibull
µg	Microgram
µm	Micrometers
5 – FU	5- fluorouracil
tg(δ)	Tangent of the phase angle
η*	Complex viscosity
η	Viscosity

ω	Frequency sweep

1. MOTIVATION

The need to study and develop new materials and composite systems based on hydrogels and microparticles as alternatives to breast cancer treatment is the main challenge that led to the development of this doctoral thesis. The main objective of this thesis is to develop a new composite Drug Delivery Systems (DDS) that can be useful in future breast cancer treatments. An outline of this thesis is presented at the end of this chapter, followed by the scientific contributions of this Ph.D. study.

1.1. Scientific context

Cancer is one of the deadliest diseases faced by our society worldwide. Despite great advances in biomedicine, cancer is still a very dangerous disease that kills many individuals each year. One of the most common types of cancer is breast cancer. It is the most prevalent cancer type diagnosed in women and has a significant mortality rate (13.6%) [1]. In 2018, approximately 627 000 women died from breast cancer. This value represents 15% of all cancer-related deaths in women [2]. Although women are the most affected, men can also suffer from breast cancer, although in extremely rare cases. Only 1% of diagnostics are found in men; however, they are normally found in later stages, with an increased risk of death [3]. In Portugal, approximately 7000 new cases were diagnosed in 2020 and, approximately 1800 women succumbed to this disease in the same year [4]. Early diagnosis is still the best way to prevent breast cancer; however, this is not possible in most cases. This leads to many women only finding that they have been developing tumours when their breast cancer is at an advanced stage. In the later stages, cancer treatment is more difficult and can be insufficient to save the patient's life.

Multiple cancer treatments are available such as hormone therapy, immunotherapy, radiation, and chemotherapy. The latter is one of the most commonly used cancer treatments; however, it has undesirable drawbacks. Systemic administration to the bloodstream leads to undesirable toxic side effects that affect all types of tissues: tumorous and healthy [5]. Another problem that might occur is multi-drug resistance (MDR). This occurs when cancerous cells develop resistance to chemotherapeutic agents, which can lead to more resistant cancer and/or tumour relapse after treatments [6]. Also, with systemic administration, drugs/bioactive agents must reach the desired tumorous area at a therapeutic concentration. Poor drug distribution and the need for high doses of chemotherapeutic drugs are the main problems of

systemic delivery since only a small amount of the drugs will reach the desired location [7]. This might lead to systemic toxicity which translates into side effects that are well known to the general public: fatigue, anaemia, nausea, weakness, and hair loss. These symptoms greatly reduce the patient's quality of life, and owing to the weakening of their immune system, patients are more susceptible to other diseases. Therefore, chemotherapeutic drugs and biological agents must be delivered only to the tumour site, thus avoiding accumulation in healthy tissues [5, 7]

To prevent systemic delivery, Drug Delivery Systems (DDS) composed of biocompatible materials have been developed. According to the National Institute of Biomedical Imaging and Bioengineering of the United States of America [8], DDS "*are engineered technologies for the targeted delivery and/or controlled release of therapeutic agents*". They are used for multiple biomedical applications including cancer treatment. DDS may be developed to regulate the *in situ* release of chemotherapeutic drugs/bioactive agents, or for co-delivery of different types of drugs and/or biological agents [9].

A possible form to introduce a DDS within the tumorous areas is through *in situ* injection. Thus, the DDS should be injectable [10–13]. A type of material that has been the focus of studies of injectable *in situ* DDS for cancer treatment is hydrogels [5, 13–15]. Hydrogels are composed of a network of hydrophilic polymers that can swell and hold a large amount of water while maintaining their structure [16]. In cancer treatments, where there is the surgical removal of a tumour, hydrogels can be used as prevention systems, where it can occupy the cavity left by the tumour to prevent cancer reoccurrence [17]. Due to their nature, hydrogels can withhold drugs/bioactive agents within their structures. Subsequently, they can be surgically placed *in situ* in the tumorous area, and the cargo can be released at a controlled rate [18]. The released cargo will only affect the surrounding area, preventing the general toxicity associated with systemic administration. Another great advantage of these materials is the so-called stimuli-responsive property. Stimuli-responsive hydrogels react to external stimuli and change their structures accordingly. Many external factors can cause this change, such as pH, ion concentration, electric field, light, and temperature [19]. This last one is the factor that characterizes Thermally Responsive Hydrogels (TRH) [20]. Due to temperature changes, the hydrogel might form/break bonds within its internal structure changing to its gel/sol form [21]. Thus, these hydrogels can be used as injectable systems. Outside the body, they can be in their sole state, facilitating their injectability and administration, and adapt their form to the injection site, and inside the body they can be at their gel state, allowing them to remain *in situ*.

Another type of DDS used in biomedical applications are polymeric microparticles [22]. They consist of a small structure, normally with a spherical shape, which can be a carrier of drugs/bioactive agents within their structure. These can be subdivided into two main types: microspheres and microcapsules. Microspheres consist of a porous matrix that has the cargo dispersed homogeneously within the structure. Microcapsules include a porous shell that surrounds an inner core, and the cargo is typically withheld within the core [23].

The combination of hydrogels and microparticles is a possible design for DDS (microparticle/hydrogel system). It has been previously proven that this system has completely different characteristics compared with microparticles and hydrogels alone [24]. With the cargo within the particles, there is a delayed release from the system when compared to microparticles alone [25]. The hydrogel serves as a protective barrier between particles and *in vivo* environment. When particles are loaded, their cargo will diffuse from the microparticle structure to the hydrogel, and then from the hydrogel to the *in vivo* environment. This can delay the release and prevent the initial burst release that typically characterizes microparticles and hydrogels drug release patterns [26]. Another advantage is the possibility of both co-delivery and sequential delivery. The delivery of more than one drug/bioactive agent has a synergistic effect in the treatment of cancer. Also, the cargo withheld in the hydrogel is released at a faster rate than the cargo within the microparticles, which in turn are within the hydrogel. Additionally, different microparticles can be loaded, allowing different release patterns [27, 28]. This opens a door for the possibility of sequential delivery, where different types of drugs are released at different periods, promoting different treatments at different stages.

Additionally, it is also possible to integrate inorganic magnetic nanoparticles (mNPs) into the system, as for example superparamagnetic iron oxide nanoparticles (SPIONs) [29]. SPIONs can increase the surrounding temperature upon application of an external alternating magnetic field, while their intrinsic properties enable diagnostic features through Magnetic Resonance Imaging (MRI). Thus, besides the drug delivery component, it is possible to induce tumour apoptosis and have diagnostic capability. The combination of treatment and diagnostics is called theranostics [30].

Thus, with the previously mentioned components (hydrogels, microparticles and mNPs) it is possible to develop a magnetically sensitive thermoresponsive injectable DDS that may be applied for injectable *in situ* breast cancer therapies. It is possible to load different chemotherapeutic drugs or other types of bioactive agents into the DDS. Different release profiles can be achieved by loading cargo within the hydrogel or microparticles. The addition of SPIONs will also add hyperthermic capabilities that allow an increase of *in situ* temperature.

1.2. Objective

This work aims to produce an injectable thermoresponsive DDS for the treatment of breast cancer. The proposed system is to be composed of microparticles within a thermoresponsive hydrogel. Microparticles are to be produced, characterized and then introduced into the hydrogel. The resulting system aims to be injected *in situ* at the tumour site to support drug release. A TRH will be used to facilitate the administration of the system. Thus, the system will be in the sol phase at operating room temperature (approximately 20-21ºC) and in the gel phase at body temperature (36-37ºC).

Therefore, different objectives must be achieved:

- Development of polymeric microspheres and mNPs ;

- Development of a TRH with and without mNPs;
- Assemble composite systems (TRH with microspheres, mNPs and drugs incorporated);
- Optimization of the composite system in terms of controlled drug release and magnetic hyperthermia;
- Validation of the composite system by *in vitro* studies.

This work will contribute to the development of a DDS for breast cancer, as well as for other types of cancer. This system can serve as a platform for *in situ* drug release, at the tumour, increasing the efficiency of treatment but also avoiding the systemic toxic side effects that current chemotherapeutic treatments have.

1.3. Thesis outline

This work will be divided into chapters following the outline:

Chapter 1: Motivation - This chapter presents a brief introduction, motivation and main objectives of this work.

Chapter 2: Background and State-of-the-Art - An introduction to breast cancer is given with statistics and current treatments. The proposed injectable DDS is given as an alternative followed by a state-of-the-art of similar DDS.

Chapter 3: Materials and methods - A general methodology of the used techniques is described in this chapter.

Chapter 4: Microparticle production - In this chapter, the production of alginate and gellan gum microparticles (GG:Alg) and their characterization are described. The introduction of SPIONs into the microparticles and the following characterization are also described in this chapter.

Chapter 5: Pluronic system - The conjugation of the produced microparticles with Pluronic gels is described in this chapter. Optimization of the system for injectable DDS is also described. Drug delivery assays are also presented and discussed, with the respective mathematical modelling to understand the release behaviour of the proposed DDS. The mixture of microparticles with mNPs within Pluronic is studied in this chapter.

Chapter 6: Chitosan System - The conjugation of the produced microparticles within a chitosan thermoresponsive hydrogel is described in this chapter. Optimization of the system for injectable DDS is also described. Drug delivery assays are also presented and discussed, with the respective mathematical modelling to understand the release behaviour of the proposed DDS.

Chapter 7: Conclusions and Future Perspectives - This work ends with a final chapter with the main conclusions and future perspectives.

1.4. Scientific contribution

This work aims to contribute to Science with a DDS that might be used in future biomedical applications. This thesis combines existing technologies and components and mixes them to produce a new system that has never been done. The conjugation of mNPs, polymeric microparticles and thermoresponsive hydrogels, and then adjusting this system for an *in vivo* environment is a great novelty that can be used for breast cancer treatments.

The following scientific articles have been produced within the scope of this work:

- Carrêlo, H.; Soares, P.I.P.; Borges, J.P.; Cidade, M.T.; "Injectable Composite Systems Based on Microparticles in Hydrogels for Bioactive Cargo Controlled Delivery". Gels 2021, 7, 147; https://doi.org/10.3390/gels7030147
- Carrêlo, H.; Soares, P.I.P.; Borges, J.P.; Cidade, M.T.; "Injectable composite systems of GG:Alg microparticles in pluronic hidrogels for bioactive cargo controlled delivery: Optimization of hydrogel composition based on rheological behavior". Fluids 2022, 7, 375; https://doi.org/10.3390/fluids7120375
- Carrêlo, H.; Soares, P.I.P.; Borges, J.P.; Cidade, M.T.; "Gelan gum/alginate microparticles: Design of experiments production optimization and drug release". Pharmaceuticals 2023, 16(7), 1029; https://doi.org/10.3390/ph16071029
- H. Carrêlo; A. R. Escoval; M. Jiménez-Rosado; A. Romero; J. P. Borges; P.I.P. Soares; "Injectable Thermoresponsive Microparticle/Hydrogel System with Superparamagnetic Nanoparticles for Drug Release and Magnetic Hyperthermia Applications" Gels 2023 9(12), 982; https://doi.org/10.3390/gels9120982
- H. Carrêlo; M. Jiménez-Rosado; Victor Perez-Puyana; A. Romero; J. P. Borges; P.I.P. Soares; "A Thermoresponsive Injectable Drug Delivery System of Chitosan/β-Glycerophosphate with Gellan Gum/Alginate Microparticles" (2023) (in preparation)

The following oral and poster presentations were carried out during this work:

- "Rheological characterization of injectable hydrogel based on bioceramic microspheres/ Pluronic (F127+F68)/Water system for bone repair"; Henrique Carrêlo, Stephanie Soares, Maria Lopes, João Paulo Borges, Maria Teresa Cidade; Young Rheologist Days 2021 (YRD 2021); Giron-France; July 6-9, 2021; oral presentation;
- "*In situ* sequential co-delivery microparticle/hydrogel system for drug delivery in cancer therapeutics" Henrique Carrêlo, Maria Teresa Cidade, João Paulo Borges, Paula I. P. Soares; 31st Conference of the European Society for Biomaterials (ESB 2021); fully virtual event; September 5-9, 2021; poster presentation;

- "A thermoresponsive injectable microparticles/hydrogel drug delivery system for cancer treatment"; Henrique Carrêlo, Paula I. P. Soares, João Paulo Borges and Maria Teresa Cidade; Materiais 2022; April, 10-13, 2022; Marinha Grande-Portugal; Oral presentation.
- "Optimization and characterization of Gellan Gum/Alginate microspheres produced via coaxial airflow"; Henrique Carrêlo, Maria Teresa Cidade, João Paulo Borges, Paula I. P. Soares; 32nd Conference of the European Society for Biomaterials (ESB 2022); September 4-8, 2022; Bordeaux-France. Oral presentation.
- "Injectable composite systems of ALG: GG microparticles in pluronic hidrogels for bioactive cargo controlled delivery: Optimization of hydrogel composition based on rheological behavior"; "; Henrique Carrêlo, Maria Teresa Cidade, João Paulo Borges, Paula I. P. Soares Annual European Rheology Conference (AERC 2022); April 26-28, 2022; Seville – Spain. Oral presentation.
- "An injectable magnetically sensitive system of GG:Alg microparticles with SPIONs in thermoresponsive hydrogels" "; Henrique Carrêlo, André Escoval, Maria Teresa Cidade, João Paulo Borges, Paula I. P. Soares. WCCE11 - 11th World Congress of Chemical Engineering. June 4- 8, 2023; Buenos Aires, Argentine. Oral presentation.

1.5. References

1. International Agency for Reseach on Cancer - World Health Organization (2022) Global Cancer Observatory. https://gco.iarc.fr/. Accessed 14 Mar 2022
2. World Health Organization. www.who.int. Accessed 18 Mar 2020
3. American Cancer Society. www.cancer.org. Accessed 17 Mar 2022
4. Liga Portuguesa Contra O Cancro. www.ligacontracancro.pt. Accessed 14 Mar 2022
5. Norouzi M, Nazari B, Miller DW (2016) Injectable hydrogel-based drug delivery systems for local cancer therapy. Drug Discov Today 21:1835–1849. https://doi.org/10.1016/j.drudis.2016.07.006
6. Wind NS, Holen I (2011) Multidrug Resistance in Breast Cancer: From In Vitro Models to Clinical Studies . Int J Breast Cancer 2011:1–12. https://doi.org/10.4061/2011/967419
7. Parhi P, Mohanty C, Sahoo SK (2012) Nanotechnology-based combinational drug delivery: An emerging approach for cancer therapy. Drug Discov Today 17:1044–1052. https://doi.org/10.1016/j.drudis.2012.05.010
8. National Institute of Biomedical Imaging and Bioengineering. https://www.nibib.nih.gov/. Accessed 16 Apr 2022
9. Carrêlo H, Soares PIP, Borges JP, Cidade MT (2021) Injectable composite systems based on microparticles in hydrogels for bioactive cargo controlled delivery. Gels 7:. https://doi.org/10.3390/gels7030147
10. Evangelopoulos M, Toledano NE, Wang X, et al (2016) Smart Hydrogels. Encycl Nanotechnol. https://doi.org/10.1007/978-94-007-6178-0
11. Bahram M, Mohseni N, Moghtader M (2016) An Introduction to Hydrogels and Some Recent Applications. Emerg Concepts Anal Appl Hydrogels.

https://doi.org/10.5772/64301
12. Yahia Lh (2015) History and Applications of Hydrogels. J Biomed Sci 04:1–23. https://doi.org/10.4172/2254-609x.100013
13. Fakhari A, Anand Subramony J (2015) Engineered in-situ depot-forming hydrogels for intratumoral drug delivery. J Control Release 220:465–475. https://doi.org/10.1016/j.jconrel.2015.11.014
14. Ta HT, Dass CR, Dunstan DE (2008) Injectable chitosan hydrogels for localised cancer therapy. J Control Release 126:205–216. https://doi.org/10.1016/j.jconrel.2007.11.018
15. Wang W, Song H, Zhang J, et al (2015) An injectable, thermosensitive and multicompartment hydrogel for simultaneous encapsulation and independent release of a drug cocktail as an effective combination therapy platform. J Control Release 203:57–66. https://doi.org/10.1016/j.jconrel.2015.02.015
16. Qiu Y, Park K (2012) Environment-sensitive hydrogels for drug delivery. Adv Drug Deliv Rev 64:49–60. https://doi.org/10.1016/j.addr.2012.09.024
17. Zhang Y, Jiang C (2021) Postoperative cancer treatments: In-situ delivery system designed on demand. J Control Release 330:554–564. https://doi.org/10.1016/j.jconrel.2020.12.038
18. Chao Y, Chen Q, Liu Z (2020) Smart Injectable Hydrogels for Cancer Immunotherapy. Adv Funct Mater 30:1–13. https://doi.org/10.1002/adfm.201902785
19. CHATTERJEE S, HUI PC (2019) Review of Stimuli-Responsive Polymers in Drug Delivery and Textile Application. Molecules 24:2547
20. Chatterjee S, Hui PCL (2021) Review of applications and future prospects of stimuli-responsive hydrogel based on thermo-responsive biopolymers in drug delivery systems. Polymers (Basel) 13:. https://doi.org/10.3390/polym13132086
21. Babu N, Vivek R, Rejeeth C (2018) Nanostructured pH-responsive biocompatible chitosan coated copper oxide nanoparticles : A polymeric smart intracellular delivery system for doxorubicin in breast cancer cells. Arab J Chem 0–10. https://doi.org/10.1016/j.arabjc.2018.04.012
22. Lengyel M, Kállai-Szabó N, Antal V, et al (2019) Microparticles, microspheres, and microcapsules for advanced drug delivery. Sci Pharm 87:. https://doi.org/10.3390/scipharm87030020
23. Kim KK, Pack DW, Ferrari M, et al (2006) Microspheres for Drug Delivery. BioMEMS Biomed Nanotechnol 19–50. https://doi.org/10.1007/978-0-387-25842-3_2
24. Carrêlo H, Soares PIP, Borges JP, Cidade MT (2021) Injectable composite systems based on microparticles in hydrogels for bioactive cargo controlled delivery. Gels 7
25. Delgado B, Carrêlo H, Loureiro M V., et al (2021) Injectable hydrogels with two different rates of drug release based on pluronic / water system filled with poly (e -caprolactone) microcapsules. J Mater Sci. https://doi.org/10.1007/s10853-021-06156-x
26. Moura MJ, Gil MH, Figueiredo MM (2019) Cisplatin delivery systems based on different drug encapsulation techniques. Eur Polym J 113:357–364. https://doi.org/10.1016/j.eurpolymj.2019.02.007
27. Ma Z, Song W, He Y, Li H (2020) A multilayer injectable hydrogel system sequentially delivers bioactive substances for each wound healing stage. ACS Appl Mater Interfaces. https://doi.org/10.1021/acsami.0c06360
28. Wu Y, Chang T, Chen W, et al (2021) Bioactive Materials Release of VEGF and BMP9 from injectable alginate based composite hydrogel for treatment of myocardial infarction. Bioact Mater J 6:520–528. https://doi.org/10.1016/j.bioactmat.2020.08.031

29. Soares PIP, Romão J, Matos R, et al (2021) Design and engineering of magneto-responsive devices for cancer theranostics : Nano to macro perspective. Prog Mater Sci 116:100742. https://doi.org/10.1016/j.pmatsci.2020.100742
30. Pene F, Courtine E, Cariou A, Mira JP (2009) Toward theragnostics. Crit Care Med 37:. https://doi.org/10.1097/CCM.0b013e3181921349

2. Background and State of the Art

This chapter is dedicated to a brief overview of the main goals of this Ph.D. thesis. The main objective was to produce a Drug Delivery System (DDS) for application in breast cancer treatment. The first part of this chapter is to give a general introduction to the target disease, breast cancer, and the available treatments. Then the aimed DDS structure will be introduced, and the state-of-the-art of similar DDS will be presented.

This chapter contains part of the original paper by the author previously published [1]: Henrique Carrêlo, Paula I. P. Soares, João Paulo Borges and Maria Teresa Cidade. "Injectable Composite Systems Based on Microparticles in Hydrogels for Bioactive Cargo Controlled Delivery". Gels, 2021, 7, 147. DOI: 10.3390/gels7030147

2.1. Cancer

Cancer is a preponderant disease that affects all ages, genders and races. According to the International Agency for Cancer Research [2], in 2020 the estimated number of new cases was around 19.3 million (22.8% of the world population), with Europe having around 4.4 million new cases. Cancer occurs when a group of cells divides uncontrollably and starts to grow to form tumours on a particular tissue depending on its origin. These primary tumours can spread to other parts of the body in a process called metastasis. This disease can occur in any part of the human body. In 2020, the types of cancer with higher incidence were breast, lung, colorectum and prostate cancers (Figure 2.1 (a)). Regarding mortality, The deadliest cancer was lung cancer, followed by colorectum and liver cancer (2020 data) [2]. Different aspects such as age, gender, and country affect the incidence and mortality rates of cancer. The incidence of cancer changes according to the gender. In men, lung and prostate cancer are the most predominant, with lung cancer having the highest mortality (Figure 2.1 (b)). In women, breast cancer has an incidence rate more than double that of colorectum cancer (the one with the second highest incidence) (Figure 2.1 (c)).

In Portugal, the incidence is similar to that worldwide. In 2020 approximately 60 thousand new cases were diagnosed [2]. According to the European Union and OECD report of 2023 [3], cancer is the second main cause of death in Portugal, representing approximately 23% of all deaths in 2020 [4]. However, cancer incidence in Portugal is one of the lowest in the European Union (EU). In 2020, the incidence rate was lower than the EU average. Regarding mortality rates, these are very close to the EU average [4].

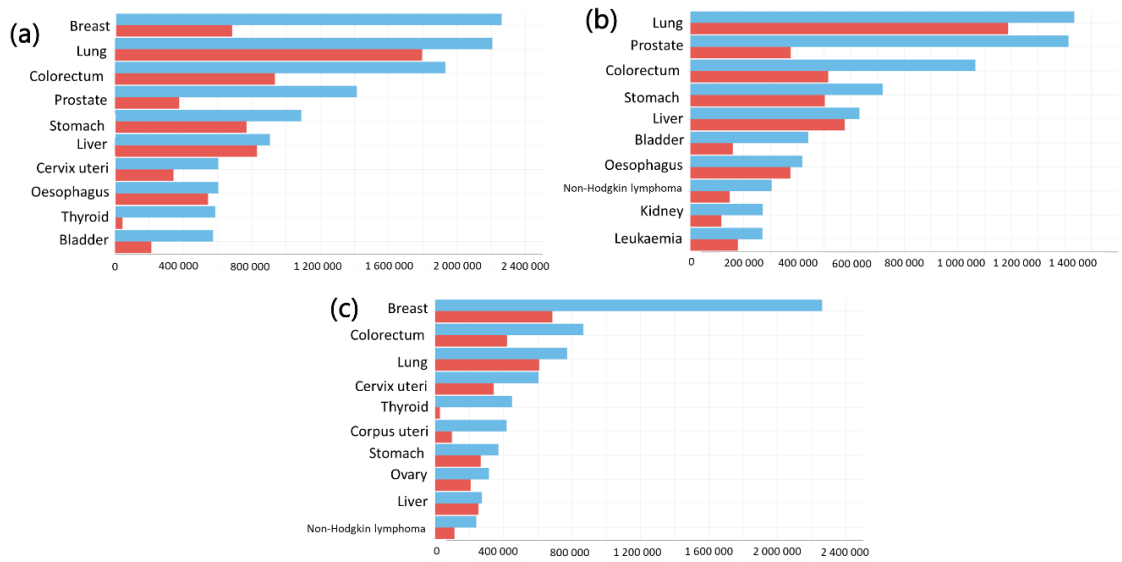

Figure 2.1 Estimated number of cancer (of 2020), divided by types in the World, including all ages (excluding non-melanoma skin cancer) of: (a) both sexes; (b) males and (c) females. Blue bars are incidence rates and red bars are mortality rates. Data source: GLOBOCAN 2020. Graph production: Global Cancer Observatory (http://gco.iarc.fr) Retrieved with permission from [2] (4-5-2023).

Cancer is an extremely complex disease, and can appear in many types of cells, at different parts of the human body, and has different responses to treatments. The deregulation of cell production and proliferation might form malignant masses of cells and also can recruit other cells and change them [49]. Hanahan and Weinberg proposed in 2000 [5] and 2011 [6] the hallmarks of cancer. These works try to understand the journey of a normal human cell to the destructive nature of a cancer cell. These eight hallmarks are:

- Acquired capabilities for sustaining proliferative signalling;
- Evading growth suppressors;
- Resisting cell death;
- Enabling replicative immortality;
- Inducing/accessing vasculature;
- Activating invasion and metastasis;
- Reprogramming cellular metabolism
- Avoiding immune destruction.

However, these hallmarks failed to address the cellular and molecular mechanisms. So, they further recognized two enabling processes that are genome instability and tumour-promoting inflammation. In 2022, Hanahan [7] added two hallmarks:

- Unlocking phenotypic plasticity;
- Senescent cells.

He also added two more enabling characteristics which are non-mutational epigenetic reprogramming and polymorphic microbiomes. What these hallmarks try to do is to describe the extremely complex characteristics/occurrences that lead to tumour development, as Hanahan best described " as heuristic tools" [7].

2.1.1. Breast cancer

Breast cancer it is the most common type of cancer in women (and also when considering both genders) with a significant mortality rate (17.7%, in 2020 worldwide) [2]. Normally, this type of cancer occurs only in one breast; however, bilateral breast cancer can also occur, even though only constitutes 0.2-3% of the cases [7, 8]. Men can also suffer from this type of cancer, however very rarely, only accounting for around 1% of all cancer cases in men [2], [9], [10].

In Portugal, around 7000 new cases (19 cases per day) were diagnosed, with 1800 women not surviving (data from 2020) [11]. However, regarding breast cancer, Portugal is the fourth country in the EU where the population most adhere to breast cancer screening. Also, due to the fact that screenings can be done within the national health system, an therefore, without associated costs for the patient, there is little difference between patients with lower or higher income. Thus, in Portugal, income is not an obstacle to breast cancer screening [3].

2.1.1.1. Stages and types of Breast cancer

Similarly to other cancers, this cancer type is classified into different stages: stage 0 - non-invasive; stages I and II - early-stage invasive; stage III - locally advanced invasive; and stage IV - metastatic or recurrent [12]. The first stage is when the cancerous cells appear but have not spread from the area where they developed. This stage is referred to as pre-cancer, such as breast carcinoma *in situ* [13], [14]. Above stage 1, cancerous cells have spread beyond their place of origin. The last stage (stage IV) is referent to the spreading of cancer to other parts of the human body and is the most advanced form. Regarding treatment effectiveness, the earlier stages have higher chances of survival. In advanced stages, treatment effectiveness is reduced, and the main goal might shift from curative to palliative care. For example, in the United States, the 5-year survival rate for women with stage IV breast cancer is around 30% [15]. Palliative care focuses on improving the patient's quality of life by managing symptoms and providing comfort within the remaining life span of the patient.

Regarding the types of breast cancer, they are defined by location, tumour size and other features. One form of defining breast cancer is by the definition of invasive or non-invasive. Invasive breast cancer is the type of cancer that has spread to other areas of the breast tissue, whilst non-invasive breast cancer has not spread to other breast tissues. Regarding invasive cancers, invasive ductal carcinoma (Figure 2.2) starts in the milk ducts and accounts for around 80% of breast cancer diagnostics [16]. In this type of breast cancer, tumour cells appeared in the milk ducts and spread beyond this area. Similarly, invasive lobular carcinoma, starts in the lobules and spreads to other breast tissues, and is the second most common type of breast cancer, with around 15% of all invasive breast cancers [16], [17]. These two breast cancer types are defined by the tissue where they appear; however, breast cancer types can be defined by other factors, including hormones and gene expression [18].

Triple-negative breast cancer is when the tumour does not present estrogen and progesterone receptors and does not have extra human epidermal growth factor receptor 2 (HER2) proteins [19]. The lack of these receptors and proteins does not allow targeted treatments such as HER2 targeted treatments and endocrine therapy (hormone therapy). This significantly lowers the survival prospects of patients, making this subtype of cancer the one with the highest metastatic occurrence and with the poorest survival rates [19].
Inflammatory breast cancer is a rare aggressive cancer that makes the breast look red [20]. Metastatic breast cancer is defined by stage IV where the cancerous cells that appeared in the breast have spread to other parts of the body [12], [20].

Non-invasive breast cancer, ductal carcinoma *in situ* (Figure 2.2) and lobular carcinoma *in situ*, are precursors to their invasive types. The former appears in the milk ducts. It might occur due to lesions on the milk ducts and might develop into invasive cancer, representing around 20-25% of diagnosed breast cancer [13]. For the latter, it is non-life threatening but might develop into an invasive breast cancer type [17].

Breast cancer is also categorized according to its gene expression profile. These include luminal A, luminal B, basal-like, normal breast-like groups, and breast cancer associated with HER2 overexpression [21]. However, hormone receptivity (for example, estrogen receptor positive) is still one of the most common forms to categorize this disease [22].

2.1.1.2. Aggressiveness of breast cancer

Tumour aggressiveness describes the degree of how the tumour cells grow and spread within the human body. Aggressive cancers are associated with metastasis, relapse and high mortality rates [23]. The aggressiveness depends on several factors that might promote proliferation, such as the type of cancer, stage, hormone receptors, and glucose metabolism, among other factors [23].

One of the most aggressive subtypes of breast cancer is the triple-negative breast cancer [19], [23]. The lack of expression of the markers of HER2 and estrogen/progesterone receptors increases the chances of rapid metastasis (faster growth rate), reoccurrence and resistance to treatments. In this subtype, the need for chemotherapy or surgery is urgent since the tumour is resistant to other treatments [23].

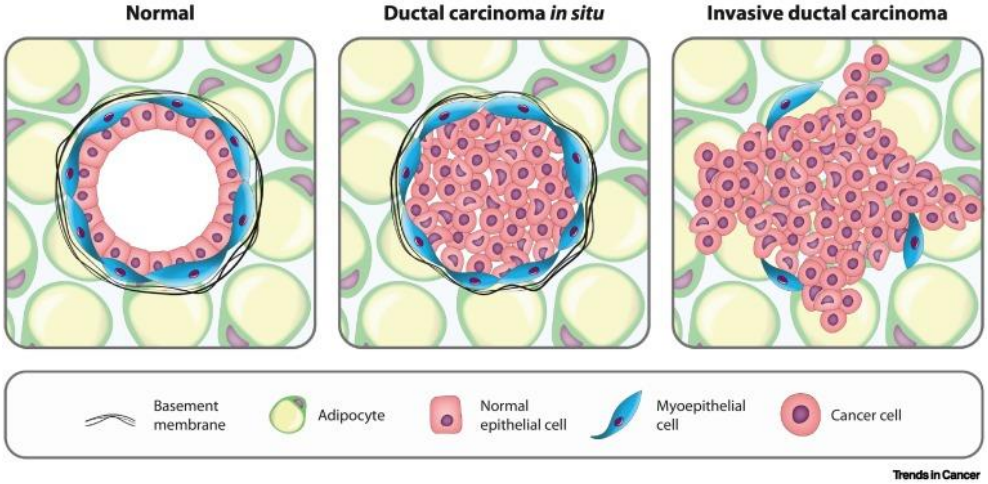

Figure 2.2 Canonical model of ductal carcinoma in situ (DCIS) progression. Breast ducts consist of luminal and myoepithelial cells. These are encapsulated by a basement membrane and surrounding adipocytes. In ductal carcinoma in situ, neoplastic cells proliferate to fill the lumen but are confined to the ductal space by an intact myoepithelial- basement membrane barrier. With time invasive ductal carcinoma can occur which is characterised by a breach in the basement membrane, loss of the myoepithelial layer, and invasion of cancer cells into the surrounding stroma. (Adapted with permission from [24]. Copyright (2023) Elsevier).

Glucose concentration and glycolysis within the tumorous areas promote cancer progression, which increases its aggressiveness. The transportation of glucose to the cancerous areas is done by the facilitative glucose transporter family and the sodium-glucose co-transporter family. The targeted therapy directed to these transporters within the tumorous region might alt the progressiveness of the tumour [23].

HER2-positive tumours are also associated with more aggressive tumours and breast cancer reoccurrence [25]. However, the introduction of HER2-targeted therapy reduced its aggressiveness. Nowadays, HER2-positive tumours are no longer worse than HER2-negative tumours [25].

Circulating tumour cells are tumour cells that have been detected in the bloodstream and are linked with higher mortality rates. Patients who exhibited higher quantities of circulating tumour cells have a higher probability of mortality [25]. Other factors that also affect the aggressiveness of the tumour are the number of metastatic sites, tumour grade and size [25]. The above-mentioned factors, among others, are important to consider during diagnostic and/or treatment to understand how breast cancer might evolve with time.

2.1.1.3. Risk factors

Several factors increase the probability of developing breast cancer. Age is a significant risk factor for breast cancer. In the United Kingdom (UK), from 2016-2018 [26], the incidence by age was studied. Each year around 25% of new cases occur in women with 75 years and older. In men, age is also a risk factor, with the incidence rate increasing at an age range from 40 to 44 years old.

Genetic mutations also contribute to the development of breast cancer. For example, the proteins BRCA1 (Breast Cancer Gene) and BRCA2 are tumour suppressor genes that are responsible to repair damaged DNA [11], [27]. By genetic inheritance, some women might be carriers of mutated BRCA1 and BRCA2. These mutated proteins might not be able to repair the damaged DNA. This in turn increases the chances of developing cancer, especially breast and ovary cancer. The mutations of BRCA1 and BRCA2 account for 30% of inheritable breast cancer cases [27].

The menstrual cycle of women can also be related to breast cancer. Women who have short and numerous menstrual cycles have higher amounts of progesterone during menstruation. Although progesterone protects against endometrial cancer, it might increase the risk of breast cancer [28]. Also, women who start menstruating before the age of 12 and women who have menopause after the age of 55 have an increased probability of developing breast cancer [29].

The tissue density also increases the probability of developing breast cancer. Dense breasts have high amounts of glandular tissue and fibrous connective tissue and low amounts of fatty tissue. Women who have dense breasts are more likely to develop breast cancer [26], [29].

Family history also needs to be considered. Women who have relatives that develop breast cancer have a higher risk of developing breast cancer [30]. The degree of relationship is also important since the risk increases with first-degree relatives (mother, sisters and daughter).

The above-mentioned risks are related to genetics and there are little to no control over them. However, there are risk factors related to behaviours. Obesity, alcohol abuse and physical inactivity increase the probability of breast cancer, as well as other cancers [3], [11]. Late pregnancy is also associated with higher risks of breast cancer. Women who have their first pregnancy after 30 years old, have a higher risk of developing breast cancer [31]. Breastfeeding reduces the chances of developing this disease. The risk is reduced by 4.3% for every 12 months of breastfeeding, and also reduces the risk of developing Triple-Negative Breast Cancer and prevents BRCA1 mutations [32].

2.1.1.4. Breast cancer microenvironment

The breast cancer microenvironment is complex and has several associated factors (Figure 2.3 and Figure 2.4). Within the tumorous area, there are tumour-infiltrating lymphocytes, complex myeloid cells, extracellular matrix (ECM), lipid-associated macrophages, cancer-associated fibroblasts and other biological agents that can promote the growth of the tumours [33], [34]. This environment can actively promote cancer tumour growth [34]. For example, endothelial cells produce new vascular branches that provide oxygen and nutrients to neoplastic cells (tumorous cells). Fibroblasts can be activated by the neoplasm into cancer-associated fibroblasts, that promote cancer cell migration and then metastasis. Also, leukocytes can be recruited to produce factors that stimulate tumour cell growth, angiogenesis, migration and suppression of the immune system [35]. The tumorous area will also change with the tumour progression since the tumorous cells will recruit biological agents and change the surrounding healthy environment to grow [35].

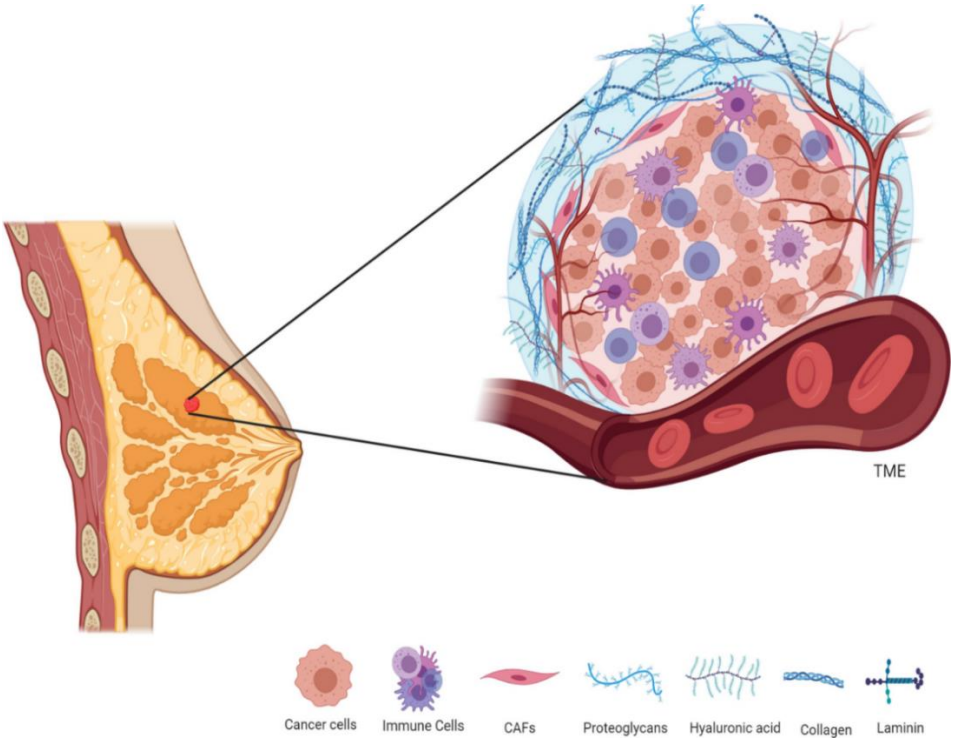

Figure 2.3 Breast tumour microenvironment. The tumour microenvironment of the breast comprises tumour cells surrounded by newly formed abnormal blood vessels, stromal cells such as CAFs, MCSCs, immune cells and non-stromal components such as ECM. The components of the TME work together to promote breast cancer progression, metastasis and resistance to therapies. (Adapted with permission from [36]. Copyright (2021) Springer).

The tumour microenvironment contains soluble, physical and cellular components. Cellular components can be subdivided into local, regional and metastatic. Local cellular components refer to the intratumoral site, specifically the biological features of the tumorous cells and the infiltrating inflammatory tumorous cells. The regional cellular components refer to the surrounding area and the relationship between healthy and cancerous cells. Regarding the metastatic components refers to the new tumorous areas that appear with cancer progression (Figure 2.4) [37].

The cancerous tissue is characterized by a lack of lymphatic vasculature, thus interstitial fluids are not normally drained. This lack of drainage leads to an increase in interstitial pressure. This pressure is also exacerbated by the invasion of the cancer cells into healthy tissues, creating more pressure [38]. Thus, there is a pressure difference between healthy and tumorous cells. The pressure also leads to an increase in ECM stiffness, leading to dense breasts [38]. With ageing, the stiffness of the ECM also increases [39].

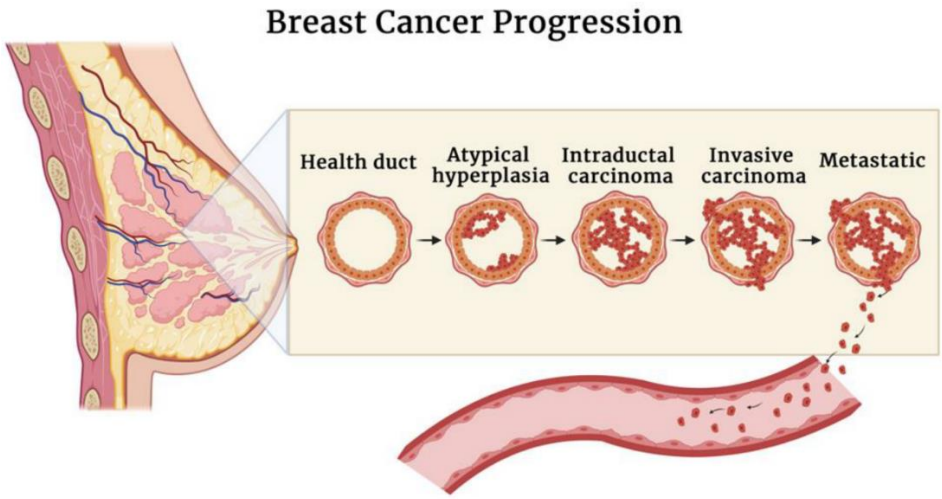

Figure 2.4 Breast cancer progression from a healthy duct to a metastatic phase. (Adapted with permission from [40]. Copyright (2022) Multidisciplinary Digital Publishing Institute).

The human body's pH is normally around 7.4, but can also be lower in certain zones such as the pancreas, colon, etc. Due to deregulated energy metabolism, insufficient perfusion and uncontrolled proliferation, the tumorous areas are characterized by acidity and hypoxia. This is due to different occurrences like low perfusion delaying the removal of acidic products and the delivery of O_2. Also, elevated oxidative metabolism consumes O_2 which creates CO_2, thus releasing H^+. Thus, the tumour microenvironment is normally acidic, in the range of 6.4-7, but it has been registered pH as low as 5.6 [34], [41].

Tumour microenvironment also changes with cancer treatments, like chemotherapy and radiation therapy [37]. For example, radiation therapy has very high anti-tumoral effects, leading to cancerous cell apoptosis. However, this therapy can also have some pro-cancerous effects. For example, after radiation, breast cancer cells release chemokine ligand CCL2, which promotes tumour-associated macrophages recruitments, leading to possible radiation resistance [37]. After surgical resection, the breast microenvironment also changes. However, data reveals that after surgery induced stress may lead to cancer growth and reoccurrence. A surgical tumour resection leads to a systemic reaction of the immune and hematologic systems. Inflammation, ischemia-reperfusion injury, sympathetic nervous system activation, and increased cytokine release are some of the responses and these can promote cancer reoccurrence [42].

2.1.2. Treatments

Different types of therapies can be used in the treatment of breast cancer, including chemotherapy, radiotherapy, surgery, and hormone therapy, amongst others. Therapies can be given before or after surgical intervention. [12]. Neoadjuvant refers to a therapy given before the main treatment, whilst adjuvant refers to a therapy given after the main therapy. For example, neoadjuvant chemotherapy is delivered before surgery to shrink the tumour, whilst adjuvant chemotherapy is given after surgery to prevent cancer reoccurrence [12]. Therapies can also be done locally, like surgery and radiation therapy that is done in the

tumorous zone, or systemically, that is the therapy is done by injecting into the patient's bloodstream [34], [43].

Chemotherapy is the most common cancer therapy. It is a systemic therapy that uses cytotoxic drugs to cause apoptosis of the cancerous cells. This therapy can be used as a primary therapy or an adjuvant one. It is used in the latter stages of breast cancer but can also be used in earlier stages [44]. A significant side effect is caused by its mode of administration, systemic delivery. Cytotoxic drugs do not distinguish cancerous cells from normal cells, which leads to severe side effects including hair loss, anaemia, nausea, gastrointestinal problems, weight loss, and among many other toxic side effects that diminish the patient's quality of life [44]. The response of tumorous cells to drugs also varies. For example, more aggressive tumours are more responsive to chemotherapy than slowly progressive cancers. Cells of aggressive tumours are actively moving through different phases of the cell cycle and this makes them more susceptible to cytotoxic drugs than cells in a resting state [44], [45]. The type of chemotherapeutic drugs to be administrated depends on the stage of breast cancer. For adjuvant therapies, some examples of possible drugs classes include anthracyclines, taxanes, 5-fluorouracil (5-FU), cyclophosphamide, and carboplatin [9]. Each drug acts differently on the cancer cells. For example, 5-FU acts as a false nucleotide building block in the genes of cancer cells, which leads to the inhibition of DNA synthesis and ultimately causes cancer cell apoptosis as the cell prepares to divide. Additionally, 5-Fluorouracil may also act on the immune system to enhance anti-tumour immune responses. However, as side effects it causes gastrointestinal symptoms (diarrhoea, nausea, vomiting), bone marrow suppression, and an increased risk of infection [45]. For metastatic cancers, some of the same drugs as taxanes are used, but other classes like ixabepilone, eribulin, and anthracyclines [9]. An example of this last class is doxorubicin (DOX) which is widely used in cancer therapy including breast cancer. However, it is also associated with severe cardiotoxicity, which often compromises the treatment duration [46].

Radiation therapy is a treatment that uses radiation to kill cancerous cells. This is done by applying sufficient doses of X-rays that alter the cancerous cell's DNA, promoting their apoptosis. This is an effective treatment, especially at the lower stages of breast cancer. This therapy affects both cancerous cells and healthy cells; however, cancer cells are less able to recover from radiation than healthy cells [20], [47]. Short-term side effects include skin rashes and inflammation of lung tissue. In the long term, damage to the heart, lungs, or blood vessels in the chest and possible development of lung cancer are possibilities [12] in addition to cancer resistance and reoccurrence [37]. After mastectomy and breast preserving surgeries, radiation therapy is commonly done to prevent cancer reoccurrence. However, especially in mastectomies, the radiation to the heart and lungs may lead to unwanted side effects [47]. There are different ways of applying radiation to tumorous areas. These can be applied by an external equipment (external radiotherapy), but can also be applied using radioactive seeds or tubes that can be placed *In vivo* near the cancerous area (Internal radiotherapy) [20]. New approaches have been researched to reduce the toxicity and improve the efficiency of this therapy, for example, radiation to regional lymph nodes [47].

Hormone therapy is also a treatment option. Two important hormones are estrogen (ESTRG) and progesterone (PRGTRS), both produced in the ovaries (and in some other tissues). The former is important for the development of women's female characteristics. The latter is important for the menstrual cycle and pregnancy [2]. Hormone-sensitive breast cancers have receptors that are sensitive to these substances (ESTRG receptor positive and PRGTRS receptor sensitive). Therefore, hormone therapies stop the production of certain hormones or interfere with the relation between the hormones and the cancerous cells. This only works in hormone-sensitive tumours. An example is blockage of the ESTRG production in ovaries using aromatase inhibitors, and thus the evolution of ESTRG receptor-positive tumours is slowed [48]. Another ESTRG blocker is tamoxifen, which has been used as an inhibitor of ESTRG signalling [22]. PRGTRS receptors in breast cancer modulate ESTRG receptors, and PRGTRS expression is dependent on ESTRG [49]. This expression aids in the classification of breast cancer since higher PRGTRS levels are registered in luminal A breast cancers than in Luminal B. Also, tumours with ESTRG receptor positivity are more common than PRGTRS. In a recent study (2022), 82.9% were ESTRG-positive/PRGTRS-positive, 15.0% were ESTRG-positive/PRGTRS-negative, and 2.0% were ESTRG-negative/PRGTRS-positive [49]. Also, it has been reported that ESTRG-positive/PRGTRS-positive cases have better survival prospects than ESTRG-positive/PRGTRS-negative since the former responded better to therapies with selective estrogen receptor modulators [49]. When a breast cancer diagnosis occurs, women should be tested for estrogen receptor and progesterone receptor status. This is important to understand since the reduction of these hormone levels can help to prevent cancer growth and reoccurrence [12].

Immunotherapy is a therapy that involves a boost of the human immune system to help in the fight against cancerous cells. For example, Immune Checkpoint Blockade (ICB) therapy uses humanized antibodies to target and neutralize certain immune checkpoint proteins. This has the goal to promote T-cell activation. By promoting the invigoration of exhausted T cells, the improvement of tumour antigen recognition and the promotion of cytotoxicity activity occurs [50]. However, these therapies are dependent on the type of cancer. Breast cancer is less responsive to ICB therapy since it is poorly infiltrated by tumour-infiltrating lymphocytes and is nonimmunogenic [50], [51]. Since this cancer was considered poor immunogenic, immunotherapy was not extensively investigated, but recent findings have found favourable clinical outcomes using this therapy in breast cancer [51]. In HER2-positive breast cancers, it is possible to use antibodies, like Herceptin, to inhibit cancer cell growth or cancer reoccurrence, by acting on these proteins [12], [50], [51].

Surgical intervention is one of the main types of intervention in breast cancer treatment. The radical removal of the breast is called mastectomy. However, for stages I and II, breast-conserving surgical interventions are preferred, even if some parts of the breast need to be removed. However, mastectomy is sometimes required for more developed stages or some specific types of patients like pregnant women or women with connective tissue diseases [12], [52]. Instead of completely removing the breast, it is possible to use implants to conserve the breast's appearance, like silicone implants [12]. The reoccurrence rates following mastectomy

are low (0-3.7%) and, together with implants, have the great benefit to provide women with the opportunity to preserve their breast appearance [52]. Nevertheless, these surgeries also have complications with possible wound dehiscence, infection, implant loss, asymmetry, and capsular contracture. Also, as previously mentioned, surgery may promote cancer reoccurrence due to the immune system's reaction. Surgery can also lead to small cancer cell dissemination, that is the spread of cancerous cells to vascular and lymphatic vessels that may lead to tumour regrowth and cancer reoccurrence [42].

2.2. Drug Delivery Systems

As presented above, there are different options for the treatment of breast cancer, but current treatments have significant side effects. Chemotherapeutic drugs are one of the most efficient anti-tumour treatments. However, the administration of chemotherapeutic drugs is performed systemically. Thus, only a small portion of the cytotoxic drugs reach the tumour site, with the rest of the drugs affecting healthy areas of the body. This systemic toxicity is responsible for the negative side effects that chemotherapy is normally associated with. Also, different chemotherapeutic drugs have rapid plasma clearance, that further diminishes the tumoural exposure to these drugs [53]. The tumours also have abnormal blood vessels that impair drug penetration into the tumour. Beyond this defective vasculature, hypoxia, acidity, defective lymphatic vessels and even multidrug resistance of cancer cells also hinders the effect of systemically administrated drugs [54]. In breast cancer, the increased stiffness of the ECM also creates a protective barrier around the tumours that reduces drug permeation [55].

These are drawbacks for an efficient drug release. When compared to traditional systemic administration of drugs, *in situ* DDS has the following advantages: controlled and sustained release profile; release of the decrease treatment efficiency and the patient's quality of life, especially when using chemotherapy. Different alternatives have been proposed, such as targeted therapies likely used in hormone and immune therapies where certain molecules and biological agents are blocked to inhibit cancer growth [56]. Another option is using DDS. As previously said in Chapter 1, these are described by the United States of America National Institute of Biomedical Imaging and Bioengineering [57] "*as technologies that carry drugs into or through the body*". Within the body, these systems can release the drugs/biochemical agents with a desired release profile rate. These can be engineered in several forms such as nanoparticles [58], microparticles [59], hydrogels [60], and many more [61]. One option is using *in situ* DDS for intratumoural treatments, which consists of the placing of a DDS near/within the tumorous cargo near the tumorous cells giving a more effective therapy and reducing the necessary drug doses; enables the release of insoluble cancer drugs; avoids the multiple drug administration cycles associated with systemic administrations; reduces the negative side effects since the drug is within the tumorous areas and with lower doses than systemic administration [53], [62]. These can serve as treatments for pre and post-surgery interventions [63]. For example, after breast-conserving surgery, DDS can also prevent tumour reoccurrence by releasing controlled amounts of agents that prevent cancer reoccurrence. To produce an

adequate DDS to be implanted *in situ* for breast cancer, and possibly for other types of cancer, it is necessary to understand the environment and to produce a system that is capable of prolonged drug-release treatment. For this, an engineering approach must be made to develop materials that can be placed *in situ* and release the drugs/biological agents within the desired patterns.

2.2.1. Hydrogels as Injectable DDS

The use of DDS for breast cancer treatment, and many other types of cancer has been the topic of many different studies. Different types of materials have been explored, and one type of them are hydrogels [64], [65]. Hydrogels are a network of hydrophilic polymers that can swell and hold a large amount of water while maintaining their structure [66]. These can adapt their structure to the *in situ* tumorous area and release their cargo.

A non-invasive strategy of placing the DDS within the area is by injection [53]. Hydrogels can be sensitive to external factors like pH or temperature [67], [68]. Hydrogels can form their structure with chemical or physical crosslinking. Chemical crosslinking of hydrogels refers to the formation of permanent, covalent bonds between polymer chains, typically through the use of crosslinking agents, like glutaraldehyde [69]. These agents are often toxic to the human body [70]. Physical-crosslinking of hydrogels refers to the formation of reversible bonds between polymer chains, typically through non-covalent interactions such as hydrogen bonding, van der Waals forces, or electrostatic interactions [70]. Physical-crosslinking is normally not associated with toxic compounds such as in the case of chemically crosslinked hydrogels. Temperature, pH, mechanical stresses, and electric fields are examples of possible triggers that lead to the formation of physical links [67], [68].

Hydrogels can be injected since they have shear thinning behaviour, and can be regain their structure with thixotropic/self-healing properties [71]–[73]. Or, they can be injected in a pre-hydrogel form, and form their structure within the *In vivo* environment, for example, Pluronic that can be injected at the sol state and within the body can form a gel structure due to temperature differences [74], [75].

2.2.2. Thermoresponsive hydrogels

Hydrogels that are sensitive to temperature are called thermoresponsive hydrogels. Thermoresponsive hydrogels undergo reversible changes in their physical properties in response to temperature [76]. They are composed of polymers that contain thermoresponsive units, which can change the structure of the hydrogel with temperature. For example, thermoresponsive hydrogels can exhibit either Lower Critical Solution Temperature (LCST) at which a polymer becomes insoluble in water or a specific solvent, leading to phase separation, or Upper Critical Solution Temperature (UCST) at which a polymer becomes soluble in water or a specific solvent. In LCST examples, hydrogel units can undergo a transition from a hydrophilic to a hydrophobic state when the temperature exceeds a certain threshold known as the LCST. With this change, hydrogels can change from a sol state at lower temperatures to

a gel state at higher temperatures. This transition occurs at the sol-gel temperature and is normally close to the LCST [68]. Thus, it is possible to develop a thermoresponsive hydrogel that is at the sol state at ambient/operating temperature and at the gel state at body temperature. The importance of the hydrogel being at the sol state at operating room temperature is to allow the hydrogel to be easily injectable into the tumorous site. With the injection to the site, the hydrogels will suffer a sol-gel transition and change to a gel structure able to regulate and deliver the biological agents for the treatment [77].

In this work two physically crosslinked hydrogels were used: Pluronic and chitosan/ beta-glycerophosphate (β-GP). Pluronic is a poloxamer is a copolymer composed of a triblock of poly(ethylene oxide) (PEO) and poly(propylene oxide) (PPO) of the following composition: PEO-PPO-PEO. This polymer is thermoresponsive due to the different affinities of both monomers. PEO blocks are hydrophilic, whilst PPO is hydrophobic. With a temperature increase, the hydrophobicity of PPO increases, and micelles form, with a hydrophobic PPO core and an outer shell of PEO chains. These micelles start to interact and form a matrix that leads to the formation of a hydrogel [78]. This transition is almost instantaneous and this hydrogel has been used as a possible DDS not only for cancer [77], [79]–[82]. Chitosan has also been a studied material in the development of DDS. It is a linear polysaccharide that is derived from chitin. Chitin is an easily accessible material since it is found in cell walls and the exoskeletons of arthropods [83]. A common source of this material is shrimp. Chitosan has several advantages including biocompatibility, biodegradability, and mucoadhesive properties, and is not cytotoxic [84]. It has been used for several types of drug delivery uses, including microparticles and nanoparticles [85], [86] and hydrogels [87]. Among the studied hydrogels, chitosan hydrogels [84], [88]–[90] have also been developed as a solution for breast cancer treatments. Within the scope of the thermoresponsive hydrogel, for injectable DDS, chitosan hydrogels are not a thermoresponsive hydrogel, however, the mixing with β-GP (β-Glycerophosphate) allows the development of a thermoresponsive hydrogel. This is due to the reduction of repulsive forces between the ammonium groups of chitosan with the presence of β-GP and a temperature increase [91]. This thermoresponsive hydrogel has been used as DDS for different purposes [92]–[94] including breast cancer treatments [95], [96].

2.2.2.1. Thermoresponsive hydrogels in cancer treatments

Santana *et al.* [97], conjugated Pluronic and hyaluronic acid into a hydrogel with nitric oxide and silica-based nanoparticles for cisplatin release. In *in vitro* trials the conjugation of nitric oxide and the chemotherapeutical drug led to synergetic effects, increasing the cytotoxicity to breast cancer cells. Rafael *et al.* [98] developed a nanosized system of cetuximab-conjugated micelles of Pluronic F127 and Gelatin hydrogels, for the delivery of small interfering RNA (siRNA) into epidermal growth factor receptor (EGFR). The developed system allowed high entrapment efficiency and an efficient gene silencing of 70% with low cytotoxicity and proper hemocompatibility.

With chitosan thermoresponsive hydrogels, Fathi *et al.* [96] developed a chitosan hydrogel with poly(N-isopropylacrylamide-co-itaconic acid) and glycerophosphate to develop a thermo

and pH-responsive hydrogel. The developed hydrogel was thermoresponsive and able to release DOX for a prolonged time, with acidic environments having higher cumulative releases. Also, the developed hydrogels were found to be non-cytotoxic to MCF-7 cells. With other materials, Qu *et al.* [63] developed a thermoresponsive hydrogel with gold nanorods for DOX release with phototherapy for cancer ablation. A near-infracted laser was used as a trigger release of the DOX due to the photothermal capacity of the gold nanorods. With the increase in temperature of the nanorods, the hydrogel mesh size decreased, releasing more DOX. *In vivo* trials showed that cancer reoccurrence rates significantly decreased with this synergetic DDS.

Wu *et al.* [99] developed a thermoresponsive hydrogel with iron oxide nanoparticles as a DDS with thermoresponsive properties. In *in vivo* trials, the hydrogel was injected into the post-surgery wound and adapted to the cavity. An alternating magnetic field (AFM) stimulated the release of the loaded drugs and also delivered heat to induce cancer cells apoptosis. Qi *et al.* [100] developed a self-assembling hydrogel in the presence of chemotherapeutic drugs like DOX. Other studies also developed different hydrogels for breast cancer reoccurrence after surgery, but others also focused on the treatment of breast cancer pre-surgery [84], [89], [101].

2.2.3. Microparticles within hydrogels: a future DDS

Hydrogels are a great solution for injectable DDS for different types of diseases beyond the scope of breast cancer treatments. Cancer treatments can take different periods. For example, chemotherapy normally takes 3 to 6 months with different cycles of administration [26]. Therefore, by using a hydrogel as a DDS, it is important to develop systems where the release profile can be adjusted. Many types of factors are involved in this, such as the hydrogel's mesh size, polymer interactions, and bio-adhesion, among other factors [102]. Another possibility is using complex DDS composites composed of at least to different architecture, as for example the combination of microparticles inside a hydrogel system [103] (Figure 2.5).

The microparticle/hydrogel system comprises the mixing of microparticles loaded with drugs/bioactive agents within a hydrogel. Microparticles alone serve as a DDS and have been used in many studies [59], [104]–[106]. By incorporating microparticles within a hydrogel structure, the drugs/bioactive agents that are released from the microparticles will have an additional barrier before the tumorous site, delaying their release. This is important for possible long-release profiles. The hydrogel will also serve as a protective barrier for the microparticles and the cargo within them. There is also the advantage of a sequential release profile. If the microparticles have one type of cargo and the hydrogel has another one, the cargo within the hydrogel will be released before the one within the microparticles. This allows for sequential treatment of complex treatments that have different phases [1]. Thus, this mixture is an interesting possibility for future DDS. The following part will focus on works that developed similar systems for biomedical applications.

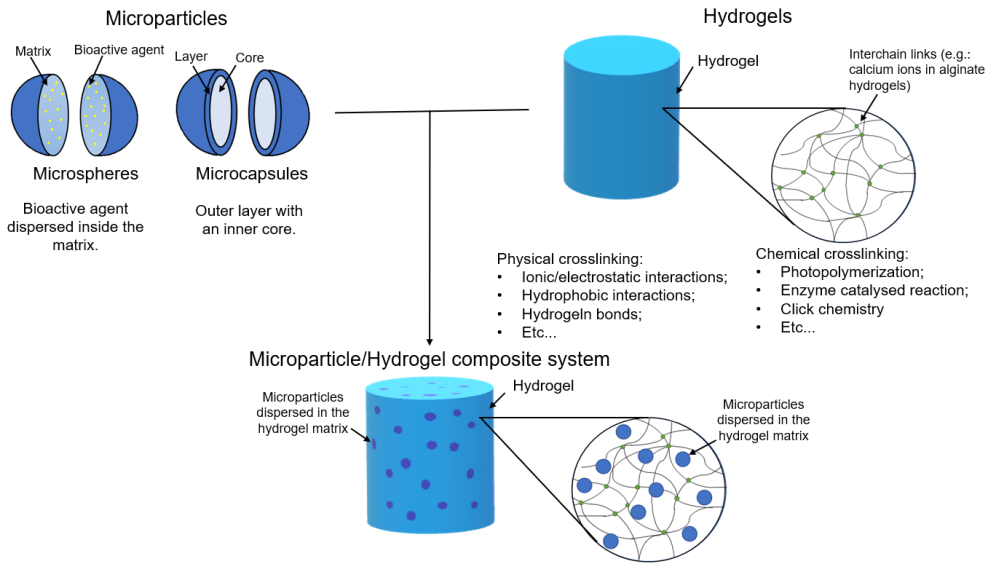

Figure 2.5 Schematic representation of microparticles (upper left), hydrogels (upper right) and the microparticle/hydrogel system (down). Image from. (Adapted with permission from [1]. Copyright (2021) Multidisciplinary Digital Publishing Institute).

2.3. State of the Art: Microparticles within hydrogels

2.3.1. Gelation of the microparticle/hydrogel system

2.3.1.1. *In situ* gelation

Thermosensitive hydrogels can undergo *in situ* gelation, where they serve as matrices capable of sustaining particles [77], [107], [108]. The hydrogel is in a sol state before injection, allowing for particles to be added and form a suspension with homogeneously distributed particles. Upon injection, the sol state changes to a gel state, resulting in a structure with particles *in situ.* When injected, the hydrogel in the sol state will fill and adapt to the injected area, and when the transition occurs it will remain there.

In addition to thermosensitive hydrogels, a blended system with a cross-linking agent can also be used for *in situ* gelation. This system involves injecting active ingredients that induce cross-linking of the precursor hydrogel mixture. However, the mixture of the precursor reagents must be done immediately before injection to allow for cross-linking to occur *in vivo*. It is important to consider how the reaction time like a quick gelation can affect injectability [71].

Another approach consists on using microparticles to deliver the cross-linking agent to the hydrogel's precursors. For example, Hori *et al.* [109] developed an injectable *in situ* ionic cross-linking alginate system using alginate microcapsules as calcium reservoirs. Microcapsules loaded with calcium ions are mixed with an alginate precursor solution and, upon injection, the capsules release the calcium ions causing gelation of the alginate solution. This system leads to quick gelation, with the release of calcium ions occurring within the first few minutes. Also with the release of ions from the microparticles, Pontremoi *et al.* [110]

developed a thermoresponsive hydrogel based on polyurethane and embedded them with mesoporous bioactive glass-based microparticles for long-term delivery of Sr^{2+} ions and an osteogenesis-enhancing molecule (*N*-acetylcysteine). The system proved to be easily injectable with a fast gelation that accommodated its form into the bone-damaged sites, thus conferring a good base for a sustained and prolonged release profile.

2.3.1.2. Gelation before injection

Hydrogel gelation before injection is another approach that can be employed. Hydrogels with rheological shear thinning behaviour, where their viscosity decreases with the applied shear rate, can be injected [111], [112]. It is also advantageous for hydrogels to exhibit thixotropic behaviour, where the lag time until the recovery of the original viscosity allows the hydrogel's structure to rearrange itself to best fit the implanted zone [32]. Self-healing hydrogels can also be utilized for this purpose, as they can repair structural damages, including formation of new bonds when older ones are broken, and recover their original forms and structures [113].

2.3.2. Mixing the microparticles within the hydrogel

Combining microparticles loaded with drugs/bioactive agents with hydrogel through blending is the most common method to prepare composite systems [77]. The mixture should be handled with care to avoid damaging the particles or cargo, and the microparticles should be uniformly distributed in the hydrogel matrix. For instance, Pluronic is a thermoresponsive polymer that undergoes a sol-gel transition at a specific temperature combination [67]. To create a hydrogel with homogeneously dispersed particles, the microparticles should be evenly distributed in a Pluronic aqueous solution at lower temperatures, followed by an increase in temperature (Figure 2.6) [77].

Alternatively, instead of keeping the microparticles separated from the hydrogel, the surface of the microparticles can be modified to create the matrix [114]. This simplifies the system by using the microparticles as crosslinking centres, eliminating the need for blending steps. For example, Zhao *et al.* [115] utilized a poly(L-lactic acid)-b-poly(ethylene glycol)-b-poly(N-isopropylacrylamide) copolymer (PLLA-PEG-PNIPAAm) to create self-assembling nanofibrous gelling microspheres that form a thermosensitive hydrogel. The PLLA branch of the copolymer creates the microspheres, and PEG provides hydrophilicity. At physiological temperature, PNIPAAm serves as physical cross-links between particles, integrating the microspheres into the hydrogel matrix. In another study, Wang *et al.* [116] developed copolymeric microspheres with acrylamide and 2-hydroxyethyl methyl acrylate. Polymerizable double bonds were introduced to the microsphere's surface, and then they were dispersed in an acrylamide solution and mixed with potassium persulfate to start the polymerization reaction and form a 3D structure. The system demonstrated a higher compression strength and endured better strain tests compared to the original hydrogel.

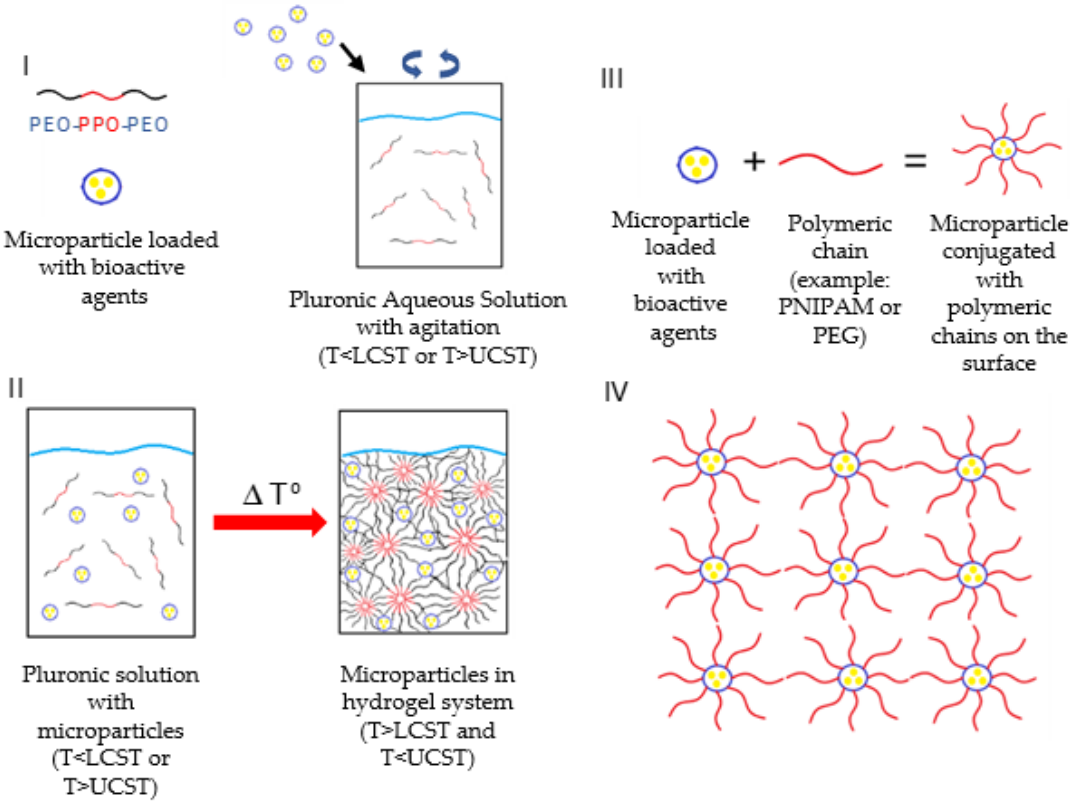

Figure 2.6 Thermoresponsive microparticles in hydrogel Pluronic system: I) Blending of Pluronic aqueous solution with microparticles, II) Microparticles in Pluronic Hydrogel system gelation with particles evenly spread in the structure. Self-forming hydrogels with microparticles as cross-linking points: III) the surfaces of the microparticles are conjugated with a polymeric chain (in red), IV) the added chains will link to other chains forming a 3D structure with the microparticles serving as linking points. (Adapted with permission from [1]. Copyright (2021) Multidisciplinary Digital Publishing Institute).

2.3.2.1. Particle release from the hydrogel: Mesh pore size and degradation of the matrix

The release mechanism of drugs/ bioactive agents from hydrogels or microparticles can be affected by various factors, such as degradation and swelling. Degradation of the matrix can occur in bulk or only at the surface, and it usually results in the exposure of particles. Swelling can cause an increase in mesh size, leading to drug/particle release, and is often sensitive to external conditions such as pH and temperature. Mechanical deformations can also cause a change in the hydrogel's structure, leading to cargo' release [102].

The cross-linking density of the hydrogel plays a significant role in the release mechanism of the cargo. A higher cross-linking density results in reduced swelling capacity and penetration of liquid into the matrix, leading to a more challenging release pathway and retardation of the release. Moreover, a higher cross-linking density also reduces the loading capacities of the matrix. Karamzadeh *et al.* [117] conducted a study using PEG-based hydrogels and polycaprolactone (PCL) microspheres for the delivery of methadone, comparing cross-

linking agents. The system with the highest cross-linking density and microspheres most delayed the release, compared to the other systems tested.

The mesh size of hydrogels is also crucial as it determines the release mechanism. If particles/bioactive agents are smaller than the mesh size, diffusion will dominate the release mechanism, resulting in a quick release. However, with increasing sizes, particles/bioactive agents become more immobilized within the matrix, leading to a slower release defined by changes in mesh size/structure. Moura *et al.* [118] compared the use of liposomes and chitosan microspheres for cisplatin transportation in a chitosan hydrogel system. The liposome/hydrogel system released cisplatin very quickly, possibly due to the encapsulation of drugs within liposomes preventing drug interaction with the chitosan matrix, resulting in a faster release. However, the presence of chitosan microspheres significantly delayed the release and initial burst compared to the free-form hydrogel, especially in chemically cross-linked hydrogels.

2.3.2.2. Surface charge and hydrophobicity of the polymers

Polymers with opposite charges can create a physical bond through electrostatic interactions, which can strengthen the bonds between particles and hydrogels. França *et al.* [119] demonstrated this by combining nano porous silicon microparticles with a hydrogel of oxidized hyaluronic acid and adipic acid dihydrazide, resulting in an electrostatic interaction between the microparticles and hydrogel.

Hydrophilic or hydrophobic polymers can also interact with drugs, affecting their release rate and incorporation into the delivery system. When designing drug delivery systems, the use of hydrophobic polymers must be carefully evaluated depending on the desired cargo hydrophilicity or hydrophobicity. Hydrophobic polymers, such as poly lactic-co-glycolic acid (PLGA), are commonly used to deliver low water-soluble drugs. The hydrophobicity of the polymer can be controlled by adjusting the ratio between glycolic acid and lactic acid in the polymer. However, increasing the hydrophobicity of the system can lead to a slower degradation rate, which may delay the release of hydrophobic drugs. On the other hand, lower drug incorporation into the system may occur with highly hydrophobic polymers [120].

2.3.2.3. Rheological properties of the system

Understanding the rheological properties of injectable systems is crucial for their design and performance. When incorporating microparticles within a hydrogel, changes in rheological properties may occur. For example, in thermoresponsive hydrogels, the presence of particles can decrease the gelation time. Hydrophilic particles can retain water within their structure, resulting in an increase in the hydrogel concentration and a decrease in its gelation time [77], [121]. The increase in cross-linking density of the hydrogel, caused by the presence of particles, can also contribute to this phenomenon. In a study using a Pluronic F127 hydrogel (15.5 w/w%), the addition of alginate microspheres decreased the gelation temperature, and an increase in particle concentration further decreased the gelation temperature [77] (Figure 2.7). This could be attributed to network formation with hydrogen bonds between carboxyl

groups from alginate and ether groups from Pluronic. The crossover point between the storage and loss modulus in a temperature sweep test in Small Angle Oscillatory Shear (SAOS) is the most common way of determining the gelation point. Alighaie *et al.* [107], in a microparticle/hydrogel system, found that microspheres' presence slightly increased the temperature of modulus crossover. However, with Fredrickson and Larson's theory, the researchers found a decrease in the transition temperature with the microparticle's presence. This phase separation theory was used to determine the bicontinuous percolation structuring point, by interpreting gelation as a phase separation phenomenon.

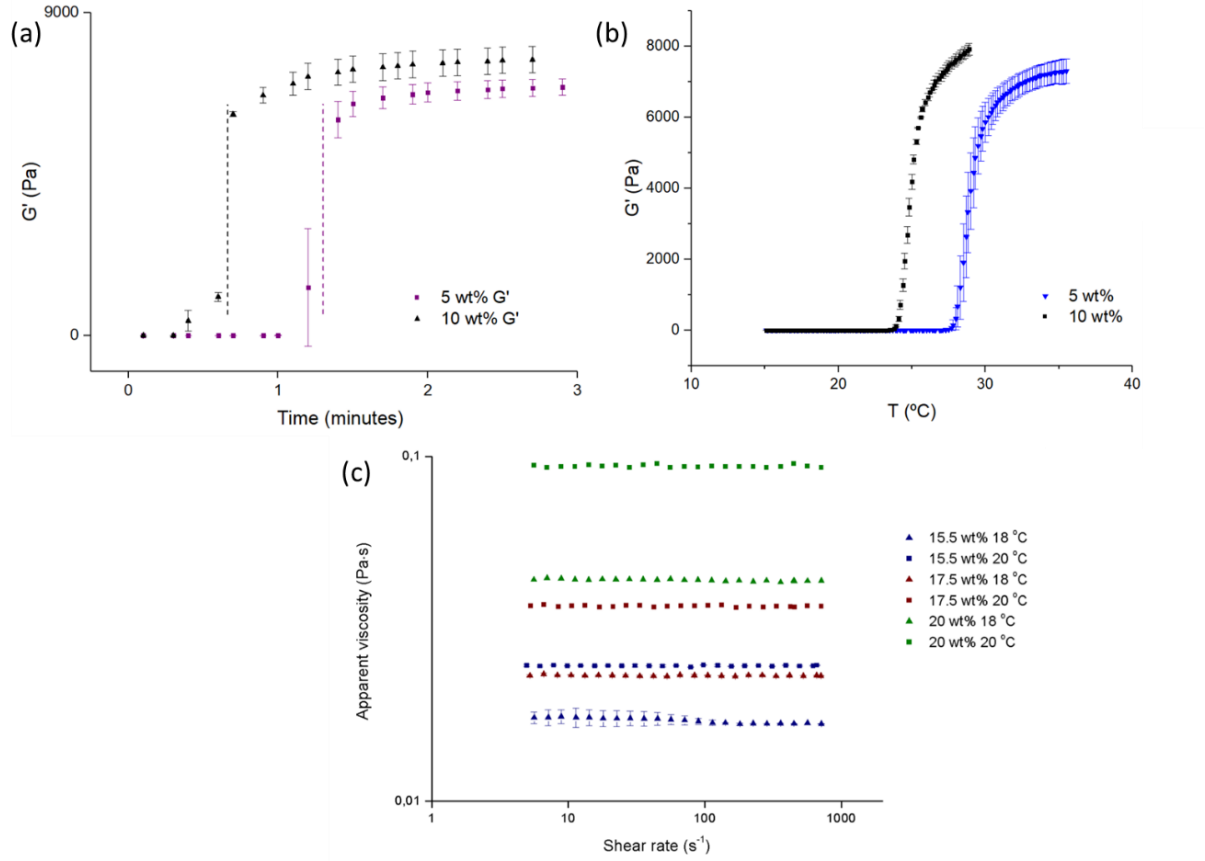

Figure 2.7 (a) Transient dynamic test with different particle concentrations; (b) Temperature sweep in a dynamic test of a microparticle/hydrogel system with different particle concentrations; Reprinted (adapted) with permission from [77]. Copyright (2021) Multidisciplinary Digital Publishing Institute; (c) Flow curve of a microparticle/hydrogel system with different particle concentrations and at different temperatures. (Adapted with permission from [77]. Copyright (2021) Multidisciplinary Digital Publishing Institute).

The presence of microparticles within a hydrogel can influence its mechanical properties. For instance, the addition of gelatine microparticles to a hyaluronic acid hydrogel resulted in an increase in both storage and loss modulus in a frequency sweep [122]. Similarly, an increase in both moduli was also observed with increasing concentrations of PCL (Polycaprolactone) microcapsules in a Pluronic hydrogel [76]. However, the extent of the increase in elastic behaviour will depend on the concentration of microparticles used [123].

The addition of microparticles to the hydrogel structure increases structural integrity, leading to an increase in the apparent viscosity of the material and a more elastic behaviour [76], [77]. The more structured material also affects the elastic modulus, which increases with

the incorporation of microparticles. In contrast, the shear-thinning behaviour of the hydrogel, which is crucial for injectability, is not significantly affected by the presence of microparticles [122].

Rheology is also an important tool to understand if the system can be injectable or not. For Alzheimer's treatment, Ji *et al.* [124] developed poly(lactic-co-glycolic acid) (PLGA) and poly lactic acid (PLA) microparticles and embedded them in a polycaprolactone-based hydrogel. The system proved to have good injectability with no clogging of the needle. The biodegradation and release profile of the microparticles was delayed due to the hydrogel protection.

More recently, other studies using the microparticles within the hydrogel system have been published in different biomedical fields. Xu *et al.* [125] developed a hyaluronic acid and carboxymethyl chitosan-based hydrogel through Schiff base reactions. Then, *Resina Darconis* microparticles were loaded into the hydrogel. The system presented good mechanical, rheological and even self-healing properties. In *in vivo* trials, the compound promoted the acceleration of wound healing by accelerating the hemostatic and inflammatory phases, thus accelerating the wound healing process. Marzaman *et al.* [126] developed chloramphenicol whey protein-based microparticles, that were then embedded in Pluronic hydrogels (F127 and F68) and hydroxypropyl methacrylate. This thermoresponsive system was developed for wound treatments, and the system was able to be at the sol state at room temperature and the gel state at 37ºC. The composite system was also able to increase bioactivity and showed antibacterial properties.

2.3.2.4. Swelling behaviour

The presence of microparticles in hydrogel systems can have an impact on their swelling behaviour. In general, the addition of microparticles tends to decrease the swelling behaviour of hydrogels, as they occupy space within the porous structure and promote physical cross-linking of the hydrogel's chains, leading to reduced swelling [121], [127]. This means that microparticles can decrease the porosity of the hydrogel [128].

The degree to which the microparticles affect the hydrogel swelling behaviour depends on their concentration and nature. Some microparticles can increase the swelling capabilities of the hydrogel, likely due to their hydrophilic nature and ability to absorb water, such as hydrophilic gelatine/heparin microspheres [129]. On the other hand, some microparticles may have no significant effect on swelling behaviour, as reported by Liu *et al.* [130] with PLGA microparticles in a PEG-PLLA-DA/NIPAAm hydrogel. But in this study, this lack of effect might be explained by the low concentrations of used cargo. The effect of microparticles on the cross-linking density can lead to a more structured system and higher degradation times, as well as a reduction in bulk degradation rate due to decreased liquid penetration within the hydrogel matrix.

2.3.3. Microparticle/hydrogel composite system as DDS: Advantages

2.3.3.1. Manipulation of the drug/bioactive agents release profile

The released concentrations must be within certain ranges after the implantation of the DDS *in vivo.* Low concentrations will have no effect on cancer, whilst too higher concentrations may have cytotoxic effects on the human body. The ideal delivery profile for any DDS would be a constant and predictable release rate. However, achieving a constant profile is challenging, and using microparticles alone makes it even more difficult. Microparticles often display an "initial burst" effect where large amounts of the loaded drug or bioactive agent are released rapidly, but subsequently, the release rate declines and becomes insufficient to maintain the desired therapeutic concentrations. To mitigate this burst effect, barriers can be added to create additional diffusion pathways that the bioactive agents must pass before reaching the *in vivo* environment [131]. Direct injection of drug/bioactive-loaded microparticles into the body exposes them directly to the physiological environment, leading to degradation and accelerated release. To slow down biodegradation and retard the release, microparticles can be embedded within a hydrogel.

In a system that used Pluronic, Heo *et al.* [132] used dexamethasone (DEX) loaded PLGA microparticles and embedded them in a Pluronic/hyaluronic acid hydrogel. In *in vivo* drug release tests, microparticles alone released 18% of DEX on day 1, 44% on day 7 and 83% at the end of 28 days, whilst the composite system released 3.2%, 32% and 78% on day 1, 7 and 28, respectively (Figure 2.8). The initial burst release was delayed, with a significant decrease in the release profile on the first day. This might be due to the interaction of DEX with the lyophilic parts of Pluronic chains after the release from the microspheres. The following rapid degradation of Pluronic led to the rapid clearance of DEX, with higher cumulative releases with time. The microspheres/HA-based system released 4.7%, 14.4% and 42% on days 1, 3 and 28. This system was capable to resist and release for long periods and retard the initial burst, maintaining therapeutic levels for longer periods.

Microparticle/hydrogel systems have been shown to release drugs at much slower rates compared to simple hydrogels with homogeneously distributed drugs. For instance, in a study conducted by our research group, methylene blue-loaded alginate particles were combined with a Pluronic hydrogel. The release of methylene blue from alginate microspheres embedded in a Pluronic hydrogel (15.5 w/w%) was 10 times slower than the one-loaded Pluronic hydrogel alone. The model drug was completely released from the Pluronic hydrogel after 24 hours, while only 38.2% was released from the composite system in the same period, achieving complete release after 240 hours (10 days) [76], [77].

In another study by Osswald and Kang-Mieler [133], the release profile of anti-vascular endothelial growth factor (VEGF) agents (ranibizumab or aflibercept) from PLGA microparticles was compared to that of microparticle/hydrogel composite systems. The microparticles alone degraded after 150 days, while the microparticle/hydrogel system lasted more than a month longer, at 196 days. The composite system also had a more prolonged release with a significantly more controlled burst release effect. The initial burst effect released 50.3% of

ranibizumab from microparticles alone, compared to only 21% from the composite system. This difference was even more pronounced with aflibercept, with the microparticles releasing 83.3% initially compared to a significantly lower 20.1% from the composite system.

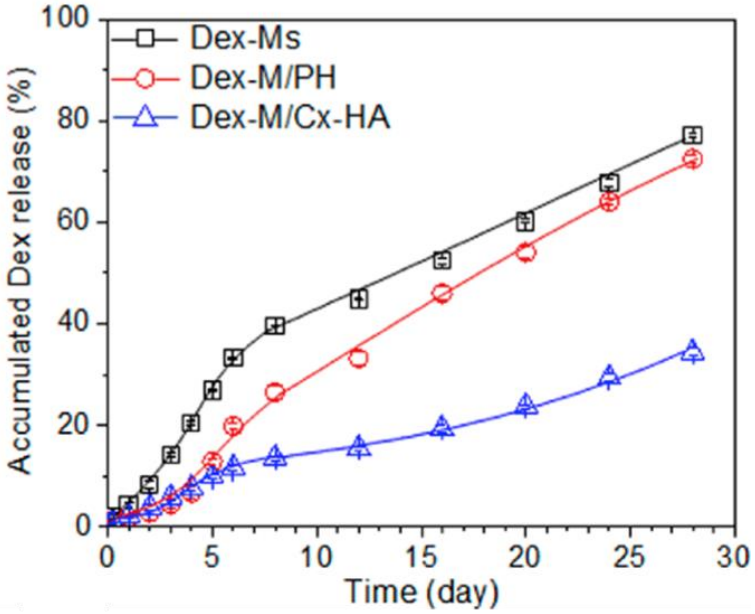

Figure 2.8 Accumulated *in vitro* release of DEX of microparticles and hydrogel alone and the composite system (Adapted with permission from [132]. Copyright (2019) Multidisciplinary Digital Publishing Institute).

2.3.3.2. *In loco* stability and drug release

Controlled release patterns can prevent the spreading of drugs or bioactive agents to other parts of the body. Chemotherapeutic drugs, for instance, are helpful in treating tumours, but they also damage healthy tissues and can decrease a patient's quality of life. An ideal DDS *in situ* should only release the necessary amount of bioactive agents to the targeted area without spreading to healthy tissues. As previously mentioned, injectable hydrogels can adapt their form to the desired area, thus facilitating the release *in loco*. Lourenço *et al.* [134] developed a system for the local delivery of strontium for bone tissue engineering. Orally administered strontium can lead to cardiovascular problems. The researchers used a hyaluronic acid microparticles/alginate hydrogel system for *in situ* delivery (Figure 2.9). *In vivo* release studies indicated that strontium was only released into the defect site, with no significant concentrations found in other organs.

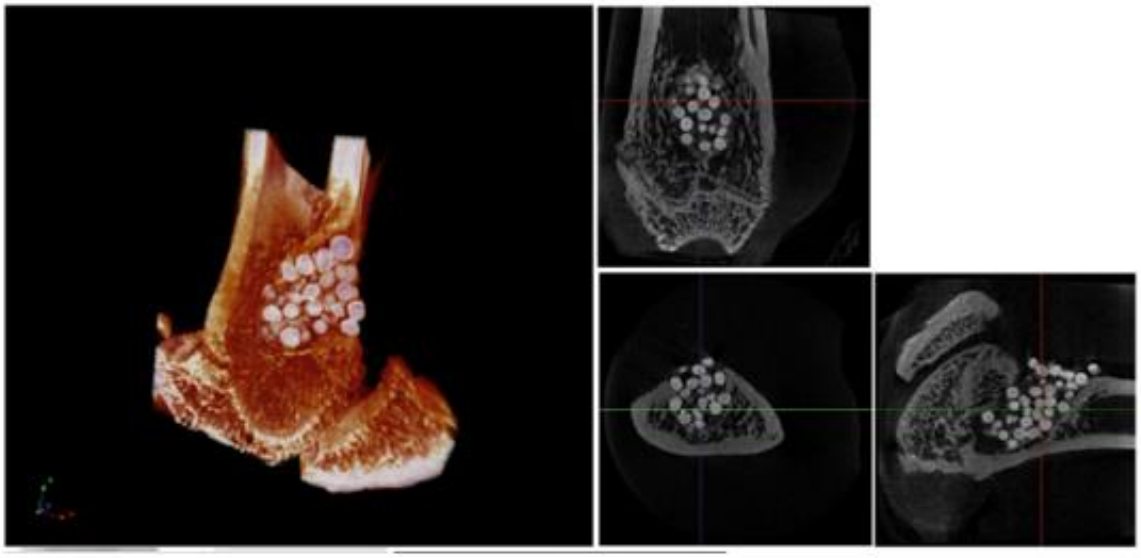

Figure 2.9 Micro-CT (microtomography) analysis of distal femur after 60 days of implantation. 3D reconstructed image and respective orthogonal slices of micro-CT acquisition of the femur with Sr-hybrid filled defect. (Adapted with permission from [134]. Copyright (2021) National Library of Medicine).

2.3.3.3. Sequential release and co-delivery

The proposed DDS that this project aims to develop can deliver multiple bioactive agents in sequential order (Figure 2.10 Figure 2.1). Medical treatments often require different drugs for different phases of treatment. Ideally, a delivery system should release the appropriate drug at the right time to achieve a maximum therapeutic effect; however, designing such DDS is not easily achievable. In a microparticle/hydrogel system, sequential delivery can be programmed. The hydrogel degrades faster than the microparticles within. Thus, releasing a possible cargo that can be loaded within the hydrogel before the cargo within the microparticles is released. The microparticles within the matrix have a delayed release, so their cargo is unloaded only after the first drug has started to be released and acted. By loading particles with different release patterns, it is possible to create a cascade treatment with progressive unloading of drugs that accompany the treatment stages [135]–[139].

A good example of this is wound healing, which has four stages of recovery from the damage to the full healing. Ma *et al.* [135] designed a system comprised of a sodium alginate/bioglass hydrogel loaded with sodium alginate microparticles, that in turn contained PLGA microparticles. This system was devised to release different products along the four different phases of recovery. For example, ionic products within the hydrogel would rapidly release at the first phase (inflammatory phase), and only afterwards PLA microparticles that were contained within the alginate microparticles would release pirfenidone to prevent scar formation.

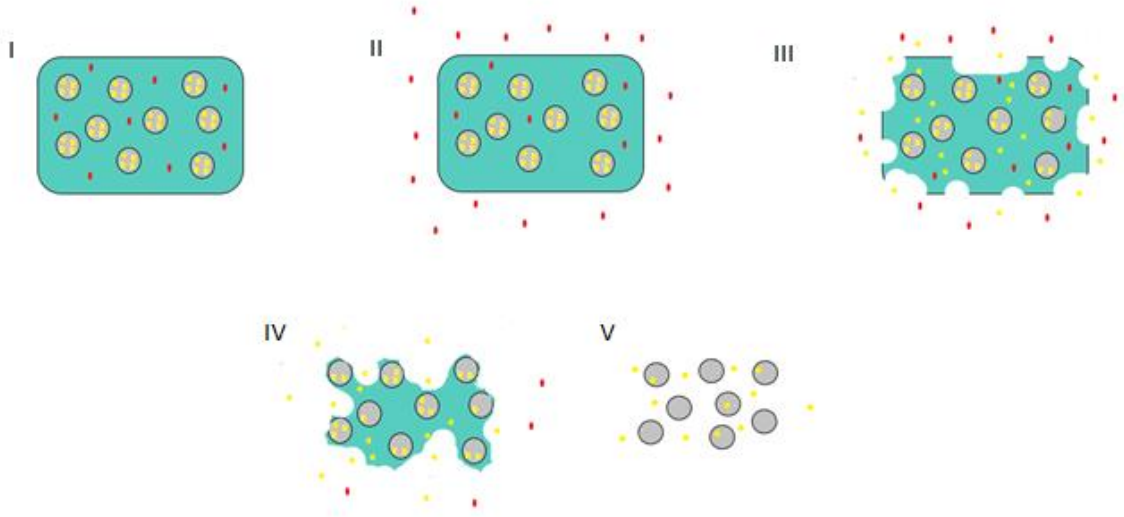

Figure 2.10 Scheme of a sequential delivery I) microcapsule/hydrogel loaded with 2 drugs (red in the hydrogel and yellow within the microparticles), II) the red drug begins to be released in an early stage, III) the hydrogel starts to degrade and the yellow drug diffuses trough the hydrogel, IV) the red drug is completely released with the degradation of the hydrogel, V) the microparticles stop being protected by the hydrogel and the yellow drug will be fully released with the complete degradation of the particles. (Adapted with permission from [1]. Copyright (2021) Multidisciplinary Digital Publishing Institute).

2.3.3.4. Encapsulation of hydrophobic drugs

Hydrophilic hydrogels have limitations in loading hydrophobic biological agents due to their nature. This means that they have been primarily used for water-soluble drugs. However, there have been various approaches to incorporating hydrophobic drugs into hydrogels [140]. For example, triblock polymers can be used to create thermosensitive hydrogels with hydrophobic chains that can form hydrophobic micelles to store drugs. This allows for a sustained release of hydrophobic drugs, while hydrophilic drugs can be released more rapidly [92]. Another strategy is to use transport agents that can carry hydrophobic drugs like liposomes [141] and niosomes [142]. Conventional hydrophilic hydrogels mixed with these transport agents loaded with hydrophobic drugs can thus serve as alternatives to deliver these types of drugs. Microparticles can also serve as hydrophobic drug carriers within hydrogels [71], [140], [143] Hydrophobic polymers such as PLGA, PLA, and PCL can also be used as carriers to deliver these drugs *in vivo*. However, unlike hydrophilic drugs, they will mainly be released by particle erosion rather than diffusion [92]. For example, Li *et al.* [144] studied the release of paclitaxel onto a thermo-sensitive hydrogel. In breast MCF-7 tumour-bearing mice models, the hydrogel was able to deliver the hydrophobic drug and had sustained release with extended drug retention within the tumour. Wang *et al.* [145] developed for oral delivery docetaxel (DTX) loaded micelles. Then these micelles were embedded within a pH-responsive hydrogel. The micelles successfully loaded the drug with high drug loading. The addition of the pH hydrogel around the micelles improved the oral bioavailability of the drug about 10 times. With a 4T1 breast cancer model the system inhibited tumour growth and decreased systemic toxicity.

2.4. Microparticles/Hydrogels systems in cancer treatment

The microparticle/hydrogel system has been used for multiple applications such as cardiovascular diseases, diabetes, bone recovery and tissue engineering [1]. Since the topic of this thesis is cancer, the following part will only focus on its use in cancer treatments. For more information on these systems in other therapies please consult the review [1].

A system for the sequential release can be useful in cancer treatment to address the different stages of the treatment. Kim *et al.* [146] developed an injectable intratumoral system for sequential co-delivery. PLGA microcapsules loaded with DOX and a thermosensitive hydrogel loaded with 5-FU. As hydrogels, they compared the behaviour of Pluronic with a poly(ethylene glycol)-b-poly(caprolactone-co-lactide) diblock copolymer. 5-FU was released first from the hydrogel, followed by a later stage of DOX release. The microcapsule/hydrogel system performed better *in vivo* and *in vitro* than the isolated microcapsules and hydrogels. *in vivo* drug biodistribution showed that the drugs were confined to the target tumours for 18 days, without distribution to normal cells. Concentrations below their toxic plasma concentrations would result in no toxicity damage. Luo *et al.* [147] developed a hyaluronic acid hydrogel with 5-FU and cisplatin and PCL-PEG-PCL microspheres loaded with paclitaxel. These two components could be used to create a sequential co-delivery system of chemotherapeutic drugs for colorectal peritoneal carcinomatosis, an advanced stage of colorectal cancer. The hydrogel alone released the drugs within a week *in vitro*, but the microspheres released only 40% of their contents at the same time.

Zheng *et al.* [139] developed a thermoresponsive injectable system for sequential co-delivery. Combretastatin A-4 (CA4) was loaded in a polypeptide hydrogel, while DTX was loaded in PLGA microparticles. CA4 would be released first to inhibit neovascularisation and reduce nutrient exchange between the tumour and surrounding tissues. Later, DTX would penetrate the new interstitial spaces, attack the surface cells of the tumour, and inhibit cell proliferation. *In vitro* release studies confirmed a more rapid release of CA4 and a slower release of DTX. The system did not suffer from burst release of DTX, unlike the PLGA microspheres alone. *In vivo* tests revealed that the total system degradation occurred after 42 days. The system was effective in inhibiting tumour cell proliferation, and drug loading in the system diminished toxicity, preventing drugs from spreading outside the cancerous area. The survival rate of the composite system with co-delivery was also the highest compared to the other systems. In another study, the co-delivery of ibuprofen as an anti-inflammatory agent and DOX as a chemotherapeutic drug was studied [148]. The study used an alginate hydrogel for early ibuprofen release and PCL microparticles for later DOX release.

Ozeki *et al.* [149] developed a system using PLGA microspheres and a thermosensitive hydrogel conjugate of PEG and PNIPAAm to treat brain tumours. They encapsulated camptothecin and vincristine separately in the PLGA microparticles and compared their efficacy. Camptothecin had a significant initial release, causing systemic toxicity. However, the use of composite systems was revealed to be more efficient, with the system containing

vincristine showing increased survival rates at lower doses compared to the system with camptothecin.

Regarding breast cancer cells, Zhu *et al*. [150] used vaterite microspheres embedded in silk nanofibers that formed a hydrogel for DOX delivery. DOX was loaded onto the vaterite particles and silk nanofibers hydrogel. The system was injectable and resolved the poor water dispersibility of vaterite and the low drug release of the silk nanofibers by combining them with the microspheres. The drug release profile was higher at lower pH, however, the release behaviour of DOX was able to be regulated by loading the drug in different particles and silk nanofibers. The injectable system had shear thinning properties due to the rupture of the silk chain's entanglement and alignment of them. The system proved to be thixotropic, with the elastic properties recovered with time. *In vitro* tests of MCF-7 cells revealed that the composite system significantly decreased the viability of the cells.

The following table (Table 2.1) gives an overview of some microparticles/hydrogel systems that have been studied as potential cancer treatments.

Table 2.1 Microparticle/hydrogel system used for cancer treatments. (Adapted with permission from [1]. Copyright (2021) Multidisciplinary Digital Publishing Institute).

Microparticles	Hydrogels	Bioactive cargo	Observations	Ref.
PLGA	PLAF-b- PEG-b- PLA	Combretastatin A-4 and docetaxel	Sequential release of drugs. The synergistic system suppressed the spread of an osteosarcoma in *in vivo* tests.	[139]
PCL–PEG–PCL	PCL–PEG–PCL	Camptothecine	The composite system had a strong anti-tumour effect. The system suppressed growth and metastasis in *in vivo* tests.	[108]
Double walled microparticles with PLGA and PDLLA	Aldehyde functionalised sodium alginate	Cisplatin and paclitaxel	Beyond the use for chemotherapeutics the hydrogel of the system also served as an antibacterial agent, due to the presence of polyethyleneimine within the hydrogel.	[143]
PLGA	Pluronic and copolymer of PEG-PCL-PLLA	DOX and 5 FU	Microparticles carried DOX and the hydrogel carried 5 FU. Pluronic rapidly cleared whilst the copolymer endured. The spread of the drug to normal tissues was not observed *in vivo*.	[146]
PCL–PEG–PCL	Hyaluronic acid	5 FU, cisplatin and paclitaxel	Hydrogel loaded with 5Fu and cisplatin and microspheres with paclitaxel. Both evaluated separately. Good *in vivo* performance.	[147]
PCL	Alginate	DOX and ibuprofen	Early release of ibuprofen as an anti-inflammatory agent followed by DOX release for cytotoxic effect.	[148]
Vaterite microspheres	Silk nanofibers	DOX	Several combinations made. The system significantly decreased viability of MCF-7 cell in *in vivo* tests.	[150]

PLGA	PEG and PNIPAAm conjugates	Camptothecin and vincristine	Drugs loaded only on the microparticles. Vincristine had a better performance than camptothecin, with longer rates of survival.	[149]
Gelatine	Alginate and chitosan	5 FU and iron oxide nanoparticles	Under an external magnetic field, the system released higher quantities of 5 FU at higher times but had no effect in the initial release.	[151]

2.5. References

[1] H. Carrêlo, P. I. P. Soares, J. P. Borges, and M. T. Cidade, "Injectable composite systems based on microparticles in hydrogels for bioactive cargo controlled delivery," *Gels*, vol. 7, no. 3. MDPI, Sep. 01, 2021. doi: 10.3390/gels7030147.

[2] International Agency for Reseach on Cancer - World Health Organization, "Global Cancer Observatory," 2022. https://gco.iarc.fr/ (accessed Mar. 14, 2022).

[3] European Cancer Inequalities Registry, "Perfil sobre cancro por país- 2023," 2023. [Online]. Available: www.oecd-ilibrary.org

[4] "PORDATA - Base de Dados Portugal Contemporâneo," 2020. www.pordata.pt (accessed Dec. 12, 2020).

[5] D. Hanahan and R. A. Weinberg, "The hallmarks of cancer," *Cell*, vol. 100, pp. 57–50, 2000, doi: 10.1016/s0092-8674(00)81683-9.

[6] D. Hanahan and R. A. Weinberg, "Hallmarks of cancer: The next generation," *Cell*, vol. 144, no. 5, pp. 646–674, 2011, doi: 10.1016/j.cell.2011.02.013.

[7] D. Hanahan, "Hallmarks of Cancer: New Dimensions," *Cancer Discov.*, vol. 12, no. 1, pp. 31–46, 2022, doi: 10.1158/2159-8290.CD-21-1059.

[8] R. Tudu, A. Kumar, R. Singh, and P. Raina, "Bilateral breast cancer: A case study," *J. Radiother. Pract.*, vol. 19, no. 3, pp. 305–308, 2020, doi: 10.1017/S1460396919000761.

[9] "National Cancer Institute." www.cancer.gov (accessed Mar. 17, 2020).

[10] S. H. Giordano, A. U. Buzdar, and G. N. Hortobagyi, "Breast Cancer in Men EPIDEMIOLOGY AND RISK FACTORS," 2002, [Online]. Available: www.annals.org

[11] "Liga Portuguesa Contra O Cancro." www.ligacontracancro.pt (accessed Mar. 14, 2022).

[12] N. Carlson and J. King, "Overview of Breast Cancer Treatment and Reconstruction for Primary Care Providers," *J. Midwifery Women's Heal.*, vol. 57, no. 6, pp. 558–568, 2012, doi: 10.1111/j.1542-2011.2012.00249.x.

[13] F. Behbod, A. M. Gomes, and H. L. Machado, "Modeling Human Ductal Carcinoma In Situ in the Mouse," *J. Mammary Gland Biol. Neoplasia*, vol. 23, no. 4, pp. 269–278, 2018, doi: 10.1007/s10911-018-9408-0.

[14] "American Cancer Society." www.cancer.org (accessed Mar. 17, 2022).

[15] "Cancer.Net." www.cancer.net (accessed Mar. 17, 2020).

[16] E. Cochrane, S. Kim, A. Kudelka, and W. Burke, "Invasive ductal breast carcinoma metastasis to the cervix: A case review and clinical correlation," *Gynecol. Oncol. Reports*, vol. 33, no. July, p. 100616, 2020, doi: 10.1016/j.gore.2020.100616.

[17] N. Wilson, A. Ironside, A. Diana, and O. Oikonomidou, "Lobular Breast Cancer: A Review," *Front. Oncol.*, vol. 10, no. January, pp. 1–13, 2021, doi: 10.3389/fonc.2020.591399.

[18] N. Eliyatkin, E. Yalcin, B. Zengel, S. Aktaş, and E. Vardar, "Molecular Classification of Breast Carcinoma: From Traditional, Old-Fashioned Way to A New Age, and A New Way," *J. Breast Heal.*, vol. 11, no. 2, pp. 59–66, 2015, doi: 10.5152/tjbh.2015.1669.

[19] X. Sun *et al.*, "Metabolic Reprogramming in Triple-Negative Breast Cancer," *Front. Oncol.*, vol. 10, no. March, 2020, doi: 10.3389/fonc.2020.00428.
[20] "National Breast Cancer Foundation, Inc.," 2023. https://www.nationalbreastcancer.org/ (accessed May 04, 2023).
[21] C. J. Campbell and B. W. Booth, "The Influence of the Normal Mammary Microenvironment on Breast Cancer Cells," *Cancers (Basel).*, vol. 15, no. 3, 2023, doi: 10.3390/cancers15030576.
[22] A. Nasrazadani, R. A. Thomas, S. Oesterreich, and A. V. Lee, "Precision medicine in hormone receptor-positive breast cancer," *Front. Oncol.*, vol. 8, no. MAY, pp. 4–11, 2018, doi: 10.3389/fonc.2018.00144.
[23] N. Afifi and C. A. Barrero, "Understanding Breast Cancer Aggressiveness and Its Implications in Diagnosis and Treatment," *J. Clin. Med.*, vol. 12, no. 4, pp. 10–12, 2023, doi: 10.3390/jcm12041375.
[24] S. V. Gibson, R. M. Roozitalab, M. D. Allen, J. L. Jones, E. P. Carter, and R. P. Grose, "Everybody needs good neighbours: the progressive DCIS microenvironment," *Trends in Cancer*, vol. 9, no. 4, pp. 326–338, 2023, doi: 10.1016/j.trecan.2023.01.002.
[25] G. Arpino, M. Milano, and S. De Placido, "Features of aggressive breast cancer," *Breast*, vol. 24, no. 5, pp. 594–600, 2015, doi: 10.1016/j.breast.2015.06.001.
[26] "Cancer Research UK," 2023. https://www.cancerresearchuk.org/ (accessed May 05, 2023).
[27] O. M. Valencia, S. E. Samuel, R. K. Viscusi, T. S. Riall, L. A. Neumayer, and H. Aziz, "The role of genetic testing in patients with breast cancer a review," *JAMA Surg.*, vol. 152, no. 6, pp. 589–594, 2017, doi: 10.1001/jamasurg.2017.0552.
[28] H. L. Olsson and M. L. Olsson, "The Menstrual Cycle and Risk of Breast Cancer: A Review," *Front. Oncol.*, vol. 10, no. January, pp. 10–13, 2020, doi: 10.3389/fonc.2020.00021.
[29] A. Surakasula, G. Nagarjunapu, and K. Raghavaiah, "A comparative study of pre- and post-menopausal breast cancer: Risk factors, presentation, characteristics and management," *J. Res. Pharm. Pract.*, vol. 3, no. 1, p. 12, 2014, doi: 10.4103/2279-042x.132704.
[30] H. R. Brewer, M. E. Jones, M. J. Schoemaker, A. Ashworth, and A. J. Swerdlow, "Family history and risk of breast cancer: an analysis accounting for family structure," *Breast Cancer Res. Treat.*, vol. 165, no. 1, pp. 193–200, 2017, doi: 10.1007/s10549-017-4325-2.
[31] M. García Manero, G. López García, L. Pina Insausti, and S. Lizarraga, "Breast cancer during pregnancy," *Rev. Med. Univ. Navarra*, vol. 52, no. 1, pp. 18–24, 2008, doi: 10.7759/cureus.2941.
[32] B. Stordal, "Breastfeeding reduces the risk of breast cancer: A call for action in high-income countries with low rates of breastfeeding," *Cancer Med.*, vol. 12, no. 4, pp. 4616–4625, 2023, doi: 10.1002/cam4.5288.
[33] Z. Tan *et al.*, "Mapping Breast Cancer Microenvironment Through Single-Cell Omics," *Front. Immunol.*, vol. 13, no. April, pp. 1–10, 2022, doi: 10.3389/fimmu.2022.868813.
[34] N. M. Anderson and M. C. Simon, "The tumor microenvironment," *Curr. Biol.*, vol. 30, no. 16, pp. R921–R925, 2020, doi: 10.1016/j.cub.2020.06.081.
[35] G. Zarrilli *et al.*, "The Tumor Microenvironment of Primitive and Metastatic Breast Cancer : Implications for Novel Therapeutic Strategies," no. i.
[36] U. Mehraj, A. H. Dar, N. A. Wani, and M. A. Mir, "Tumor microenvironment promotes breast cancer chemoresistance," *Cancer Chemother Pharmacol*, vol. 87, no. 2, pp. 147–158, 2021, doi: 10.1007/s00280-020-04222-w.

[37] J. J. Li, J. Y. Tsang, and G. M. Tse, "Tumor Microenvironment in Breast Cancer — Updates on Therapeutic Implications and Pathologic Assessment," 2021.
[38] K. P. Valente, S. S. Thind, M. Akbari, A. Suleman, and A. G. Brolo, "Collagen Type I-Gelatin Methacryloyl Composites: Mimicking the Tumor Microenvironment," *ACS Biomater. Sci. Eng.*, vol. 5, pp. 2887–2898, 2019, doi: 10.1021/acsbiomaterials.9b00264.
[39] X. Jiang *et al.*, "Recent Advances in the Aging Microenvironment of Breast Cancer," *Cancers (Basel).*, vol. 14, no. 20, 2022, doi: 10.3390/cancers14204990.
[40] S. Moroni, L. Casettari, and D. A. Lamprou, "3D and 4D Printing in the Fight against Breast Cancer," *Biosensors*, vol. 12, no. 8, 2022, doi: 10.3390/bios12080568.
[41] E. Boedtkjer and S. F. Pedersen, "The Acidic Tumor Microenvironment as a Driver of Cancer," *Annu. Rev. Physiol.*, vol. 82, pp. 103–126, 2020, doi: 10.1146/annurev-physiol-021119-034627.
[42] Z. Chen *et al.*, "Surgical stress and cancer progression : the twisted tango," pp. 1–11, 2019.
[43] C. Núñez, J. L. Capelo, G. Igrejas, A. Alfonso, L. M. Botana, and C. Lodeiro, "An overview of the effective combination therapies for the treatment of breast cancer," *Biomaterials*, vol. 97, pp. 34–50, 2016, doi: 10.1016/j.biomaterials.2016.04.027.
[44] E. Å. Lundqvist, K. Fujiwara, and M. Seoud, "Principles of chemotherapy," *Int. J. Gynecol. Obstet.*, vol. 131, pp. S146–S149, 2015, doi: 10.1016/j.ijgo.2015.06.011.
[45] R. Ponce-cusi and G. M. Calaf, "Apoptotic activity of 5-fluorouracil in breast cancer cells transformed by low doses of ionizing α-particle radiation," pp. 774–782, 2016, doi: 10.3892/ijo.2015.3298.
[46] M. Argenziano *et al.*, "Improvement in the Anti-Tumor E ffi cacy of Doxorubicin Nanosponges in In Vitro and in Mice Bearing Breast Tumor Models," pp. 1–19.
[47] J. Haussmann *et al.*, "Recent advances in radiotherapy of breast cancer," pp. 1–10, 2020.
[48] P. Bhardwaj *et al.*, "Estrogens and breast cancer: Mechanisms involved in obesity-related development, growth and progression," *J. Steroid Biochem. Mol. Biol.*, vol. 189, no. March, pp. 161–170, 2019, doi: 10.1016/j.jsbmb.2019.03.002.
[49] D. Design, "The Role of Progesterone Receptors in Breast Cancer," no. January, pp. 305–314, 2022.
[50] J. Goldberg *et al.*, "The Immunology of Hormone Receptor Positive Breast Cancer," vol. 12, no. May, pp. 1–22, 2021, doi: 10.3389/fimmu.2021.674192.
[51] V. Debien *et al.*, "Immunotherapy in breast cancer: an overview of current strategies and perspectives," *npj Breast Cancer*, vol. 9, no. 1, 2023, doi: 10.1038/s41523-023-00508-3.
[52] V. Galimberti *et al.*, "Nipple-sparing and skin-sparing mastectomy: Review of aims, oncological safety and contraindications," *Breast*, vol. 34, pp. S82–S84, 2017, doi: 10.1016/j.breast.2017.06.034.
[53] A. Fakhari and J. Anand Subramony, "Engineered in-situ depot-forming hydrogels for intratumoral drug delivery," *J. Control. Release*, vol. 220, pp. 465–475, 2015, doi: 10.1016/j.jconrel.2015.11.014.
[54] P. Prasad, A. Shuhendler, P. Cai, A. M. Rauth, and X. Y. Wu, "Doxorubicin and mitomycin C co-loaded polymer-lipid hybrid nanoparticles inhibit growth of sensitive and multidrug resistant human mammary tumor xenografts," *Cancer Lett.*, vol. 334, no. 2, pp. 263–273, 2013, doi: 10.1016/j.canlet.2012.08.008.
[55] J. M. Fleming, S. T. Yeyeodu, A. McLaughlin, D. Schuman, and D. K. Taylor, "In Situ Drug Delivery to Breast Cancer-Associated Extracellular Matrix," *ACS Chem. Biol.*, vol. 13, no. 10, pp. 2825–2840, 2018, doi: 10.1021/acschembio.8b00396.

[56] V. Masoud and G. Pagès, "Targeted therapies in breast cancer: New challenges to fight against resistance," *World J. Clin. Oncol.*, vol. 8, no. 2, pp. 120–134, 2017, doi: 10.5306/wjco.v8.i2.120.
[57] "National Institute of Biomedical Imaging and Bioengineering." https://www.nibib.nih.gov/ (accessed Apr. 16, 2022).
[58] A. Z. Wang, R. Langer, and O. C. Farokhzad, "Nanoparticle Delivery of Cancer Drugs," *Annu. Rev. Med.*, vol. 63, no. 1, pp. 185–198, 2012, doi: 10.1146/annurev-med-040210-162544.
[59] S. Bale, A. Khurana, A. S. S. Reddy, M. Singh, and C. Godugu, "Overview on therapeutic applications of microparticulate drug delivery systems," *Crit. Rev. Ther. Drug Carrier Syst.*, vol. 33, no. 4, pp. 309–361, 2016, doi: 10.1615/CritRevTherDrugCarrierSyst.2016015798.
[60] M. Norouzi, B. Nazari, and D. W. Miller, "Injectable hydrogel-based drug delivery systems for local cancer therapy," *Drug Discov. Today*, vol. 21, no. 11, pp. 1835–1849, 2016, doi: 10.1016/j.drudis.2016.07.006.
[61] J. K. Patra *et al.*, "Nano based drug delivery systems: Recent developments and future prospects," *J. Nanobiotechnology*, vol. 16, no. 1, pp. 1–33, 2018, doi: 10.1186/s12951-018-0392-8.
[62] A. Aung, V. Kumar, J. Theprungsirikul, S. K. Davey, and S. Varghese, "An Engineered Tumor-on-a-Chip Device with Breast Cancer–Immune Cell Interactions for Assessing T-cell Recruitment," *Cancer Res.*, vol. 80, no. 2, pp. 263–275, 2020, doi: 10.1158/0008-5472.CAN-19-0342.
[63] Y. Qu *et al.*, "A biodegradable thermo-responsive hybrid hydrogel: Therapeutic applications in preventing the post-operative recurrence of breast cancer," *NPG Asia Mater.*, vol. 7, no. 8, pp. e207-10, 2015, doi: 10.1038/am.2015.83.
[64] J. H. Lee and A. Nan, "Combination Drug Delivery Approaches in Metastatic Breast Cancer," *J. Drug Deliv.*, vol. 2012, pp. 1–17, 2012, doi: 10.1155/2012/915375.
[65] A. D. Wong, L. M. Russell, M. E. Katt, and P. C. Searson, "Chemotherapeutic Drug Delivery and Quantitative Analysis of Proliferation, Apoptosis, and Migration in a Tissue-Engineered Three-Dimensional Microvessel Model of the Tumor Microenvironment," *ACS Biomater. Sci. Eng.*, vol. 5, no. 2, pp. 633–643, 2019, doi: 10.1021/acsbiomaterials.8b00877.
[66] Y. Qiu and K. Park, "Environment-sensitive hydrogels for drug delivery," *Adv. Drug Deliv. Rev.*, vol. 64, no. SUPPL., pp. 49–60, 2012, doi: 10.1016/j.addr.2012.09.024.
[67] C. Tipa, M. T. Cidade, T. Vieira, J. C. Silva, P. I. P. Soares, and J. P. Borges, "A new long-term composite drug delivery system based on thermo-responsive hydrogel and nanoclay," *Nanomaterials*, vol. 11, no. 1, pp. 1–22, 2021, doi: 10.3390/nano11010025.
[68] S. Chatterjee and P. C. L. Hui, "Review of applications and future prospects of stimuli-responsive hydrogel based on thermo-responsive biopolymers in drug delivery systems," *Polymers (Basel).*, vol. 13, no. 13, 2021, doi: 10.3390/polym13132086.
[69] S. R. Gomes, G. Rodrigues, G. G. Martins, C. M. R. Henriques, and J. C. Silva, "In vitro evaluation of crosslinked electrospun fish gelatin scaffolds," *Mater. Sci. Eng. C*, vol. 33, no. 3, pp. 1219–1227, 2013, doi: 10.1016/j.msec.2012.12.014.
[70] D. Y. Fan, Y. Tian, and Z. J. Liu, "Injectable Hydrogels for Localized Cancer Therapy," *Front. Chem.*, vol. 7, no. October, pp. 1–11, 2019, doi: 10.3389/fchem.2019.00675.
[71] J. H. Seo *et al.*, "Monopotassium phosphate-reinforced in situ forming injectable hyaluronic acid hydrogels for subcutaneous injection," *Int. J. Biol. Macromol.*, vol. 163,

pp. 2134–2144, 2020, doi: 10.1016/j.ijbiomac.2020.09.089.
[72] S. Mantha, S. Pillai, P. Khayambashi, A. Upadhyay, and Y. Zhang, "Smart Hydrogels in Tissue Engineering and," *Materials (Basel).*, vol. 12, 2019, doi: 10.3390/ma12203323.
[73] Y. Sugioka, J. Nakamura, C. Ohtsuki, and A. Sugawara-narutaki, "Thixotropic hydrogels composed of self-assembled nanofibers of double-hydrophobic elastin-like block polypeptides," *Int. J. Mol. Sci.*, vol. 22, no. 8, 2021, doi: 10.3390/ijms22084104.
[74] J. Yao, C. Zhu, T. Peng, Q. Ma, and S. Gao, "Injectable and Temperature-Sensitive Titanium Carbide-Loaded Hydrogel System for Photothermal Therapy of Breast Cancer," vol. 9, no. December, pp. 1–11, 2021, doi: 10.3389/fbioe.2021.791891.
[75] J. García-Couce, M. Tomás, G. Fuentes, L. J. Cruz, I. Que, and A. Almirall, "Chitosan/Pluronic F127 Thermosensitive Hydrogel as an Injectable Dexamethasone Delivery Carrier," *Gels*, vol. 8, p. 44, 2022.
[76] B. Delgado, H. Carrêlo, M. V. Loureiro, A. C. Marques, J. P. Borges, and M. T. Cidade, "Injectable hydrogels with two different rates of drug release based on pluronic / water system filled with poly (e -caprolactone) microcapsules," *J. Mater. Sci.*, 2021, doi: 10.1007/s10853-021-06156-x.
[77] M. T. Cidade, D. J. Ramos, J. Santos, H. Carrelo, N. Calero, and J. P. Borges, "Injectable hydrogels based on pluronic/water systems filled with alginate microparticles for biomedical applications," *Materials (Basel).*, vol. 12, no. 7, pp. 1–14, 2019, doi: 10.3390/ma12071083.
[78] H. Carrêlo, A. R. Escoval, P. I. P. Soares, J. P. Borges, and M. T. Cidade, "Injectable Composite Systems of Gellan Gum : Alginate Microparticles in Pluronic Hydrogels for Bioactive Cargo Controlled Delivery : Optimization of Hydrogel Composition based on Rheological Behavior," *Fluids*, vol. 7, no. 375, 2022, doi: 10.3390/fluids7120375.
[79] B. Shriky *et al.*, "Pluronic F127 thermosensitive injectable smart hydrogels for controlled drug delivery system development," *J. Colloid Interface Sci.*, vol. 565, pp. 119–130, 2020, doi: 10.1016/j.jcis.2019.12.096.
[80] S. Y. Park, Y. Lee, K. H. Bae, C. Ahn, and T. G. Park, "Temperature / pH-Sensitive Hydrogels Prepared from Pluronic Copolymers End-Capped with Carboxylic Acid Groups via an Oligolactide Spacer," pp. 1172–1176, 2007, doi: 10.1002/marc.200600914.
[81] E. Gioffredi *et al.*, "Pluronic F127 hydrogel characterization and biofabrication in cellularized constructs for tissue engineering applications .," *Procedia CIRP*, vol. 49, no. iii, pp. 125–132, 2016, doi: 10.1016/j.procir.2015.11.001.
[82] N. Rapoport, "Physical stimuli-responsive polymeric micelles for anti-cancer drug delivery," *Prog. Polym. Sci.*, vol. 32, no. 8–9, pp. 962–990, 2007, doi: 10.1016/j.progpolymsci.2007.05.009.
[83] V. Patrulea, V. Ostafe, G. Borchard, and O. Jordan, "Chitosan as a starting material for wound healing applications," *Eur. J. Pharm. Biopharm.*, vol. 97, pp. 417–426, 2015, doi: 10.1016/j.ejpb.2015.08.004.
[84] M. Fathi, M. Alami-milani, M. H. Geranmayeh, J. Barar, H. Erfan-niya, and Y. Omidi, "Dual thermo-and pH-sensitive injectable hydrogels of chitosan/(poly(N-isopropylacrylamide-co-itaconic acid)) for doxorubicin delivery in breast cancer," *Int. J. Biol. Macromol.*, p. #pagerange#, 2019, doi: 10.1016/j.ijbiomac.2019.01.122.
[85] S. A. Agnihotri, N. N. Mallikarjuna, and T. M. Aminabhavi, "Recent advances on chitosan-based micro- and nanoparticles in drug delivery," *J. Control. Release*, vol. 100, no. 1, pp. 5–28, 2004, doi: 10.1016/j.jconrel.2004.08.010.
[86] P. H. Yassue-Cordeiro *et al.*, "Chitosan-based nanocomposites for drug delivery," *Appl.*

Nanocomposite Mater. Drug Deliv., pp. 1–26, 2018, doi: 10.1016/b978-0-12-813741-3.00001-7.

[87] F. Ebru, K. Tuba, and G. Altıncekic, "Investigation of gelatin / chitosan as potential biodegradable polymer films on swelling behavior and methylene blue release kinetics," *Polym. Bull.*, no. 0123456789, 2020, doi: 10.1007/s00289-020-03280-7.

[88] H. Hyun, Y. B. Yoo, S. Y. Kim, H. S. Ko, and H. J. Chun, "Hydrogel-Mediated DOX · HCl / PTX Delivery System for Breast Cancer Therapy".

[89] C. Tsao, F. M. Kievit, K. Wang, A. E. Erickson, and R. G. Ellenbogen, "Chitosan-Based Thermoreversible Hydrogel as an in Vitro Tumor Microenvironment for Testing Breast Cancer Therapies," 2014.

[90] F. Chang, C. Tsao, A. Lin, M. Zhang, and S. L. Levengood, "PEG-Chitosan Hydrogel with Tunable Stiffness for Study of Drug Response of Breast Cancer Cells," 2016, doi: 10.3390/polym8040112.

[91] E. Assaad, M. Maire, and S. Lerouge, "Injectable thermosensitive chitosan hydrogels with controlled gelation kinetics and enhanced mechanical resistance," *Carbohydr. Polym.*, vol. 130, pp. 87–96, 2015, doi: 10.1016/j.carbpol.2015.04.063.

[92] P. S. Chan, J. W. Xian, Q. Li, C. W. Chan, S. S. Y. Leung, and K. K. W. To, "Biodegradable Thermosensitive PLGA-PEG-PLGA Polymer for Non-irritating and Sustained Ophthalmic Drug Delivery," *Am. Assoc. Pharm. Sci.*, pp. 1–13, 2019, doi: 10.1208/s12248-019-0326-x.

[93] M. Yang, S. He, Z. Su, Z. Yang, X. Liang, and Y. Wu, "Thermosensitive injectable chitosan/collagen/β-glycerophosphate composite hydrogels for enhancing wound healing by encapsulating mesenchymal stem cell spheroids," *ACS Omega*, vol. 5, no. 33, pp. 21015–21023, 2020, doi: 10.1021/acsomega.0c02580.

[94] K. D. Roehm and S. V. Madihally, "Bioprinted chitosan-gelatin thermosensitive hydrogels using an inexpensive 3D printer," pp. 0–11, 2011.

[95] Z. Karimi, T. Somayeh, M. Mohsen, and M. Mirian, "Evaluation of thermosensitive chitosan hydrogel containing gefitinib loaded cellulose acetate butyrate nanoparticles in a subcutaneous breast cancer model," *Int. J. Pharm.*, vol. 624, p. 122036, 2022, doi: 10.1016/j.ijpharm.2022.122036.

[96] M. Fathi, M. Alami-Milani, M. H. Geranmayeh, J. Barar, H. Erfan-Niya, and Y. Omidi, "Dual thermo-and pH-sensitive injectable hydrogels of chitosan/(poly(N-isopropylacrylamide-co-itaconic acid)) for doxorubicin delivery in breast cancer," *Int. J. Biol. Macromol.*, vol. 128, pp. 957–964, 2019, doi: 10.1016/j.ijbiomac.2019.01.122.

[97] B. D. M. Santana, J. C. Pieretti, R. N. Gomes, and G. Cerchiaro, "Cytotoxicity towards Breast Cancer Cells of Pluronic F-127 / Hyaluronic Acid Hydrogel Containing Nitric Oxide Donor and Silica Nanoparticles Loaded with Cisplatin," 2022.

[98] D. Rafael *et al.*, "Efficient EFGR mediated siRNA delivery to breast cancer cells by Cetuximab functionalized Pluronic® F127/Gelatin," *Chem. Eng. J.*, vol. 340, pp. 81–93, 2018, doi: 10.1016/j.cej.2017.12.114.

[99] H. Wu *et al.*, "Injectable magnetic supramolecular hydrogel with magnetocaloric liquid-conformal property prevents post-operative recurrence in a breast cancer model," *Acta Biomater.*, vol. 74, pp. 302–311, 2018, doi: 10.1016/j.actbio.2018.04.052.

[100] Y. Qi *et al.*, "Injectable Hexapeptide Hydrogel for Localized Chemotherapy Prevents Breast Cancer Recurrence," *ACS Appl. Mater. Interfaces*, vol. 10, no. 8, pp. 6972–6981, 2018, doi: 10.1021/acsami.7b19258.

[101] R. Li *et al.*, "Injectable and In Situ -Formable Thiolated Chitosan-Coated Liposomal

Hydrogels as Curcumin Carriers for Prevention of *In vivo* Breast Cancer Recurrence," *ACS Appl. Mater. Interfaces*, vol. 12, p. 17936−17948, 2020, doi: 10.1021/acsami.9b21528.
[102] J. Li and D. J. Mooney, "Designing hydrogels for controlled drug delivery," *Nat. Publ. Gr.*, vol. 1, pp. 1–18, 2016, doi: 10.1038/natrevmats.2016.71.
[103] H. Carrêlo, P. I. P. Soares, J. P. Borges, and M. T. Cidade, "Injectable composite systems based on microparticles in hydrogels for bioactive cargo controlled delivery," *Gels*, vol. 7, no. 3, 2021, doi: 10.3390/gels7030147.
[104] M. N. Ravi Kumar, "Nano and microparticles as controlled drug delivery devices.," *J. Pharm. Pharm. Sci.*, vol. 3, no. 2, pp. 234–258, 2000.
[105] G. Murtaza, A. Waseem, Nisar-ur-Rehman, and I. Hussain, "Alginate microparticles for biodelivery: A review," *African J. Pharm. Pharmacol.*, vol. 5, no. 25, pp. 2726–2737, 2011, doi: 10.5897/AJPP11.706.
[106] M. Lengyel, N. Kállai-Szabó, V. Antal, A. J. Laki, and I. Antal, "Microparticles, microspheres, and microcapsules for advanced drug delivery," *Sci. Pharm.*, vol. 87, no. 3, 2019, doi: 10.3390/scipharm87030020.
[107] M. Aliaghaei, H. Mirzadeh, E. Dashtimoghadam, and S. Taranejoo, "Investigation of gelation mechanism of an injectable hydrogel based on chitosan by rheological measurements for a drug delivery application," *Soft Matter*, vol. 8, no. 27, pp. 7128–7137, 2012, doi: 10.1039/c2sm25254f.
[108] L. Liu, Q. Wu, X. Ma, D. Xiong, C. Gong, and Z. Qian, "Colloids and Surfaces B : Biointerfaces Camptothecine encapsulated composite drug delivery system for colorectal peritoneal carcinomatosis therapy : Biodegradable microsphere in thermosensitive hydrogel," *Colloids Surfaces B Biointerfaces*, vol. 106, pp. 93–101, 2013, doi: 10.1016/j.colsurfb.2013.01.047.
[109] Y. Hori, A. M. Winans, and D. J. Irvine, "Modular injectable matrices based on alginate solution / microsphere mixtures that gel in situ and co-deliver immunomodulatory factors," *Acta Biomater.*, vol. 5, no. 4, pp. 969–982, 2009, doi: 10.1016/j.actbio.2008.11.019.
[110] C. Pontremoli *et al.*, "Mesoporous Bioactive Glasses Incorporated into an Injectable Thermosensitive Hydrogel for Sustained Co-Release of Sr 2 + Ions and N - Acetylcysteine," 2022.
[111] J. Feng *et al.*, "Sustained release of bioactive IGF-1 from a silk fibroin microsphere-based injectable alginate hydrogel for the treatment of myocardial infarction," *J. Mater. Chem. B*, vol. 8, pp. 308–315, 2019, doi: 10.1039/c9tb01971e.
[112] F. Zhao *et al.*, "An Injectable Particle-Hydrogel Hybrid System for Glucose-regulatory Insulin Delivery," *Acta Biomater.*, 2017, doi: 10.1016/j.actbio.2017.09.044.
[113] S. Talebian *et al.*, "Self-Healing Hydrogels: The Next Paradigm Shift in Tissue Engineering?," *Adv. Sci.*, vol. 6, no. 16, 2019, doi: 10.1002/advs.201801664.
[114] W. Zhang *et al.*, "Precision-guided long-acting analgesia by hydrogel-immobilized bupivacaine-loaded microsphere," *Theranostics*, vol. 8, no. 12, pp. 3331–3347, 2018, doi: 10.7150/thno.25276.
[115] C. Zhao *et al.*, "Biodegradable Nanofibrous Temperature-Responsive Gelling Microspheres for Heart Regeneration," *Adv. Funct. Mater. 2020,* pp. 1–12, 2020, doi: 10.1002/adfm.202000776.
[116] Z. Wang *et al.*, "Polymerizable Microsphere-Induced High Mechanical Strength of Hydrogel Composed of Acrylamide," *Materials (Basel).*, 2018, doi: 10.3390/ma11060880.

[117] Y. Karamzadeh, A. A. Asl, and S. Rahmani, "PCL microsphere / PEG-based composite hydrogels for sustained release of methadone hydrochloride," *J. Appl. Polym. Sci.*, vol. 48967, pp. 1–11, 2020, doi: 10.1002/app.48967.
[118] M. J. Moura, M. H. Gil, and M. M. Figueiredo, "Cisplatin delivery systems based on different drug encapsulation techniques," *Eur. Polym. J.*, vol. 113, no. September 2018, pp. 357–364, 2019, doi: 10.1016/j.eurpolymj.2019.02.007.
[119] C. G. França *et al.*, "Microporous and Mesoporous Materials Nanoporous silicon microparticles embedded into oxidized hyaluronic acid / adipic acid dihydrazide hydrogel for enhanced controlled drug delivery Carla Giometti Franc a," *Microporous Mesoporous Mater.*, vol. 310, 2021, doi: 10.1016/j.micromeso.2020.110634.
[120] M. Mohammadi, K. Patel, S. P. Alaie, R. B. Shmueli, and C. G. Besirli, "Injectable drug depot engineered to release multiple ophthalmic therapeutic agents with precise time profiles for postoperative treatment following ocular surgery," *Acta Biomater.*, 2018, doi: 10.1016/j.actbio.2018.04.037.
[121] X. Zhang *et al.*, "Doubly crosslinked biodegradable hydrogels based on gellan gum and chitosan for drug delivery and wound dressing," *Int. J. Biol. Macromol.*, vol. 164, pp. 2204–2214, 2020, doi: 10.1016/j.ijbiomac.2020.08.093.
[122] R. Tsaryk *et al.*, "Collagen-low molecular weight hyaluronic acid semi-interpenetrating network loaded with gelatin microspheres for cell and growth factor delivery for nucleus pulposus regeneration," *Acta Biomater.*, 2015, doi: 10.1016/j.actbio.2015.03.041.
[123] J. Yan *et al.*, "Injectable alginate / hydroxyapatite gel scaffold combined with gelatin microspheres for drug delivery and bone tissue engineering," *Mater. Sci. Eng. C*, vol. 63, pp. 274–284, 2016, doi: 10.1016/j.msec.2016.02.071.
[124] Y. B. Ji *et al.*, "Preparation and evaluation of injectable microsphere formulation for longer sustained release of donepezil," *J. Control. Release*, vol. 356, pp. 43–58, 2023, doi: 10.1016/j.jconrel.2023.02.024.
[125] L. Xu, Z. Zhou, Y. Chen, H. Lu, and P. Hu, "Resina Draconis Particles Encapsulated in a Hyaluronic-Acid-Based Hydrogel to Treat Complex Burn Wounds," 2022.
[126] A. Marzaman, Sartini, M. Mudjahid, T. Roska, A. Sam, and A. Permana, "Development of chloramphenicol whey protein-based microparticles incorporated into thermoresponsive in situ hydrogels for improved wound heaaling treatment," *Int. J. Pharm.*, vol. 628, p. 122323, 2022, doi: 10.1016/j.ijpharm.2022.122323.
[127] M. Fan *et al.*, "Covalent and injectable chitosan-chondroitin sulfate hydrogels embedded with chitosan microspheres for drug delivery and tissue engineering," *Mater. Sci. Eng. C*, vol. 71, pp. 67–74, 2017, doi: 10.1016/j.msec.2016.09.068.
[128] E. Pérez-Herrero, P. García-García, J. Gómez-Morales, M. Llabrés, A. Delgado, and C. Évora, "New injectable two-step forming hydrogel for delivery of bioactive substances in tissue regeneration," *Regen. Biomater.*, vol. 6, no. 3, pp. 149–162, 2019, doi: 10.1093/rb/rbz018.
[129] Y. Pan *et al.*, "Covalently injectable chitosan/chondroitin sulfate hydrogel integrated gelatin/heparin microspheres for soft tissue engineering," *Int. J. Polym. Mater. Polym. Biomater.*, vol. 70, no. 3, pp. 149–157, 2021, doi: 10.1080/00914037.2019.1695210.
[130] W. Liu, M. A. Borrell, D. C. Venerus, W. F. Mieler, and J. J. Kang-mieler, "Characterization of Biodegradable Microsphere-Hydrogel Ocular Drug Delivery System for Controlled and Extended Release of Ranibizumab," *Transl. Vis. Sci. Technol.*, vol. 8, 2019, doi: 10.1167/tvst.8.1.12.
[131] J. Yoo and Y. Y. Won, "Phenomenology of the Initial Burst Release of Drugs from PLGA

Microparticles," *ACS Biomater. Sci. Eng.*, vol. 6, no. 11, pp. 6053–6062, 2020, doi: 10.1021/acsbiomaterials.0c01228.
[132] J. Y. Heo *et al.*, "An injectable click-crosslinked hydrogel that prolongs dexamethasone release from dexamethasone-loaded microspheres," *Pharmaceutics*, vol. 11, no. 9, 2019, doi: 10.3390/pharmaceutics11090438.
[133] C. R. Osswald and J. J. Kang-Mieler, "Controlled and Extended In Vitro Release of Bioactive Anti-Vascular Endothelial Growth Factors from a Microsphere-Hydrogel Drug Delivery System," *Curr. Eye Res.*, vol. 41, no. 9, pp. 1216–1222, 2016, doi: 10.3109/02713683.2015.1101140.
[134] A. H. Lourenço *et al.*, "Injectable hybrid system for strontium local delivery promotes bone regeneration in a rat critical- sized defect model," *Sci. Rep.*, pp. 1–15, 2017, doi: 10.1038/s41598-017-04866-4.
[135] Z. Ma, W. Song, Y. He, and H. Li, "A multilayer injectable hydrogel system sequentially delivers bioactive substances for each wound healing stage," *ACS Appl. Mater. Interfaces*, 2020, doi: 10.1021/acsami.0c06360.
[136] Y. Wu *et al.*, "Release of VEGF and BMP9 from injectable alginate based composite hydrogel for treatment of myocardial infarction," *Bioact. Mater.*, vol. 6, no. 2, pp. 520–528, 2021, doi: 10.1016/j.bioactmat.2020.08.031.
[137] X. Zhang *et al.*, "Dual-responsive Nanoparticles Based on Chitosan for Enhanced Breast Cancer Therapy," *Carbohydr. Polym.*, 2019, doi: 10.1016/j.carbpol.2019.05.081.
[138] M. Loepfe *et al.*, "Electrospray-Based Microencapsulation of Epigallocatechin 3-Gallate for Local Delivery into the Intervertebral Disc," *Pharmaceutics*, vol. 11, 2019, doi: 10.3390/pharmaceutics11090435.
[139] Y. Zheng *et al.*, "Injectable Hydrogel − Microsphere Construct with Sequential Degradation for Locally Synergistic Chemotherapy," *ACS Appl. Mater. Interfaces*, 2017, doi: 10.1021/acsami.6b15245.
[140] E. Larrañeta, S. Stewart, M. Ervine, R. Al-Kasasbeh, and R. F. Donnelly, "Hydrogels for Hydrophobic Drug Delivery . Classification , Synthesis and Applications," *J. Funct. Biomater.*, vol. 9, no. 13, 2018, doi: 10.3390/jfb9010013.
[141] R. Li *et al.*, "Injectable and in Situ-Formable Thiolated Chitosan-Coated Liposomal Hydrogels as Curcumin Carriers for Prevention of *In vivo* Breast Cancer Recurrence," *ACS Appl. Mater. Interfaces*, vol. 12, no. 15, pp. 17936–17948, 2020, doi: 10.1021/acsami.9b21528.
[142] D. S. Shaker, M. A. Shaker, A. Klingner, and M. S. Hanafy, "In situ thermosensitive Tamoxifen citrate loaded hydrogels : An effective tool in breast cancer loco-regional therapy," *J. Drug Deliv. Sci. Technol.*, vol. 35, pp. 155–164, 2016, doi: 10.1016/j.jddst.2016.05.007.
[143] P. Davoodi, W. C. Ng, W. C. Yan, M. P. Srinivasan, and C. H. Wang, "Double-walled microparticles-embedded self-cross-linked, injectable, and antibacterial hydrogel for controlled and sustained release of chemotherapeutic agents," *ACS Appl. Mater. Interfaces*, vol. 8, no. 35, pp. 22785–22800, 2016, doi: 10.1021/acsami.6b03041.
[144] Z. Lin *et al.*, "Novel thermo-sensitive hydrogel system with paclitaxel nanocrystals: High drug-loading, sustained drug release and extended local retention guaranteeing better efficacy and lower toxicity," *J. Control. Release*, vol. 174, no. 1, pp. 161–170, 2014, doi: 10.1016/j.jconrel.2013.10.026.
[145] Y. J. Wang *et al.*, "PEG-PCL based micelle hydrogels as oral docetaxel delivery systems for breast cancer therapy," *Biomaterials*, vol. 35, no. 25, pp. 6972–6985, 2014, doi:

10.1016/j.biomaterials.2014.04.099.
[146] D. Yeon *et al.*, "Biomaterials Synergistic anti-tumor activity through combinational intratumoral injection of an in-situ injectable drug depot," *Biomaterials*, vol. 85, pp. 232–245, 2016, doi: 10.1016/j.biomaterials.2016.02.001.
[147] J. Luo *et al.*, "Intraperitoneal administration of biocompatible hyaluronic acid hydrogel containing multi-chemotherapeutic agents for treatment of colorectal peritoneal carcinomatosis," *Int. J. Biol. Macromol.*, vol. 152, pp. 718–726, 2020, doi: 10.1016/j.ijbiomac.2020.02.326.
[148] V. Pawar, V. Borse, R. Thakkar, and R. Srivastava, "Dual-purpose Injectable Doxorubicin Conjugated Alginate Gel Containing Polycaprolactone Microparticles for Anti-Cancer and Anti-Inflammatory Therapy," *Curr Drug Deliv .*, vol. 15, no. 5, pp. 716–726, 2018, doi: 10.2174/1567201814666171013151750.
[149] T. Ozeki, D. Kaneko, K. Hashizawa, Y. Imai, T. Tagami, and H. Okada, "Improvement of survival in C6 rat glioma model by a sustained drug release from localized PLGA microspheres in a thermoreversible hydrogel," *Int. J. Pharm.*, pp. 299–304, 2012, doi: 10.1016/j.ijpharm.2012.02.012.
[150] C. Zhu *et al.*, "Injectable Silk-Vaterite Composite Hydrogels with Tunable Sustained Drug Release Capacity," *ACS Biomater. Sci. Eng.*, vol. 5, no. 12, pp. 6602–6609, 2019, doi: 10.1021/acsbiomaterials.9b01313.
[151] X. Chen *et al.*, "Magnetic and self-healing chitosan-alginate hydrogel encapsulated gelatin microspheres via covalent cross-linking for drug delivery," *Mater. Sci. Eng. C*, vol. 101, no. April 2018, pp. 619–629, 2019, doi: 10.1016/j.msec.2019.04.012.

3. Materials and Methods

This chapter serves as a comprehensive repository detailing all the materials and methods employed throughout the course of the PhD research. Each subsequent chapter will delve into distinct concepts and systems utilized, with the current chapter dedicated to explicating the methodologies employed for their production. Within the scope of this thesis, microparticles crafted from Alginate and Gellan Gum, hydrogels synthesized using Pluronic and Chitosan, and microparticles incorporating Superparamagnetic Iron Oxide Nanoparticles were the principal materials under investigation.

3.1. Materials

For microparticles production, high acyl gellan gum, branded as Phytagel (Molecular weight (Mw): ~1000g/mol), was obtained from Sigma-Aldrich (U.S.A), while the alginic acid sodium salt (Mw: 10000 – 600000 g/mol) was obtained from BioChemica (Panreac Química SLU, Spain) and the methylene blue powder from Alfa Aesar (U.S.A.). Ultrapure water was obtain from Millipore system, Milli-Q from Merck.

To produce the phosphate-buffered saline (PBS) solution with pH 7.4, 4 g of sodium chloride (Mw: 58.44) (NaCl 100%) (J.T. Baker, Avantor U.S.A.), 0.1 g of potassium chloride (Mw: 74.55 g/mol) (KCl ≥99%) (Sigma-Aldrich, U.S.A.), 0.72 g of disodium hydrogen phosphate (Mw: 141.96 g/mol) (Na2HPO4) (Panreac Química SLU, Spain), and 0.12 g of potassium dihydrogen phosphate (Mw: 136.09 g/mol) (KH2PO4) (Panreac Química SLU, Spain) were added to 800 mL of ultrapure water, followed by the addition of 200 mL of ultrapure water after pH adjustment. In the case of PBS with pH 6.5, the quantities were adjusted accordingly: 8 g of NaCl, 0.2 g of KCl, 0.61 g of Na2HPO4, and 0.19 g of KH2PO4. For the preparation of the aqueous solution of 3.5 w/v%, calcium chloride (Mw: 110.99 g/mol) from Carl Roth (Germany) was used.

The hydrogels, Pluronic F-127 (Mw: ~12600 g/mol) and Pluronic F68 (Mw: ~8350 g/mol) were purchased from Sigma Aldrich (USA). Sigma Aldrich also supplied the low molecular weight chitosan (Ch) (Mw: 50,000-190,000 g/mol (based in viscosity)), while Merck (Germany) provided β-glycerophosphate disodium salt pentahydrate (β-GP) (Mw: 306.11 g/mol).

For the Superparamagnetic Iron Oxide Nanoparticles (SPIONs), Iron (III) chloride hexahydrate (Mw: 270.3 g/mol) was sourced from Fluka (Germany), while Iron (II) chloride tetrahydrate (Mw: 198.805 g/mol) was purchased from ThermoFisher (Germany). Ammonia (25%) (Mw: 35.05 g/mol) was purchased from VWR International (USA) and 3-(Triethoxysiliyl)-propylamine (APTES) (Mw: 221.37 g/mol) was purchased from Sigma Aldrich (USA).

3.1.1. GG:Alg Microparticles Production

For the polymeric solutions, alginate and gellan gum aqueous solutions were used (2 w/v%) (with ultrapure water). These two polymers were mixed with determined ratios to obtain the 2 w/v% final solution. To dissolve them, the solutions were blended at 40ºC for 4 hours. To produce the microparticles, the coaxial air-flow technique was used, by a Nisco® Encapsulation Unit – VARJ1 [13] (Figure 3.1) using a needle with an internal diameter of 0.25 mm and an outer diameter of 0.5 mm. With this system, the solution was extruded in small droplets to a 500 mL calcium chloride aqueous solution (3.5 w/v%). The microparticles were maintained within the bath overnight to harden and then filtered and washed with ethanol.

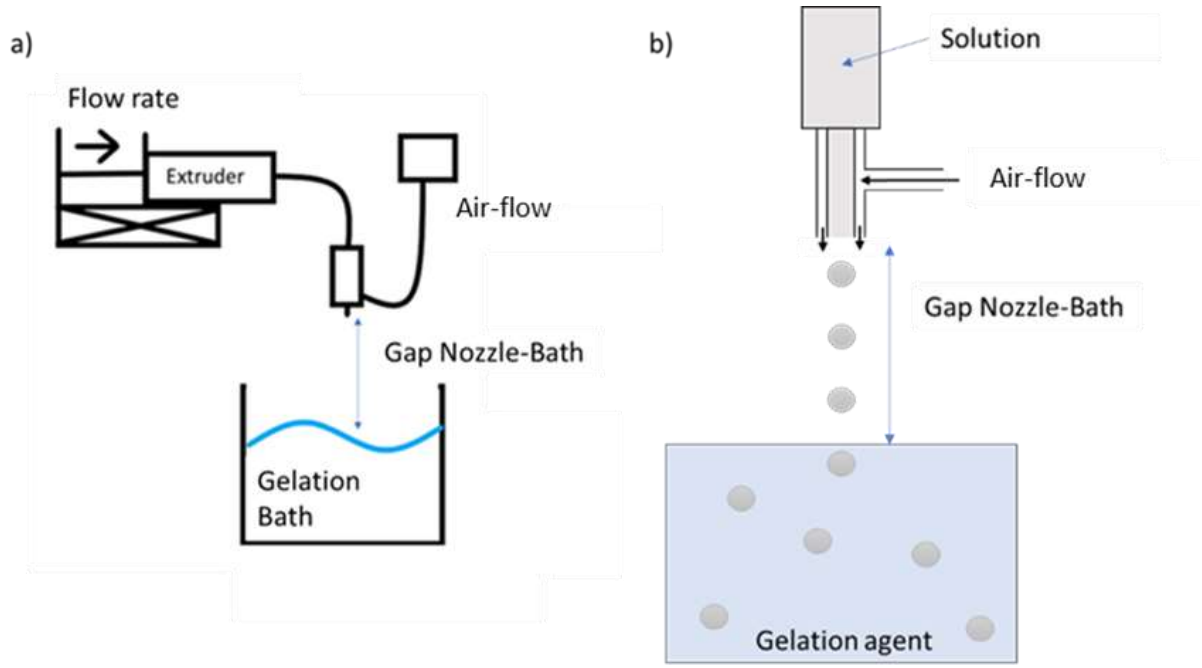

Figure 3.1 (a) General scheme of the coaxial air-flow system, (b) magnification of (a), scheme of microparticle's production near the nozzle, adapted from [13].

3.1.1.1. GG:Alg Microparticles Production optimization

A Design of Experiments (DOE) was used to optimize the microparticle production. A two-level fractional factorial design was used with 4 factors with a degree of fractionation 2 (24-1), with 3 replicas and a design resolution of IV. Design-Expert Software® Version 11 (Stat-Ease Inc., USA) was used to analyse the results. The chosen factors were: A: GG:Alg Ratio within a 2 w/v% aqueous solution; B: Gap bath-nozzle; C: Air-flow; D: Pump flow. Factor C, the air-flow, is the velocity at which the air-flow is expelled, and the pump flow (Factor D) is the flow rate that the extruder has, in order to extrude the solution. Three responses were chosen: the diameter of the microparticles at the wet stage (size) and the Coefficient of Variation (COV) and SPAN, used to evaluate the distribution of particle size (dispersibility). COV is the standard deviation divided by the mean whilst the normalised SPAN is given by (d(0.9)-d(0.1))/d(0.5)), with the d being the percentiles.

The objective was to optimize the coaxial air-flow method to produce microparticles with minimal particle size and dispersibility. The study focused on microparticle production at the wet stage. After the optimization process, the particles were dried. The microparticles were filtered and subjected to a water-ethanol exchange using various ultrapure water and ethanol blend solutions with increasing ethanol concentrations, as follows: 90:10, 75:25, 50:50, 25:75, 10:90, and 0:100 (water (v/v%): ethanol (v/v%)). The microparticles were immersed in each solution for 1 hour, starting from the 90:10 solution, and then dried using a vacuum pump.

3.1.2. GG:Alg microparticles loaded with Methylene Blue (MB)

The microparticles were loaded with MB via absorption of this model drug. PBS solutions with different pH (6.5 and 7.4) were prepared previously, and different batches of both were mixed with different concentrations of MB (10, 30, 60, 100, 140, 250 and 290 µg/mL). Then, 0.02 g of GG:Alg microparticles were added to 5 mL of each batch and left for 4 days in an orbital shaker at 37ºC, to allow the maximum swelling of the microparticles. The concentration of unencapsulated MB in the solution was determined using UV-VIS spectroscopy at its maximum absorbance of 664 nm using a T90+ UV/VIS Spectrometer (PG Instruments Ltd, UK). Calibration curves for MB concentration in PBS at pH 7.4 and pH 6.5 were established to be abs=0.1919conc+0.0559 (R2=0.99) and abs=0.1865conc+0.0578 (R2=0.99), respectively (where abs represent absorbance and conc represents the concentration of MB). The Encapsulation Efficiency (EE%) (Equation 3.1) and Loading Capacity (LC%) (Equation 3.2) were determined using the following equations:

$$EE\ (\%) = \left(\frac{ms_0 - ms_f}{ms_0}\right).100 \qquad \text{Equation 3.1}$$

$$LC(\%) = \frac{m_{encap.MB}}{m_{GG:Alg}}.100 \qquad \text{Equation 3.2}$$

Where ms_0 is the mass of MB in the initial solution, ms_f is the mass after the swelling of the particles, $m_{encap.MB}$ is the mass of encapsulated MB (measuring the MB concentration in the solution after encapsulation) and $m_{GG:Alg}$ the weight of the particles. At least four replicas were used.

3.1.1. SPIONs and SPIAPTS production

Magnetite nanoparticles (mNPs) were produced via a co-precipitation method [1, 2]. Ferrous (F^{2+}) and ferric (Fe^{3+}) chlorides were dissolved in ultrapure water with a concentration of 1 M. The two solutions were mixed, in a round bottom spherical flask with 3 necks, with vigorous agitation (600 rpm), with a molar ratio of 1:2 (Fe^{2+}:Fe^{3+}) and diluted with 100 ml of deionized water with deaeration of O_2 with bubbling N_2. Afterwards, 10 mL of ammonia was added and kept for 5 minutes. With the introduction of ammonia, the colour changed from orange to black. The reaction was stopped by adding 60 mL of ultrapure water. To disperse

the nanoparticles suspensions, they were sonicated. Afterwards, the SPIONs were washed by magnetic separation 5 times with ultrapure water.

SPIONs that were to be coated with APTES followed a previously described method [3, 4]. An APTES solution was prepared (20 mL; 20 v/v%), and added to the SPIONs suspension together with 60 mL of glycerol. The mixture was mixed for 2 hours with rotational mixing (500rpm) at 90ºC for 2 hours. Afterwards, the suspension was washed five times similarly to SPIONs protocol. For the rest of the study, SPIONs coated with APTES will be denominated as SPIAPTs (SPIONs/APTES). Also, mNPs refer to both types of nanoparticles used in this thesis.

3.1.2. GG:Alg microparticles with mNPs

The combination of the microparticles with SPIONs was done via adsorption [5]. Freeze-dried GG:Alg microparticles were submerged in mNPs suspensions with different concentrations (1, 2.5 and 5 mg/mL). The microparticles were submerged into the suspensions and left for 4 days (allowing the maximum swelling of the microparticles) at 37ºC in an orbital shaker. Afterwards, the microparticles were washed with distilled water and freeze-dried. Then they were sieved to separate the microparticles from possible mNPs aggregates.

To determine the Absorption Efficiency (AE%) and Absorption Capacity (AC%), 0.02 g of GG:Alg microparticles were added to 5 mL of mNPs suspensions with different concentrations (1, 2.5, and 5 mg/mL) (Equations 3.3 and 3.4). After 4 days, the concentration of free SPIONs in the suspension was measured using the 1,10-phenanthroline method [6, 7], and the maximum absorbance at 510 nm was recorded using a T90+ UV/VIS Spectrometer (PG Instruments Ltd, UK). The calibration curves for determining the SPIONs concentration were calculated using the equation abs=4.5079$conc$+0.0753 (R^2=0.99), where abs represent the absorbance and $conc$ represents the concentration of iron (mg/mL).

$$AE\ (\%) = \left(\frac{msn_0 - msn_f}{msn_0}\right).100 \qquad \text{Equation 3.3}$$

$$AC(\%) = \frac{m_{mNPs}}{m_{GG:Alg}}.100 \qquad \text{Equation 3.4}$$

Where msn_0 is the mass of nanoparticles in the initial suspension, msn_f is the mass of nanoparticles in suspension, after the swelling of the particles, m_{mNPs} is the mass of adsorbed nanoparticles, and $m_{GG:Alg}$ is the weight of the particles. Four replicas were used.

3.1.2.1. Microparticles/SPIONs/SPIAPTS characterization

The microparticles morphology was analysed using an S9 Stereo Optical Microscope (Leica®, Germany), an SEM Tabletop microscope TM3030 Plus (Hitachi®, Japan) and an Olympus BX51 microscope (Olympus®, Japan) equipped with an Olympus DP73 CCD camera. Optical microscope images were acquired with the Stream Basic v.1.9 Olympus software, and a halogen lamp (KL 2500 LCD, SCHOTT) was used to provide cold illumination. All the images obtained were automatically scaled by the software. Samples for SEM were previously freeze

dried and then coated with iridium. The particles' size at the wet stage and dried was determined using the Leica S9 Stereo Microscope and measured using Image J software. A minimum of 100 diameters were measured for each run of the DOE.

Regarding pristine SPIONs and SPIAPTs, Dynamic Light Scattering (DLS) measurements, an SZ-100 nanoparticle series instrument (Japan) was used with a 532 nm laser and a Peltier system (25ºC). The mNPs suspensions (0.05 mg/mL) were diluted in ultrapure water and measured 3 times using a disposable cell with a scattering angle of 90º. Using cumulants statistics, the hydrodynamic diameter and polydispersity of the mNPs were determined. Additionally, the zeta potential and average values were also determined. Transmission Electron Microscopy (TEM) images were obtained using a Hitachi H-8100 thermionic emission LaB (Japan). Samples for TEM analysis were prepared in suspensions in ultrapure water with 5 mg/mL.

Thermal gravimetric analyses (TGA) were carried out using a TGA-DSC – STA 449 F3 Jupiter equipment from Netzsch (Germany) under a nitrogen atmosphere with a heating rate of 10 ºC/min in a temperature range of 25-800ºC. The samples were prepared by vacuum drying them and weighing 50 mg each sample.

Fourier transform infrared (FTIR) analyses of the microparticles with and without nanoparticles were performed using a Perkin-Elmer – Spectrum Two (USA) instrument equipped with an attenuated total reflection cell (ATR) in the range of 4000-500 cm^{-1}. For the GG:Alg microparticles, with and without MB or nanoparticles, the samples were all vacuum dried. The chitosan hydrogels were analysed in their swollen state and after being freeze-dried (Zirbus VaCo 2 (Zirbus, Germany)).

Powder X-ray diffraction (DRX) was performed using a D81 90 powder diffractometer (Malvern Pananalytical, Spain), with X-rays at 40 kV and 30 mA impacting the samples at a pitched angle of 0.015º for a passing time of 0.1s. All samples were previously vacuum dried before the test.

3.5. Hydrogels preparation and the Microparticle-Hydrogel system

Two thermoresponsive hydrogels were used in this work: a Pluronic gel system and a chitosan/β-glycerophosphate system (Ch/β-GP).

3.5.1. Pluronic hydrogels

Two types of Pluronic were used: Pluronic F127 and Pluronic F68. These two differ in the ratio of PEO and PPO, and their mixture can be used to regulate the transition temperature [8, 9]. The Pluronic system was prepared in an aqueous solution (with ultrapure water) with always 20 w/w%. Different ratios of F127 and F68 were studied (F127:F68 – 14:6; 15:5; 16:4;

17:3; 18:2 and 20:0). After their mixing within ultrapure water, they were stored at 4ºC for the Pluronic to dissolve and maintain the system at the sol state.

The addition of the microparticles was done by adding the microparticles in gel at the sol state (in solution) and then manually mixing, preparing a homogenously dispersed solution with the particles. Different microparticle concentrations were added and studied: 2%, 5%, 10% and 15% (w/v%).

3.5.2. Ch/β-GP hydrogels

Chitosan solutions with a concentration of 3 w/v% were prepared in aqueous solutions of acetic acid (0.05 M) and stored at 10ºC. Meanwhile, solutions of β-GP with different concentrations (0, 2, 3, 4, and 5 w/v%) were prepared by mixing acetic acid solutions (0.05 M) (1.66 mL) with varying amounts of β-GP (Table 3.1), which were also refrigerated at 10ºC. Next, the β-GP solutions were added dropwise to the chitosan solutions with magnetic stirring at 10ºC, and the resulting solutions were left to mix for 1 hour at the same temperature. The final solutions had a chitosan concentration of 2.25 w/v% and different concentrations of β-GP (Table 3.1). After the 1-hour mixing period, microparticles with concentrations of 2 and 5 w/v% were added to the solution and mixed at 10ºC before analysis.

Table 3.1 Concentrations of chitosan, β -GP and GG:Alg microparticles within the microparticles/hydrogel system

Batch Ch/β-GP	[Ch] (w/v%)	[β-GP] (w/v%)	[microparticles] (w/v%)
Ch/β-GP 0%	2.25	0	0
Ch/β-GP 2%		2	
Ch/β-GP 3%		3	
Ch/β-GP 4%		4	
Ch/β-GP 5%		5	
Ch/β-GP/GG:Alg 2%		4	2
Ch/β-GP/GG:Alg 5%			5

3.5.3. Degradation tests

Different methods were used to understand the way the systems degraded with time. For microparticles with and without mNPs, the degradation was done by submerging the microparticles in PBS solutions with pH 6.5 and pH 7.4. Different batches were collected at different times when the microparticles were filtered, rinsed with water and freeze-dried. Then the mass loss was determined following the next equation:

$$mass\ loss\ (\%) = \left(\frac{m_0 - m_{td}}{m_0}\right).100$$ Equation 3.5

Where m_0 is the initial mass and m_{td} is the registered mass at the different times.

The Pluronic system stability was evaluated to understand how it behaved at different pH and if it retained the gel state in aqueous solutions. Pluronic solutions (F127:F68 17:3) were introduced in dialysis membranes. Then these were kept at 37ºC until the Pluronic was at the gel state. Then these membranes were submerged in 50 mL PBS solutions (pH 7.4 and 6.5) at 37ºC. At different times (1, 3, 6 and 24 h) the recipients were taken out of PBS and their content was analyzed via rheology, using frequency sweeps. Four replicas were used. Also, Pluronic degradation was done with mass loss. With at least 5 replicas, Pluronic solutions (4 mL) (F127:F68 17:3) were introduced to falcons (50 mL), and then the temperature increased to 37ºC to allow the solutions to turn gel. Then 15 mL of PBS solutions (pH 6.5 and 7.4 (at 37ºC)) were introduced to the falcons. These were stored at 37ºC with orbital agitation. At different times (1, 2, 3, 4, 6, 24 and 48 h) the PBS was removed and the gels dried and the mass variation was done.

3.5.4. Rheological characterization

An Anton Paar MCR 501 rheometer with a plate/plate geometry of 50 mm diameter (PP50) with a gap of 3 mm for Pluronic solutions and a geometry of 25 mm diameter (PP25) with a 1 mm gap for the GG:Alg solutions. For the chitosan hydrogels, an AR 2000 rheometer from *TA Instruments* (New Castle, USA) was used with a PP of 40 mm and a gap of 2 mm. These gaps were used in order to conform to the dimensions of the microparticles. Firstly, strain sweep tests (results not shown) were performed to determine the linear viscoelastic range (the zone where elastic (G') and viscous (G'') moduli remain constant) for all materials.

For the GG:Alg solutions, flow curves were performed at ambient temperature. At least 3 replicas were done.

For Pluronic gels, temperature ramps in an oscillatory state were done at a constant frequency (1 Hz) and with a strain of 2% (within the linear viscoelastic region). The temperature ramps had an increased rate of 1ºC/min. Frequency sweeps were carried out at 37ºC with 2% of strain, obtaining G', G'' and the associated complex viscosity (η*). Flow curves were carried out at 21ºC (operating room temperature).

For the chitosan hydrogel, a strain of 1% was chosen in accordance with the linear viscoelastic region. An oscillation procedure was done to understand the variation of the moduli with time at different temperatures. Three different temperatures were evaluated: 10°C (for 10 minutes), which is the production temperature, 20°C (for 30 minutes), which is the operating room temperature, and 37°C (for 1 hour and 30 minutes), which is the body temperature. This was done to understand the effect of time and temperature on the transition of chitosan with β-GP to the gel state. The 20°C temperature was studied to assess the behaviour of the hydrogel before injection. Flow curves were done at 10°C and 20°C, ranging

from 0.1 s^{-1} to 100 s^{-1}, to analyse the injectability of the system. Frequency sweeps were conducted at 10°C, 20°C, and 37°C, with a strain of 1%. At 37°C, frequency sweeps were performed at different time intervals to assess the behaviour of the hydrogel over time (0, 1, 2, and 5 h).

3.6. Release profiles

For drug release profiles, the production method that enables the highest loading of MB was used. For microparticles alone, batches with 0.025 g of MB loaded microparticles were loaded within a donor-recipient made of the permeable membrane. This was then loaded in 50 mL of PBS solutions with pH of 7.4 and 6.5. The system was kept within an orbital shaker at 37ºC. At regular intervals of time, 2 mL of PBS were extracted and replaced with fresh PBS. Then the concentration of MB was analyzed to understand the release profiles.

For microparticles within Pluronic solutions, a similar method was used, but 0.02 g of microparticles loaded with MB were mixed in Pluronic solutions (with an F127:F68 ratio of 17 w/w%:3 w/w%) and then introduced in a donor-recipient made of the permeable membrane. The concentration of microparticles within the Pluronic solution was 2 and 5 w/v%. The membranes were then immersed in 10 mL of PBS solutions (previously heated at 37ºC) and put in an orbital shaker at 37ºC. The concentration of released MB was retrieved at different intervals of time.

With microparticles with SPIONs that were mixed with Pluronic, a similar procedure was used. However, the microparticles loaded were divided with a ratio of 1:1 (50% of microparticles loaded with MB and 50% of microparticles loaded with SPIONs or SPIAPTEs (1:1 ratio)). In this case, the concentration of microparticles within the Pluronic solution was 2 w/v% (1 w/v% MB loaded GG:Alg and 1 w/v% mNPs loaded GG:Alg).

Pluronic hydrogels loaded with MB without microparticles were also studied to understand their release profile. To produce these hydrogels, MB with similar quantities to the ones within the microparticles were mixed in the sol phase of the Pluronic hydrogels (ratio of 17:3). Then the solutions were put in similar permeable membranes and then placed within PBS solutions with pH 6.5 and 7.4 at 37ºC.

Regarding the release profiles using the chitosan/beta-glycerophosphate, 0.02 g of MB-loaded microparticles were mixed in the Ch/4%β-GP solution at 10ºC, with a 2 w/v% of MB loaded microparticle concentration in the solution. Then the system was introduced in the recipient made from the permeable membrane. The recipient was then immersed in 20 mL of PBS with pH of 7.4 and 6.5. Batches with and without the hydrogel were done to understand the release profile of the MB-loaded microparticles.

In all MB release profiles, at least five replicas were performed.

3.6.1. Mathematical fittings of the release profiles.

To fit a mathematical model, three models were selected: the Korsmeyer-Peppas (KP), Weibull (W), and Peppas-Sahlin (PS) models [10–12].

In the KP model (Equation 3.6), Q_t represents the concentration of the drug released at each time point (t). The constant k is associated with the structural and geometric properties of the system, while n is linked to the mechanism of drug release. For particles shaped as spheres, Fickian diffusion occurs if $n \leq 0.43$. This type of release is mainly controlled by the diffusion of the drug molecules to the release medium. Case II transport, occurs when $n = 0.85$, where the swelling and relaxation of the system mainly control the release [10]. Swelling controlled releases are associated with more glassy polymers [11]. Anomalous transport, a mix of the previous two, occurs between the previous two ($n \in]0.43, 0.85[$). With $n > 0.85$ a Super case II transport occurs. With this last one, the release is affected by the mobility of the polymeric chains and by erosion [10, 12]. A modified KP model (KP T_{lag}) (Equation 3.7), is more suited for swellable systems [13, 14] where the lag time prior to drug release (T_{lag}) [15] at the beginning of the release is accounted for. This lag times is the interval for the drug to diffuse/dissolve before their release, and it can be affected by the swelling of the polymeric matrixes, due to the increase of the diffusion pathways, decrease the drug concentration gradients [13, 14].

$$Q_t = kt^n \quad \text{Equation 3.6}$$

$$Q_t = k\left(t - T_{lag}\right)^n \quad \text{Equation 3.7}$$

With the Weibull model [12, 15] (Equation 3.8), a is a time scale parameter of the process, and b is a shape parameter of the release, that can be correlated to the release mechanism: Fickian diffusion with $b \leq 0.75$, a complex mechanism if $b > 1$ and a combination of the former two with $b \in]0.75,1[$.

$$Q_t = 100\left(1 - e^{-tb/a}\right) \quad \text{Equation 3.8}$$

Peppas-Sahlin model (PS) (Equation 3.9) uses two constants that correlate with the contribution of Fickian diffusion (k_1) and the contribution of case II transport (k_2) [16]. The exponent m correlates with the KP model and can be associated with the release profile just like n in the KP model [17]. A variation of the PS model (PS T_{lag}) was also studied (Equation 10), that like the KP T_{lag}, model, also accounts for T_{lag}. Table 3 presents the models' parameters and adjusted R^2 (R^2_{adj}) given by the DDSolver program.

$$Q_t = k_1 t^m + k_2 t^{2m} \quad \text{Equation 3.9}$$

$$Q_t = k_1 (t - T_{lag})^m + k_2 (t - T_{lag})^{2m} \quad \text{Equation 3.10}$$

The mathematical models were chosen to fit the data obtained from the experimental data set. These models were selected based on their ability to capture the release behavior of the

drug over time. The KP model is often used to describe the release of drugs from polymeric systems, while the Weibull model is commonly used to model the release of drugs from complex systems. The PS model is often used to describe the release of drugs from systems with a complex release mechanism. By fitting the experimental data to these models, it was possible to gain insight into the release mechanism of the drug from the system under study. The adjustments were done by the Excel (Microsoft, USA) add on DDSolver [14, 15] .

3.7. Magnetic Hyperthermia

Magnetic hyperthermia tests were conducted using a nanoScale Biomagnetics device from the D5 series, operating at a frequency of 388.5 kHz and a field intensity of 300 Gauss for 10 minutes. Each test was performed with three replicates, and all samples contained an equal amount of SPIONs. The analysis included aqueous suspensions of pristine SPIONs at a concentration of 5 mg/mL, aqueous suspensions of SPIONs-APTES at a concentration of 5 mg/mL, microparticles loaded with mNPs, and the same particles within a Pluronic hydrogel (17:3) in its gel state. The specific absorption rate (SAR) indicates the heating efficiency of the magnetic nanoparticles through energy absorption with the application of an alternating magnetic field [18] (Equation 3.11).

$$SAR\ (W/g)\ = \frac{C_{NP}.m_{Fe}+C_l.m_l}{m_{Fe}}.\left(\frac{dT}{dt}\right)_{max} \qquad \text{Equation 3.11}$$

$(dT/dt)_{max}$ is the maximum derivative of the temperature ramp, C_{NP} is the specific heat of Fe_3O_4, C_l is of the liquid, m_{Fe} is the iron mass and m_l of the liquid.

3.8. Cytotoxicity

3.8.1. Microparticles with and without SPIONs/SPIAPTS

Cytotoxicity tests of the microparticles with and without SPIONs/SPIAPTS were performed according to ISO-10993 standard "Biological evaluation of medical devices, Part 5: Tests for in vitro cytotoxicity". The extract method was used with a Vero cell line provided by the American Type Culture Collection (ATCC CCL-81)). The extract was produced using a concentration of 5 mg/mL. Each sample was placed in 1 mL of complete culture medium, DMEM (Dulbecco's modified Eagle's medium with 1.0 g/L glucose, stable glutamine and sodium pyruvate, Biowest #L0066) supplemented with penicillin (100 U/mL), streptomycin (100 µg/mL) (Invitrogen, #15140122) and 10% FBS (Fetal Bovine Serum, S. America origin, Biowest, #S1810), at 37 °C for 48h. The Vero cells were seeded in 96 well plates at a density of 30 000 cells/cm^2. After 24h, the medium was replaced by the extract and their dilutions (2.5 mg/mL and 1 mg/mL). A negative control corresponded to cells fed with a complete cell culture medium, and a positive control corresponded to cells cultured in a cytotoxic environment caused by the supplementation of the culture medium with 10% dimethyl sulfoxide (DMSO)

were also defined. After 48 h of incubation, the medium was removed from each well and replaced with a resazurin solution containing 50% of the complete medium and 50% of a 0.04 mg/mL resazurin solution in PBS. After 3 hours of incubation at 37 ºC and 5% of CO_2, the absorbance was measured at 570 and 600 nm. Cell viability is given as a percentage of viable cells in the samples to test relative to the negative control.

3.8.2. Pluronic and Ch/β-GP systems

The cytotoxicity tests with the hydrogels were also carried out according to ISO-10993 standard "Biological evaluation of medical devices, Part 5: Tests for in vitro cytotoxicity". The tests were made using the direct contact and the extract method and Vero cell line provided by the American Type Culture Collection (ATCC CCL-81). The cells were cultured in complete culture medium: DMEM (Dulbecco's modified Eagle's medium with 1.0 g/L glucose, stable glutamine and sodium pyruvate, Biowest #L0066) supplemented with penicillin (100 U/mL), streptomycin (100 µg/mL) (Invitrogen, #15140122) and 10% FBS (Fetal Bovine Serum, S. America origin, Biowest, #S1810). The tests were carried out in hydrogels with different concentrations of Pluronic (20, 15, 10, 7.5, 5 and 2.5%) in aqueous solutions and chitosan solutions with different concentrations of β-GP (2, 4 and 5 w/v%). Both systems were analyzed with and without GG:Alg microparticles. Also, Pluronic gels of F127 and F68 were studied separately (concentrations: 20, 15 ,10, 5 and 3 w/v%). For extract preparation, the samples were weighted and sterilized under UV light for 120 min, immersed in complete culture medium (50 mg per mL of medium) and incubated at 37 ºC for 48 h while for direct contact the samples were cut with an area of 0.8 cm^2 and were also sterilized under UV light for 120 min. Vero cells were seeded at a density of 30×10^3 cells/cm^2 in 96 well plates and in 24 well plates for the extract and the direct method, respectively, and incubated for 24 h at 37 ºC and 5% CO_2. After that period, the culture medium was replaced by the extracts and their dilutions in the extract method while in the direct contact, the samples were placed directly over the cells. The negative control was defined as cells fed with a complete cell culture medium, and the positive control corresponded to cells cultured in a cytotoxic environment caused by the supplementation of the culture medium with 10% dimethyl sulfoxide (DMSO). After 48 h, the colorimetric assay based on resazurin and its reduction to resorufin by metabolic active cells was used to determine the viability of the living cells. As the absorption peak of resazurin shifts from 600 nm to 570 nm upon reduction, absorbance measurements allow quantifying the number of active cells relative to the negative cell control, and consequently the assessment of the cytotoxicity of the material being studied. The medium was removed from each well and replaced with a resazurin solution containing 50 % of the complete medium and 50 % of a 0.04 mg/mL resazurin solution in PBS. After 3 hours of incubation at 37 ºC and 5 % CO_2, the absorbance was measured at 570 and 600 nm. The results are expressed as the average of the corrected absorbance normalized to the negative control ± the combined standard uncertainty. For Pluronic systems, Pluronic alone, and Pluronic with microparticles were studied using the direct contact method, as described earlier, by preparing the gel with DMEM.

Different concentrations of Pluronic solutions (with DMEM) were used (20, 15, 10, 7.5, 5 and 2.5 v/v%). After 48h in contact with the samples, a colorimetric viability assay was performed to determine cell viability. The microparticles were previously sterilized under UV light (254 nm) for 30 min.

3.9. References

1. Soares PIP, Alves AMR, Pereira LCJ, et al (2014) Effects of surfactants on the magnetic properties of iron oxide colloids. J Colloid Interface Sci 419:46–51. https://doi.org/10.1016/j.jcis.2013.12.045
2. Soares PIP, Laia CAT, Carvalho A, et al (2016) Iron oxide nanoparticles stabilized with a bilayer of oleic acid for magnetic hyperthermia and MRI applications. Appl Surf Sci 383:240–247. https://doi.org/10.1016/j.apsusc.2016.04.181
3. Villa S, Riani P, Locardi F, Canepa F (2016) Functionalization of Fe3O4 NPs by silanization: Use of amine (APTES) and thiol (MPTMS) silanes and their physical characterization. Materials (Basel) 9:. https://doi.org/10.3390/ma9100826
4. Liu Y, Li Y, Li XM, He T (2013) Kinetics of (3-aminopropyl)triethoxylsilane (aptes) silanization of superparamagnetic iron oxide nanoparticles. Langmuir 29:15275–15282. https://doi.org/10.1021/la403269u
5. Matos RJR, Chaparro CIP, Silva JC, et al (2018) Electrospun composite cellulose acetate/iron oxide nanoparticles non-woven membranes for magnetic hyperthermia applications. Carbohydr Polym 198:9–16. https://doi.org/10.1016/j.carbpol.2018.06.048
6. Soares PIP, Machado D, Laia C, et al (2016) Thermal and magnetic properties of chitosan-iron oxide nanoparticles. Carbohydr Polym 149:382–390. https://doi.org/10.1016/j.carbpol.2016.04.123
7. Soares PIP, Sousa AI, Ferreira IMM, et al (2016) Towards the development of multifunctional chitosan-based iron oxide nanoparticles: Optimization and modelling of doxorubicin release. Carbohydr Polym 153:212–221. https://doi.org/10.1016/j.carbpol.2016.07.109
8. Zhang M, Djabourov M, Bourgaux C, Bouchemal K (2013) Nanostructured fluids from pluronic® mixtures. Int J Pharm 454:599–610. https://doi.org/10.1016/j.ijpharm.2013.01.043
9. Rio LG, Diaz-rodriguez P, Landin M (2020) New tools to design smart thermosensitive hydrogels for protein rectal delivery in IBD. Mater Sci Eng C 106:110252. https://doi.org/10.1016/j.msec.2019.110252
10. Prezotti FG, Cury BSF, Evangelista RC (2014) Mucoadhesive beads of gellan gum/pectin intended to controlled delivery of drugs. Carbohydr Polym 113:286–295. https://doi.org/10.1016/j.carbpol.2014.07.021
11. Bruschi ML (2015) Strategies to Modify the Drug Release from Pharmaceutical Systems Related titles. Elsevier, Cambridge

12. Costa P, Lobo JMS (2001) Modeling and comparision of dissolution profiles. Eur J Pharm Sci 13:123–124

13. Kim H, Fassihi R (1997) Application of binary polymer system in drug release rate modulation. 2. Influence of formulation variables and hydrodynamic conditions on release kinetics. J Pharm Sci 86:323–328. https://doi.org/10.1021/js960307p

14. Zuo J, Gao Y, Bou-Chacra N, Löbenberg R (2014) Evaluation of the DDSolver software applications. Biomed Res Int 2014:. https://doi.org/10.1155/2014/204925

15. Zhang Y, Huo M, Zhou J, et al (2010) DDSolver: An add-in program for modeling and comparison of drug dissolution profiles. AAPS J 12:263–271. https://doi.org/10.1208/s12248-010-9185-1

16. Arifin DY, Lee LY, Wang CH (2006) Mathematical modeling and simulation of drug release from microspheres: Implications to drug delivery systems. Adv Drug Deliv Rev 58:1274–1325. https://doi.org/10.1016/j.addr.2006.09.007

17. Peppas NA, Sahlin JJ (1989) A simple equation for the description of solute release. III. Coupling of diffusion and relaxation. Int J Pharm 57:169–172. https://doi.org/10.1016/0378-5173(89)90306-2

18. Gonçalves A, Almeida F V., Borges JP, Soares PIP (2021) Incorporation of dual-stimuli responsive microgels in nanofibrous membranes for cancer treatment by magnetic hyperthermia. Gels 7:1–17. https://doi.org/10.3390/GELS7010028

4. PRODUCTION, OPTIMIZATION AND CHARACTERIZATION OF MAGNETIC GELLAN GUM/ALGINATE MICROPARTICLES

The following chapter will focus on the development and optimization of microparticles, followed by their characterization *in vitro*. Afterwards the microparticles were loaded with a model drug and their release profile was characterized. Also, magnetic nanoparticles were produced and characterized, and further loaded with the produced microparticles. The obtained composite microparticles were then characterized *in vitro.*

This chapter contains part of the original papers by the author:

Henrique Carrêlo, Maria Teresa Cidade, João Paulo Borges, Paula Soares, "Gellan Gum/Alginate Microparticles as Drug Delivery Vehicles: DOE Production Optimization and Drug Delivery". Pharmaceuticals 2023, 16(7), 1029; https://doi.org/10.3390/ph16071029

H. Carrêlo; A. R. Escoval; M. Jiménez-Rosado; A. Romero; J. P. Borges; P.I.P. Soares; "An injectable thermoresponsive magnetically-sensitive drug microparticles/hydrogel system with superparamagnetic nanoparticles." (2023) (in preparation)

4.1.Introduction

4.1.1. Polymeric microparticles

Polymeric microparticles consist of small particles made from a polymeric structure, that range from 1 to 1000 μm [1, 2]. Microparticles typically have spherical shapes, but their shape can vary (Figure 4.1 (a) to (j)). Microparticles can have irregular shapes (Figure 4.1 (k)), or torus shape (similar to a doughnut format) (Figure 4.1 (l)), bullet shape (Figure 4.1 (m)), a cylindrical shape (Figure 4.1 (n)) or even a cubic form (Figure 4.1 (o)) [2].

The shape and geometry of particles (either micro or nanoparticles) deeply affect their possible use as DDS. For example, their elimination by phagocytosis is dependent on the curvature of particles, with phagocytosis velocity decreasing with a higher curvature angle [3]. Also, in the case of nanoparticles, nanorods have been found to remain for longer periods in the bloodstream than nanospheres [3]. Needle and plate shape nanoparticles present higher cytotoxicity when compared to spherical and rod-shaped nanoparticles. Particles shape can also alter the drug release profile. In 3D-printed tablets with polyvinyl alcohol filaments, Goyanes *et al.* [4] printed different geometries of particles for paracetamol release, maintaining

the same surface area. The spherical and cylinder tablets released at a slower rate than the pyramid, torus, and cube-shaped tablets.

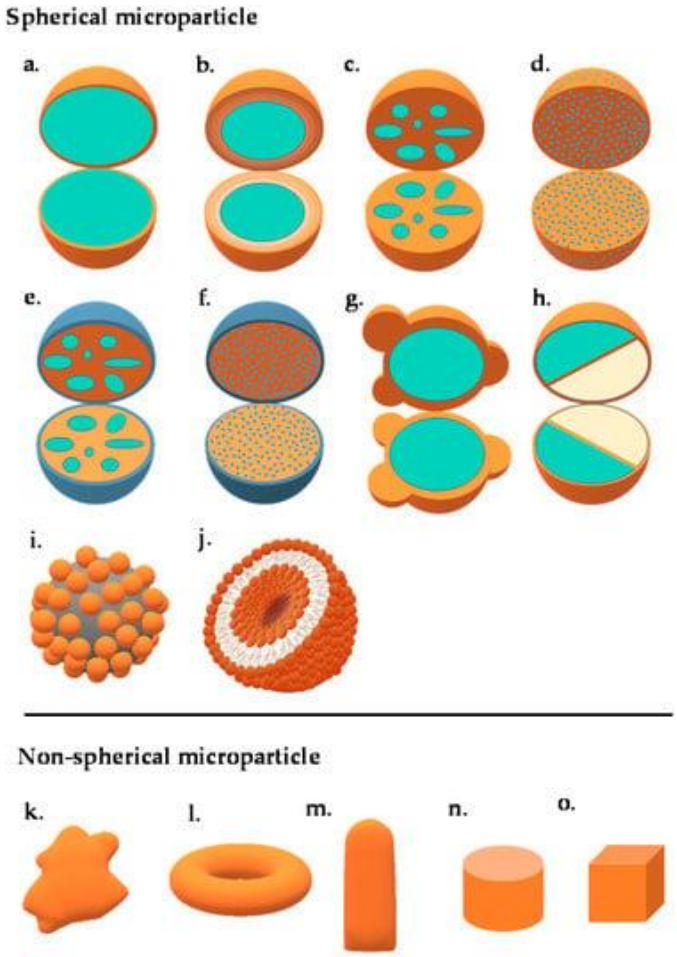

Figure 4.1 Schematic illustration of the different microparticle structures: (**a**) mononuclear/single core/core-shell, (**b**) multi-wall, (**c**) polynuclear/multiple core, (**d**) matrix, (**e**) coated polynuclear core, (**f**) coated matrix particle, (**g**) patchy microparticle, (**h**) dual-compartment microcapsule, (**i**) colloidosome, (**j**) giant liposome, (**k**) irregular-shaped microparticle, (**l**) torus-shaped microparticle, (**m**) bullet-shaped microparticle, (**n**) microtablet, and (**o**) cubic-shaped microparticle. (Adapted with permission from [2]. Copyright (2022) Multidisciplinary Digital Publishing Institute).

4.1.1.1. Internal structure

Spherical microparticles can be classified according to their internal structure into microspheres and microcapsules (Figure 4.2). Microspheres have a continuous matrix, and within this structure, they can have homogenously dispersed cargo (Figure 4.1 (d)). In contrast, microcapsules have a shell layer that surrounds a reservoir core. This core is where the cargo can be stored and the shell serves as a barrier that protects the core from external factors (Figure 4.1 (b)) [2]. Microparticles can also exhibit different types of regions within them [2]. For example, Janus particles are particles that exhibit two or more distinct physical properties. For example, one-half of the particles can be composed of hydrophilic material, and the other one can be made of a hydrophobic one [5]. Also, layers can be added to store different types

of cargo (such as hydrophilic and hydrophobic cargo [6]) or even add more protection to the cargo.

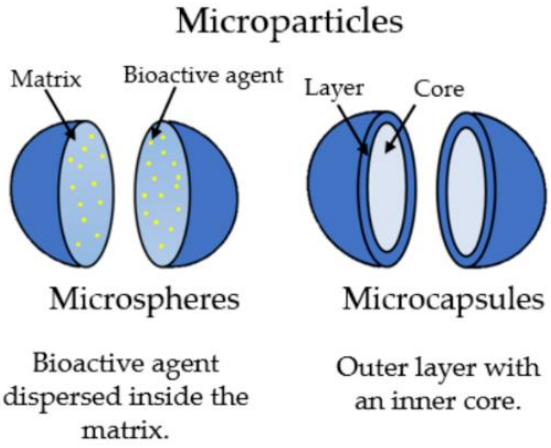

Figure 4.2 Scheme of microspheres and microcapsules internal structure. (Adapted with permission. From [7]. Copyright (2021) Multidisciplinary Digital Publishing Institute).

4.1.1.2. Release profiles

Regarding the release profile, differences in microparticle structure affect how the microparticles will release the cargo. In the case of a microsphere, the release profile depends on the polymeric matrix. Diffusion of drugs and the pores of the matrix will affect the release profile. Additionally, water uptake also influences the drug release profile, since swelling increases the rate of release. Surface erosion will also affect the release profile [2]. On the other hand, in microcapsules the release will depend on the protective shell. The shell might dissolve or erode (shell erosion) and release the cargo, but can also be permeable or semi impermeable allowing for the drug to be released by the osmotic phenomenon [2].

The ideal release profile of a microparticle is to release in a sustained way (in a monophasic release) (Figure 4.3 (a.1)). This is to release cumulatively with time with a constant diffusion rate to the blood circulation (Figure 4.3 (a.2)) [8]. This is important to maintain the drug concentration above a therapeutical threshold concentration, for the therapy to have effect, but below the toxicity threshold, to avoid any toxic side effects. Thus, it would be easier to predict and to tailor the drug release profile for the desired treatment when particles are placed *in vivo.* However, a common occurrence with microparticles is the effect of initial burst release, where a large amount of cargo is released in the early hours of the release [2, 8] (Figure 4.3 (b.1)). This might have negative side effects caused by a high concentration of drug in the blood stream (Figure 4.3 (b.2)). The initial burst release effect can also be delayed after placement of the microparticles in the *in vivo* environment (delayed biphasic) (Figure 4.3 (c.1) and (c.2)), and can also be triphasic, with an early burst release followed by a second one (Figure 4.3 (d.1) and (d.2)) [8]. This process is associated with different factors such as size, porosity, water intake, erosion of the particle (in bulk or at the surface), type of drug/bioactive agent among other factors [8].

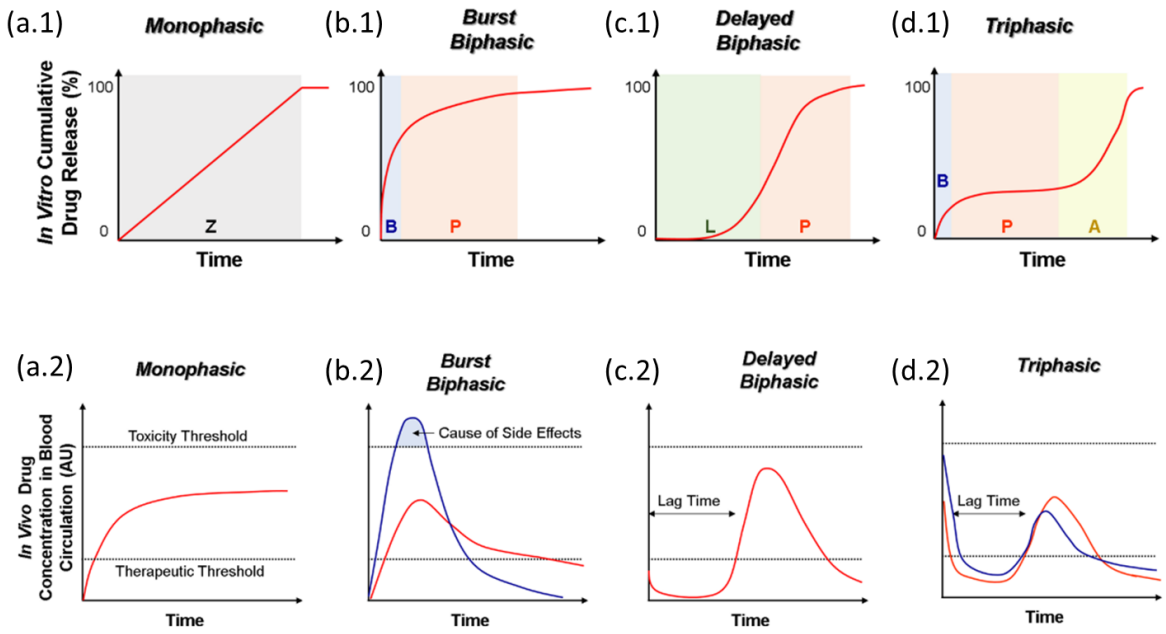

Figure 4.3 (a.1), (b.1), (c.1) and (d.1) Different types of in vitro overall drug release profiles from polymer microparticles systems; (a.2), (b.2), (c.2) and (d.2) Respective time-dependent *in vivo* drug concentration profiles for the respective types of drug release profiles. (Adapted with permission from [8]. Copyright (2020) American Chemical Society).

4.1.1.3. Materials

Microparticles can be made from multiple types of polymers, including synthetic [9, 10] and natural polymers [1, 11]. Natural polymers are derived from natural sources such as in plants, algae, and animals, among others, and are the result of natural processes or biological processes [1, 11]. Based on their structure, natural polymers can be categorized into three classes: polypeptide- and protein-based (such as collagen, fibrin, gelatine); polysaccharide (such as alginate, chitosan, gellan gum) and polynucleotide-based (such as DNA) [12]. Due to their natural origin, they have biofunctional molecules that ensure bioactivity and biomimetic natures, assuring biocompatibility and biodegradation for possible biomedical purposes. However, they also have some disadvantages such as microbial contamination, poor mechanical strength, and uncontrollable rate of degradation [12].

On the other hand, synthetic polymers are man-made materials that are synthesized from monomers using chemical reactions. Examples of synthetic polymers include poly(e-caprolactone) (PCL), polyglycolic acid (PGA), polylactic acid (PLA), and their copolymer poly(glycolic acid) (PLGA) [12]. Synthetic polymers can be designed with specific properties, such as mechanical strength, thermal stability, biocompatibility, and biodegradability. They can be synthesized in large quantities, and their properties can be precisely controlled, allowing them to be tailored for specific applications and can also be more resistant to degradation than natural [12]. However, they lack bio-mimicking properties. For example, for tissue engineering they lack cell adhesion sites, thus requiring further chemical modifications [12]. Also, synthetic polymers have a great environmental impact. The production of these polymers

involves petroleum extraction thus having environmentally damaging processes [13]. Also, their production to determined shapes, such as microparticles or fibres, involves the use of chemical solvents, such as organic solvents, that are associated with health and environmental hazards. For example, PLA is commonly dissolved in chloroform. This is a volatile substance that when inhaled can cause severe health damage such as liver, kidney, and heart diseases. Also, it is an extremely toxic substance to be disposed into the environment [13]. Other solvents used for synthetic polymer manipulation like dichloromethane, toluene and methanol have similar side effects.

Although natural polymers can also be dissolved with organic solvents, due to environmental, health and biomimicking causes, natural polymers serve as an alternative to synthetic polymers for the biomedical industry. With natural polymers it is possible to develop microparticles that can be naturally sourced and produced with an eco-friendly production, developing microparticles that can more easily mimic the human body without resorting to further chemical processes.

4.1.1.4. Alginate and Gellan Gum microparticles

Within the natural polymers, polysaccharides like alginate (Alg) and gellan gum (GG) have been used for biomedical purposes. Alginate is an anionic polysaccharide linear copolymer of β-(1–4) linked d-mannuronic acid and β-(1–4)-linked l-guluronic acid units and is derived from brown seaweeds [14] (Figure 4.4 Chemical structures of (a) alginate and (b) gellan gum (low acyl). (Adapted with permission from [16, 17]. Copyright (2019 and 2015) Elsevier).Figure 4.4 (a)). Gellan gum is also an anionic polysaccharide with a linear structure composed of α-L-rhamnose, β-D-glucuronate and β-D-glucose, and has good mucoadhesive properties [15] (Figure 4.4 (b)).

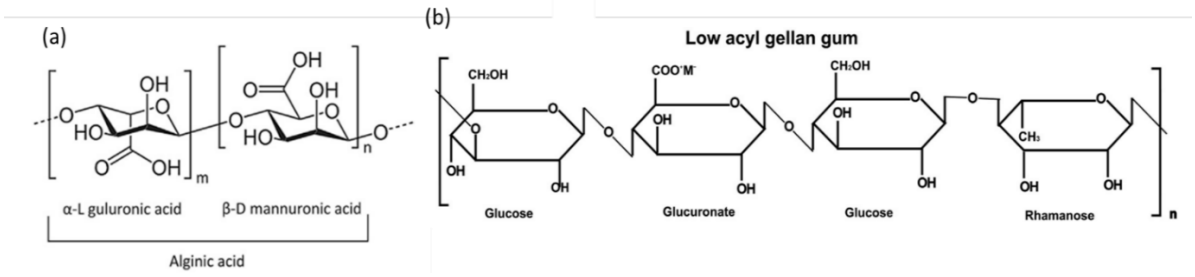

Figure 4.4 Chemical structures of (a) alginate and (b) gellan gum (low acyl). (Adapted with permission from [16, 17]. Copyright (2019 and 2015) Elsevier).

Due to the anionic nature of these polymers, in the presence of ions, especially divalent ions like Ca^{2+}, their chains interact with these ions. These ions serve as a linkage between chains, thus forming a hydrogel. This type of physical crosslinking is called ionic gelation [18]. Both alginate and gellan gum are sensitive to ionic gelation, thus, can be easily used to produce microparticles or microspheres. Alginate and gellan gum hydrogels have been extensively used in the biomedical industry as DDS [14, 19–21], but they are also used in the food industry as gelling agents [22, 23].

Regarding breast cancer and other types of cancer, different microparticle DDS have been made using these polymers. Alginate microspheres have been used as DDS of chemotherapeutic drugs [24–26]. Joseph and Sangeetha [26] developed alginate particles for exemestane release profiles for breast cancer treatments. Xue *et al.* [24] developed magnetically responsive alginate and chitosan microspheres for DOX (Doxorubicin) release, capable of releasing DOX on demand. Román *et al.* [27] developed alginate microcapsules with attached epidermal growth factor on the surface of the microparticles to specifically target non-small lung cancer cells. Also, cisplatin was added as a chemotherapeutic drug to be released. *In vitro* experiments showed a faster mortality rate in H460 lung cancer cell plates using the designed DDS. Other drugs such as 5-FU (5- Fluorouracil) have also been combined with alginate beads for breast cancer treatments [28].

Gellan gum also has been used in the development of DDS for cancer treatment [29]. Zhou *et al.* [29] developed glutathione-gellan gum conjugate hydrogels for DOX release. This composite system had a slower release profile on acidic pH's, ideal for cancerous areas. Also, higher cytotoxicity was found on cancer cells (4T1 cell lines) than on normal epithelial cells in cytotoxicity *in vitro* tests. Hsu *et al.* [30] used gellan gum microspheres to deliver hyaluronic-based nanosized DOX carriers. The system that combined the gellan gum microparticles was prolonged due to the gellan gum's slow degradation rate and good biocompatibility thanks to gellan gum. Also, gellan gum surface has been functionalized with antibodies to stimulate T cells for immunotherapeutic approach [31]. Although not in microparticle form, gellan gum hydrogels have been used in the design of local therapies for breast cancer, for paclitaxel delivery in post-surgery treatment of HER2+breast tumours (human epidermal growth factor receptor 2) [32]. Gellan gum hydrogels were prepared in different solutions (acetate buffer and phosphate buffer solution) and with different L-cysteine concentrations to better adapt to breast cancer areas, such as the high glutathione concentrations that exist in this type of cancer. Swelling rate, pore size and dynamic modulus were dependent on the type of solution and on the used concentration of L-cysteine. In HER2+ breast carcinoma cell lines, the hydrogel proved to have an antiproliferative effect over the tumorous cells.

Microparticles composed of alginate and gellan gum have been used for other biomedical purposes. The blending of two or more polymers is useful since it combines the attributes of each polymer into the blend. The mixture of alginate with gellan gum has been studied for microparticle production. The similarity to the ECM (extracellular matrix) of alginate can be combined with the mucoadhesive properties of gellan gum for example. Farias *et al.* [33] developed microparticles, films and oral tablets of the mixture of these two polymers to form a morin oral DDS. The developed systems were found to have good mucoadhesive properties, with the tablets and films being better than microparticles. However, microparticles revealed a more prolonged release profile in artificial saliva. Jana *et al.* [34] developed alginate and gellan gum microparticles loaded with aceclofenac (anti-inflammatory). The results revealed that the microparticles entrapped the drug with efficiencies ranging from 39.30 ± 1.28% to 98.46 ± 0.40%. The variation of alginate and gellan gum changed the release profile

with a higher concentration of gellan gum changing the release profile from Fickian to anomalous diffusion. Microparticles made from these two polysaccharides have also been used as encapsulators of bacteria such as *Bifidobacterium bifidu*, *Lactobacillus helveticus* and *Lactobacillus delbrueckii* [35]. Also, gellan gum and alginate sponges with antibacterial peptide nisin-loaded stearic acid-based nanoparticles have also been developed for wound treatments [36]. Other studies focused on alginate and gellan gum blends [37, 38]

4.1.2. Methods of microparticle production

When selecting the appropriate production method, it is important to consider various factors including the materials used, the intended application, the microparticle's diameter, the stability of both the drug and particles, as well as the desired release time. Loading the drug onto the carrier can be achieved through encapsulation during the production of the carrier or through diffusion after the carrier has been produced. Regardless of the used method, it is crucial to ensure that the drug's bioactivity is not compromised, and that high loading efficiency, low particle size span, and reproducibility are achieved cost-effectively, avoiding any particle aggregation. Furthermore, it is important to ensure that the degradation and release profiles of the carrier are appropriate for the intended application [39, 40]. Here, some production methods are listed.

4.1.2.1. Extrusion-based methods

Droplet generation through a nozzle followed by its hardening in a bath is a method that has been used in several studies since it can produce millimetric particles and microparticles with excellent production rates and reproducibility [41–43] (Figure 4.5 (a)). The crosslinking can be of chemical or physical nature, as explained in the previous Chapter 2 [44, 45]. The particle diameter can be controlled with the nozzle diameter, viscosity of the fluid, and flow rate but also with the particle detachment.

For a particle to detach from a nozzle, the force dragging the particle to fall must exceed the maximum capillary force [46]. The dragging force can be aided by other forces, such as an air-flow (Figure 4.5 (b)). The addition of a parallel air-flow to the nozzle will add a force that will promote droplet detachment. This technique is called coaxial air-flow [47]. With this additional force, smaller particles can be produced at a faster rate. The same principle can be used with the application of an electric field between the nozzle and the bath (coaxial electrospray) (Figure 4.5 (c)) [48, 49], and also with the vibration of the nozzle (Figure 4.5 (d)) [47]. The jet-cutting technology is a method that uses a mechanical cut of a flow (jet) with cutting wires (Figure 4.5 (d)). It has a high production rate and can be operated in 2 modes. The normal mode, where the drop falls vertically to the bath, and the soft-landing mode, where the drop is projected diagonally to reduce the bead deformation. The latter is adequate for high-scale production [47]. Coaxial electrospray also allows the production of multi-layered particles, using a nozzle with an inner and an outer needle, creating a liquid stream with an inner and an outer phase. The application of an electric field will promote the elongation of

the liquid creating a cone, a Taylor cone. Due to hydrodynamic shears the cone breaks in layered particles that fall to a collector [50–53].

During the fall, spheres might acquire non-spherical shapes. This must be accounted for when defining the nozzle-bath gap, as well as temperature and humidity conditions. The height of the bath must be adequate so that spheres reach the bottom fully crosslinked, avoiding further deformation [46]. Optimization steps are required to adjust the production parameters. Flow rate, nozzle diameter, bath size and height, nozzle-bath gap, viscosity, and crosslinking solution, are some that the previously mentioned methods share, whilst each one has its specific parameters, like in the coaxial air-flow technique the air-flow itself and in coaxial electrospray the electric field.

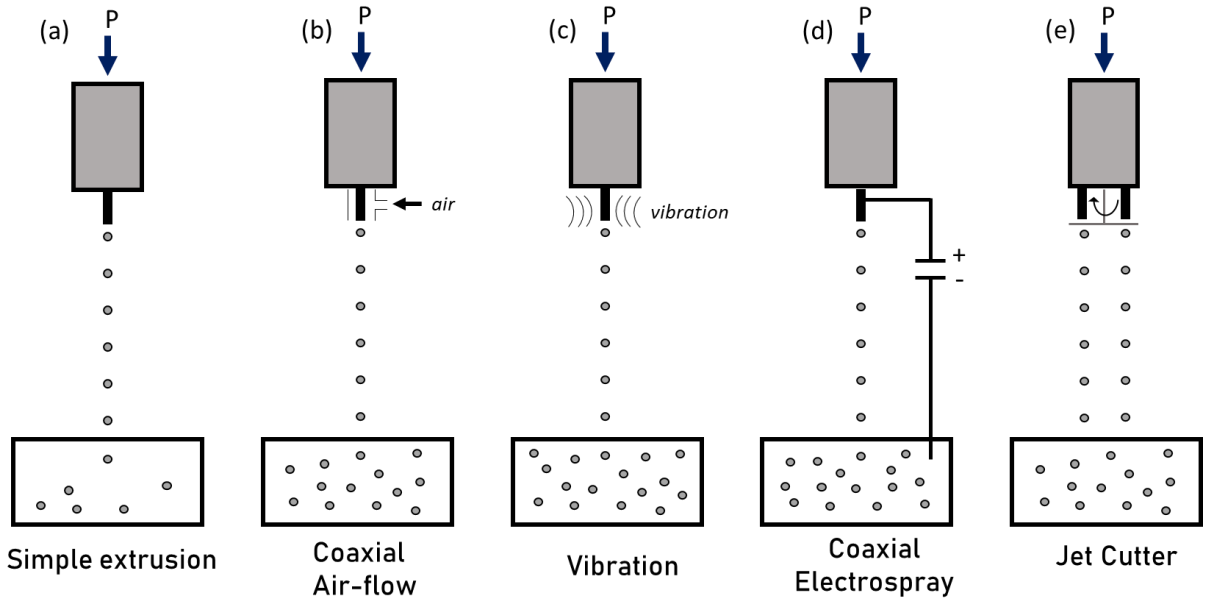

Figure 4.5 Scheme of microparticle production via extrusion techniques: (a) Simple extrusions; (b) Coaxial air-flow; (c) Vibration; (d) Coaxial electrospray; (e) Jet cutter.

4.1.2.2. Emulsion-based methods

Emulsion-based techniques are commonly used to produce polymeric microparticles for drug delivery. In this technique, a water-in-oil (w/o) or oil-in-water (o/w) emulsion is formed with the drug and polymer dissolved or dispersed in the appropriate phase [54, 55]. The emulsion is then subjected to mechanical shear forces that forms a droplet within a matrix solution. Then, the solidification of the droplet to form microparticles containing the drug might occur via chemical or physical crosslinking.

The choice of emulsion type (w/o or o/w) depends on the solubility of the drug and polymer in different phases, as well as the desired release kinetics. For example, hydrophilic drugs are dissolved in water phases, whereas lipophilic drugs must be dissolved in oil phases. However, there are other options like water-in-oil-in-water (w/o/w), that better encapsulates hydrophilic compounds. This double emulsion consists in a first w/o emulsion that is then added to a water bath [6]. There is also water-in-oil-in-oil-in-water (w/o/o/w), which produces

double-walled microspheres that allow better protection and a more prolonged and sustainable release profile [56, 57].

Microparticles made via the emulsion technique have high drug-loading capacity. In addition, the size and shape of microparticles can be controlled by adjusting the emulsion conditions, such as the addition of surfactants, the intensity of the applied shear force, and the viscosity of the components, among other factors [57]. Also, this technique is scalable and might be adapted for large-scale production. However, emulsion stability must be carefully controlled to prevent phase separation, which can result in uneven drug distribution and poor microparticle formation. Additionally, the use of organic solvents in the oil phase can be problematic because it may result in residual solvents in the final product, which can have toxic effects, and many washing steps must be made to remove the totality of the residues [45, 55, 56, 58, 59]. Another option is to use physical crosslinkers instead of chemical ones, to avoid the toxicity associated with the latter ones [52].

4.1.2.3. Microfluidic techniques

Microfluidic techniques allow the formation of discrete polymeric droplets in a continuous phase (Figure 4.6). It is considered a bottom-up approach where the production components are miniaturized to manipulate the flow of fluids [60]. The dispersed phase, such as a polymeric solution, is injected through a microscopic channel into a continuous, immiscible phase. At the intersection of the channel, the droplet will form with the dragging force being higher than the viscous force, and the break-off of the droplet occurs with free surface instabilities, promoted by different effects, such as the flow of the continuous phase [60]. Afterwards, the droplet will be polymerised, for example, using UV radiation (using photosensitive monomers) or thermal procedures [5]. Different geometries can be used in microfluidics, where the most used ones are co-flow, flow-focusing and T-junctions [102]. This technique can create micro and nanoparticles, where flow rates, phase ratios, viscosity, channels and orifices diameters and other factors will be determined. This technique allows the creation of different particles like Janus particles (these combine two or more distinct materials on their surface) [62] and even double emulsions for layered capsules (with a core and a shell) [63, 64].

Microfluidic techniques have the advantage to be able to create reproducible monodispersed particles [66]. Additionally, it allows good control over particle production, regarding size, size distribution, structure, surface properties and precise concentration gradients [62]. The production of biopolymeric lignin particles comparing microfluidics and emulsification techniques showed that microfluidic-produced carriers with higher encapsulation efficiency and narrower size distribution [67]. Proteins have also been encapsulated with microfluidic techniques without denaturation [68]. However, the production rates can be low and expensive due to the complexity of the equipment, and these systems are very prone to channel blockage, stopping the operation [62].

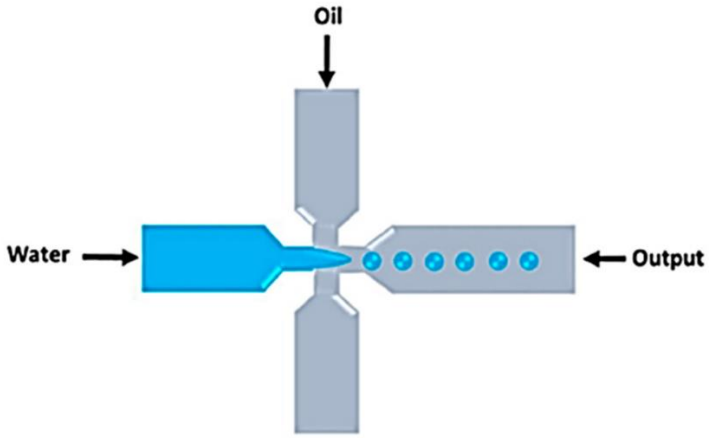

Figure 4.6 Droplet microfluidic system to create immiscible liquid droplets. (Adapted with permission from [65]. Copyright (2020) Multidisciplinary Digital Publishing Institute).

4.1.2.4. Other production methods

The spray drying technique is a continuous technique that allows the encapsulation of hydrophobic and hydrophilic drugs. It consists of spraying a liquid through a nozzle, followed by evaporation of the solvent using a drying gas and collection of the particles in a hot drying medium [69, 70]. Chemotherapeutic drugs can be encapsulated using this technique [71, 72] [73]. A derivative of this technique is the spray-freeze drying technique, where the particles are sprayed, frozen and then sublimated [74], a useful process to create inhalable particles [75, 76].

Another method for microparticle formation is using superhydrophobic surfaces. Aqueous solutions are put on a superhydrophobic surface that will form spherical particles that can be polymerized in a dried condition [77]. Different forms of crosslinking can be done, using either UV lights or atmospheres with a crosslinker, among others [40, 78]. Pectin-coated chitosan microgels have been crosslinked on superhydrophobic surfaces encapsulating 5-FU. Coating the microspheres allowed the prevention of early drug release. The sizes obtained were in the micro-sized range suited for colon cancer treatments [79].

4.1.3. Magnetic microparticles for cancer treatment

As previously stated, microparticles have been used for cancer treatment [24–26, 28, 30], including breast cancer [32]. There are other bioactive agents that can be loaded onto the microparticles to be used for breast cancer treatments. One of these agents is superparamagnetic iron oxide nanoparticles (SPIONs) [80], which are a type of magnetic nanoparticles (mNPs). These nanoparticles can be used for the following reasons [81]:

- Magnetic resonance imaging – SPIONs can be used as contrast agents since they generate a magnetic signal that is detected by the MRI equipment;

- Drug Delivery: SPIONs can be coated with specific drugs/molecules serving as DDS. Also, they can be functionalized with targeting molecules for targeting tissues, such as tumors;
- Magnetic hyperthermia: superparamagnetic nanoparticles can increase temperature when submitted to an alternating magnetic field. The heat stress (between temperatures of 41 to 46ºC) causes the degradation of cellular structures and functions that will cause cell death.

SPIONs are useful for cancer treatment and their combination with microparticles/polymeric matrixes has been used in the past [24, 82, 83]. The combination of drug delivery and magnetic hyperthermia can cause a synergistic effect on cancer treatments. The following part will analyze the production of these mNPs and their conjugation with polymeric microparticles for possible cancer therapies, especially breast cancer.

4.1.3.1. Magnetic Nanoparticles (mNPs)

When SPIONs are exposed to an alternating magnetic field (AMF), their magnetic moments align with the field direction and can rapidly switch back and forth in response to changes in the magnetic field (MF) direction. This results in rapid reorientation of the magnetic moments, generating heat via relaxation losses [84–86] These magnetic relaxations can be described in two regimes: Néel and Brownian relaxations [87]. The amount of heat generated by SPIONs depends on several factors, such as particle size, magnetic moment, magnetic anisotropy, and frequency of the magnetic field. By controlling these parameters, it is possible to achieve selective heating of SPIONs in specific regions of the body, allowing targeted hyperthermia therapy for cancer treatment, as previously stated [88].

Additionally, SPIONs can also be used as contrast agents in MRI, which can be used for the detection of tumors and treatment monitoring, as previously stated. Also, SPIONs tend to accumulate in tumorous areas due to the enhanced permeability and retention effect (EPR). Solid tumors have leaky vasculature and have poor lymphatic drainage, resulting in the accumulation of nanoparticles in the tumor [89]. This allows for better monitoring of tumor progression with MRI, but also for possible treatments via magnetic hyperthermia and drug delivery. Also, functionalization and coating of SPIONs can be done for targeted therapies [86].

4.1.3.2. Synthesis of SPIONs

The synthesis of SPIONs, especially the magnetite nanoparticles, involves the mixing of the Fe^{2+} and Fe^{3+} ions from salts or organic iron precursors. To prevent agglomeration and control particle size, stabilizing agents are also required [90]. A very brief overview of some techniques is here presented. The co-precipitation method [83, 90, 91] (Figure 4.7 (a)) is one of the most conventional methods to produce magnetite SPIONs since it uses non-toxic solvents, has a high yield, and is easily reproducible. The precipitation ferric precipitation and ferrous salts aqueous solutions by adding a base, within an inert atmosphere and temperature below 100ºC. This was the chosen method for this study. The polyol method [90] permits the control of the shape and size of the particles. Liquid polyols (such as triethylene glycol and

PEG (Polyethylene glycol)) serve as reducing agents and solvents to metal precursors that are dissolved within them. The hydrothermal method [90] (Figure 4.7 (b)) uses high-pressure/high-temperature conditions to produce the nanoparticles, using an autoclave, where chemical reactions occur. This method has the advantage to produce highly crystalline and uniform-sized nanoparticles. In the technique that uses high-temperature decomposition of organic precursors, the nanoparticles are formed by decomposing organometallic precursors at higher temperatures in the presence of organic solvents and surfactant capping agents. It is a precise method but involves high temperatures and expensive reagents. SPIONs can also be produced via microemulsions [90], allowing for precise control of the size of the nanoparticles. Another inexpensive production technique is sol-gel processing [90], which involves two reactions: hydrolysis of the precursor in the acidic or basic mediums and polycondensation of the hydrolyzed products.

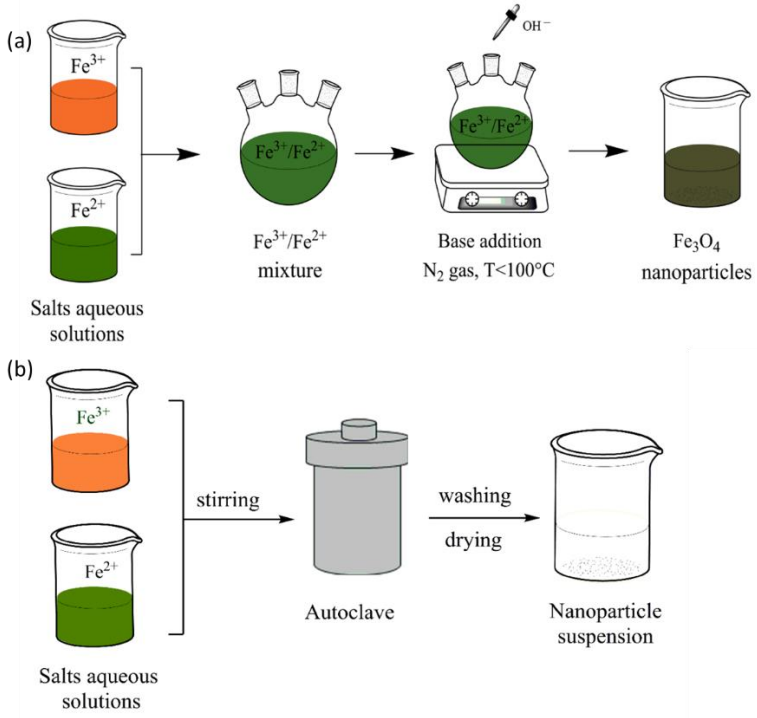

Figure 4.7 (a) Scheme Co-precipitation syntheses of SPIONs (b) Scheme of hydrothermal synthesis of SPIONs. (Adapted with permission from [90]. Copyright (2020) Multidisciplinary Digital Publishing Institute).

4.1.3.3. Magnetic properties of SPIONs

The magnetic properties of nanoparticles depend on their size. Magnetic effects are caused by masses and electric charges, such as electrons and protons. The magnetic dipole is created by the spinning of an electric-charged particle. A ferromagnetic material is composed of magnetic domains, and in each domain, all magnetic dipoles are aligned in the same direction, by exchange forces. Large ferromagnetic materials have several magnetic domains. However, when the particle size is small enough, the state of lowest energy has uniform magnetization and the particle is composed of a single domain (Figure 4.8 (a)) [92].

The magnetic susceptibility is the ratio of the induced magnetization and the applied magnetic field (H). Another two parameters are the remanence which is the magnetization that remains after an applied field has been removed, and the coercivity is the required applied magnetic field to reduce the saturated magnetic materials to zero [93]. However, coercivity is size-dependent (Figure 4.8 (a)). In the case of ferromagnetic particles, there are multi-domains, and with the application of an MF, the magnetic dipoles align with the field. With the removal of the MF, the magnetization remains, and the dipoles are still aligned in the different domains (Figure 4.8 (b) left). At lower sizes, in the range of superparamagnetism, the coercivity is null, this means that there is no longer a required applied magnetic field to reduce the saturated magnetic dipoles to zero. Thus, with the application of an AMF, the dipoles align, but with the removal of the AMF, the superparamagnetic nanoparticles revert to the nonmagnetic state [92]. This phenomenon of the magnetic field is thus associated with the energy loss associated with temperature increase with the application of AMF.

As previously stated, there are two regimes that govern the SPIONs reaction to an AMF: Néel and Brownian relaxations [87]. The former involves the flipping of magnetic moments of individual atoms within the nanoparticle to align with the magnetic field, this regime is more prevalent in smaller nanoparticles. The latter mechanism is associated with the rotational motion of the entire nanoparticle in response to a magnetic field. This is more associated with larger nanoparticles, and is highly affected by the viscosity of the matrix that surrounds the nanoparticle [87].

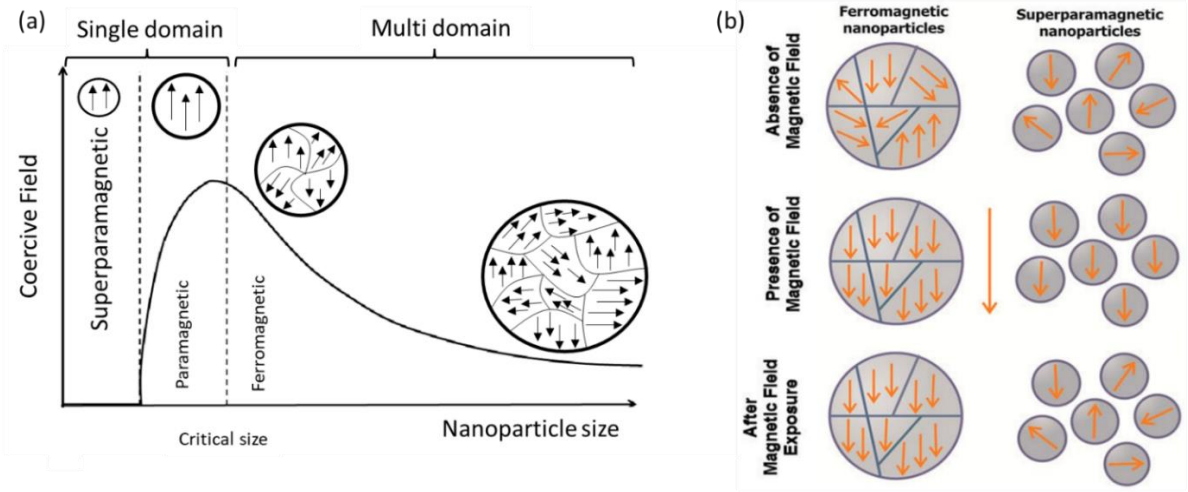

Figure 4.8 (a) Illustration of the relationship of coercivity, size and the magnetic domain structures, with the arrows symbolizing the magnetic dipoles; (b)Illustration of superparamagnetic and ferromagnetic particles in the presence and absence of an AMF, and after exposure to an AMF. In the presence of an alternating magnetic field, the magnetic moment of both superparamagnetic and ferromagnetic nanoparticles are aligned. With the removal of the AMF, the ferromagnetic nanoparticles maintain the magnetic state, while the superparamagnetic revert to the nonmagnetic state. (Adapted with permission from [65, 86]. Copyright (2017) Multidisciplinary Digital Publishing Institute).

4.1.3.4. Coatings of SPIONs

In aqueous mediums, SPIONs may agglomerate and form large clusters of particles that could even be seen by the naked eye. Since the superparamagnetic properties are size dependent, this effect will affect the SPIONs response with the application of an AMF [94, 95]. Thus, it is important to obtain colloidal stability, which refers to the capacity of mNPs to remain stable and dispersed in a liquid medium at physiological conditions. Different mechanisms contribute to the colloidal stability of SPIONs, such as electrostatic and repulsive forces. Within a liquid medium, the charged groups at the mNPs surface may interact with oppositely charged ions and molecules, which might aid in the repulsive forces between nanoparticles. pH or charged stabilizing agents like surfactants can aid in the electrostatic interactions to stabilize SPIONs. On the other hand, steric repulsions refer to physical barriers that are at SPIONs surface that, due to steric hindrance, prevent the aggregation of the nanoparticles (Figure 4.9) [94, 95]. In addition to stabilization, SPIONs coating allows conjugation with different bioactive agents, like drug molecules and targeting ligands [86]. PEG can serve as a coating to prolong the circulation time in blood since it can reduce the absorption by macrophages and promotes penetration through the cell membrane. Inorganic materials, like gold, protect the magnetic core against oxidation, corrosion, and aggregation and also increase biocompatibility [86]. Also using folic acid, it is possible to improve tumour cell targeting, with the connection to the folate receptor of the cell [81]. Soares *et al.* [96] developed magnetite SPIONs with chitosan coating for DOX delivery. DOX entrapment increased with the combination of chitosan with SPIONs, and the release rate was dependent on SPIONs concentration.

After being coated, SPIONs can be conjugated with targeting species that serve as targeting agents (Figure 4.9). Some examples include proteins (transferrin, antibodies, and lectins), peptides, DNA, and others. Covalent bonds can be formed between functional groups such as amine ($–NH_2$), aldehyde (–CHO), carboxyl (–COOH), and sulfhydryl (–SH) on the SPIONs coating and ligands [90]. These targeting species can be useful in breast cancer therapies, for example, HER2+ positive cancer with Herceptin targeting HER-2/neu on breast cancer [97]. Also, conjugating SPIONs can be conjugated with antibodies that can promote T cells to act. Proteins such as CTLA-4 and PD-1 act as blockers of T cell activation. Using Immune Checkpoint Therapy, it is possible to block CTLA-4 and/or PD-1 using antibodies to restore immune activation, and SPIONs can be linked with these types of agents [97].

APTES (3-aminopropyltriethoxysilane) coating is a widely used steric surface modification technique for SPIONs to improve their colloidal stability and biocompatibility [98, 99]. APTES is a silane compound that can react with hydroxyl groups on the surface of SPIONs to form a stable amine-functionalized layer. APTES coating can improve the colloidal stability of SPIONs by providing a positive charge on their surface, which creates electrostatic repulsion between the particles and prevents aggregation [100, 101]. Additionally, amine groups on the surface can serve as reactive sites for further functionalization with biomolecules or targeting

ligands [102, 103]. APTES coating can also improve the biocompatibility of SPIONs by reducing their cytotoxicity and immunogenicity [104].

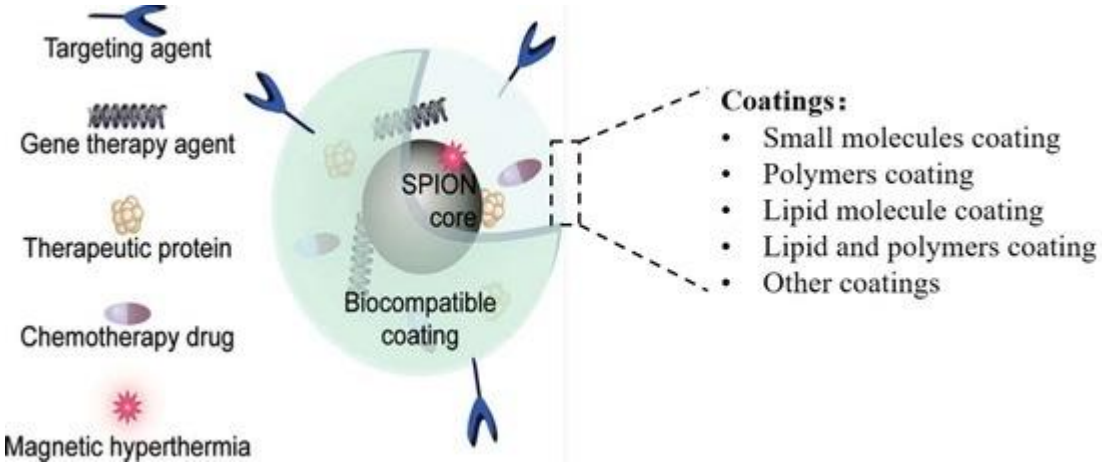

Figure 4.9 Possible architecture of SPIONs that can be coated or functionalized with different materials/bioactive agents. (Adapted with permission from [105]. Copyright (2020) Multidisciplinary Digital Publishing Institute).

4.1.3.5. Combination of SPIONs with polymeric matrixes

The combination of mNPs with polymeric structures for biomedical purposes can be of great benefit. Besides DDS, the polymeric matrix can serve as a transport for the mNPs. SPIONs presence in the hydrogel structure can confer magnetic properties and change the structure of the polymer. For example in hydrogels, high concentrations of SPIONs can lead to stiffer structures [90].

There are different forms to combine SPIONs with polymers. For example, it is possible via incorporation, that is before crosslinking the matrix, where SPIONs are present in the precursors of the polymeric matrix. Another form is by adsorption, with the adhesion of the nanoparticles onto the surface of the crosslinked matrix and even by absorption via swelling of the matrix [90]. Matos *et al.* [82] developed electrospun cellulose acetate membranes loaded with SPIONs for magnetic hyperthermia applications. SPIONs were coated with oleic acid (OA) and dimercaptosuccinic acid (DMSA) to obtain stable suspensions. The magnetic membranes were produced in 2 ways: via incorporation during electrospinning, where SPIONs incorporation into the produced fibres was successful; and via adsorption, where the produced fibres were submerged into mNPs suspensions and adsorbed to the fibres surface. The incorporation of SPIONs into the fibres conferred hyperthermic properties, with the ones that were produced via adsorption having higher temperature variations than the ones that were made via incorporation. Also, the fibres were revealed to be non-cytotoxic for Vero cell lines. However, higher concentrations of mNPs increased cytotoxicity. Thus, the method of incorporating the mNPs within the polymeric matrix is important. In this case, the mNPs at the surface produced far better temperature variations with AMF than the ones in the middle of the fibre.

One other method is *in situ* precipitation. In this method, SPIONs are produced in the presence of the hydrogel. Onto the hydrogel network, an iron solution (ratio of 1:2 of Fe^{2+} : Fe^{3+}) is loaded. The swollen hydrogel is immersed in an alkaline solution that promotes the crystallisation of the magnetite [90]. Freire *et al.* [106] developed a chitosan-based magnetite nanocomposite where ultrasounds were used for an *in situ* method with just one step. Superparamagnetic spheroidal magnetite nanoparticles with diameters between 10 and 24 nm were produced. And the incorporation of the SPIONs was confirmed, with a production time of around 2 minutes.

4.1.3.6. Polymeric microparticles and SPIONs

The production of polymeric particles with mNPs has been previously done. Finotelli *et al.* [41] produced alginate/chitosan beads via extrusion into an ionically crosslinking bath of $CaCl_2$ solution. Insulin was incorporated within the polymeric beads along SPIONs. Chitosan coating of the beads was added to improve the encapsulation efficiency of the drug, but no improvements were noted, although chitosan slowed the release profile of insulin. Regarding SPIONs, their introduction to the microparticles allowed for a tunable release profile of insulin. With the application of an AMF, the release rate of insulin was faster. Wen *et al.* [42] also used alginate and chitosan to produce composite microparticles containing SPIONs for on-demand cell separation within the structure of the bead. The SPIONs were integrated within the inner structure of the microparticles, where solutions with alginate and SPIONs were extruded into a $CaCl_2$ bath. Afterwards, the microparticles were embedded in a chitosan solution. SEM (Scanning electron microscopy) mapping confirmed that the mNPs were distributed homogenously in the cross-sections of the beads. Also, the swelling of the microparticles was affected by the presence of SPIONs within the structure of the bead, possibly due to the steric hindrance by the SPIONs with alginate.

In a different study, sorafenib, a cancer drug that suppresses kinase proteins, was encapsulated within alginate microspheres and SPIONs were added [107]. The microspheres were made via the emulsion technique. The addition of SPIONs into the microspheres allowed for an increase in temperature of around 4ºC under the application of an AMF. The alginate/SPIONs microspheres did not exhibit cytotoxicity in HEPG2 liver cancer and L929 fibroblast cell lines. Xue *et al.* [24] developed DOX-loaded microspheres that were AMF responsive for postsurgical breast cancer treatments, primarily to avoid cancer reoccurrence. Alginate and chitosan were used to produce these DOX and SPIONs loaded microspheres. The application of the AMF altered the release profile of the microspheres, with the cumulative release being able to reach 22.5% within 10 minutes with the application of AMF, whilst without AMF the release was around 0.2%. *In vitro,* cytotoxicity tests on MCF-7 breast cancer cells revealed that the combined therapy of AMF and DOX lead to a cell death of 96%. A significantly higher rate than the treatments with only the application of the AMF or DOX alone.

The combination of polymeric microparticles with mNPs is of great interest for cancer treatment applications, since it can serve as a DDS and a hyperthermia system. Gellan gum

and alginate are biocompatible polymers used for biomedical purposes. SPIONs were chosen for their hyperthermia capabilities, and the APTES coating was chosen due to the positive charge of this aminosilane, that might better interact with the negatively charged alginate and gellan gum structure. Therefore, this chapter will focus on the production, optimization, and characterization of alginate and gellan gum microparticles with SPIONs to obtain a magnetically sensitive DDS. This chapter introduces a novel approach by synergistically incorporating both coated and uncoated SPIONs into alginate/gellan gum microparticles. Additionally, the optimization procedure for the production of these microparticles is presented, filling a research gap as it has not been reported in the existing literature, based on thorough searches conducted. The first part will focus on the production and optimization of polymeric microparticles via the coaxial air-flow technique. A Design of Experiments (DOE) was used to optimize the physicochemical properties of the obtained microparticles, followed by extensive characterization. Polymeric microparticles were combined with SPIONs, with and without APTES coating, followed by extensive characterization. Materials and methods (production and characterization) used are described in Chapter 3.

4.2. Results and discussion

4.2.1. Production and optimization of the GG:Alg microparticles

4.2.1.1. Preliminary tests

The goal of this DOE was to understand the effect of the chosen parameters into the diameter of gellan gum and alginate microspheres. Preliminary tests were performed to determine the best factors (production parameters) and levels that should be used in the DOE. For these tests, it is necessary to choose 2 levels for each factor to determine the effect that each factor has on the selected responses. 4 factors were chosen: A: GG:Alg Ratio; B: Gap bath-nozzle; C: Air-flow and D: Pump flow. In this case, the chosen responses were the diameter (size) of the particles without drying (wet stage) and to evaluate dispersibility, the Coefficient of Variation (COV) (standard deviation/mean) and normalized SPAN (=(d(0.9)-d(0.1))/d(0.5)) (d is percentile) were both chosen.

Regarding factor A (GG:Alg Ratio), the concentration of the solution was studied to understand if the solutions passed throw the coaxial air-flow system and if the microparticles were formed after the ionic gelation in the $CaCl_2$ bath (3.5 w/v%). The calcium chloride concentration was chosen according to previous studies to induce the fastest gelation possible [108, 109]). Solutions with high viscosities clogged the air-flow system. Gellan gum aqueous solutions (1 w/v%) had a high viscosity and clogged the needle with an internal diameter of 0.25 mm and an outer diameter of 0.5 mm. of the coaxial flow system. The mixture of gellan gum with alginate solutions decreased the viscosity of the final mixture [34, 38]. Maintaining the same ratio of GG:Alg (50%:50%), four concentrations were tested (1, 1.5, 2 and 2.5 w/v%) in the coaxial air-flow equipment. The rest of the parameters were put at the minimum levels:

(air-flow: 2.5 L/min, pump flow: 5 mL/h and gap nozzle-bath: 10 cm). These levels were just chosen to understand the best polymer concentrations of the solutions in a preliminary test. Concentrations of 1 and 1.5 w/v% led the microparticles to deform and collapsed after falling into the $CaCl_2$ bath. With 2.5 w/v% the nozzle clogged due to the high viscosity of the solution. With 2w/v% no clogging occurred. Thus, maintaining the polymer's solution with a concentration of 2%, three different GG:Alg ratios were chosen: 75%:25%, 50%:50% and 25%:75%. With 75%:25% clogging occurred due to the high viscosity associated with gellan gum. Therefore, for factor A the chosen concentration was 2 w/v% and the GG:Alg ratios were: 50%50% (considered the lower level) and 25%:75% (considered the higher level). Figure 4.10 depicts the viscosity between the two solutions. Both had a shear thinning behaviour and the solutions with higher GG and lower Alg concentrations had higher viscosity. Gellan gum has a higher viscosity than Alg, hence the differences in viscosities [34, 38]. With higher shears, the viscosities converged, possibly due to the alignment of the polysaccharide chains with the flow.

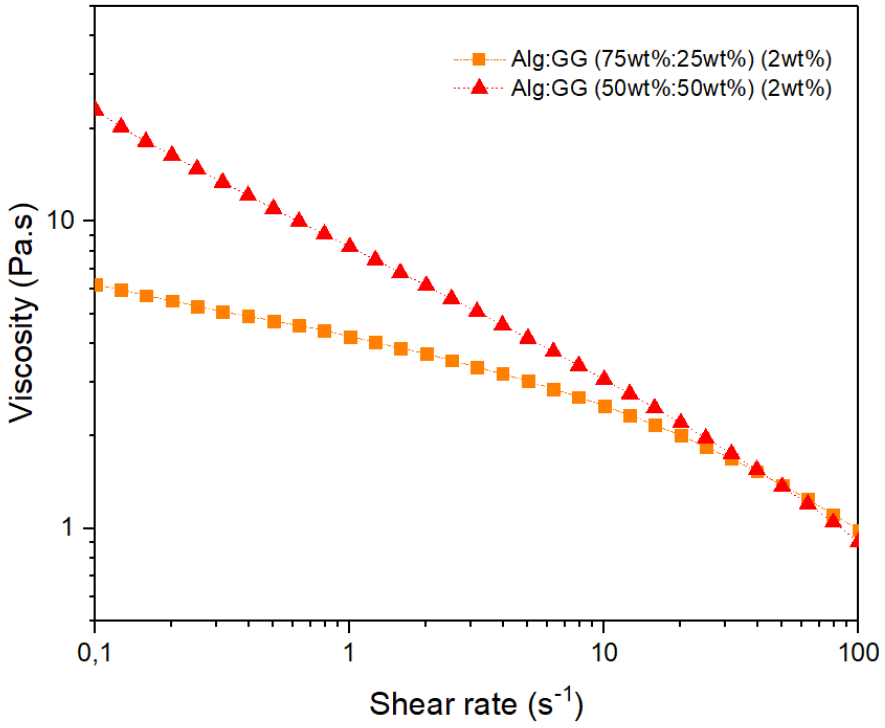

Figure 4.10 Flow curves (25ºC) of the Alg:GG solutions (2w/v%) with different ratios of GG and Alg.

Regarding factor B, the lower level of the bath-nozzle gap was set at a height of 10 cm and the higher level at 20 cm. Below 10 cm the equipment was very close to the calcium chloride recipient, thus 10 cm was chosen to confer a safety distance. 20 cm was chosen according to previous studies, with a 20 cm height sufficient to produce the smallest droplets [46] (Figure 4.11).

For factor C, the air-flow was set as the lower level of 2.5 L/min and the higher level as 5 L/min (the equipment's maximum). Below 2.5 L/min some clogging at the end of the nozzle occurred, thus this was set as the minimum.

For factor D, the pump flow, the lower level was set as 5 mL/h and the high-level set as 10 mL/h. Below 5 mL/h some clogging of the system occurred, so this level was defined as the minimum. Pump flows above 10 mL/h exerted a high pressure that led to the detachment of the link tube (Figure 4.11) between the nozzle and the pump. Thus, 10 mL/h was chosen as the maximum limit to prevent this link to detach and guarantee good production.

The chosen needle diameter was the previously mentioned with an internal diameter of 0.25 mm and an outer diameter of 0.5 mm. Another needle with a lower diameter (internal: 0.17 mm; outer: 0.3mm) was used but the clogging of the system also occurred using the GG:Alg solutions with the previously mentioned ratios. With lower diameters, higher shear rates are applied to the solutions, accordingly to Poiseuille's equation [110]. Even though higher shear rates are acquired and GG:Alg solutions are shear thinning, thus diminishing the solution's viscosity, the needles with lower diameters clogged frequently and were not able to be used in this study. Thus, needle diameter was maintained as a constant, with the study with larger diameters as a possible topic to be studied for future studies.

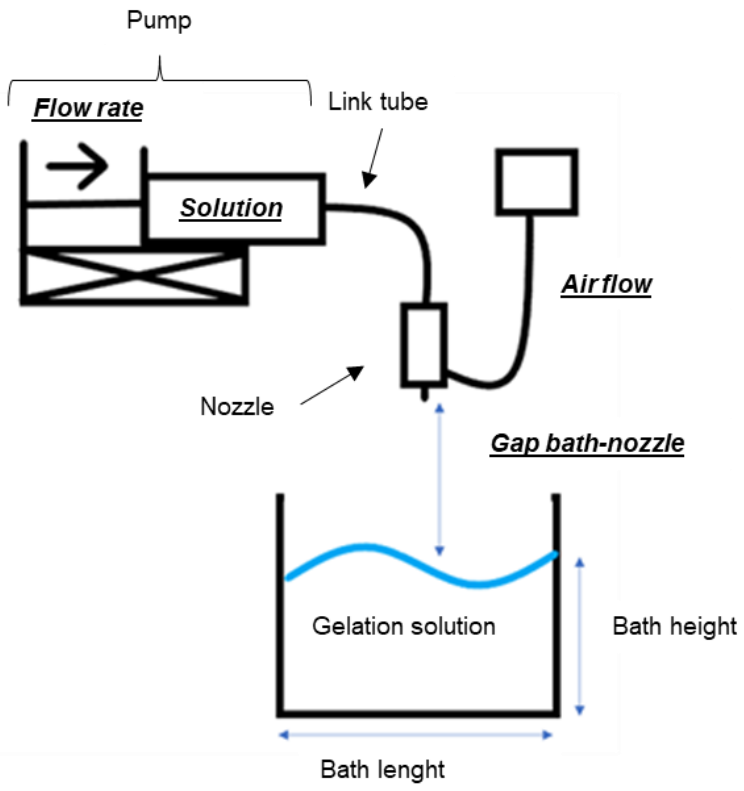

Figure 4.11 Schematic representation of the coaxial air-flow system and its components.

Table 4.1 depicts the 24 runs done in a random sequence with the established levels for each run. All particles had a spherical shape. All results were found to be normally distributed.

Table 4.1 Design of Experiments and responses. In each run, the variations of levels of the factors are assigned randomly (by the DOE software), to avoid influences from the previous run. In each run, the following responses are determined and assigned in the table.

RUN	Factors				Responses		
	A: GG: Alg ratio (%)	B: Gap bath-nozzle (cm)	C: Air-flow (L/min)	D: Pump flow (mL/h)	Size (μm)	COV	SPAN
1	25:75	20	5	10	383.4	0.0770	0.1969
2	50:50	20	5	5	434.6	0.0662	0.1486
3	50:50	10	2.5	5	652.6	0.0659	0.1582
4	50:50	10	5	10	496.1	0.0400	0.1611
5	25:75	20	2.5	5	617.6	0.0648	0.1610
6	25:75	10	5	5	427.0	0.1200	0.2460
7	25:75	20	5	10	441.7	0.0949	0.2311
8	25:75	10	5	5	418.1	0.1109	0.2496
9	50:50	20	2.5	10	666.9	0.0619	0.1473
10	50:50	10	2.5	5	607.4	0.0618	0.1447
11	25:75	10	2.5	10	649.0	0.0600	0.1447
12	50:50	20	5	5	453.3	0.0690	0.1740
13	25:75	10	2.5	10	655.6	0.0718	0.1723
14	50:50	20	2.5	10	619.5	0.0653	0.1604
15	50:50	10	5	10	435.0	0.0589	0.1505
16	50:50	10	2.5	5	591.0	0.0587	0.1623
17	25:75	20	5	10	490.6	0.0853	0.1935
18	50:50	20	2.5	10	692.8	0.0735	0.1838
19	50:50	20	5	5	405.2	0.0825	0.1752
20	25:75	10	2.5	10	676.4	0.0586	0.1679
21	50:50	10	5	10	418.4	0.0820	0.2185
22	25:75	20	2.5	5	527.9	0.0796	0.1928
23	25:75	20	2.5	5	588.0	0.0619	0.1646
24	25:75	10	5	5	474.1	0.0907	0.2184

4.2.1.2. Microparticle size

Regarding the microparticle's size (diameter), only air-flow (factor C) and pump flow (factor D) were found to be statistically significant, with a p-value < 0.05. The GG:Alg ratio (factor A) and the bath-nozzle gap (factor B) were not significant, and thus, they were excluded from the ANOVA analysis, as can be observed in Table 4.2, where only air-flow and pump flow were analyzed. Additionally, no significant lack of fit was detected in the ANOVA analysis, as can be observed in Table 4.2, which was obtained from the Design-Expert Software® (Version 11).

Table 4.2 Obtained ANOVA table parameters for the particles size (diameter) (p-value < 0.05). df is degrees of freedom.

Source	Sum of Squares	df	Mean Square	F-Value	*p*-Value	
Model	2.218×10^5	2	1.109×10^5	81.830	<0.0001	significant
C-Air-flow	2.141×10^5	1	2.141×10^5	158.020	<0.0001	
D-Pump flow	7647.260	1	7647.260	5.640	0.0271	
Residual	28455.610	21	1355.030			
Lack of Fit	6958.180	5	1391.640	1.040	0.4303	not significant
Pure Error	21497.430	16	1343.590			
Cor Total	2.502×10^5	23				

Figure 4.12 (a) displays the Pareto chart of microparticle sizes, with the Y axis indicating the t-value effect. The higher the t-value, the more significant the factor is to the response, which is the microparticle size [111]. A factor is considered significant if it surpasses the t-value limit [112]. As previously said, air-flow had the most significant effect on microparticle size, as it had the highest t-value (Figure 4.12 (a)). It had a negative effect, resulting in smaller diameters with higher air-flow. Pump flow (D) had a positive effect on particle size, with higher flows resulting in larger diameters. However with a lower significance than air-flow, as it did not even surpass the Bonferroni Limit. The Bonferroni Limit is another limit that is higher than the t-value limit that serves as a threshold that confirms that the factors have a significant effect [113]. Even though the Bonferroni line confirms that the factor is significant, factors between the Bonferroni and the t-values also are accounted as significant [113]. The remaining factors, GG:Alg ratio (A) and Gap bath-nozzle (B), had no significant impact on microparticle size under the tested experimental conditions.

Figure 4.12 (b) displays the interaction between air-flow (C) and pump flow (D), the two statistically significant factors, confirming the data in Figure 4.12 (a) that indicates that this interaction is not significant. It can also be seen the increase of microparticle size with higher pump flows. Therefore, these factors do not affect each other. The expected change in microparticle size between the studied levels of the significant factors (A and D) is shown graphically in Figure 4.12 (c), where the slope of air-flow is far superior to the pump flow, indicating its superior impact on the particle size.

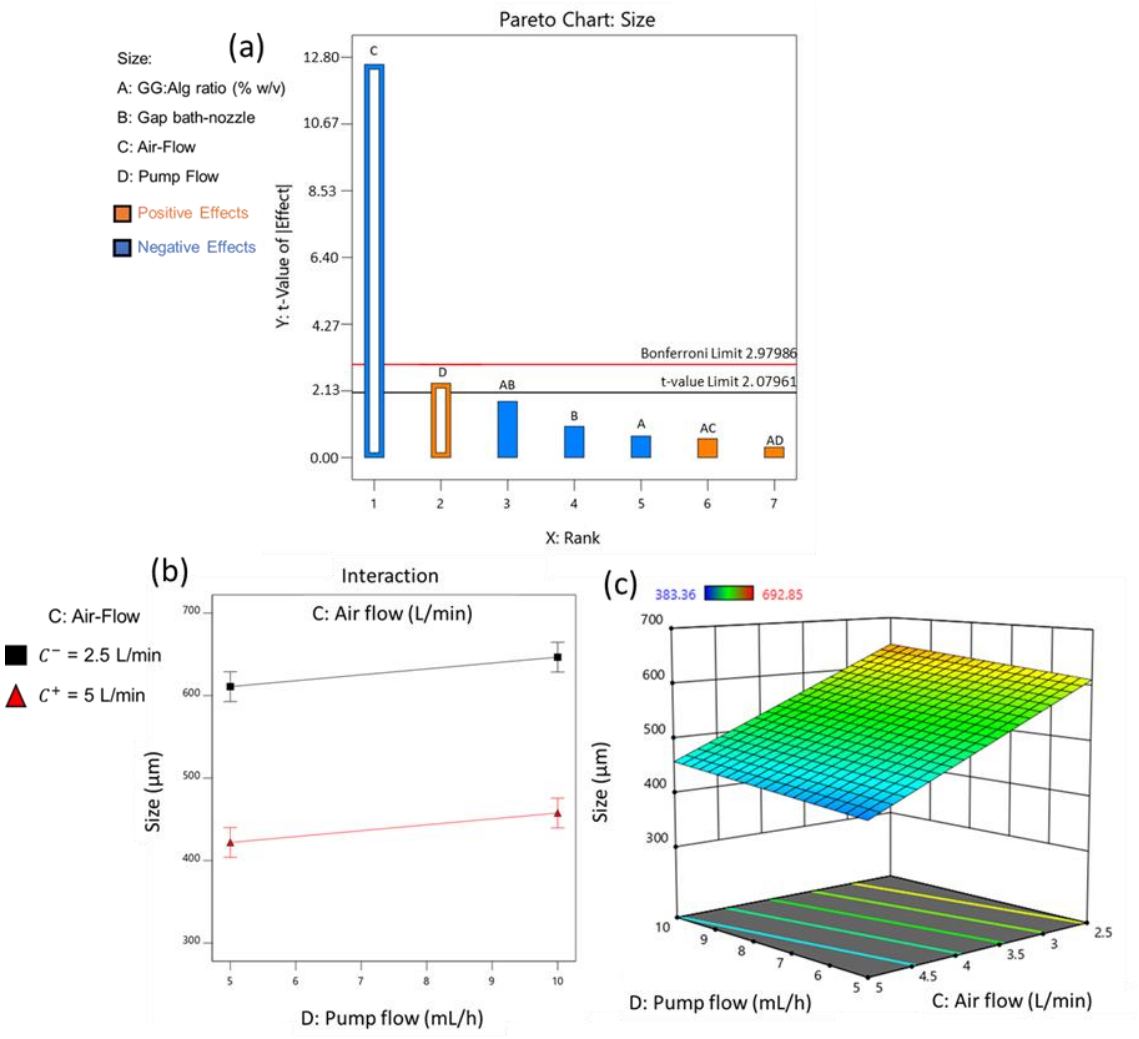

Figure 4.12 (a) Pareto charts with the effects of the different variables on the particle's diameter. Empty bars mean significant factor whilst full ones are of non-significant; (b) Interaction plots for particle's diameter between the significant factors the C: Air-flow and D: Pump flow (A: GG:Alg ratio (% w/v) = 50:50; B: Gap bath-nozzle = 15 cm); (c) Response surface plot for the particle's size, with the effect of C: Air-Flow and D: Pump Flow (A: GG:Alg ratio = 50:50; B: Gap bath-nozzle = 15 cm).

Observations indicate that higher air-flow rates led to a significant decrease in particle size while increasing pump flow resulted in larger particles. It is worth noting that the effect of pump flow on particle size was less significant than air-flow. Workamp *et al.* [46] reported a similar trend, where polyacrylamide and gelatine particles decreased in diameter with increasing volumetric air-flow rates, using a coaxial air-flow device. Chan *et al.* [114] found similar results for an atomization process, where an increase in volumetric liquid flow rate (equivalent to pump flow in this study) resulted in larger particles. In this study, neither height (equivalent to gap bath-nozzle) nor flow (equivalent to pump flow) had a significant impact on particle size, consistent with previous research [115].

In sum, the diameter of the microparticles at the wet stage was found to be affected in a statistically significant way by the Air-Flow (C) and the Pump Flow (D). GG:Alg ratio (A) and

the Gap nozzle-bath had no statistically significant effect and were excluded from the ANOVA analysis. Also, there was no significant lack of fit detected in the ANOVA analysis.

4.2.1.3. Dispersibility: COV and SPAN

Regarding dispersibility, COV varied between 0.4000 and 0.1200 and SPAN be-tween 0.1486 and 0.2496. There was no lack of fit for COV (Table 4.3) and for SPAN (Table 4.4). In both responses, the GG:Alg ratio (A) and air-flow (C) were statistically significant factors. The interaction between these factors (AC) was also significant. The bath-nozzle gap (B) and pump flow (D) were not significant and were excluded from the analysis.

Table 4.3 Obtained ANOVA table parameters for the particles size's COV (p-value < 0.05).

Source	Sum of Squares	df	Mean Square	F-Value	p-Value	
Model	0.0043	3	0.0014	9.43	0.0004	significant
A-Percentage in 2%	0.0015	1	0.0015	9.93	0.0050	
C-Air-flow	0.0016	1	0.0016	10.33	0.0044	
AC	0.0012	1	0.0012	8.02	0.0103	
Residual	0.0030	20	0.0002			
Lack of Fit	0.0010	4	0.0002	1.96	0.1499	not significant
Pure Error	0.0020	16	0.0001			
Cor Total	0.0073	23				

Table 4.4 Obtained ANOVA table parameters for the particles size's SPAN (p-value < 0.05).

Source	Sum of Squares	df	Mean Square	F-Value	p-Value	
Model	0.0148	3	0.0049	11.81	0.0001	significant
A-Percentage in 2%	0.0052	1	0.0052	12.48	0.0021	
C-Air-flow	0.0068	1	0.0068	16.19	0.0007	
AC	0.0028	1	0.0028	6.78	0.0170	
Residual	0.0084	20	0.0004			
Lack of Fit	0.0019	4	0.0005	1.17	0.3588	not significant
Pure Error	0.0065	16	0.0004			
Cor Total	0.0232	23				

As previously said, for COV and SPAN, factors A and C were statistically significant, including their interaction (AC) and factors B and D had no significant impact as it is observed in the Pareto charts of Figure 4.13 (a.1) and (b.1). The interaction between air-flow and GG:Alg ratio (AC) was found to be significant, being with a positive sign, although it was below the Bonferroni Limit in both cases. As shown in Figure 4.13 (a.2) and (b.2), the effect of air-flow was influenced by the GG:Alg ratio for COV and SPAN, respectively. The air-flow had a greater impact on the particle size distribution at the higher (C+ = 5 L/min) and lower level (C- = 2.5 L/min) with a GG:Alg ratio of 25:75 than with 50:50. This can be attributed to the differences

in viscosity between the two ratios, and their susceptibility with the air-flow, where a higher viscosity (GG:Alg ratio of 50%:50%) limits the effect of air-flow on the particle size distribution. Figure 4.13 (a.3) and (b.3) demonstrate how the COV and SPAN, respectively, are expected to change with air-flow and gap bath-nozzle. However, the effect of the bath-nozzle gap on the particle size distribution was found to be insignificant in this study.

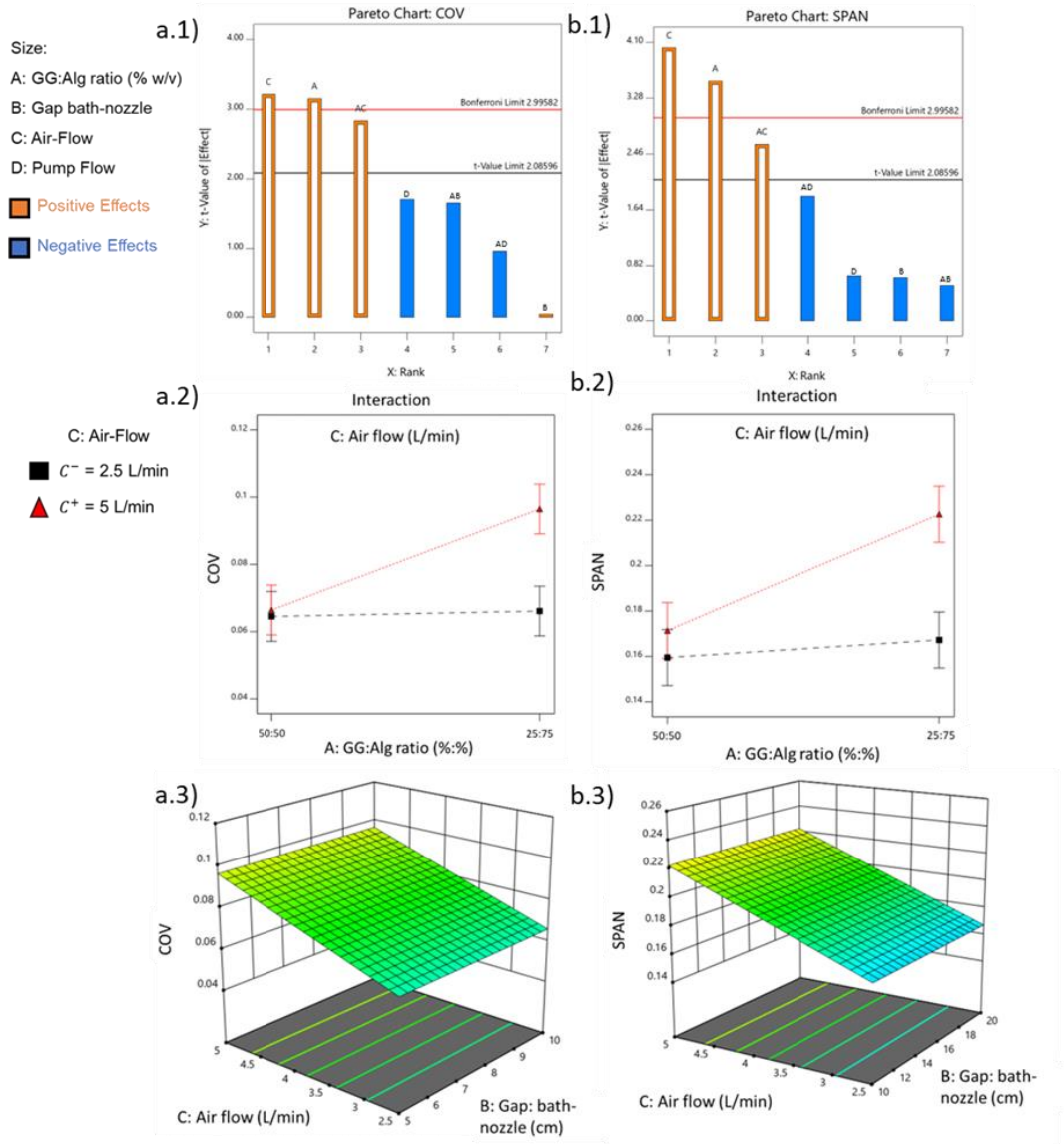

Figure 4.13 Pareto charts with the effects of the different variables on the particle's dispersibility a.1) COV, b.1) SPAN. a.2) Interaction plots for particle's diameter COV between the significant factors the A: GG:Alg ratio and C:Air-flow (B: Gap bath-nozzle = 15 cm; D: Pump Flow = 5 mL/h); b.2) Interaction plots for particle's diameter SPAN between the significant factors the A: GG:Alg ratio and C: Air-flow (B: Gap bath-nozzle = 15 cm; D: Pump Flow = 5 mL/h); a.1) Response surface plot for the particle's diameter COV, with the effect of C: Air-flow and D: Pump Flow (A: GG:Alg ratio = 25:75; B: Gap bath-nozzle = 15 cm); c.3) Response surface plot for the particle's diameter SPAN, with the effect of C: Air-flow and D: Pump Flow (A: GG:Alg ratio = 25:75; B: Gap bath-nozzle = 15 cm).

At higher air-flows, SPAN and COV values were observed to increase. Chan *et al.* [114] reported similar findings, where a lower air-to-liquid mass flow rate ratio resulted in a smaller particle size distribution. Air-flow had a higher effect on SPAN compared to COV, as indicated

by the higher t-value. The GG:Alg ratio (A) also had a significant effect on dispersibility, with a positive correlation. A higher dispersibility was observed at the higher level of 25%:75% (GG:Alg), which was attributed to the viscosity of the solutions [34, 38]. Higher levels of gellan gum increased the solution's viscosity, leading to lower dispersibility, while lower-viscosity solutions resulted in higher dispersibility.

Defining the optimized levels

With the main goal of decreasing the microparticle diameter and the diameter dispersibility, the GG:Alg ratio of 50%:50% (A) was selected, since higher viscosities decreased the dispersibility. Factor B, which represented the gap between the bath and nozzle, did not have a significant effect on particle size or dispersibility, so an intermediary level of 15 cm was chosen. Air-flow (C) had a significant impact on all responses, with higher air-flow resulting in smaller microparticle diameters but increased dispersibility. Additionally, air-flow had a stronger effect on microparticle size than on COV and SPAN. Consequently, a higher level of 5 L/min was chosen to minimize the particle size. Pump flow (D) had a positive effect on the particle diameter, but no impact on dispersibility, so the lower level of 5 mL/h was selected. Under these conditions, the polymeric microparticles produced had wet diameters ranging from 400 to 450 μm (414.3 ±36.4 μm).

4.2.1.4. Drying and swelling of the microparticles

The microparticle production using the coaxial air-flow system was optimized and the drying of the microparticles was carried out. The microparticles were dried using a vacuum drier. Before drying, a solvent exchange method from water to ethanol was done to prevent aggregation. Figure 4.14 (a) shows the dried microparticles. With the drying stage, the water and ethanol from the microparticles were removed and only the polymeric matrix remained, reducing the mobility and establishing hydrogen or van der Waals bonds between the molecules [34]. Thus, reducing the size of the microparticle. The drying stage is ideal for the preservation of the particles and for future drug encapsulation, where the reswelling of the microparticles allows the drug-loaded solution to enter/adhere to the polymeric matrix [2]. They had an average diameter of 171 ± 36 μm. Figure 4.14 (b) is an approximated version of (a), where the morphology of the surface is rough, due to the shrinking of the polymeric matrix.

In Figure 4.14 (c) the swelling in mass of the microparticles in PBS 6.5 and 7.4 is observed, where the maximum swelling occurred at 72 hours. In Figure 4.14 (d) the Swelling in Volume is also depicted. The particles within PBS pH 7.4 swelled to a diameter of 433.6 ± 67.8 μm and within PBS pH 6.5 swelled to a diameter of 398.3 ± 52.4 μm. Higher swelling indexes were obtained at pH 7.4. The reduction in swelling of the microparticles was attributed to the anionic nature of the polymers. When exposed to basic environments (in this case pH 7.4), the carboxylic acid groups in both polymers deprotonate, increasing the number of negatively charged groups and a decrease in the strength of intermolecular hydrogen bonds [116, 117]. This leads to repulsive electrostatic charges between the chains, which promotes the formation of a larger mesh and facilitates solvent penetration. Conversely, at lower pH (in

this case pH 6.5), the calcium ions dissociate from the structure, facilitating the formation of hydrogen bonds and leading to a tightly packed structure, preventing higher swellings [118].

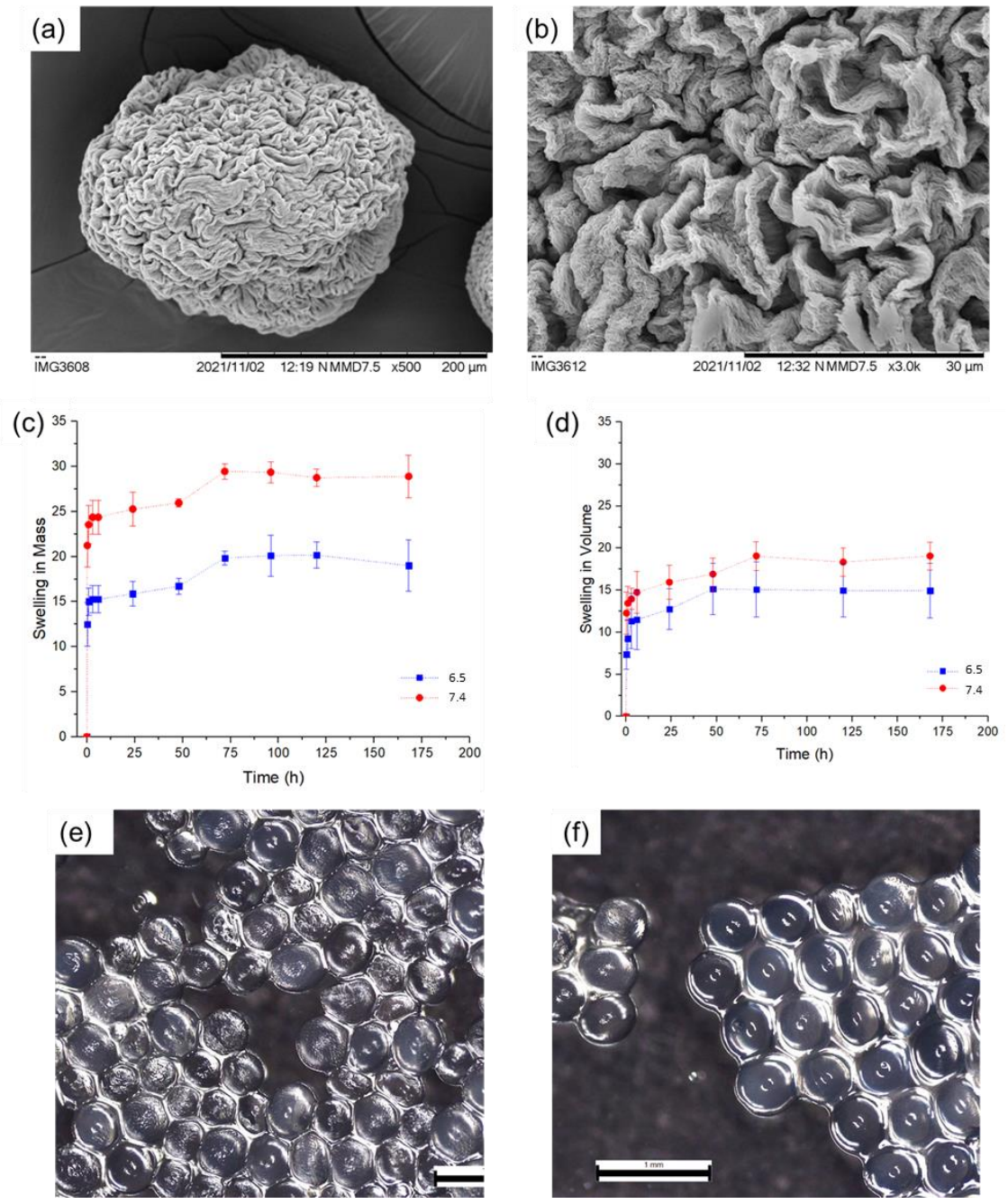

Figure 4.14 (a) SEM analysis of dried GG:Alg microparticles; (b) SEM analysis of the surface of the GG:Alg microparticles (approximation of (a)); (c) Swelling indexes in mass of microparticles submerged in PBS (pH 7.4 and 6.5); (d) Swelling in Volume of the microparticles after being submerged in PBS with similar pH; (e) Microscope image of microparticles after being swollen in PBS 6.5 (at the end 175 h); (f) Microscope image of microparticles after being swollen in PBS 7.4 (at the end 175 h).

This finding is consistent with previous studies that have reported reduced swelling with lower pH levels. For example, in the study with alginate beads [117] that studied alginate beads from pH 2 to 11, lower particles diameter were obtained and higher surface charges were recorded with lower pH. In gellan gum microparticles, similar swelling behaviours occur.

Narkar *et al.* [119] recorded lower swelling indexes with pH 1.2 than with pH 7.4, and Prezotti et al. [120] also had similar results with pectin/gellan gum beads in similar pH levels. Figure 4.14 (e) and (f) depict the microparticle's rough surfaces after being swollen in PBS pH 6.5 (e) and PBS pH 7.4 (f). Particles that were swollen at pH 6.5 conditions presented a non-smooth surface when compared to the ones at pH 7.4. With PBS pH 6.5 the surfaces did not swell up to their original sizes (Figure 4.14 (d)), leaving some roughness on their surfaces. This different reaction to pH 6.5 and pH 7.4 reveals that the microparticles will behave differently if *placed in vivo* in a tumorous area. Since tumorous areas have lower pH than the normal body pH (7.4) [121], the microparticles will have lower swelling indexes in tumorous areas.

4.2.1.5. Degradation of the microparticles

To understand how the microparticles can degrade within the tumorous environment, *in vitro* degradation tests were done. Using PBS solutions with physiological pH (7.5), and an acidic pH (6.5), the mass loss with time was registered. The degradation process did not occur during the first 7 days of the assay. In the first 35 days, microparticles lost mass, with no significant difference between the pH. However, at the end of the 57-day assay period, particles exposed to pH 7.4 experienced a more pronounced mass loss compared to those exposed to pH 6.5. Specifically, the particles lost an average of 50% mass at pH 7.4 and 40% at pH 6.5 (Figure 4.15 (a)). The loss of structural integrity resulting from degradation was also visually evident in the particles' morphology after drying (Figure 4.15 (b)). The degradation rate of the microparticles was affected by the pH of the solution. At pH 7.4, the particles had a higher mass loss when compared to pH 6.5, with a mass loss of around 50% at the end of 57 days. In previous studies [14, 122, 123], alginate degradation was found to be dependent on the pH. Alginate is more stable in solutions between pH 5 to 10. For low pH, degradation via proton-catalyzed hydrolysis is predominant, while for the higher pH (more basic) degradation occurs via β-alkoxy-elimination [122]. However, alginates can also degrade at neutral pH in the presence of reducing compounds [123]. In this case, the higher mass losses at pH 7.4 can be attributed to the deprotonation of the carboxylic acid, when compared to pH 6.5, leading to a faster dissolution of the alginate structure. Ionically crosslinked alginate also lose the divalent cations that form the structure and degrade at pH 7.4 [14]. On the other hand, gellan gum tends to be more stable in PBS with pH 7.4 [124, 125]. However, gellan gum is more deformable and fragile in more neutral pH medium compared to acidic ones [126, 127]. For example, Franco e*t al.* [127] revealed that gellan gum gels had lower mechanical properties (stress of fracture and young modulus) when the gels were prepared at pH 7 than the ones prepared at pH 5 .3 and 3.5. In an artificial urine solution, Barros *et al.* [128] compared the degradation of alginate and gellan gum. At the end of 60 days, alginate had lost all the weight, whilst gellan gum maintained more than 50% of the weight.

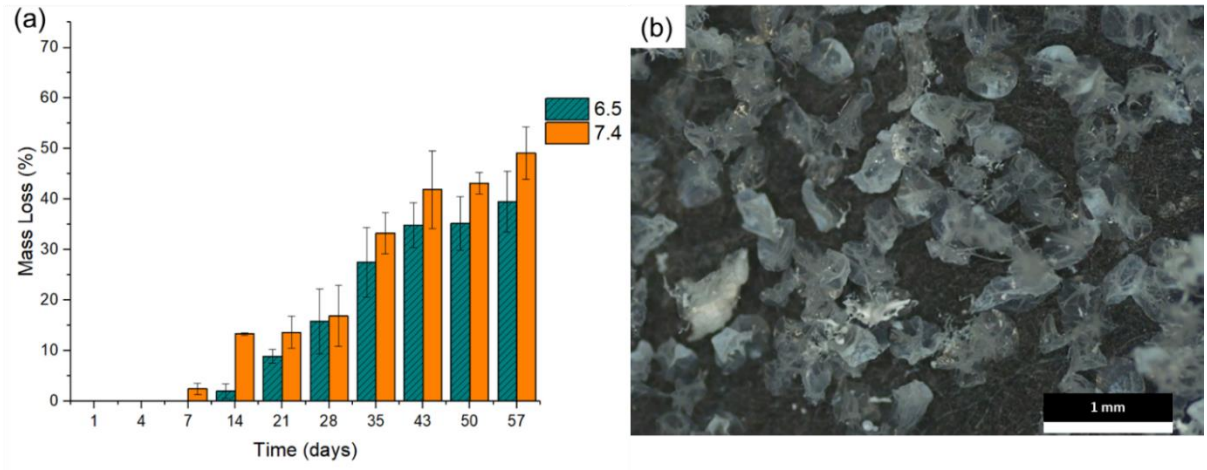

Figure 4.15 (a) Degradation of microparticles within PBS with pH 6.5 and pH 7.4 along 57 days; (b) GG:Alg particles after 28 days in PBS (pH 7.4).

4.2.1.6. Fourier-transform infrared spectroscopy (FTIR)

FTIR analysis was done to characterize the composition of the GG;Alg microparticles and the GG and Alg powders, and to confirm that both polymers were within the microparticles. FTIR analysis of alginate and gellan gum are well documented [26, 34, 129]. In the case of alginate (Figure 4.16) a band at 3606 cm^{-1} corresponds to the stretching of OH, and a band at 1614 cm^{-1} represents the asymmetric stretching of -COO. Another band at 1417 cm^{-1} indicates the symmetric stretching of -COO, and a band at 1032 cm^{-1} is due to the stretching of C-O-C. For gellan gum a characteristic band at 3627 cm^{-1} represents the stretching of -OH, a band in the range of 3300–2930 cm^{-1} is due to -C-H stretching, a band at 1660 cm^{-1} indicates -C-O stretching, a band at 1405 cm^{-1} for methyl -C-H bonding, and a band at 891 cm^{-1} is for -C-O stretching of alkyl ether. Figure 4.16 also depicts the analysis of GG:Alg microparticles [34]. The band around 3400 and 3100 cm^{-1} was attributed to the -C-H stretching of gellan gum, while the band at 1598 cm^{-1} was attributed to -COO stretching (asymmetric) of alginate. The bands at 1417 cm^{-1} (symmetric -COOH stretching) and 1023 cm^{-1} (C-O-C stretching) were also observed, indicating the presence of alginate in the microparticles [34].

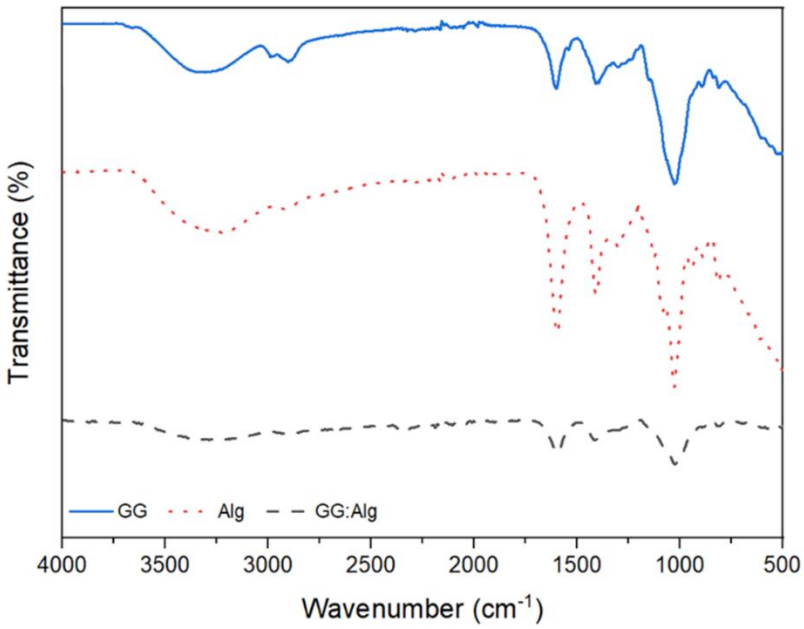

Figure 4.16 FTIR of Alg and GG powders and of GG:Alg microparticles

4.2.1.7. Loading of Methylene Blue (MB) into the microparticles

To understand if the produced GG:Alg microparticles could be used as DDS, a model drug was used to simulate the entrapment and release of drugs. Methylene blue, a cationic model dye was chosen to simulate a drug. Since the microparticles react differently to different pH, two pH were chosen for encapsulation. Further characterisation was also done with MB loaded microparticles to better understand the better conditions of drug encapsulation.

Solutions with different concentrations of MB (10 to 290 µg/mL) were used to understand how the encapsulation efficiency varied with MB concentrations. Higher MB concentrations led to increased efficiency and loading capacity in GG:Alg microparticles (Figure 4.17 (a) and (b)). This is due to a decrease in mass transfer resistance against MB diffusion from the solution to the beads, resulting in higher drug diffusion with the increase in MB concentration [130]. The optimal conditions for MB encapsulation were achieved using solutions of 290 µg/mL with pH 7.4, resulting in an encapsulation efficiency of 77.83% (±0.56) and a loading capacity of 5.71% (±0.06).

For each MB concentration, two pH (6.5 and 7.4) were studied. Solutions prepared at pH 7.4 had higher EE% and LC% values than the solutions at pH 6.5. Since MB is a cationic compound, there might be interactions between the cationic MB and the anionic polysaccharide [131]. At pH 7.4, due to deprotonation of the moieties of gellan gum and alginate, more anionic moieties are present (compared with pH 6.25), thus increasing the interaction with the cationic MB [131]. Also, at acidic pH (6.5), there is a higher concentration of H^+ protons that compete with MB molecules for the vacant anionic moieties of the polysaccharide chains, reducing the interaction of the polymeric chains with MB, and thus lowering the entrapment efficiency [117]. These findings are consistent with a study conducted

by Othman *et al.* [130] who used alginate particles for MB removal and observed an improvement in adsorption capacity with an increase in pH. After MB entrapment, the microparticles were vacuum dried, without solvent exchange as previously done. The dried microparticles loaded with MB also had similar diameters to the particles without the model drug, however, the original spherical shape of the microparticles was not fully preserved, possibly due to the interaction with the PBS, with also MB and with the drying stages (Figure 4.17 (c) and (d)).

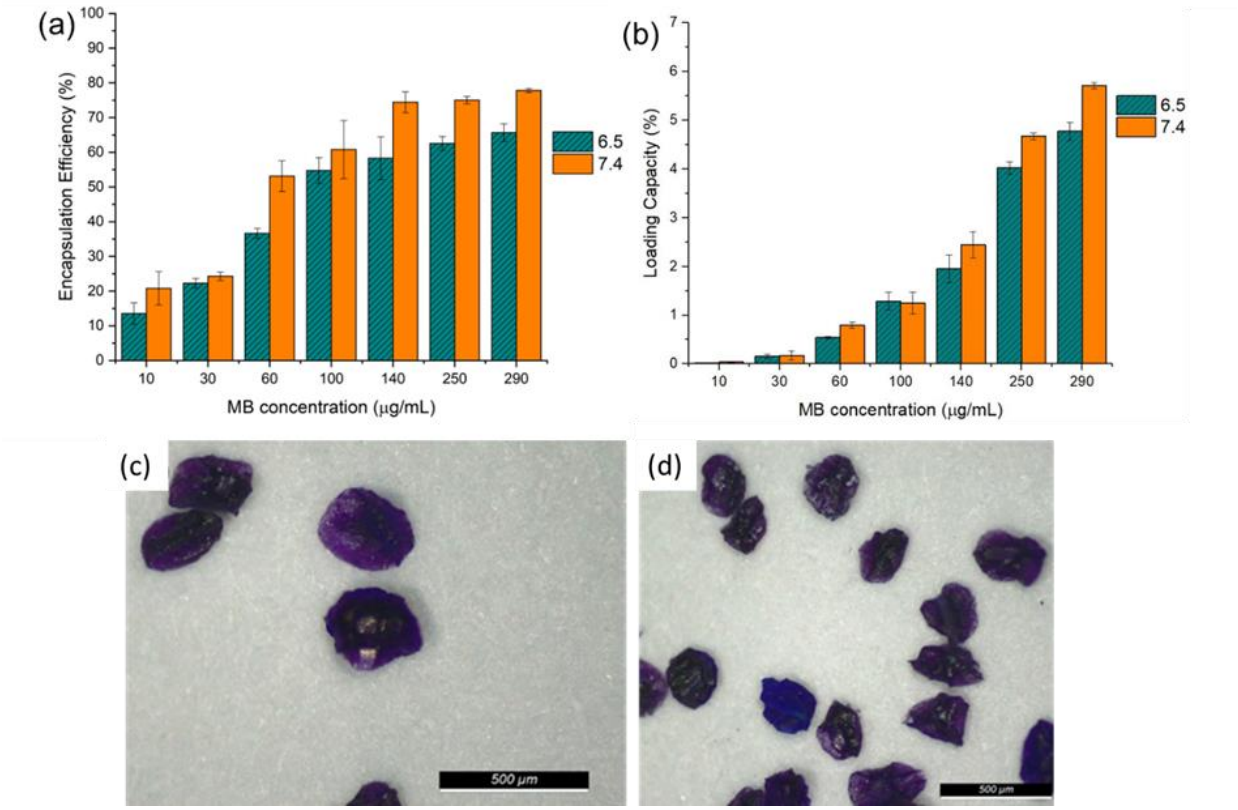

Figure 4.17 (a) Encapsulation Efficiency (E.E.%); (b) Loading Capacity (L.C.) with different concentrations of methylene blue (MB) in PBS solutions with pH of 6.5 and 7.4.; (c) and (d) microscopic images of MB loaded GG:Alg after vacuum drying.

4.2.1.8. Thermogravimetric Analysis (TGA)

TGA tests were performed to study the thermal stability of microparticles with and without MB (Figure 4.18). Regarding TGA results of microparticles without MB, a first thermal event between 25ºC and 100ºC occurred associated with water loss, with a weight loss of 15 %. A significant decrease in mass (33%) occurred between 220ºC and 280ºC. This was associated with depolymerization of alginate and gellan gum, associated with the loss of volatile components, chains broken and fragmentation of the material, observed in the mass loss in the GG and Alg samples and as previously mentioned [108, 132–134]. At 700ºC another thermal event occurred, possibly linked with the degradation of Na_2CO_3 of alginate [135]. The final residue of the sample without MB was 6.95%. In literature, TGA of sodium alginate and gellan gum are available, and results were similar to the ones obtained in this project. For

alginate, Bajas *et al.* [136] studied the alginate degradation with temperature. A mass loss event between 35ºC and 210ºC occurred, possibly related to water loss. From 210 to 272ºC a major degradation of alginate occurred, associated with the loss of volatile components, chains broken and fragmentation of the material. From 200 to 500 ºC the alginate degradation occurred, but the final residue was around 40% (at 500ºC). Similar results were found in other studies [108, 137]. Sodium alginate decomposes by dehydration followed by degradation of Na_2CO_3 and a carbonized material that decomposes slowly from 600-750 °C in N_2 atmospheres [135]. For gellan gum, Noor *et al.* [134] did the same test for pure gellan gum. Between 25 to 160ºC a weight loss was registered, associated with water loss. The degradation of pure gellan gum started at 230ºC with a weight loss of 35%, followed by a gradual weight loss of 44% until 850ºC, with the final residue around 6%. MB alone had a constant mass loss until its final value of 41.01% at 850ºC.

Regarding the MB-loaded GG:Alg microparticles, similar behaviours to the non-loaded microparticles occurred, but with less weight loss. At the end of the tests, microparticles loaded in PBS with pH 6.5 retained 15.24% and those loaded within PBS with pH 7.4 retained 23.34%. In these MB loaded microparticles, around 600ºC a thermal event is also observed, with a different slope shift around 600ºC. This was also attributed to the degradation of Na_2CO_3 of alginate, that in particles without MB was observed at 700ºC. The different mass losses between the microparticles that were loaded in PBS solutions with different pH were attributed to the loading capacity previously studied (Figure 4.17). Where higher loading capacities occurred for pH 7.4, thus higher masses.

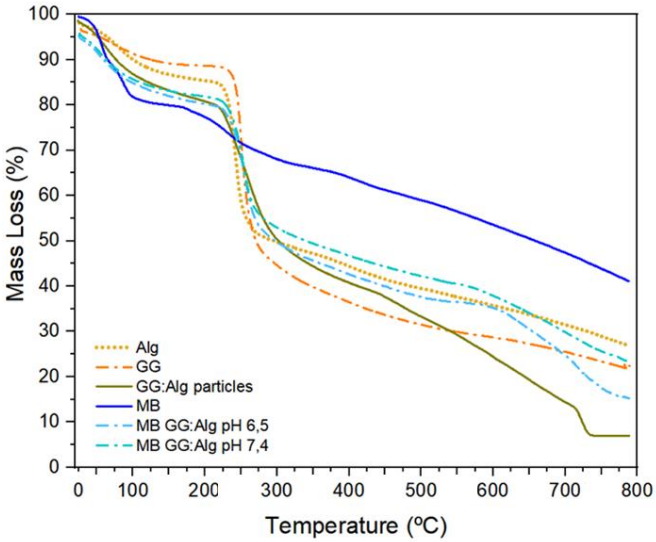

Figure 4.18 TGA of GG and Alg powders; GG:Alg microparticles; GG:Alg microparticles loaded with MB in PBS solutions with pH 6.5 and 7.4;, and MB powder alone.

4.2.2. Drug release assays

The microparticles had an early burst release pattern with MB [7] (Figure 4.19). In the first 24 hours, over 50% of MB was released, and by 72 hours, more than 75%. This

phenomenon has been previously reported in alginate particles [138] and in gellan gum particles [139, 140]. The rapid release could be attributed to the presence of MB molecules on or near the particle's surface, which are easily released upon hydration [141]. After the initial burst release, the release rate reached a steady state, with the majority of MB released. Throughout the release period, the concentration of MB released was marginally higher at pH 6.5 than at pH 7.4, however, no significantly differences were observed between the two release profiles, as can be observed in Table 4.5, where one-way ANOVA tests were performed each time from 24 h onward, to understand if there were statistically significant differences between the release profiles in PBS with pH 6.5 and pH 7.4. As can be observed, only at the times of 144 and 192h did the release profile were statistically significant. However, for the rest of the analysed times, that was the majority, there were no differences in the release profiles in PBS with pH 6.5 and pH 7.4. So, in general, although the average release is larger in PBS pH 6.5, no statistical significance exists with the release profile in PBS pH 7.4.

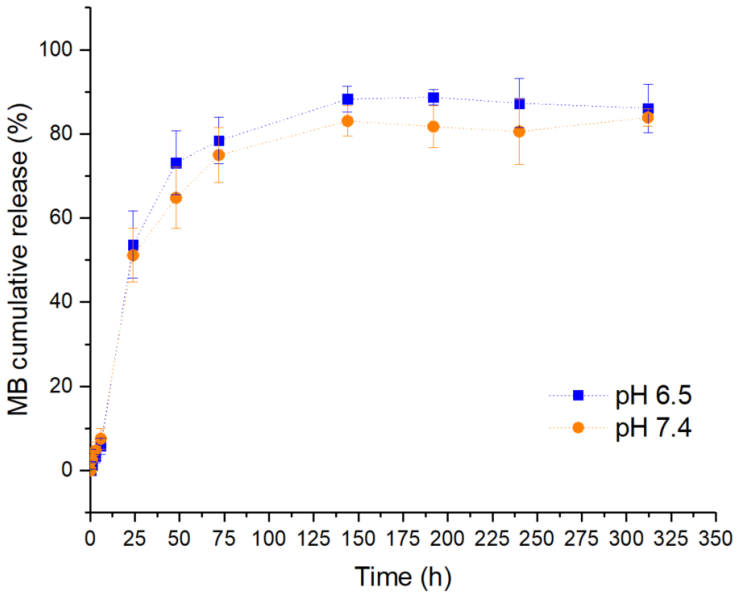

Figure 4.19 MB cumulative release from GG:Alg microparticles in PBS solutions with pH of 6.5 and 7.4

Table 4.5 ANOVA parameters (p - value < 0.05) comparing the release profiles of GG:Alg microparticles in PBS with pH 7.4 and 6.5. Statistically significant times are indicated with an *.

Time (h)	ANOVA parameters between pH 6.5 and 7.4
24	F(1,8) = 0.311, p = 0.592
48	F(1,8) = 3.131, p = 0.115
72h	F(1,8) = 0.797, p = 0.398
144	F(1,8) = 11.673, p = 0.009 *
192	F(1,8) = 17.586, p = 0.003 *
240	F(1,8) = 0.405, p = 0.542
312	F(1,8) = 0.658, p = 0.441

4.2.2.1. Mathematical fittings

Three mathematical models for fitting the experimental data were chosen as previously explained on Chapter 3. The KP (Korsmeyer-Peppas) and the PS (Peppas-Sahlin) models had two variants that included the T_{lag} parameter associated with swellable microparticles, thus in total 5 types of fittings were performed.

In Table 4.6, the obtained fitting parameters are demonstrated. All models had R^2_{adj} above 0.90, with the exception of the KP model. The highest R^2_{adj} were obtained with the KP T_{lag} and SP T_{lag} models, thus better mathematical fittings were obtained using the modified models. T_{lag} accounts for the lag time that is the time that it takes for the drug to diffuse/dissolve before being released, and this lag time can be affected by the swelling of the polymeric matrixes since it increases the diffusion pathways, decrease the drug concentration gradients and thus might affect the time before the release [142, 143]. Thus, since the GG:Alg have high swelling indexes (Figure 4.14 (d)) the introduction of T_{lag} to the KP and SP models accounted the swelling of the microparticles, leading to better fittings [142, 143].

Regarding the release profiles, the KP T_{lag} and SP T_{lag} models, both models revealed a Fickian release profile with $n \leq 0.43$. The normal KP model also revealed a Fickian release profile; however, the PS model revealed an anomalous transport, that is a mixture between a Fickian release profile and a case II transport profile. However, the k_1, that is the contribution of the Fickian release profile in the KP and KP T_{lag} models was far higher than the k_2 contribution, related with the case II transport. The Weibull (W) model also revealed a Fickian release profile, with $b \leq 0.75$. These results are in accordance with previous studies with alginate [33, 34, 144] and gellan gum microparticles [145], where also Fickian release profiles were obtained for microparticles made from similar polysaccharides.

Thus, the release profile was Fickian, and thus, was more dominated by the concentration gradient than by swelling. Regarding pH, the MB release profiles were similar between pH 6.5 and 7.4, with no significant difference between them; however, the release profile with pH 6.5 was slightly higher. Since the swelling impact over the release profile is not

significant, the different swelling indexes between pH 7.4 and pH 6.5 will not affect the release profile of MB from the microparticles.

Table 4.6 Parameter values and R^2_{adj} from the fittings of mathematical models from the release profiles, from DDSolver software. The adjusted R^2 is in bold. The parameters are divided into two columns, one for the PBS with pH of 6.5 and the other for the PBS with pH of 7.4.

pH		pH 6.5	pH 7.4
KP	k	20.760	19.675
	n	0.239	0.238
	R^2adj	**0.8313**	**0.8461**
KP T_{lag}	k	67.111	50.531
	n	0.044	0.081
	T_{lag}	23.994	14.713
	R^2adj	**0.9915**	**0.9819**
W	a	10.989	8.095
	b	0.591	0.466
	R^2adj	**0.9279**	**0.9201**
PS	k_1	12.637	11.920
	k_2	-0.428	-0.405
	m	0.446	0.445
	R^2adj	**0.9228**	**0.9365**
PS T_{lag}	k_1	35.742	31.730
	k_2	-3.575	-2.991
	m	0.264	0.273
	T_{lag}	5.999	5.994
	R_2adj	**0.9893**	**0.9914**

4.2.3. Magnetic microparticles: Combination of the GG:Alg microparticles with SPIONs

The microparticles previously produced, optimized, and characterized via coaxial air-flow technique can be used as a DDS. However, to create a more complex DDS that might be able to be used *in situ* in cancer treatments, we developed a combined system of GG:Alg microparticles with SPIONs to confer hyperthermic properties to the microparticles. As previously mentioned in the introduction, we used SPIONs without coating and SPIONs with APTES coating (addressed as SPIAPTS), to understand if the addition of this type of coating differed when combined with the microparticles.

4.2.3.1. Preparation of the SPIONs with and without APTES coating (SPIAPTS)

SPIONs and SPIAPTs were produced accordingly with the coprecipitation method as explained in Chapter 3. With the DLS technique (Dynamic light scattering), the hydrodynamic diameter, the polydispersity indexes and the Zeta-potential (at ultrapure water pH) are

described in Table 4.7. The increase in charge with APTES coating to above +26 mV are attributed to the coating of amino groups [91, 146].

Table 4.7 Parameters obtained via DLS, hydrodynamic diameter with associated polidispersibilty and Zeta-potential for SPIONs and SPIAPTs

mNPs	Hydrodynamic diameter (nm)	Polydispersity Index	Zeta-Potential (mV)
SPIONs	145.15 ± 23.85	0.13 ± 0.07	+ 4.25 ± 1.28
SPIAPTs	165.44 ± 33.97	0.16 ± 0.09	+ 38.04 ± 7.01

Figure 4.20 (a) and (b) depicts the TEM analysis of the mNPs. Using these images it was found that the average size of the iron core for SPIONs was 8.59±2.03 nm (Figure 4.20 (c)). For SPIAPTs the diameters had 7.55±1.37 nm (Figure 4.20 (d)). A difference between the average and the d(0.5) was noticed, although they were close in both types of nanoparticles. The lower diameters obtained in SPIAPTs might be related to the lower aggregation that the APTES coating confers, thus allowing better viewing of the nanoparticles in TEM. The different diameters obtained from DLS and TEM images are attributed to agglomerations. The DLS technique analysis might detect mNPs agglomerations as one particle. Thus, the DLS analysis gave higher mNPs diameters than the TEM analysis depicts.

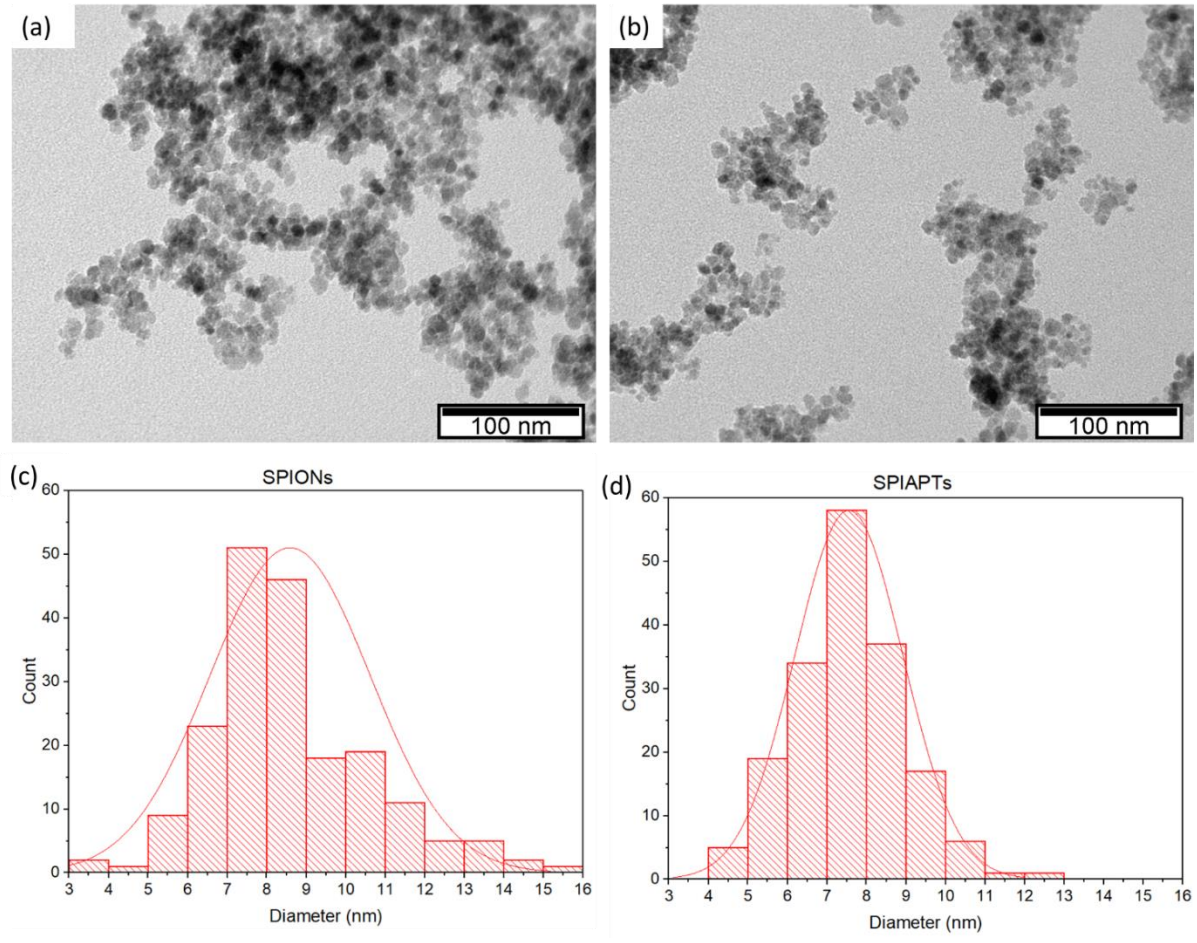

Figure 4.20 TEM analysis of (a) SPIONs and (b) SPIAPTs, and their respective distribution in (c) and (d).

4.2.3.2. Introduction of the mNPs onto the microparticles

The nanoparticles were introduced into the microparticles via adsorption method [82]. The microparticles were introduced within the suspensions with the mNPs with different concentrations of SPIONs and SPIAPTs, to let them swell and adsorb the mNPs to the microparticle's surface.

Figure 4.21 depicts the adsorption efficiency (AE%) of the nanoparticles into the microparticles and adsorption capacity (AC%). Higher adsorption efficiencies were obtained with higher concentrations of mNPs. The coating with APTES appeared to have no influence in the AE% and AC% (See Chapter 3).

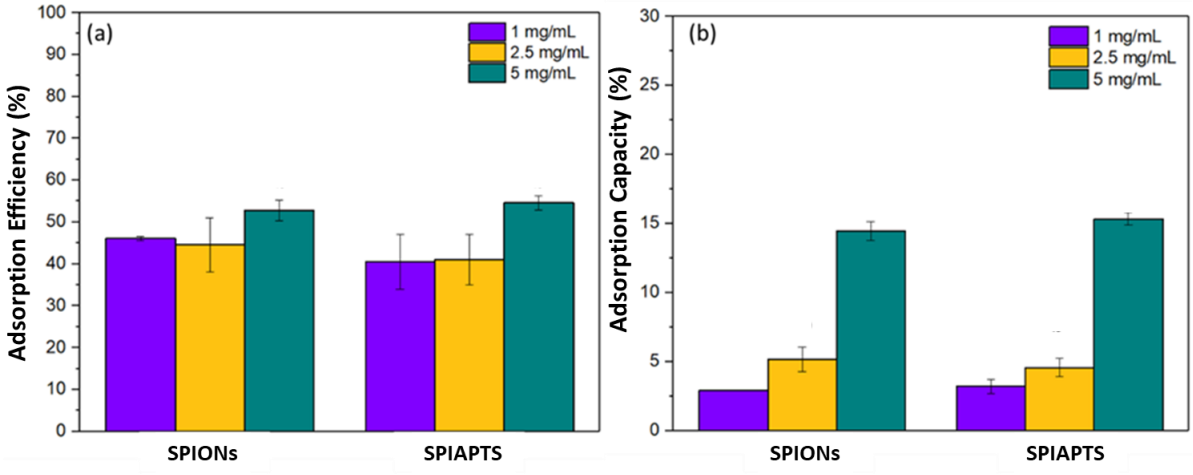

Figure 4.21 Adsorption Efficiency and Adsorption Capacity of SPIONs and SPIAPTs in microparticles and different nanoparticle concentrations (1, 2.5 and 5 mg/mL) via adsorption technique.

After retrieving the microparticles from the nanoparticles suspensions, washing with ultrapure water and drying, the microparticles kept their diameter when compared with the bare microparticles between 150 and 200 µm (Figure 4.14 (a)) [147]. Figure 4.22 depicts the SEM analysis and (b) the EDX (Energy dispersive X-ray) analysis. With this analysis, it is possible to observe agglomerations of mNPs at the microparticles' surface. The EDX analysis confirms that these agglomerations have a high content of iron. Figure 4.22 (c) and (d) show the GG:Alg microparticles loaded with SPIONs under an optical microscope.

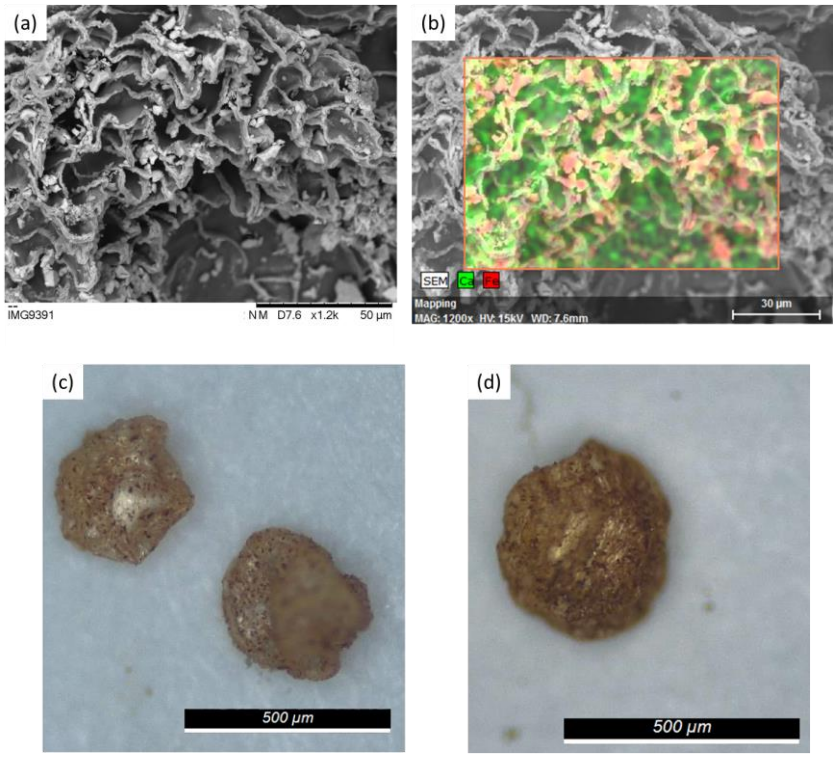

Figure 4.22 SEM analysis (a) and EDX analysis (b) of the surface of a microparticle loaded with SPIONs. In Figure (b) the red zones depict the presence of Iron and the green zones the presence of Calcium. Optical microscope images of (c) polymeric microparticles loaded with SPIONs and (d) SPIAPTs.

4.2.3.3. Magnetic microparticles FTIR, TGA and X-ray Diffraction (XRD)

TGA analysis of the microparticles revealed that the first thermal event at approximately 70 °C was associated with the loss of water from the microparticles (Figure 4.23 (a)). Around 230 °C, all the samples exhibited significant mass loss, associated with the depolymerization of gellan gum and alginate [108, 132–134]. The microparticles that had nanoparticles exhibited a lower weight loss than the microparticles without nanoparticles, likely owing to the inorganic nature of the nanoparticles that did not undergo degradation during thermal analysis [148]. Also, microparticles that were submerged within suspensions of 5 mg/mL had lower weight losses than the ones with 2.5 and 1 mg/mL. This was correlated with the adsorption capacity of the microparticles (Figure 4.21 (b)).

FTIR spectra (Figure 4.23 (b)) show that the GG:Alg microparticles without SPIONs had a band around 3400 and 3100 cm^{-1}, attributed to the -C-H stretching of gellan gum and O-H groups [137]. The -COO stretching (asymmetric) was observed at 1598 cm^{-1}, followed by a symmetric -COOH stretching at 1417 cm^{-1}, and a C-O-C stretching at 1023 cm^{-1} of alginate [34]. The -COO stretching band of gellan gum was likely overlapped with the O-H stretching vibration modes at 1630 cm^{-1}. The microparticles containing SPIONs and SPIAPTs had similar bands to those without mNPs, except for a band at 560 cm^{-1} attributed to the Fe-O stretching vibration mode. The band around 1100 and 800 cm^{-1} can also be associated with Si-O-Si and Si-O stretching vibrations of APTES, respectively [102, 146].

XRD analysis (Figure 4.23 (c)) confirms the presence of mNPs at the GG:Alg microparticles surface. For the two types of microparticles adsorbed with SPIONs and SPIAPTs, peaks at 30º (2 2 0), 35.5º (3 1 1), 57º (5 1 1) and 62.5º (4 4 0) were obtained, typical of iron oxide nanoparticles [149]. The presence of magnetite is confirmed by the peaks at 2θ at 30.1, 35.5, 42.6, 53.6, 57.0 and 62.8 which can be assigned to diffraction of the (220), (311), (400), (422), (511), (440) planes of this phase, respectively [150]. This is corroborated by Khalkhali *et al.* [149]. A peak with a significant width appeared at around 21º, which might have conflicted with the significant peak at 18.25º (1 1 1) significant of SPIONs [149]. This peak was attributed to alginate and gellan gum, and even though they have an amorphous structure, they affect the intensity and peaks in XRD analysis as shown by Mun *et al.* [37].

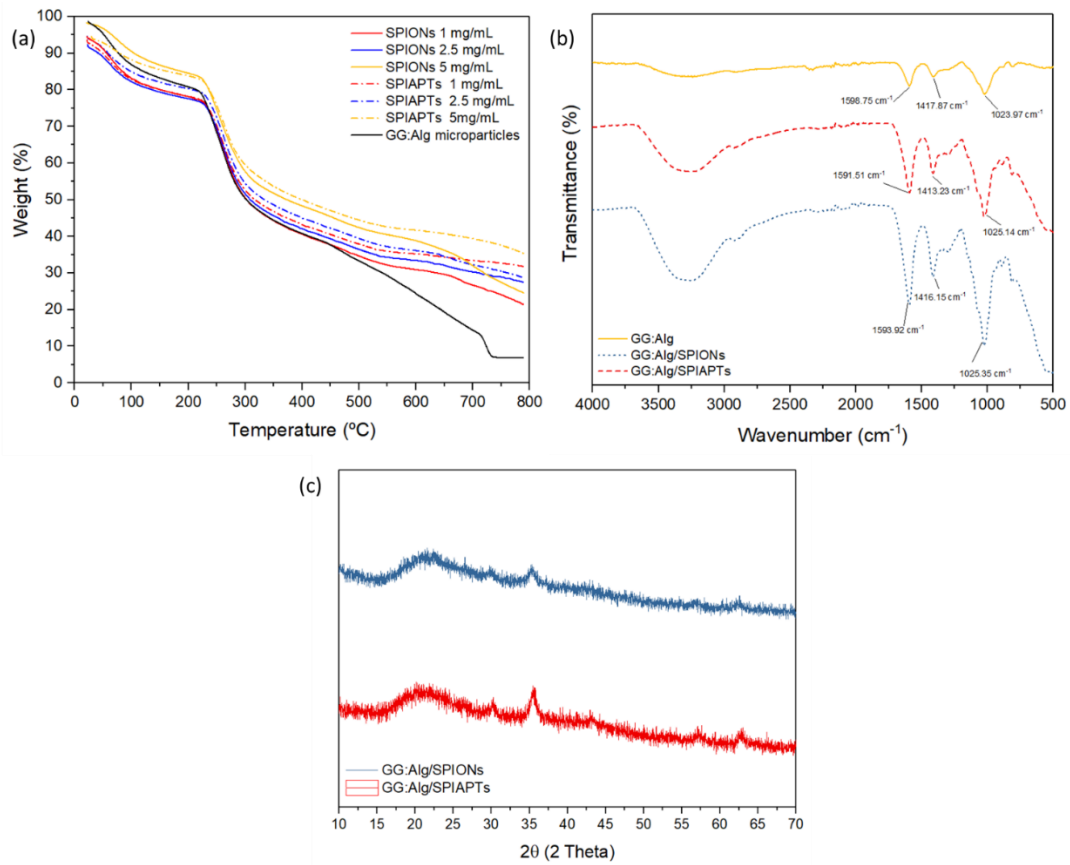

Figure 4.23 (a) Thermal Gravimetry Analysis of GG:Alg microparticles with and without nanoparticles (SPIONs and SPIAPTs) with different concentrations. (b) Fourier-transform infrared spectroscopy of the microparticles with and without nanoparticles (SPIONs and APTES). (c) XRD of the microparticles loaded with SPIONs and SPIAPTs.

4.2.3.4. Swelling and degradation of magnetic microspheres

The adsorption of mNPs to the microparticles appeared to have no significant effect on the microparticle's swelling. All swelling values were similar at the end of 3 days (Figure 4.24 (a)). To understand if the swelling released mNPs, the concentration of mNPs in the PBS solution was measured at the end of 3 days. After 3 days, the microparticles had released 6.57 ±0.58 wt.% of SPIONs and 6.24 ± 1.27 wt.% of SPIAPTs to the respective PBS solutions. Hence, the percentage in weight of mNPs released after swelling was similar between the non-coated

and coated nanoparticles. In Figure 4.24 (b) the mass loss in PBS (pH 6.5) with the time of the microparticles is given. This was attributed to the dissolution of alginate and gellan gum into the PBS, and also of the breakage of the calcium links between the polysaccharidic chains. The microparticles with mNPs lost more mass than the microparticles without mNPs. We attribute this to conjugation between the degradation of the gellan gum/alginate structure and the release of the nanoparticles from the microparticles, hence a higher mass loss was observed.

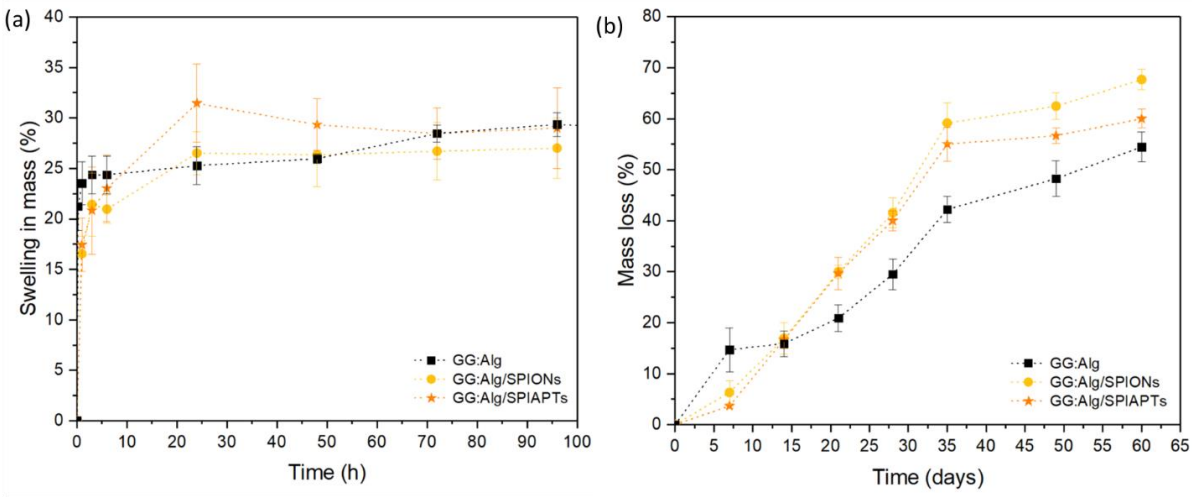

Figure 4.24 (a) Swelling in mass in PBS (pH 6.5) with and without mNPs; (b) Degradation (mass loss) in microparticles with and without mNPs.

4.2.3.5. *in vitro* cytotoxicity of the microparticles

Before conjugating the GG:Alg microparticles with and without mNPs into a thermoresponsive hydrogel, it is fundamental to understand if they have a benign or harmful impact on the surrounding cells. Thus, cytotoxicity assays were performed, and are displayed in Figure 4.25. No cytotoxicity was found on the microparticles with and without mNPs. Different microparticles with SPIONs that were submerged in suspensions with different concentrations of mNPs were tested and showed no significant differences between them. Although viable, the microparticles with SPIAPTs caused lower cell viability than the ones with SPIONs. Cytotoxicity depends on many factors, such as the type of cell and type of coating [151]. For example, Alpdemir *et al.* [107] found that alginate microparticles containing SPIONs had no negative effects on L929 fibroblast and HEPG2 liver cancer cell lines. T-tests (two-tailed and independent with unequal variance) were performed comparing each sample to the control. No statistically significant differences were found for the different samples.

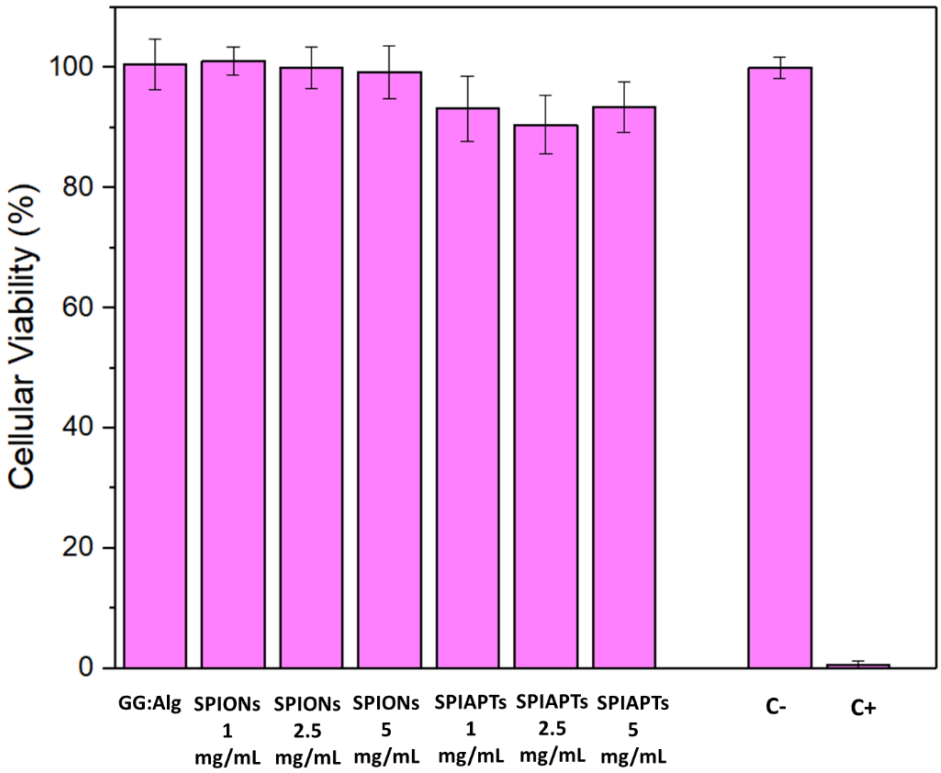

Figure 4.25 VERO cell viability (%) after 48h of indirect exposure to the developed microparticles with and without mNPs (GG:Alg). Microparticles that were submerged in different concentrations of mNPs (1, 2.5 and 5 mg/mL) were analyzed. Data were expressed as mean ± standard deviation for at least four experiments. C- is the negative control (no medium alterations) and C+ is the positive control (medium with 10 µL of DMSO).

4.2.4. Magnetic hyperthermia assays

Magnetic hyperthermia tests were conducted to determine whether the mNPs were capable of increasing their temperature within the microparticle structure under the application of an Alternating Magnetic Field (AMF). Figure 4.26 (a) shows the temperature increase of microparticles with mNPs and the original mNPs suspensions. The aqueous suspensions of SPIONs and SPIAPTs exhibited different temperature increases, with the former being significantly higher. This was attributed to the presence of the APTES coating. With the GG:Alg microparticles the temperature variations were lower, from 3 to 4 ºC. This was attributed to restriction of Brownian movements, since the nanoparticles were mobilized at the surface of the microparticles, and the temperature increase only occurring due to Néel relaxation with the application of the AMF, reducing the temperature variation [87, 146, 152]. The microparticles with SPIONs had a temperature increase of 3.03 ± 0.51ºC and the microparticles with SPIAPTs 4.40 ± 0.75ºC. With a ANOVA study, it was revealed that no statistically significant differences was observed between the two types of microparticles (with SPIONs and SPIAPTEs) ($F(1, 4) = [6.724]$, $p = 0.06$). Table 4.8 presents the specific absorption rate (SAR) values, has previously explained in Chapter 3. The values follow the trend from the temperature variations of Figure 4.26, where higher SAR was obtained from the free nanoparticle suspensions, with the SPIONs suspension having a higher energy absorption rate.

These temperatures might be further optimized in the future by increasing the concentration of mNPs within the microparticles, for example by increasing the concentration of the original suspension (above 5 mg/mL) [82]. However, even with these temperature increases, sufficient *in vivo* temperatures capable of tumour cells apoptosis might be achieved, since for tumour cell apoptosis the temperature should be in the range from 42ºC to 46ºC [153].

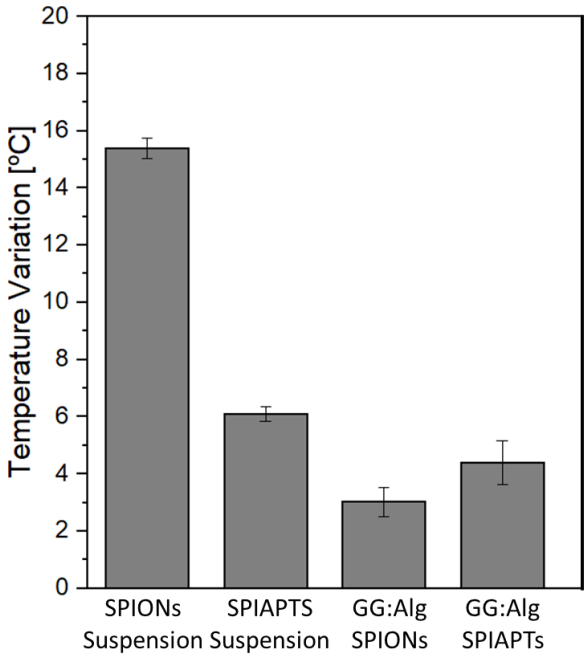

Figure 4.26 Magnetic hyperthermia study: Temperature variation with the application of an alternating magnetic field (300 Gauss and 388.5 kHz, 10 minutes).

Table 4.8 SAR values of the magnetic hyperthermia study over the SPIONs and SPIAPTs suspensions and the microparticles loaded with the nanoparticles.

Sample	SAR (W/g)
SPIONs suspension	21.04±0.51
SPIAPTs suspension	8.34±0.36
GG:Alg SPIONs	4.14±0.70
GG:Alg SPIAPTs	6.02±1.03

4.3. Conclusions

In this chapter, the objective was to optimize the production of microparticles made from alginate (Alg) and gellan gum (GG) using the coaxial air-flow technique with the goals of understanding the factors that most influenced the production, and of minimizing the microparticles size and size dispersibility. Then, after the characterization of the microparticles, SPIONs were added to the microparticles to add sensibility to an AMF for hyperthermia purposes.

In GG:Alg microparticles production optimization, the goal was to identify the factors that most significantly influenced production, while minimizing particle size and dispersibility. The parameters chosen to study were: pump flow, air-flow, the distance between the nozzle and $CaCl_2$ bath, and the ratio between GG and Alg (which mainly affected the viscosity).

The particle size was mostly influenced by the air-flow, with higher flows leading to smaller diameters. However, the air-flow also significantly affected dispersibility, where higher air-flow increasing COV and SPAN values. Thus, a compromise was achieved by sacrificing dispersibility and decreasing the size of the microparticles. The GG:Alg ratio also significantly affected the dispersibility, whereas the more viscous solutions had lower dispersibility. The pump flow also influenced the size of the microparticles, which had a positive effect. The distance between the nozzle and the $CaCl_2$ bath had no statistically significant effect.

The produced microparticles had an average diameter of 414.30 ±36.40 µm at the wet stage but decreased to 171.0 ± 36.0 µm when dried. The swelling, degradation, and encapsulation of MB are affected by the pH of the solution, with pH 7.4 leading to higher degradation, swelling and EE% and LC%. This was due to the anionic nature of gellan gum and alginate.

Following the characterization of the microparticles, SPIONs were adsorbed into the microparticles to develop systems suitable for use in magnetic hyperthermia therapy. mNPs, were successfully adsorbed onto microparticles' surface. Suspensions of different concentrations were used to determine the optimal conditions for producing these magnetic microparticles. Submerging the microparticles in suspensions with higher concentrations of mNPs (5 mg/mL) produced higher adsorption efficiency and adsorption capacity The nanoparticles formed clusters on the microparticle surface. SPIONs and SPIAPTs were used, with no significant differences between them when adsorbed onto microparticles' surface. The microparticles produced with and without mNPs were found to be non-cytotoxic. Magnetic hyperthermia tests revealed that the mNPs adsorbed onto the microparticle's surface produced a lower temperature variation than the mNPs suspensions, but the temperature variations were around 3 to 4 °C. Higher variations could be achieved by increasing the number of mNPs in the microparticles, but further studies need to be done.

4.4. References

1. Kim KK, Pack DW, Ferrari M, et al (2006) Microspheres for Drug Delivery. BioMEMS Biomed Nanotechnol 19–50. https://doi.org/10.1007/978-0-387-25842-3_2
2. Lengyel M, Kállai-Szabó N, Antal V, et al (2019) Microparticles, microspheres, and microcapsules for advanced drug delivery. Sci Pharm 87:. https://doi.org/10.3390/scipharm87030020
3. Nejati S, Mohseni Vadeghani E, Khorshidi S, Karkhaneh A (2020) Role of particle shape on efficient and organ-based drug delivery. Eur Polym J 122:109353.

https://doi.org/10.1016/j.eurpolymj.2019.109353

4. Goyanes A, Robles Martinez P, Buanz A, et al (2015) Effect of geometry on drug release from 3D printed tablets. Int J Pharm 494:657–663. https://doi.org/10.1016/j.ijpharm.2015.04.069

5. Serra CA, Cortese B, Khan IU, et al (2013) Coupling Microreaction Technologies , Polymer Chemistry , and Processing to Produce Polymeric Micro and Nanoparticles with Controlled Size , Morphology , and Composition. 414–439. https://doi.org/10.1002/mren.201300101

6. Delgado B, Carrêlo H, Loureiro M V., et al (2021) Injectable hydrogels with two different rates of drug release based on pluronic / water system filled with poly (e -caprolactone) microcapsules. J Mater Sci. https://doi.org/10.1007/s10853-021-06156-x

7. Carrêlo H, Soares PIP, Borges JP, Cidade MT (2021) Injectable composite systems based on microparticles in hydrogels for bioactive cargo controlled delivery. Gels 7:. https://doi.org/10.3390/gels7030147

8. Yoo J, Won Y (2020) Phenomenology of the Initial Burst Release of Drugs from PLGA Microparticles. ACS Biomater Sci Eng. https://doi.org/10.1021/acsbiomaterials.0c01228

9. Brzeziński M, Kost B, Wedepohl S, et al (2019) Stereocomplexed PLA microspheres: Control over morphology, drug encapsulation and anticancer activity. Colloids Surfaces B Biointerfaces 184:. https://doi.org/10.1016/j.colsurfb.2019.110544

10. Xu K, An N, Zhang H, et al (2020) Sustained-release of PDGF from PLGA microsphere embedded thermo-sensitive hydrogel promoting wound healing by inhibiting autophagy. J Drug Deliv Sci Technol 55:. https://doi.org/10.1016/j.jddst.2019.101405

11. Devi N, Kakati DK (2013) Smart porous microparticles based on gelatin/sodium alginate polyelectrolyte complex. J Food Eng 117:193–204. https://doi.org/10.1016/j.jfoodeng.2013.02.018

12. Reddy MSB, Ponnamma D, Choudhary R, Sadasivuni KK (2021) A comparative review of natural and synthetic biopolymer composite scaffolds. Polymers (Basel) 13:. https://doi.org/10.3390/polym13071105

13. Amarakoon M, Alenezi H, Homer-Vanniasinkam S, Edirisinghe M (2022) Environmental Impact of Polymer Fiber Manufacture. Macromol Mater Eng 307:1–20. https://doi.org/10.1002/mame.202200356

14. Augst AD, Kong HJ, Mooney DJ (2006) Alginate hydrogels as biomaterials. Macromol Biosci 6:623–633. https://doi.org/10.1002/mabi.200600069

15. Bacelar AH, Silva-Correia J, Oliveira JM, Reis RL (2016) Recent progress in gellan gum hydrogels provided by functionalization strategies. J Mater Chem B 4:6164–6174. https://doi.org/10.1039/c6tb01488g

16. Milivojevic M, Pajic-Lijakovic I, Bugarski B, et al (2019) Gellan gum in drug delivery applications. In: Natural Polysaccharides in Drug Delivery and Biomedical Applications. Elsevier Inc., pp 145–186

17. Liang Y, Kashdan T, Sterner C, et al (2015) Algal Biorefineries. In: Industrial Biorefineries

and White Biotechnology. Elsevier B.V., pp 35–90

18. Morris ER, Nishinari K, Rinaudo M (2012) Gelation of gellan - A review. Food Hydrocoll 28:373–411. https://doi.org/10.1016/j.foodhyd.2012.01.004

19. Alvarez-Lorenzo C, Blanco-Fernandez B, Puga AM, Concheiro A (2013) Crosslinked ionic polysaccharides for stimuli-sensitive drug delivery. Adv Drug Deliv Rev 65:1148–1171. https://doi.org/10.1016/j.addr.2013.04.016

20. Mahajan HS, Gattani SG (2009) Gellan gum based microparticles of metoclopromide hydrochloride for intranasal delivery: Development and evaluation. Chem Pharm Bull 57:388–392. https://doi.org/10.1248/cpb.57.388

21. Gasperini L, Mano JF, Reis RL (2014) Natural polymers for the microencapsulation of cells. J R Soc Interface 11:. https://doi.org/10.1098/rsif.2014.0817

22. Voo WP, Ooi CW, Islam A, et al (2016) Calcium alginate hydrogel beads with high stiffness and extended dissolution behaviour. Eur Polym J 75:343–353. https://doi.org/10.1016/j.eurpolymj.2015.12.029

23. Sanderson GR, Ortega D (1994) Alginates and Gellan Gum: Complementary Gelling Agents. 83–89. https://doi.org/10.1007/978-1-4615-2486-1_8

24. Xue W, Liu XL, Ma H, et al (2018) AMF responsive DOX-loaded magnetic microspheres: Transmembrane drug release mechanism and multimodality postsurgical treatment of breast cancer. J Mater Chem B 6:2289–2303. https://doi.org/10.1039/c7tb03206d

25. Hunter Joyce M, Lu C, James ER, et al (2018) Phenotypic basis for matrix stiffness-dependent chemoresistance of breast cancer cells to doxorubicin. Front Oncol 8:. https://doi.org/10.3389/fonc.2018.00337

26. Jayapal JJ, Dhanaraj S (2017) Exemestane loaded alginate nanoparticles for cancer treatment: Formulation and in vitro evaluation. Int J Biol Macromol 105:416–421. https://doi.org/10.1016/j.ijbiomac.2017.07.064

27. Román J V., Galán MA, Del Valle EMM (2016) Preparation and preliminary evaluation of alginate crosslinked microcapsules as potential drug delivery system (DDS) for Human lung cancer therapy. Biomed Phys Eng Express 2:1–13. https://doi.org/10.1088/2057-1976/2/3/035015

28. Arica B, Çaliş S, Kaş HS, et al (2002) 5-Fluorouracil encapsulated alginate beads for the treatment of breast cancer. Int J Pharm 242:267–269. https://doi.org/10.1016/S0378-5173(02)00172-2

29. Zhou S, Zheng X, Yi K, et al (2022) Temperature-Ion-pH Triple Responsive Gellan Gum as In Situ Hydrogel for Long-Acting Cancer Treatment

30. Hsu MF, Tyan YS, Chien YC, Lee MW (2018) Hyaluronic acid-based nano-sized drug carrier-containing Gellan gum microspheres as potential multifunctional embolic agent. Sci Rep 8:1–10. https://doi.org/10.1038/s41598-018-19191-7

31. Rodrigues DB, Moreira HR, Cerqueira MT, et al (2022) Highly tailorable gellan gum nanoparticles as a platform for the development of T cell activator systems. Biomater Res 26:1–19. https://doi.org/10.1186/s40824-022-00297-z

32. Nieto C, Vega MA, Rodríguez V, et al (2022) Biodegradable gellan gum hydrogels loaded with paclitaxel for HER2+ breast cancer local therapy. Carbohydr Polym 294:. https://doi.org/10.1016/j.carbpol.2022.119732

33. de Farias AL, Meneguin AB, da Silva Barud H, Brighenti FL (2020) The role of sodium alginate and gellan gum in the design of new drug delivery systems intended for antibiofilm activity of morin. Int J Biol Macromol 162:1944–1958. https://doi.org/10.1016/j.ijbiomac.2020.08.078

34. Jana S, Das A, Nayak AK, et al (2013) Aceclofenac-loaded unsaturated esterified alginate/gellan gum microspheres: In vitro and in vivo assessment. Int J Biol Macromol 57:129–137. https://doi.org/10.1016/j.ijbiomac.2013.03.015

35. Rosas-Flores W, Ramos-Ramírez EG, Salazar-Montoya JA (2013) Microencapsulation of Lactobacillus helveticus and Lactobacillus delbrueckii using alginate and gellan gum. Carbohydr Polym 98:1011–1017. https://doi.org/10.1016/j.carbpol.2013.06.077

36. Reczyńska-kolman K, Hartman K, Kwiecień K, et al (2022) Composites based on gellan gum, alginate and nisin-enriched lipid nanoparticles for the treatment of infected wounds. Int J Mol Sci 23:. https://doi.org/10.3390/ijms23010321

37. Mun S, Kim HC, Yadave M, Kim J (2015) Graphene oxide-gellan gum-sodium alginate nanocomposites: Synthesis, characterization, and mechanical behavior. Compos Interfaces 22:249–263. https://doi.org/10.1080/09276440.2015.1018716

38. Akkineni A, Ahlfeld T, Funk A, et al (2016) Highly Concentrated Alginate-Gellan Gum Composites for 3D Plotting of Complex Tissue Engineering Scaffolds. Polymers (Basel) 8:170. https://doi.org/10.3390/polym8050170

39. Young S, Wong M, Tabata Y, Mikos AG (2005) Gelatin as a delivery vehicle for the controlled release of bioactive molecules. J Control Release 109:256–274. https://doi.org/10.1016/j.jconrel.2005.09.023

40. Lima AC, Sher P (2012) Production methodologies of polymeric and hydrogel particles for drug delivery applications. 231–248

41. Finotelli PV, Da Silva D, Sola-Penna M, et al (2010) Microcapsules of alginate/chitosan containing magnetic nanoparticles for controlled release of insulin. Colloids Surfaces B Biointerfaces 81:206–211. https://doi.org/10.1016/j.colsurfb.2010.07.008

42. Wen H, Gao T, Fu Z, et al (2017) Enhancement of membrane stability on magnetic responsive hydrogel microcapsules for potential on-demand cell separation. Carbohydr Polym 157:1451–1460. https://doi.org/10.1016/j.carbpol.2016.11.022

43. Ramana Reddy KV, Gupta J, Izharuddin P (2019) Alginate Microspheres: The Innovative Approaches to Production of the Microbeads/Micro-Particles. J Drug Deliv Ther 9:774–781. https://doi.org/10.22270/jddt.v9i4-s.3413

44. Mahou R, Vlahos AE, Shulman A, Sefton M V. (2018) Interpenetrating Alginate-Collagen Polymer Network Microspheres for Modular Tissue Engineering. ACS Biomater Sci Eng 4:3704–3712. https://doi.org/10.1021/acsbiomaterials.7b00356

45. Čalija B, Cekić N, Savić S, et al (2013) PH-sensitive microparticles for oral drug delivery

based on alginate/oligochitosan/Eudragit® L100-55 "sandwich" polyelectrolyte complex. Colloids Surfaces B Biointerfaces 110:395–402. https://doi.org/10.1016/j.colsurfb.2013.05.016

46. Workamp M, Alaie S, Dijksman JA (2016) Coaxial air-flow device for the production of millimeter-sized spherical hydrogel particles. Rev Sci Instrum 87:. https://doi.org/10.1063/1.4972587

47. Prüsse U, Bilancetti L, Bučko M, et al (2008) Comparison of different technologies for alginate beads production. Chem Pap 62:364–374. https://doi.org/10.2478/s11696-008-0035-x

48. Enayati M, Ahmad Z, Stride E, Edirisinghe M (2010) Preparation of Polymeric Carriers for Drug Delivery with Different Shape and Size Using an Electric Jet. 600–608

49. Park S, Hwang S, Lee J (2011) pH-responsive hydrogels from moldable composite microparticles prepared by coaxial electro-spray drying. Chem Eng J 169:348–357. https://doi.org/10.1016/j.cej.2011.02.063

50. Davoodi P, Feng F, Xu Q, et al (2014) Coaxial electrohydrodynamic atomization : Microparticles for drug delivery applications. J Control Release. https://doi.org/10.1016/j.jconrel.2014.12.004

51. Sosnik A (2014) Production of Drug-Loaded Polymeric Nanoparticles by Electrospraying Technology. 10:. https://doi.org/10.1166/jbn.2014.1887

52. Zhang L, Huang J, Si T, X Xu R (2012) Coaxial electrospray of microparticles and nanoparticles for biomedical applications. Expert Rev Med Devices 9:596–612. https://doi.org/10.1586/erd.12.58.

53. John J V, Mccarthy A, Wang H, et al (2020) Engineering Biomimetic Nanofiber Microspheres with Tailored Size , Predesigned Structure , and Desired Composition via Gas Bubble – Mediated Coaxial Electrospray. 1907393:1–9. https://doi.org/10.1002/smll.201907393

54. Sakaeda T (1998) O / W Lipid Emulsions for Parenteral Drug Delivery . 111 . Lipophilicity Necessary for Incorporation in Oil Particles Even After Intravenous Injection. 6:119–127

55. Kietzmann D, Béduneau A, Pellequer Y, Lamprecht A (2009) pH-sensitive microparticles prepared by an oil / water emulsification method using n-butanol. 375:61–66. https://doi.org/10.1016/j.ijpharm.2009.04.006

56. Zheng W (2009) A water-in-oil-in-oil-in-water (W / O / O / W) method for producing drug-releasing , double-walled microspheres. 374:90–95. https://doi.org/10.1016/j.ijpharm.2009.03.015

57. Ansary RH, Rahman MM, Awang MB, et al (2016) Preparation, characterization and in vitro release study of BSA-loaded double-walled glucose-poly(lactide-co-glycolide) microspheres. https://doi.org/10.1007/s12272-016-0710-3

58. Grenha A, Gomes ME, Rodrigues M, et al (2010) Development of new chitosan/carrageenan nanoparticles for drug delivery applications. J Biomed Mater Res - Part A 92:1265–1272. https://doi.org/10.1002/jbm.a.32466

59. Obaidat RM, Alnaief M, Mashaqbeh H (2018) Investigation of Carrageenan Aerogel Microparticles as a Potential Drug Carrier. AAPS PharmSciTech 19:2226–2236. https://doi.org/10.1208/s12249-018-1021-4

60. Liu D, Zhang H, Fontana F (2017) Microfluidic-assisted fabrication of carriers for controlled drug delivery. 1856–1883. https://doi.org/10.1039/c7lc00242d

61. Tran TM, Lan F, Thompson CS, Abate AR (2013) From tubes to drops: Droplet-based microfluidics for ultrahigh-throughput biology. J Phys D Appl Phys 46:. https://doi.org/10.1088/0022-3727/46/11/114004

62. Khan IU, Serra CA, Anton N, Vandamme T (2013) Microfluidics: A focus on improved cancer targeted drug delivery systems. J Control Release 172:1065–1074. https://doi.org/10.1016/j.jconrel.2013.07.028

63. Yoon DH, Hasegawa K, Kaneko Y, et al (2015) Formation of polymeric hollow microcapsules and microlenses using gas-in-organic-in-water droplets. Micromachines 6:622–633. https://doi.org/10.3390/mi6050622

64. Kong T, Wu J, Yeung KWK, et al (2013) Microfluidic fabrication of polymeric core-shell microspheres for controlled release applications. Biomicrofluidics 7:1–9. https://doi.org/10.1063/1.4819274

65. Qamar AZ, Shamsi MH (2020) Desktop fabrication of lab-on-chip devices on flexible substrates: A brief review. Micromachines 11:. https://doi.org/10.3390/mi11020126

66. Lababidi N, Sigal V, Koenneke A, et al (2019) Microfluidics as tool to prepare size-tunable PLGA nanoparticles with high curcumin encapsulation for efficient mucus penetration. Beilstein J Nanotechnol 10:2280–2293. https://doi.org/10.3762/bjnano.10.220

67. Busatto CA, Taverna ME, Lescano MR, et al (2019) Preparation and Characterization of Lignin Microparticles-in-Alginate Beads for Atrazine Controlled Release. J Polym Environ 27:2831–2841. https://doi.org/10.1007/s10924-019-01564-2

68. Martins C, Chauhan VM, Selo AA, et al (2020) Modelling protein therapeutic co-formulation and co-delivery with PLGA nanoparticles continuously manufactured by microfluidics. React Chem Eng 5:308–319. https://doi.org/10.1039/c9re00395a

69. Ré M (2007) Formulating Drug Delivery Systems by Spray Drying Formulating Drug Delivery Systems by Spray Drying ˆ s Re. Dry Technol An Int J 37–41. https://doi.org/10.1080/07373930600611877

70. Helmy W, Sallam M, Fang J, Elkhodairy KA (2018) Dual-targeted casein micelles as green nanomedicine for synergistic phytotherapy of hepatocellular carcinoma. J Control Release #pagerange#. https://doi.org/10.1016/j.jconrel.2018.08.026

71. Iglesias I, Benedı J (2011) Paclitaxel-loaded polyester nanoparticles prepared by spray-drying technology : in vitro bioactivity evaluation. 28:417–429. https://doi.org/10.3109/02652048.2011.576785

72. Sastre RL, Olmo R, Blanco MD (2007) 5-Fluorouracil plasma levels and biodegradation of subcutaneously injected drug-loaded microspheres prepared by spray-drying poly (

d , l -lactide) and poly (d , l -lactide-co-glycolide) polymers. 338:180–190. https://doi.org/10.1016/j.ijpharm.2007.02.001

73. Lopedota A, Cutrignelli A, Laquintana V, et al (2016) Spray Dried Chitosan Microparticles for Intravesical Delivery of Celecoxib : Preparation and Characterization. 2195–2208. https://doi.org/10.1007/s11095-016-1956-7

74. Vishali DA, Monisha J, Sivakamasundari SK, et al (2019) Spray freeze drying : Emerging applications in drug delivery. J Control Release 300:93–101. https://doi.org/10.1016/j.jconrel.2019.02.044

75. Fukushige K, Tagami T, Naito M, et al (2020) Developing spray-freeze-dried particles containing a hyaluronic acid-coated liposome – protamine – DNA complex for pulmonary inhalation. Int J Pharm 583:119338. https://doi.org/10.1016/j.ijpharm.2020.119338

76. Roa WH, Azarmi S, Al-hallak MHDK, et al (2011) Inhalable nanoparticles , a non-invasive approach to treat lung cancer in a mouse model. 150:49–55. https://doi.org/10.1016/j.jconrel.2010.10.035

77. Costa AMS, Alatorre-meda M, Alvarez-lorenzo C, Mano JF (2015) Superhydrophobic Surfaces as a Tool for the Fabrication of Hierarchical Spherical Polymeric Carriers. 1–5. https://doi.org/10.1002/smll.201500192

78. Song B (2018) Lotus leaf-inspired design of calcium alginate particles with superhigh drug encapsulation efficiency and pH responsive release. Colloids Surfaces B Biointerfaces. https://doi.org/10.1016/j.colsurfb.2018.09.001

79. Puga AM, Catarina A, Mano JF, et al (2013) Pectin-coated chitosan microgels crosslinked on superhydrophobic surfaces for 5-fluorouracil encapsulation. 98:331–340

80. Emer C, Hildebrand LS, Friedrich B, et al (2023) In Vitro Analysis of Superparamagnetic Iron Oxide Nanoparticles Coated with APTES as Possible Radiosensitizers for HNSCC Cells. Nanomaterials 13:. https://doi.org/10.3390/nano13020330

81. Musielak M, Piotrowski I, Suchorska WM (2019) Superparamagnetic iron oxide nanoparticles (SPIONs) as a multifunctional tool in various cancer therapies. Reports Pract Oncol Radiother 24:307–314. https://doi.org/10.1016/j.rpor.2019.04.002

82. Matos RJR, Chaparro CIP, Silva JC, et al (2018) Electrospun composite cellulose acetate/iron oxide nanoparticles non-woven membranes for magnetic hyperthermia applications. Carbohydr Polym 198:9–16. https://doi.org/10.1016/j.carbpol.2018.06.048

83. Soares PIP, Sousa AI, Silva JC, et al (2016) Chitosan-based nanoparticles as drug delivery systems for doxorubicin: Optimization and modelling. Carbohydr Polym 147:304–312. https://doi.org/10.1016/j.carbpol.2016.03.028

84. Martins PM, Lima AC, Ribeiro S, et al (2021) Magnetic Nanoparticles for Biomedical Applications : From the Soul of the Earth to the Deep History of Ourselves. https://doi.org/10.1021/acsabm.1c00440

85. Soares PIP, Alves AMR, Pereira LCJ, et al (2014) Effects of surfactants on the magnetic properties of iron oxide colloids. J Colloid Interface Sci 419:46–51.

https://doi.org/10.1016/j.jcis.2013.12.045

86. Belyanina I, Kolovskaya O, Zamay S, et al (2017) Targeted magnetic nanotheranostics of cancer. Molecules 22:1–19. https://doi.org/10.3390/molecules22060975

87. Ota S, Takemura Y (2019) Characterization of Néel and Brownian Relaxations Isolated from Complex Dynamics Influenced by Dipole Interactions in Magnetic Nanoparticles. J Phys Chem C 123:28859–28866. https://doi.org/10.1021/acs.jpcc.9b06790

88. Ivkov R, Denardo SJ, Daum W, et al (2005) Application of High Amplitude Alternating Magnetic Fields for Heat Induction of Nanoparticles Localized in Cancer. 11:7093–7104. https://doi.org/10.1158/1078-0432.CCR-1004-0016

89. Arami H, Khandhar A, Liggitt D, Krishnan KM (2015) In vivo delivery, pharmacokinetics, biodistribution and toxicity of iron oxide nanoparticles. Chem Soc Rev. https://doi.org/10.1039/C5CS00541H

90. Bustamante-Torres M, Romero-Fierro D, Estrella-Nuñez J, et al (2022) Polymeric Composite of Magnetite Iron Oxide Nanoparticles and Their Application in Biomedicine: A Review. Polymers (Basel) 14:. https://doi.org/10.3390/polym14040752

91. Chaparro CIP, Loureiro LR, Valente M, et al (2019) Application of Hyperthermia for Cancer Treatment: Synthesis and Characterization of Magnetic Nanoparticles and their internalization on Tumor Cell Lines. In: 2019 IEEE 6th Portuguese Meeting on Bioengineering (ENBENG). IEEE, Lisbon, Portugal

92. Soares PIP (2015) Chitosan-based magnetic nanoparticles for osteosarcoma theranostic. Universidade Nova de Lisboa- Faculdade de Ciências e Tecnologias

93. Soares PIP, Machado D, Laia C, et al (2016) Thermal and magnetic properties of chitosan-iron oxide nanoparticles. Carbohydr Polym 149:382–390. https://doi.org/10.1016/j.carbpol.2016.04.123

94. Cardoso VF, Francesko A, Ribeiro C, et al (2017) Advances in Magnetic Nanoparticles for Biomedical Applications. 1700845:1–35. https://doi.org/10.1002/adhm.201700845

95. Schneider M, Otarola J, Vakarelska E, et al (2022) Biomedical Applications of Iron Oxide Nanoparticles : Current Insights Progress and Perspectives

96. Soares PIP, Sousa AI, Ferreira IMM, et al (2016) Towards the development of multifunctional chitosan-based iron oxide nanoparticles: Optimization and modelling of doxorubicin release. Carbohydr Polym 153:212–221. https://doi.org/10.1016/j.carbpol.2016.07.109

97. Janko C, Ratschker T, Nguyen K, et al (2019) Functionalized superparamagnetic iron oxide nanoparticles (SPIONs) as platform for the targeted multimodal tumor therapy. Front Oncol 9:1–9. https://doi.org/10.3389/fonc.2019.00059

98. Turrina C, Oppelt A, Mitzkus M, et al (2022) Silica - coated superparamagnetic iron oxide nanoparticles : New insights into the influence of coating thickness on the particle properties and lasioglossin binding Materials and methods Synthesis of IONs @ TEOS Peptide binding Characterization Results a. MRS Commun 12:632–639. https://doi.org/10.1557/s43579-022-00228-y

99. Liu Y, Li Y, Li XM, He T (2013) Kinetics of (3-aminopropyl)triethoxylsilane (aptes) silanization of superparamagnetic iron oxide nanoparticles. Langmuir 29:15275–15282. https://doi.org/10.1021/la403269u

100. Sodipo BK, Aziz AA (2014) A sonochemical approach to the direct surface functionalization of superparamagnetic iron oxide nanoparticles with (3-aminopropyl)triethoxysilane. Beilstein J Nanotechnol 5:1472–1476. https://doi.org/10.3762/bjnano.5.160

101. Lu A, Salabas EL, Schüth F (2007) Magnetic Nanoparticles : Synthesis , Protection , Functionalization , and Application Angewandte. 1222–1244. https://doi.org/10.1002/anie.200602866

102. Villa S, Riani P, Locardi F, Canepa F (2016) Functionalization of Fe3O4 NPs by silanization: Use of amine (APTES) and thiol (MPTMS) silanes and their physical characterization. Materials (Basel) 9:. https://doi.org/10.3390/ma9100826

103. Sypabekova M, Hagemann A, Rho D, Kim S (2023) Review : 3-Aminopropyltriethoxysilane (APTES) Deposition Methods on Oxide Surfaces in Solution and Vapor Phases for Biosensing Applications

104. Chavez DH, Juarez-moreno K, Hirata GA (2016) Aminosilane Functionalization and Cytotoxicity Effects of Upconversion Nanoparticles Y 2 O 3 and Gd 2 O 3. 1–7. https://doi.org/10.5772/62252

105. Wu Y, Lu Z, Li Y, et al (2020) Surface modification of iron oxide-based magnetic nanoparticles for cerebral theranostics: Application and prospection. Nanomaterials 10:1–21. https://doi.org/10.3390/nano10081441

106. Freire TM, Dutra LMU, Queiroz DC, et al (2016) Fast ultrasound assisted synthesis of chitosan-based magnetite nanocomposites as a modified electrode sensor. Carbohydr Polym 151:760–769. https://doi.org/10.1016/j.carbpol.2016.05.095

107. Alpdemir Ş, Vural T, Kara G, et al (2020) Magnetically responsive, sorafenib loaded alginate microspheres for hepatocellular carcinoma treatment. IET Nanobiotechnology 14:623–627. https://doi.org/10.1049/iet-nbt.2020.0139

108. Patel N, Lalwani D, Gollmer S, et al (2016) Development and evaluation of a calcium alginate based oral ceftriaxone sodium formulation. Prog Biomater 5:117–133. https://doi.org/10.1007/s40204-016-0051-9

109. Li J, Wu Y, He J, Huang Y (2016) A new insight to the effect of calcium concentration on gelation process and physical properties of alginate films. J Mater Sci 51:5791–5801. https://doi.org/10.1007/s10853-016-9880-0

110. Amer MH, Rose FRAJ, Shakesheff KM, et al (2017) Translational considerations in injectable cell-based therapeutics for neurological applications: concepts, progress and challenges. npj Regen Med 2:. https://doi.org/10.1038/s41536-017-0028-x

111. Iordache TV, Banu ND, Giol ED, et al (2020) Factorial design optimization of polystyrene microspheres obtained by aqueous dispersion polymerization in the presence of poly(2-ethyl-2-oxazoline) reactive stabilizer. Polym Int 69:1122–1129. https://doi.org/10.1002/pi.5974

112. Quarta E, Sonvico F, Bettini R, et al (2021) Inhalable microparticles embedding calcium phosphate nanoparticles for heart targeting: The formulation experimental design. Pharmaceutics 13:. https://doi.org/10.3390/pharmaceutics13111825

113. Hu X, Wang H, Liu Y (2016) Statistical Analysis of Main and Interaction Effects on Cu(II) and Cr(VI) Decontamination by Nitrogen-Doped Magnetic Graphene Oxide. Sci Rep 6:1–11. https://doi.org/10.1038/srep34378

114. Chan ES, Lim TK, Ravindra P, et al (2012) The effect of low air-to-liquid mass flow rate ratios on the size, size distribution and shape of calcium alginate particles produced using the atomization method. J Food Eng 108:297–303. https://doi.org/10.1016/j.jfoodeng.2011.08.010

115. Nastruzzi A, Pitingolo G, Luca G, Nastruzzi C (2020) DoE analysis of approaches for hydrogel microbeads' preparation by millifluidic methods. Micromachines 11:. https://doi.org/10.3390/mi11111007

116. Rizwan M, Yahya R, Hassan A, et al pH Sensitive Hydrogels in Drug Delivery : Brief History , Properties , Swelling , and Release Mechanism , Material Selection and Applications. https://doi.org/10.3390/polym9040137

117. Zeeb B, Saberi AH, Weiss J, McClements DJ (2015) Retention and release of oil-in-water emulsions from filled hydrogel beads composed of calcium alginate: Impact of emulsifier type and pH. Soft Matter 11:2228–2236. https://doi.org/10.1039/c4sm02791d

118. Rayment P, Wright P, Hoad C, et al (2009) Investigation of alginate beads for gastro-intestinal functionality, Part 1: In vitro characterisation. Food Hydrocoll 23:816–822. https://doi.org/10.1016/j.foodhyd.2008.04.011

119. Narkar M, Sher P, Pawar A (2010) Stomach-specific controlled release gellan beads of acid-soluble drug prepared by ionotropic gelation method. AAPS PharmSciTech 11:267–277. https://doi.org/10.1208/s12249-010-9384-1

120. Prezotti FG, Cury BSF, Evangelista RC (2014) Mucoadhesive beads of gellan gum/pectin intended to controlled delivery of drugs. Carbohydr Polym 113:286–295. https://doi.org/10.1016/j.carbpol.2014.07.021

121. Madhusudhan A, Reddy GB, Venkatesham M (2014) Efficient pH Dependent Drug Delivery to Target Cancer Cells by Gold Nanoparticles Capped with Carboxymethyl Chitosan. 8216–8234. https://doi.org/10.3390/ijms15058216

122. Guarino V, Caputo T, Altobelli R, Ambrosio L (2015) Degradation properties and metabolic activity of alginate and chitosan polyelectrolytes for drug delivery and tissue engineering applications. AIMS Mater Sci 2:497–502. https://doi.org/10.3934/matersci.2015.4.497

123. Pawar SN, Edgar KJ (2012) Alginate derivatization: A review of chemistry, properties and applications. Biomaterials 33:3279–3305. https://doi.org/10.1016/j.biomaterials.2012.01.007

124. Xu Z, Li Z, Jiang S, Bratlie KM (2018) Chemically Modified Gellan Gum Hydrogels with Tunable Properties for Use as Tissue Engineering Scaffolds. ACS Omega 3:6998–7007. https://doi.org/10.1021/acsomega.8b00683

125. Correia JS, Oliveira JM, Caridade SG, et al (2011) Gellan gum-based hydrogels for intervertebral disc tissue-engineering applications. J Tissue Eng Regen Med 5:97–107. https://doi.org/10.1002/term.363

126. Zhao X, Wang Z (2019) A pH-sensitive microemulsion-filled gellan gum hydrogel encapsulated apigenin: Characterization and in vitro release kinetics. Colloids Surfaces B Biointerfaces 178:245–252. https://doi.org/10.1016/j.colsurfb.2019.03.015

127. Picone CSF, Cunha RL (2011) Influence of pH on formation and properties of gellan gels. Carbohydr Polym 84:662–668. https://doi.org/10.1016/j.carbpol.2010.12.045

128. Barros AA, Rita A, Duarte ARC, et al (2015) Bioresorbable ureteral stents from natural origin polymers. J Biomed Mater Res - Part B Appl Biomater 103:608–617. https://doi.org/10.1002/jbm.b.33237

129. Zheng Y, Liang Y, Zhang D, et al (2018) Gelatin-Based Hydrogels Blended with Gellan as an Injectable Wound Dressing. https://doi.org/10.1021/acsomega.8b00308

130. Othman I, Abu Haija M, Kannan P, Banat F (2020) Adsorptive Removal of Methylene Blue from Water Using High-Performance Alginate-Based Beads. Water Air Soil Pollut 231:. https://doi.org/10.1007/s11270-020-04751-3

131. Temeepresertkij P, Iwaoka M, Iwamori S (2021) Molecular interactions between methylene blue and sodium alginate studied by molecular orbital calculations. Molecules 26:1–7. https://doi.org/10.3390/molecules26227029

132. Halim NFA, Majid SR, Arof AK, et al (2012) Gellan Gum-LiI gel polymer electrolytes. Mol Cryst Liq Cryst 554:232–238. https://doi.org/10.1080/15421406.2012.634344

133. Khampieng T, Aramwit P, Supaphol P (2015) Silk sericin loaded alginate nanoparticles: Preparation and anti-inflammatory efficacy. Int J Biol Macromol 80:636–643. https://doi.org/10.1016/j.ijbiomac.2015.07.018

134. Noor ISM, Majid SR, Arof AK, et al (2012) Characteristics of gellan gum-LiCF3SO3polymer electrolytes. Solid State Ionics 225:649–653. https://doi.org/10.1016/j.ssi.2012.03.019

135. Soares JP, Santos JE, Chierice GO, Cavalheiro ETG (2004) Thermal behavior of alginic acid and its sodium salt. Eclet Quim 29:57–63. https://doi.org/10.1590/S0100-46702004000200009

136. Bajas D, Vlase G, Mateescu M, et al (2021) Formulation and characterization of alginate-based membranes for the potential transdermal delivery of methotrexate. Polymers (Basel) 13:1–18. https://doi.org/10.3390/polym13010161

137. Kloster GA, Muraca D, Moscoso Londoño O, et al (2020) Alginate based nanocomposites with magnetic properties. Compos Part A Appl Sci Manuf 135:105936. https://doi.org/10.1016/j.compositesa.2020.105936

138. Witzler M, Vermeeren S, Kolevatov RO, et al (2021) Evaluating Release Kinetics from Alginate Beads Coated with Polyelectrolyte Layers for Sustained Drug Delivery. ACS Appl Bio Mater 4:6719–6731. https://doi.org/10.1021/acsabm.1c00417

139. Boni FI, Prezotti FG, Cury BSF (2016) Gellan gum microspheres crosslinked with trivalent

ion: Effect of polymer and crosslinker concentrations on drug release and mucoadhesive properties. Drug Dev Ind Pharm 42:1283–1290. https://doi.org/10.3109/03639045.2015.1125915

140. Xu H, Shi M, liu Y, et al (2014) A Novel In Situ Gel Formulation of Ranitidine for Oral Sustained Delivery. Biomol Ther (Seoul) 22:161–165. https://doi.org/10.4062/biomolther.2013.109

141. Fredenberg S, Wahlgren M, Reslow M, Axelsson A (2011) The mechanisms of drug release in poly(lactic-co-glycolic acid)-based drug delivery systems - A review. Int J Pharm 415:34–52. https://doi.org/10.1016/j.ijpharm.2011.05.049

142. Kim H, Fassihi R (1997) Application of binary polymer system in drug release rate modulation. 2. Influence of formulation variables and hydrodynamic conditions on release kinetics. J Pharm Sci 86:323–328. https://doi.org/10.1021/js960307p

143. Zuo J, Gao Y, Bou-Chacra N, Löbenberg R (2014) Evaluation of the DDSolver software applications. Biomed Res Int 2014:. https://doi.org/10.1155/2014/204925

144. Tu J, Bolla S, Barr J, et al (2005) Alginate microparticles prepared by spray-coagulation method: Preparation, drug loading and release characterization. Int J Pharm 303:171–181. https://doi.org/10.1016/j.ijpharm.2005.07.008

145. Mukesh Dhanka, Chaitra Shetty RS (2017) Methotrexate loaded gellan gum microparticles for drug delivery Authors: Int J ofBiological Macromol. https://doi.org/10.1016/j.ijbiomac.2017.12.026

146. Stanković A, Mihailović J, Mirković M, et al (2020) Aminosilanized flower-structured superparamagnetic iron oxide nanoparticles coupled to 131I-labeled CC49 antibody for combined radionuclide and hyperthermia therapy of cancer. Int J Pharm 587:. https://doi.org/10.1016/j.ijpharm.2020.119628

147. Carrêlo H, Escoval AR, Soares PIP, et al (2022) Injectable Composite Systems of Gellan Gum : Alginate Microparticles in Pluronic Hydrogels for Bioactive Cargo Controlled Delivery : Optimization of Hydrogel Composition based on Rheological Behavior. Fluids 7:. https://doi.org/10.3390/fluids7120375

148. Soares PIP, Lochte F, Echeverria C, et al (2015) Thermal and magnetic properties of iron oxide colloids: Influence of surfactants. Nanotechnology 26:. https://doi.org/10.1088/0957-4484/26/42/425704

149. Khalkhali M, Rostamizadeh K, Sadighian S, et al (2015) The impact of polymer coatings on magnetite nanoparticles performance as MRI contrast agents: A comparative study. DARU, J Pharm Sci 23:1–12. https://doi.org/10.1186/s40199-015-0124-7

150. Shukla S, Jadaun A, Arora V, et al (2015) In vitro toxicity assessment of chitosan oligosaccharide coated iron oxide nanoparticles. Toxicol Reports 2:27–39. https://doi.org/10.1016/j.toxrep.2014.11.002

151. Wei H, Hu Y, Wang J, et al (2021) Superparamagnetic iron oxide nanoparticles: Cytotoxicity, metabolism, and cellular behavior in biomedicine applications. Int J Nanomedicine 16:6097–6113. https://doi.org/10.2147/IJN.S321984

152. Chandra S, Mehta S, Nigam S, Bahadur D (2010) Dendritic magnetite nanocarriers for drug delivery applications. New J Chem 34:648–655. https://doi.org/10.1039/b9nj00609e

153. Liu X, Zhang Y, Wang Y, et al (2020) Comprehensive understanding of magnetic hyperthermia for improving antitumor therapeutic efficacy. Theranostics 10:3793–3815. https://doi.org/10.7150/thno.40805

5. THE GG:ALG/PLURONIC SYSTEM

5.1. Introduction

In this chapter, the development of the GG:Alg/Pluronic system will be addressed. Firstly, the GG:Alg (Gellan Gum: Alginate) microparticles without mNPs (magnetic nanoparticles) were combined with Pluronic to optimize the thermoresponsive system. The main goal was to optimize the sol-gel transition temperature so that the system is in the sol state at 21ºC (operating room temperature) and in the gel state at 37ºC (human body temperature). The second part concerns the use of microparticles with mNPs within the Pluronic gel and the optimization of the properties of this system.

This chapter will be based on the following article:

Carrêlo, H.; Escoval, A.R.; Soares, P.I.P.; Borges, J.P.; Cidade, M.T. "Injectable Composite Systems of Gellan Gum:Alginate Microparticles in Pluronic Hydrogels for Bioactive Cargo Controlled Delivery: Optimization of Hydrogel Composition based on Rheological Behavior". Fluids 2022, 7, 375. https://doi.org/10.3390/fluids7120375

5.1.1. Pluronic

Pluronic refers to a family of block copolymers consisting of poly(ethylene oxide) (PEO) and poly(propylene oxide) (PPO) units. This poloxamer is used for several applications owing to its unique ability to form temperature-sensitive and reversible gels and is approved by the Food and Drug Administration (FDA) of the USA for pharmaceutical purposes [1]. When Pluronic copolymers are dissolved in water, the hydrophilic PEO blocks extend into the water. In contrast, hydrophobic PPO blocks tend to aggregate to minimize their exposure to water. With a temperature increase , the hydrophobic PPO segments begin to aggregate at lower temperatures, forming micelles [2] (Figure 5.1). As the temperature continues to increase, PPO blocks become more ordered, leading to the formation of a physical gel network almost instantaneously [2]. This process is called micellization. Pluronic is a hydrogel [3]–[5], but due to this type of reticulation, that it is not permanent within aqueous solutions, Pluronic will be addressed has a gel in this thesis, since Pluronic gels can be dissolved in aqueous solution [3], [6], [7]. This gel network can also be disrupted at higher temperatures because of the increased solubility of PPO blocks in water, leading to the gel collapse [8].

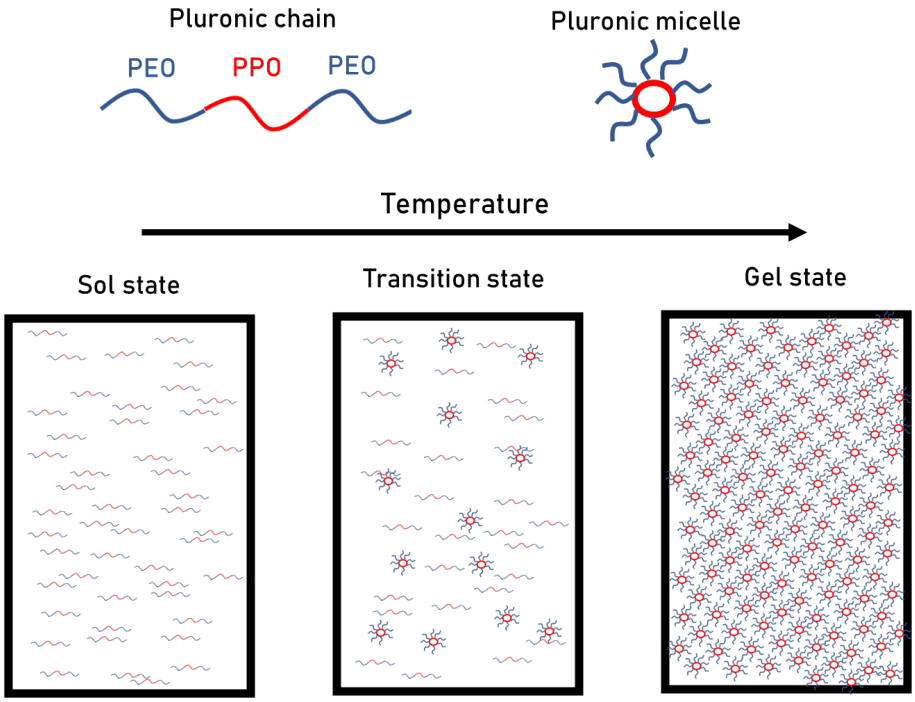

Figure 5.1 Pluronic chain and micelle (upper part) and the sol state to the gel state (lower part)

5.1.1.1. Types of Pluronic

Pluronic polymers can be divided into four different categories according to hydrophilic-lipophilic balance (HLB) ratio and PPO chain length (examples in brackets) (Figure 5.2) [1]:

- (I) HLB of 20-29 (Pluronic F127, F108 and F68);
- (II) HLB < 20 and PPO chain <30 (Pluronic L35, L44 and L64);
- (III) HLB<20 and PPO chain of 30-60 (Pluronic P85, P105 and L61);
- (IV) HLB<20 and PPO chain > 60 (Pluronic P123 and L121)

The first category includes Pluronic polymers with high hydrophilicity and biocompatibility [1]. Pluronic F127 and F68 are two of the most commonly used types of Pluronic, especially F127 [9]. They differ in molecular weight with F127 having a higher molecular weight than F68. The composition of F127 is 70% PEO and 30% PPO, whereas F68 has 80% PEO and 20% PPO [8]. The differences in the molecular weight and PEO:PPO ratios between F127 and F68 affect their physical properties and performance as hydrogels. F127 is more hydrophobic and more likely to form micelles at lower concentrations, leading to more elastic gel networks. F68 is more hydrophilic and easier to dissolve in water [8].

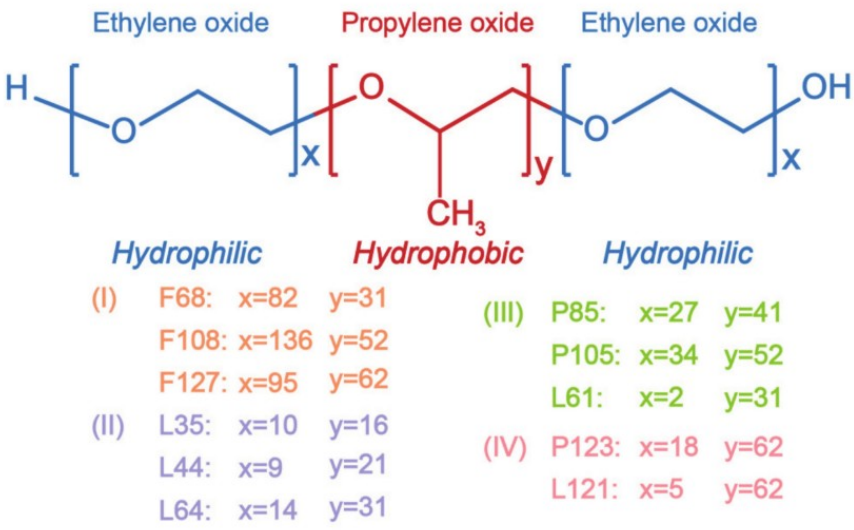

Figure 5.2 Structure of the different Pluronic polymers. (Adapted with permission from [1]. Copyright (2021) Multidisciplinary Digital Publishing Institute).

5.1.1.2. Pluronic polymer applications

In biomedical applications, Pluronic gels have been extensively used, due to the capacity of Pluronic, especially F127, of forming 3D structures [1], [10], [11]. For example, Pluronic has been used in different cancer studies [1], wound healing treatments, bioinks, bone treatments and neurological treatments [10], [11]. It has also been used for drug delivery using Pluronic's micelles, has coating agent for pharmaceutical formulations and even as biological response modifiers [12]. The fact that Pluronic is able of being in a viscous state at lower temperatures (room temperature) and at a gel state at body temperature, offers the possibility of developing injectable systems. Shriky *et al.* [5] studied the effects of flow on Pluronic F127, with the formed structure being affected by the direction of the flow. Also, beyond their use in DDS, Pluronics have been used for possible tissue engineering applications, serving as bioinks [13]. Previous studies have also tried to conjugate these poloxamers with SPIONs [14].

F127-based Pluronics have been used to develop an intratumoral injectable breast cancer DDS. Rafael *et al.* [15] studied the delivery of small interfering RNA (siRNA) of epidermal growth factor receptors (EGFR) using micelles of Pluronic and gelatine. The combination of gelatine with Pluronic allowed the cationic groups necessary for the complexation of siRNA. High entrapment efficiencies were obtained with gene silencing levels of 70% with low cytotoxicity and adequate hemocompatibility. Functionalized micelles showed higher rates of internalization in EGFR expressing cells than non-functionalized ones. Santana *et al.* [16] studied the delivery of nitric oxide and cisplatin loaded into silica nanoparticles within a thermoresponsive F-127/hyaluronic acid hydrogel matrix. The combination of nitric oxide and cisplatin led to lower cancerous cell viability than the systems with just one of them. Cheng *et al.* [17] used Pluronic F127 with ester-grafted Pluronic F123 (with 4-hydroxymethylphenylboronic acid pinacol ester) as a DDS to efficiently

deliver DOX (Doxorubicin), and as a detoxification regulator to prevent multidrug resistance (MDR) in breast cancer cells. The hybrid micelles had higher stability and DOX encapsulation than the non-ester grafted F127/F123 micelles, due to the lower critical micelle concentration of the former. The system also induced more apoptosis in MDR-cells compared to non-functionalized Pluronic micelles. The ester groups prevented detoxification that reduces DOX concentration and efficacy in tumour cells, thus preventing MDR. *in vivo* tests showed that the system accumulated at the tumour regions and had the highest tumour growth inhibition.

5.1.2. Microparticles within Pluronic

In previous works of our group, the Pluronic polymer was used in combination with microparticles. Cidade *et al.* [18] combined alginate microparticles with Pluronic F127. The introduction of microparticles led to a decrease in the systems temperature transition and a slowing of the release profile compared to the drug-loaded gel. Delgado *et al.*[19] produced poly(e-caprolactone) (PCL) microcapsules via W/O/W (Water/Oil/Water) production techniques and combined them with Pluronic, where, the microcapsules also diminished the transition temperatures. The poloxamer gel structure delayed the release when compared with the drug-loaded Pluronic and the drug loaded microparticles without Pluronic. Tipa *et al.*[20] combined nanoclays with Pluronic F127:F68 mixtures. The addition of nanoclays decreased the transition temperatures and delayed the model drug release. In another study [7], Pluronic was also used to deliver dexamethasone within PLGA (poly(lactic-co-glycolic acid) microparticles. Pluronic delayed the release and endured 6 days *in vivo*. Also, Pluronic was compared with a hyaluronic acid hydrogel. However, the hyaluronic acid hydrogel persisted much longer *in vivo* than the Pluronic gel and had a slower release profile. Giovagnoli *et al.* [21] developed alginate microparticles incorporating DOX and embedded them in Pluronic F127. The release profile of DOX was delayed by the Pluronic F127 gel. For breast cancer application, but with nanoparticles with cisplatin, Pluronic was also used as a transport matrix in combination with hyaluronic acid [16].

GG:Alg microparticle, as far as the research showed, been studied have not been used in combination with Pluronic gels, neither GG:Alg microparticles with SPIONs (Superparamagnetic Iron Oxide Nanoparticles) and SPIAPTs (Superparamagnetic Iron Oxide Nanoparticles with APTES), since the developed GG:Alg microparticles with and without nanoparticles are unique. Also, the variation of Pluronic F127 and F168 is used to alter the transition temperature of the system. This variation in combination with the GG:Alg is a study never done before that delves into the relation of these factors to fabricate an adequate thermoresponsive system. Hence, this chapter will focus on the study and characterization of GG:Alg microparticles with thermoresponsive Pluronic gel. Materials and methods (production and characterization) are described in Chapter 3.

5.2. Results and Discussion

5.2.1. GG:Alg microparticles within the Pluronic hydrogel system

5.2.1.1. Development of the Pluronic hydrogel

Before incorporation of the GG:Alg microparticles, Pluronic gel had to be optimized regarding its sol-gel temperature. To regulate the transition temperature, two Pluronic polymers (HLB of 20-29) were chosen: Pluronic F127 and F68. Pluronic F127 (20 w/w%) has a sol gel transition temperature of 22ºC whilst F68 (20 w/w%) is around 50 ºC. The concentration of Pluronic polymer also influences the transition temperature. Higher concentrations of Pluronic F127 decrease the transition temperature, whilst lower concentrations increase it [20]. However, mixing F127 with F68 allows tailoring the transition temperature. For this study, solutions with the same concentration of F127 and F68 were used (20 w/w%), which were mixed in different proportions (Pluronic F127:F68 ratios (20:0; 18:2; 17:3; 16:4; 15:5; 14:6 w/w:w/w%)).

Figure 5.3 depicts the temperature profiles for the Pluronic systems in 20 w/w% aqueous solutions during oscillation tests. The temperature ramps exhibited three distinct regions: the sol region, the transition region, and the gel region, similar to earlier works [5]. In the first region, the system was fully in the sol state, with G''>G', indicating a viscous behaviour. As the temperature increased, the moduli began to rise, indicating the onset of the second region. This increase occurred around a specific temperature, referred to as Ti (initial temperature), and corresponded to the Pluronic's micellization [8], [22]. The transition region ended with an abrupt transition into a plateau, which marks the beginning of the gel state (final region). This transition is where the plateau temperature can be found. The gel state is characterized by a full micellized structure of the gel, where G'>G'', indicating an elastic structure, and with the moduli being independent of temperature (Figure 5.3 (b)).

The Ti and Tp temperatures indicate the start and finish, respectively, of the transition stage. This transition stage occurs due to the coexistence between formed micelles and loose chains within the solution [23]. With temperatures close to Tp the loose chains micellize until the point of full micellization of the system. The gel state occurs due to the interaction of micelles. After micelle saturation, these interactions form a structure that leads to the gel state. This gel state in Pluronic maintains within a temperature range; however, at a higher temperature, the structure collapses [24].

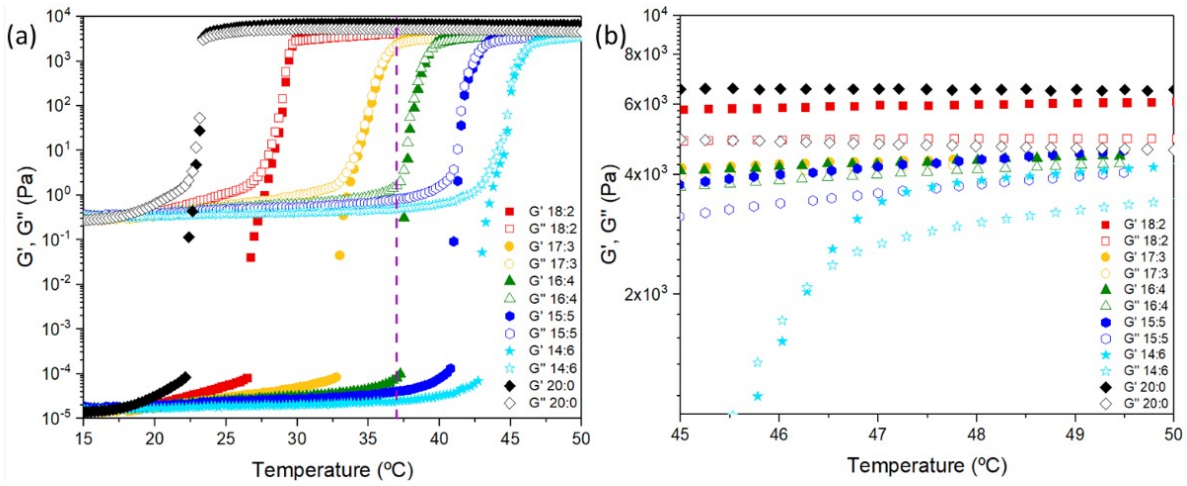

Figure 5.3 Elastic (G') and viscous (G'') moduli of different ratios of Pluronic F127 and F68, of a Pluronic aqueous solution of 20 w/w% (**a**). The violet line represents 37 ºC. On the (**b**), there is an approximation of the region between 45 and 50 ºC of the image on the left. Image from, with permission. (Adapted with permission from [2]. Copyright (2021) Multidisciplinary Digital Publishing Institute).

The transition temperatures (Table 5.1) increased with a decrease of F127 concentration and an increase of F68. For example, with a Pluronic ratio of 20:0 (F127:F68), the Tp was 23.62 ± 0.11 °C, whilst with a ratio of 14:6, the Tp increased more than 20 °C, to a Tp of 45.81 ± 0.11 °C. In this system, F127 is the main phase and is the one that micellizes. Pluronic F68 does not form a micellized phase at these concentrations. In addition, Pluronic F68 has a much higher gelation temperature than Pluronic F127 (when the concentrations are similar) [8], [25]. This is attributed to the higher PPO content of F127 ($PEO_{99}PPO_{69}PEO_{99}$) in comparison with F68 ($PEO_{80}PPO_{27}PEO_{80}$). It is this moiety that leads to the thermoresponsivity of the hydrogel [26]. Decreasing F127 presence within the solution will lead to fewer moieties of PPO, and thus fewer available chains that can micellize [8], [26]. Between 21ºC (operating room temperature) [27] and 37ºC (body temperature), the systems with the ratios of 17:3 and 16:4 were the ones chosen closer to 37ºC.

Table 5.1 Transient temperatures (Tp and Ti) of the Pluronic systems with GG:Alg (w/w%).

Tp (°C)									
ratio	**0%**		**2%**		**5%**		**10%**		**15%**	
17:3	34.62	± 1.78	34.77	± 0.29	33.58	± 0.19	31.06	± 0.10	27.92	± 0.09
16:4	39.67	± 0.67	38.05	± 0.75	35.23	± 1.48	33.27	± 0.18	32.88	± 0.65
15:5	42.24	± 0.20	42.08	± 0.33	40.12	± 0.02	38.47	± 0.64	35.13	± 0.51
14:6	45.81	± 0.11	44.00	± 0.76	43.67	± 0.09	40.78	± 0.25	38.56	± 0.05
Ti (°C)										
ratio	**0%**		**2%**		**5%**		**10%**		**15%**	
17:3	31.81	± 0.66	30.84	± 0.87	29.25	± 2.73	26.33	± 1.17	24.69	± 0.31
16:4	36.12	± 1.01	35.02	± 1.12	30.74	± 0.84	30.70	± 2.59	28.89	± 0.78
15:5	39.40	± 1.21	35.90	± 0.91	35.54	± 0.61	34.97	± 0.74	31.58	± 0.49
14:6	41.58	± 1.54	39.65	± 0.76	40.00	± 0.50	37.72	± 2.23	31.74	± 0.50

The moduli at the gel phase increase with higher concentrations of F127 and lower F68 (Figure 5.3 (b)). Thus, in this case, lower transition temperatures lead to more elastic structures. This is again associated with the previously mentioned, that with lower concentrations of F127, fewer moieties capable of forming the gel structure are available in the hydrogel and, thus, a less condensed structure is formed, with a lower elasticity.

These results are in accordance with previous studies, with the variation of ratios between F127 and F68 also producing similar results [8], [20], [28], [29]. The interaction between F127 and F68 has been previously studied, where two views have been proposed: either micellization occurs with micelles from the two types of Pluronic (mixed micelles) or that two micelles populations exist independently, with the last one being the one that was presented as the more probable [8], [26], [30]. Cooperative aggregation (mixed micelles) might occur with similar core block compositions and a PPO:PPO ratios (examples of Pluronic F77/F87) [31]. However, Pluronic F127 and F68 do not share similar PPO:PPO ratios. Zhang *et al.* [30] studied this question with Pluronic solutions (20 w/w%) of mixtures of F127 and F68. Results showed that no mixed micellization occurred. The sol gel transition is heavily dependent on the Pluronic F127, since it is the gel forming phase, but the presence of F68 also alters the transition, since it can delay the movements of the F127 micelles, preventing gelation.

5.2.1.2. The sol gel transition temperature of the microparticle-gel composite system.

With the previously tested Pluronic ratios, different dried GG:Alg microparticle concentrations (0, 2, 5, 10 and 15 w/v%) were introduced into the systems and the sol gel transition temperatures were analysed. Figure 5.4 depicts temperature ramps in an oscillation test of the gel systems with the microparticles. The temperature ramps present a similar profile to those of gels alone (Figure 5.3). The microparticle's presence decreased the transition temperatures of the Pluronic gels. The increase in the microparticle concentration further decreased the transition temperatures of the systems. This decrease might be explained by the swelling of the microparticles within the Pluronic solution, thus increasing the Pluronic concentration within the solution, and then decreasing the sol gel temperature [18], [19]. It is also possible that the carboxylic groups of the polysaccharidic GG:Alg microparticles interacted with the ether groups of Pluronic and promoted the formation of the gel structure [18], [32].

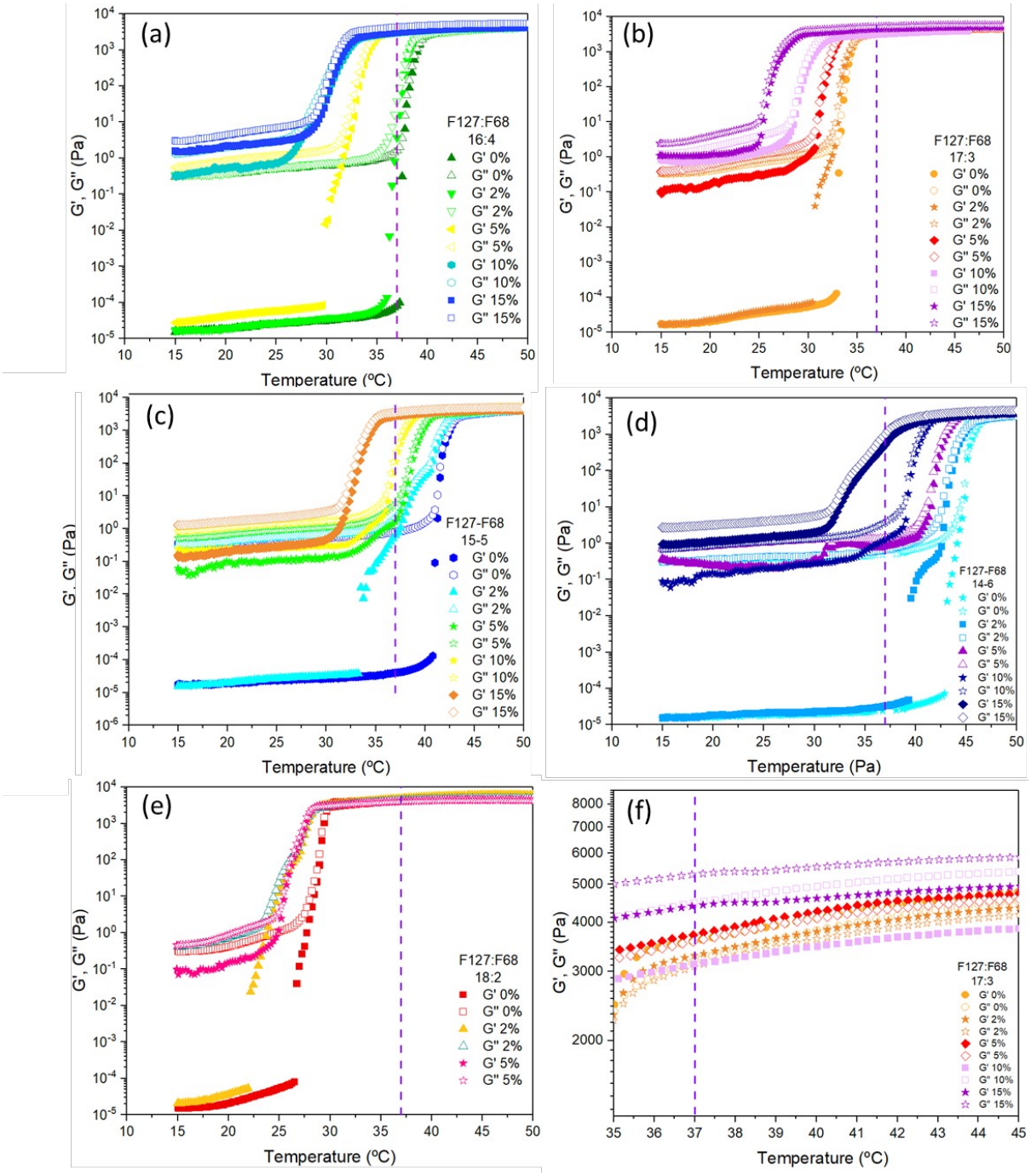

Figure 5.4 Elastic (G') and viscous (G'') moduli of different microparticle concentrations (in w/v%) within Pluronic F127:F68 ratios of (a) 16:4; (b) 17:3; (c) 15:5; (d) 14:6; (e) 18:2. (f) is an approximation of the (b) 17:3 from 35 to 45 ºC. The violet dotted line represents 37 °C. (Adapted with permission from [2]. Copyright (2021) Multidisciplinary Digital Publishing Institute).

In the first region, in the sol state, the presence of the microparticles increased the moduli, but maintaining the viscous behaviour of the gel system. In this state, a small slope was detected before the transition temperature. This was attributed to the formation of micelles, although in small numbers that did not significantly alter the viscous behaviour, but promoted some micellization and structuration that was detected. Like in the Pluronic without microparticles (Figure 5.3), once the temperature reached Ti, the moduli suddenly

increased several orders of magnitude until Tp was reached and the gel state commenced. With the introduction of microparticles, for lower concentrations, the moduli were as expected: G'>G'' or very close (Figure 5.5). However, for higher concentrations (Figure 5.5, that depicts the 16:4 and 17:3 ratios as examples), at the gel state, G'' and G' were very close but with G''>G'. The system was at the gel state, as can be observed in Figure 5.6 (the 17:3 ratio at 37ºC), but G''>G' is not the rheological response expected for gels. This could be attributed to the interaction between the microparticles within the gel state. The moduli increased due to the particles' presence, giving it a more elastic state. However, the friction between particles within the rheometer's gap, and within the gel state, might have led to interparticle lubrication. This energy dissipation might have contributed to G'' increase [33]–[36] Also, wall slip might have also occurred. This effect is linked of suspensions of large particles [37]. The presence of microparticles decreased the elasticity, this was corroborated by the fact that the distance between G'' and G' increased with the higher concentrations of microparticles observed at the gel state (Figure 5.5). Also, this effect might be due to the used angular frequency, with the necessity of frequency sweep tests to corroborate. Also, given the size of the microparticles (around 200 µm) the rheometer gap might have been not well adjusted for the higher microparticle concentrations, creating interactions that lead to these results. Despite this, the microparticle/gel system was still able to be at the sol and gel state. The decrease in transition temperatures of Pluronic was similar to previous works, with the introduction of microparticles also being described in previous works [18], [19], [32], [38].

Also, for the system with 14:6 (Figure 5.4 (d)) It appears to be a 2-step gelation mechanism that is enhanced by the presence of microparticles. For example, the system with 2% of microparticles appears to have two different slops with temperature increase. This can also be observed for the system with 15%.

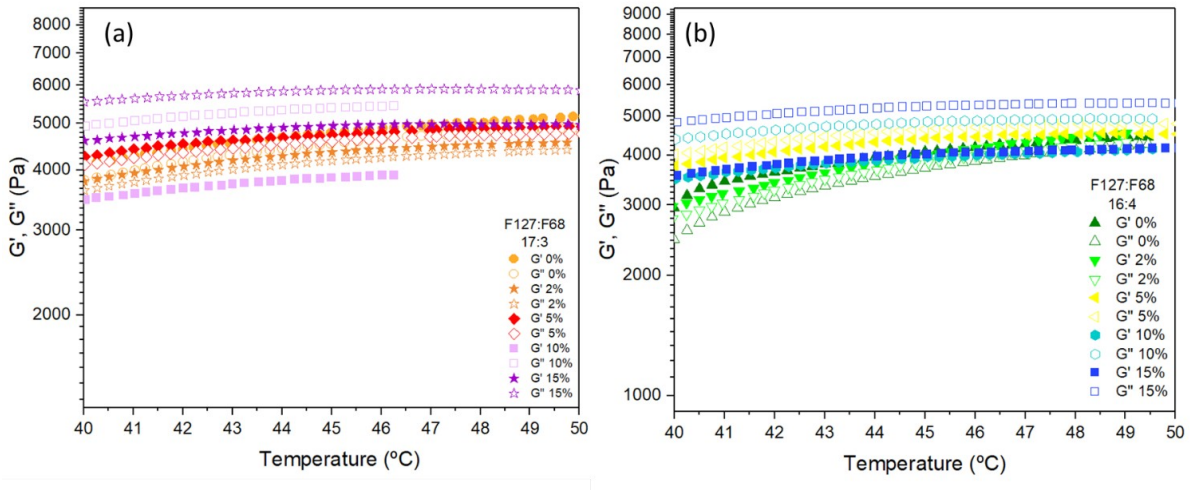

Figure 5.5 Elastic (G') and viscous (G'') moduli of different microparticle concentrations (in w/v%) within Pluronic F127:F68 ratios of (a) 17:3 and (b) 16:4 within 40 to 50ºC.

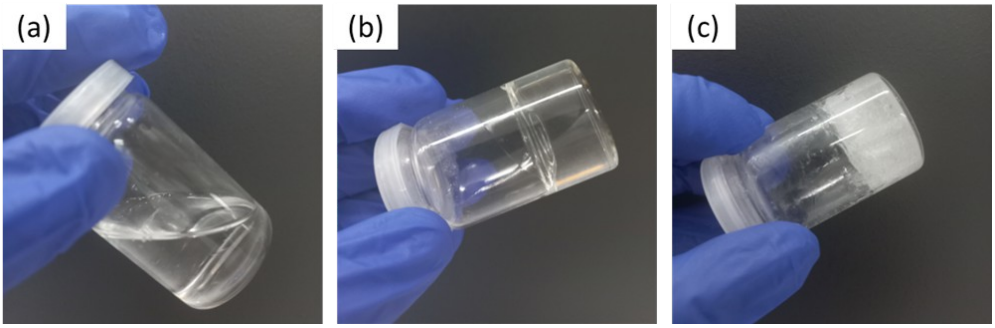

Figure 5.6 Images of Pluronic F127:F68 with 17:3 ratio within a flask: (**a**) 0 w/v% of microparticles at 21 °C (sol state), (**b**) 0 w/v% microparticles at 37 °C (gel state) and (**c**) 15 w/v% microparticles at 37 °C (gel state). (Adapted with permission from [2]. Copyright (2021) Multidisciplinary Digital Publishing Institute).

Figure 5.7 depicts the relation between the microparticle concentration and the Pluronic F127:F68 ratios (Figure 5.7 (a) and (b) for Tp and (c) for Ti) regarding the transition temperatures. The variation of Pluronic ratios had a more significant impact on the systems' transition temperatures than the microparticle concentration (Figure 5.7 (a)) since higher temperature variations were obtained with Pluronic concentration. As previously observed, the increase in microparticle concentration led to a decrease in Ti and Tp (Figure 5.7 (b) and (c)).

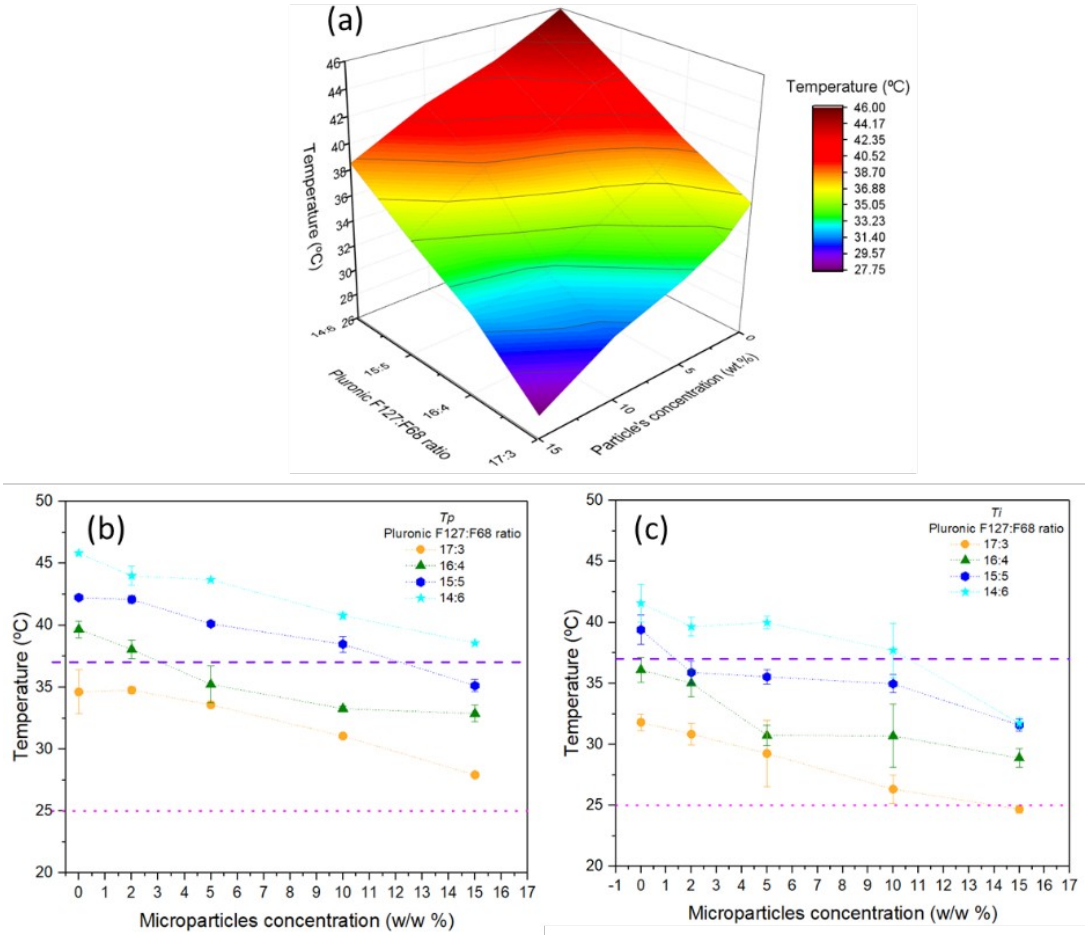

Figure 5.7 (**a**) 3D representation of the sol–gel transition temperatures (Tp) of the microparticle/gel composite system with variation of Pluronic F127:F68 ratio and microparticle concentration; (**b**) variation in the Tp of the microparticle–Pluronic gel composite system with microparticle concentration at different ratios of F127:F68; (**c**) similar graphic depiction for Ti. In (**b**) and (**c**), the dashed line in purple represents the 37 °C limit, and the dotted line in pink represents the ambient temperature of 25°C. (Adapted with permission from [2]. Copyright (2021) Multidisciplinary Digital Publishing Institute).

5.2.1.2.1. Mathematical fittings of the Transition Temperatures

With the previous results, some mathematical fittings can be done to understand the relationship between the concentration of the microparticles and the transition temperatures. Thus, a linear model was used following the next equation:

$$T = m.c + T_0 \qquad \text{Equation 5.1}$$

T represents either Tp or Ti (°C), m is the slope of the linear regression, c is the microparticle concentration and T_0 is the intercept, i.e., the transition temperature of the Pluronic solution without microparticles. R^2 is the adjusted error. Linear regression was calculated for each ratio. Table 5.2 depicts the obtained parameters of the linear fittings for Ti and Tp.

Pluronic polymers ratio did not influence the microparticle concentration effect on Tp (Table 5.2) since all slopes are similar regardless of ratio. Thus, no interaction between the concentration and ratio effect on Tp was observed. The obtained R^2 was high. The 16:4 (F127:F68) ratio was the one with the lowest R^2; however, the value was still adequate for the microparticle/gel system to be in the sol state at 21ºC and in the gel state at 37ºC. The obtained T_0, that in this case it is the Tp of the hydrogel without microparticles, where similar to the previously registered (Figure 5.3 Figure 5.4), indicating a good-fitting model that describes the effect of the microparticle concentration on the Pluronic transition temperatures.

For Ti (Table 5.2), also no influence between the concentration and ratio was detected. The slopes were also similar, however, the R^2 are lower than the ones obtained for Tp. This was attributed to the start of micellization, which showed higher dispersibility, as can be observed in Figure 5.7 (c) where higher standard deviations are obtained when compared to Tp. Regarding T_0, the obtained transition temperatures were also similar to the hydrogels without microparticles (Figure 5.3 Figure 5.4).

Table 5.2 Linear regression of the obtained Pluronic systems sol gel transition temperatures according to microparticle concentration (w/v%). Left table for Tp and right table for Ti. M is the slope of the regression and T_0 is the intercept, i.e., the modelled temperature with 0 w/v%. (Adapted with permission from [2]. Copyright (2021) Multidisciplinary Digital Publishing Institute).

Tp			
F127:F68 Ratio	***m* (°C/(w/w%))**	**T_0 (°C)**	**R^2**
14:6	–0.4658	45.55	0.9799

15:5	–0.4762	42.66	0.9764
16:4	–0.4564	38.74	0.8805
17:3	–0.4668	35.38	0.9616

Ti			
F127:F68 Ratio	***m*** **(°C/(w/w%))**	T_0 **(°C)**	R^2
14:6	–0.5886	41.91	0.8804
15:5	–0.4182	38.16	0.8413
16:4	–0.4646	35.27	0.8341
17:3	–0.4900	31.72	0.9900

5.2.1.3. Determination of the optimal system for injectable purposes

With the obtained data it was possible to understand the effect of the Pluronic ratio and the microparticle concentration on the transition temperatures. The F127:F68 ratio effect is independent of the microparticle concentration effect. Furthermore, these data allows defining the best Pluronic ratio and microparticle concentration to be used in the desired DDS. Figure 5.7 (b) and (c) show lines that represent the temperatures of 37ºC and 21ºC, which serve as a visual aid to select the optimal systems. The ratio 17:3 can be used with almost all microparticles concentrations, except 15 w/v%. With 16:4, the microparticles concentration of 5, 10 and 15 w/v% also can be used. With 15:5 ratio, only with 15 w/v%. The ratios of 14:6 and 18:2 did not meet the criteria, having transition temperatures far higher and lower, respectively. For the following works, only the ratios of 16:4 and 17:3 were chosen due to their more adequate transition temperatures to produce an injectable system into the human body.

5.2.2. Rheological Characterization of the GG:Alg microparticles/Pluronic system

Figure 5.8 (a) and (b) depict the dependence of G′ and G′′ with frequency at 37ºC of the microparticle/gel system with Pluronic ratios of 17:3 and 16:4. The ratio of 16:4 with 0 and 2 w/v% of microparticles presented lower moduli than the other concentrations. For these systems, Ti is below 37ºC and Tp is above 37ºC, as can be observed in Figure 5.4 (a) and in Figure 5.7 (b) and (c). Thus, in these conditions, the samples were within the transition region, with micelles forming, but not within the gel state. For the higher concentrations (5, 10 and 15 w/v%), all samples had similar moduli, but at much higher values than those with 0 and 2 w/v%, indicating that they were at the gel state. However, G′′>G′ was still observed with frequency sweeps, being interparticle lubrication or wall slip the explanations for this, as previously said. The moduli presented an almost null slope with frequency, typical of gel structures. For the ratio of 17:3 all systems were also at the gel state, with G′′>G′, except for

the system without microparticles that had G′>G′′. The introduction of microparticles slightly increased the moduli but had the previously described effect of G′′>G′, and with increasing microparticle concentration the difference between G′′ and G′ increased.

As noted earlier, the addition of microparticles to a material increases its rigidity, resulting in an increase in G'. The friction between the particles can cause energy dissipation, increasing G'' [33], [34]. This effect was also described in a previous work by Zheng *et al.* [35] with a similar test with PLGA microparticles within a polypeptide hydrogel. In this thesis, within the studied range of angular frequency (0.1-10 $rad.s^{-1}$) the phenomenon was maintained, indicating that this phenomenon is related to the microparticles concentration and not to the used angular frequency.

These gels can be called soft/weak gels. They have a dependency on frequency, even though the slopes are low. Also, the moduli are parallel and very close to each other, to the point that G′′>G′ within the gel state. Thus, with tg(δ) >1 (tg(δ) = G′′/G′), indicating a soft gel structure [39]. The microparticles did not alter the gel state but increased the loss modulus to a point that surpassed the elastic modulus within a gel, something that differs from the common literature [39–41].

Figure 5.8 (b) depicts flow curves of the 16:4 and 17:3 ratios at 21ºC with different microparticles concentrations. The Pluronic solutions had a Newtonian behaviour within the studied shear rate ranges. The introduction of the microparticles led to an increase in the apparent viscosity but maintained a general Newtonian behaviour, with the exception for the systems with 15 w/v% of microparticles, with a tendency for shear thinning behaviour. These results are in accordance with the previous results since all studied systems are within the sol state region at 21ºC (Figure 5.4). In previous studies, Newtonian behaviour was also obtained at lower temperatures in the sol state [20,21]. Tipa *et al.* [20] analyzed similar Pluronic F127 and F68 ratios but with nanoclays. Similar viscosities were obtained when compared with the results of this study, especially for the systems with 2 and 5 w/v% of microparticles. The great increase of viscosities with 10 and 15 w/v% might jeopardize the injectability of the system.

These rheological studies were done to characterize and confirm if the hydrogels were in fact at the gel state at 37ºC and how the viscosity of the Pluronic sol state systems at 21ºC was affected by the introduction of the microparticles. With these results, the following studies will only use the concentrations of 0, 2, and 5 w/v% of microparticles.

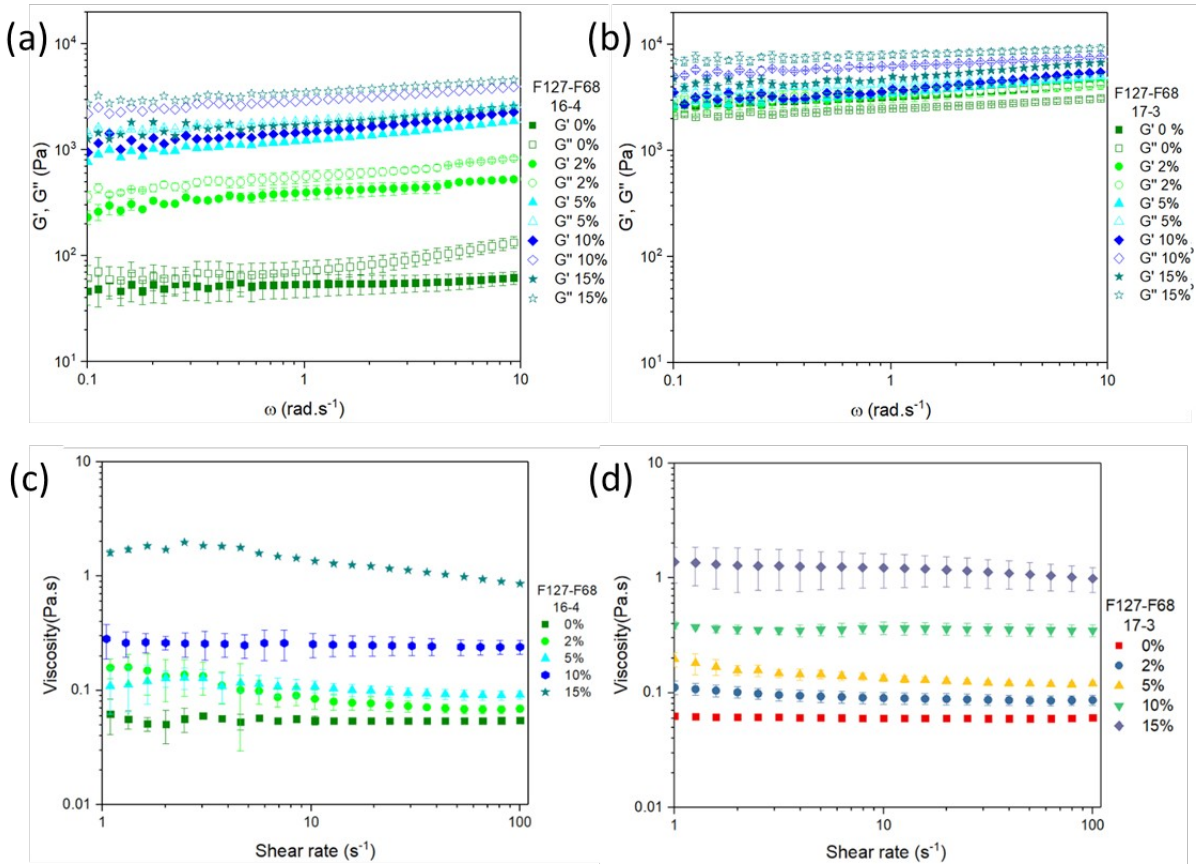

Figure 5.8 Frequency sweeps of the microparticle/Pluronic gel composite system with different microparticle concentrations (w/v%) at 37 °C. On (a), a Pluronic ratio of 16:4 and on (b) of 17:3. Flow curves of the microparticle/Pluronic gel system with different microparticle concentrations (w/v%) at 21 °C. On the (c) is a Pluronic ratio of 16:4 and on (d) of 17:3. (Adapted with permission from [2]. Copyright (2021) Multidisciplinary Digital Publishing Institute).

5.2.2.1. The behaviour of Pluronic in PBS solutions

To understand how the microparticle/Pluronic system behaves in solution, with time and pH, the studied hydrogel was submerged in PBS solutions with pH 6.5 and pH 7.4. Figure 5.9 depicts frequency sweeps of the Pluronic gel with a ratio of 17:3 after being in PBS solutions at different intervals of time. Rheological tests were carried out to depict a degradation profile with time. Before submitting the system to PBS, the Pluronic was at a normal gel state with G'>G'' and independent of frequency. After 1 h in PBS, no significant differences were observed. After 3 h the moduli decreased but retained the gel state. However, at 6 h the gel mostly fully dissolved in the PBS solution with only fragments of the remaining Pluronic. No differences were observed between 6 h and 24 h. No significant differences were also observed between using PBS with pH 6.5 and 7.4. This was attributed to the fact that Pluronic does not have any ionizable groups within its structure [44].

Figure 5.9 (c) depicts the mass variation after the hydrogels was within PBS solutions. At the end of 6 hours the hydrogel was not fully dissolved but had significantly decreased in mass (23.05 ± 7.47% for pH 6.5 and 11.91 ± 10.94% for pH 7.4 of remaining mass). After 6, 24 and 48h the remaining Pluronic masses were also fragmented, and at 48h, below 5 % of

remaining mass. In this test the Pluronic gel almost dissolved within a day, however at the end of 6h the Pluronic had lost over more than 75% of the mass, not even been detected in the obtained rheological tests, so it can be said that at the end of 6h the Pluronic gel had almost disappeared. No significant differences were detected between the two studied pH regarding mass loss of Pluronic.

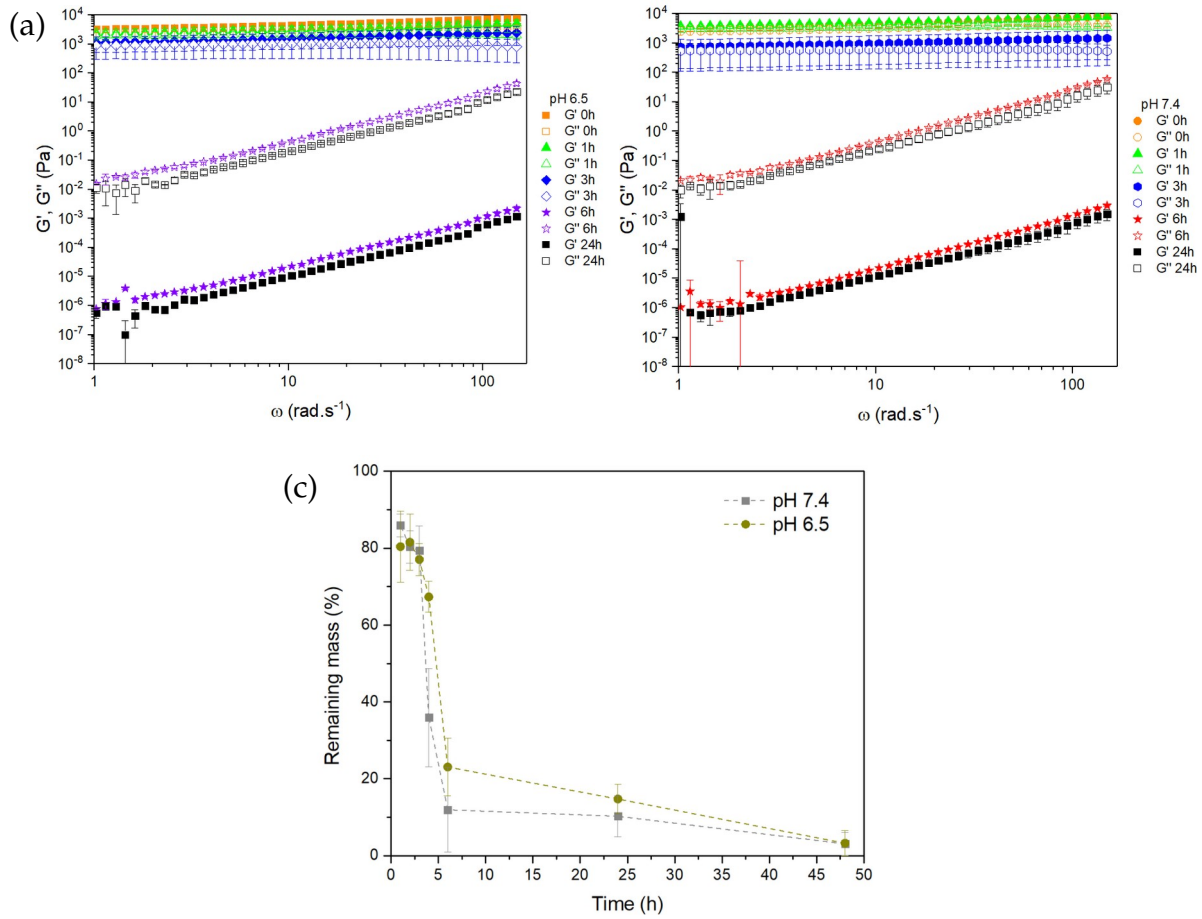

Figure 5.9 Frequency sweeps of Pluronic 17:3 ratio gel submerged for different times in PBS with pH 6.5 (a) and 7.4 (b) at 37 °C and mass variation in similar conditions (c). (Adapted with permission from *[2]*. Copyright (2021) Multidisciplinary Digital Publishing Institute).

Pluronic gels dissolved at this rate due to its lack of crosslinking, where this gel is formed only by a micellar structure. When put within the PBS solutions, the Pluronic concentrations lowers closer to the critical micelle concentration, leading the micelle structure to disassemble, hence the dissolution of the gel structure [45]. Thus, since this structure was not able to withhold in aqueous solutions it was referred as a gel and not as a hydrogel, since hydrogels are not supposed to dissolve in solutions [6]. Of course, the volume of PBS used greatly affects the dissolution rate of this gel [7]. For example, Diniz *et al.* [3] analysed the degradation of Pluronic F127 in a cell culture medium by placing 500 µL of Pluronic in the gel state in contact with the medium (1 mL). After a week, the gel had broken down into fragments, and 85% of its initial weight had disappeared within 2 weeks. This fragmentation also occurred in our study, but the used volumes are very different from the

ones used in this thesis. Also, in *in vivo* conditions, this rapid dilution effect has been observed to be not so pronounced. In *in vivo* studies, Heo et *al.* [7] observed that the Pluronic (in PBS solutions 20 w/v%) fully disappeared after 6 days. However, in *in vitro* studies the Pluronic systems disappeared in a matter of hours, similarly to the obtained results of this thesis. This means that the Pluronic hydrogel has different degradation/dilution velocities depending on the applied conditions.

5.2.2.2. MB release tests and cytotoxicity

This next part will evaluate both microparticles/hydrogel systems under drug release tests and cytotoxicity. Methylene blue (MB) was used as a model drug.

Figure 5.10 (a) shows the release profile of the Pluronic system (without microparticles) (F127:F68 - 17:3) loaded with MB, and (b) is the release profile from MB loaded microparticles within Pluronic gels with 16:4 and 17:3 ratio and (c) is the release profile form MB loaded microparticles within a 17:3 ratio gel with microparticles concentrations of 2 and 5 w/v%.

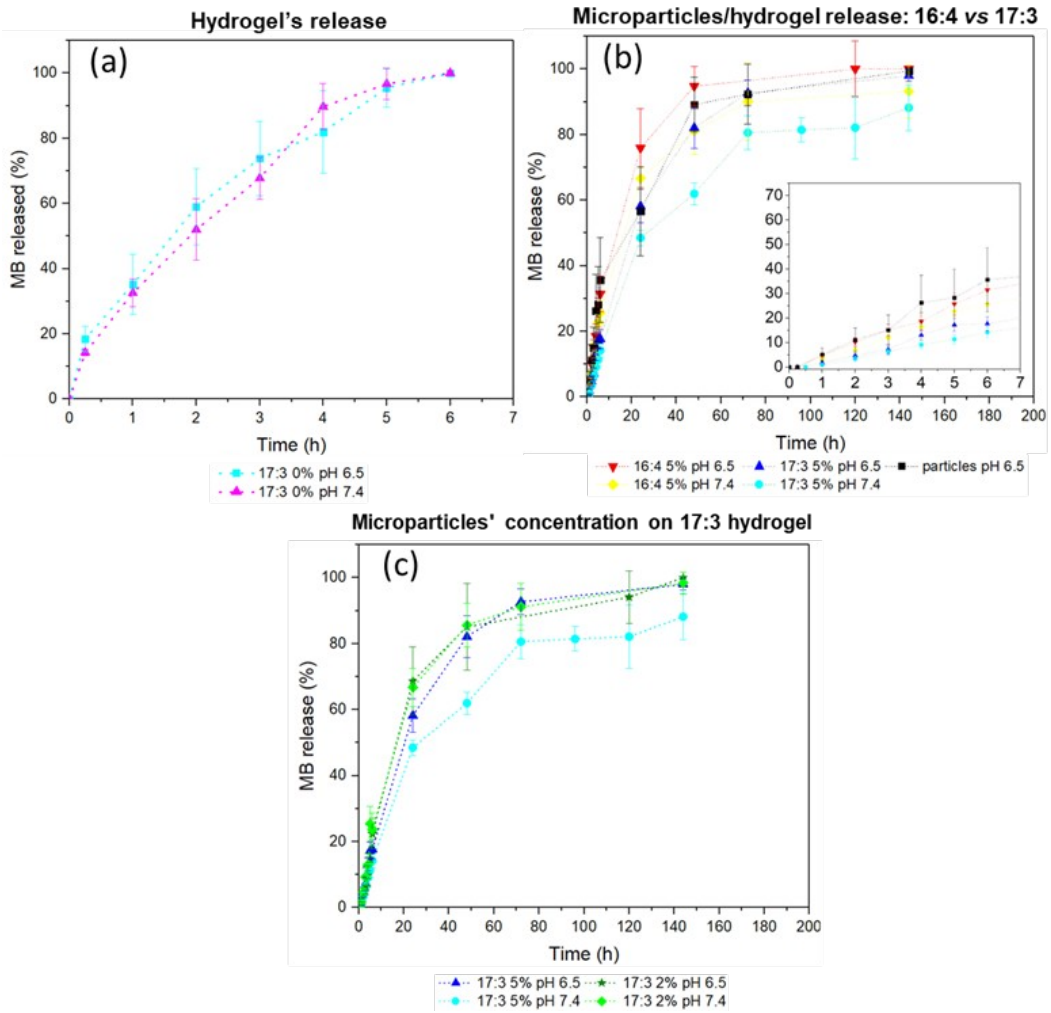

Figure 5.10 (a) Release profile of MB-loaded Pluronic gel, 17:3 F127:F68 ratio, in PBS pH 6.5 and pH 7.4; (b) Release profiles of microparticles (in PBS pH 6.5) and microparticle/gel composite system for 16:4 and 17:3

F127:F68 ratios (5 w/v% of microparticles) in PBS pH 6.5 and pH 7.4; (c) Release profile of microparticle/gel composite system with F127:F68 ratio 17:3 with 2 and 5 w/v% microparticles in PBS pH 6.5 and pH 7.4. (Adapted with permission from [2]. Copyright (2021) (Multidisciplinary Digital Publishing Institute).

In Figure 5.10 (a), after 6 hours all MB was released. No differences were detected between the systems at different pH. This great release might be related to the dissolution observed in Figure 5.9 , where after 6 hours in PBS, a great part Pluronic gel was dissolved. Also, the diffusion of MB molecules to the PBS solution also contributed to the fast release of the drug [46]. The number of micelles affects the aqueous path within the gel structure, and with the dissolution of the structure, these paths increase accelerating the drugs release [46].

In Figure 5.10 (b) the release profiles of Pluronic with ratio of 16:4 and 17:3 with MB-loaded GG:Alg microparticles were compared with a microparticles concentration of 5 w/v%. Also, the release profile of microparticles alone was compared with the microparticle/hydrogel system. There were no significant differences between the release profiles of the system with Pluronic 16:4. However, with the 17:3 ratio gel, the release profile was delayed when compared to the microparticles alone, especially at the first hours. In longer times, no significant differences between the Pluronic ratios and the microparticles alone were observed. This might explained by the significant dissolution of the Pluronic at the end of 6 hours. Thus, at the end of 6 hours, the a great percentage of the gel had been diluted. The pH did not affect the release profile of the systems, regardless of the Pluronic ratio.

In Figure 5.10 (c), it can be observed that using of 2 or 5 w/v% of microparticle concentrations did not change the release profile. The pH also did not affect the release profile, even though a pH of 7.4 at the 5 w/v% concentration was lower than the rest.

The obtained results showed that the Pluronic did not have a significant retardation effect within PBS solutions, only in the first hours. It did not delay the burst effect nor altered the release profile of the microparticles. However, the used *in vitro* environment is very different from the *in vivo*. Previous investigations [47] have revealed that Pluronic systems have a delaying effect on the release profiles of drug-loaded microparticles. Pluronic systems, in an *in vivo* study of DEX (Dexamethasone)-loaded PLGA microspheres [7], showed a delaying effect on the initial burst release, potentially owing to the interaction between DEX and the hydrogel. The hydrogel degraded at a faster rate than the microparticles, so a first drug/bioactive agent can be loaded onto the hydrogel and first released. Then the cargo within the microparticles was released. In this thesis Pluronic did not have a delaying effect in *in vitro* tests. More release studies should be conducted under similar *in vivo* conditions to determine if the Pluronic affects the release of the GG: Alg microparticle MB. This DDS can also serve as a dual-drug delivery system for complex therapeutic systems that require this dual-release profile.

5.2.2.2.1. Mathematical Fitting

Mathematical fittings of the obtained data from the drug release assays were done using the KP (Korsmeyer-Peppas) model and the PS (Peppas-Sahlin) model, and the respective modified models, the KP T_{lag} and the PS T_{lag} models, since they best fitted the GG:Alg microparticles alone Table 5.3. Good fittings were obtained and the models with T_{lag} had better fittings than the non-modified models. Between the modified KP T_{lag} and PS T_{lag} models, the latter model obtained higher R_{adj}^2, thus the obtained release profiles better fitted this model, However, even with the KP T_{lag} module the fittings were also good. With the KP T_{lag} model, the release profiles were revealed to be Fickian, according to the parameter n < 0.43. However, with the PS T_{lag} model, a mixed contribution of the Fickian release profile and a case II transport profile was obtained. But in the PS T_{lag} model, the contribution of k_1 is far higher than the contribution of k_2, thus indicating a higher Fickian contribution of the release profile than case II.

Comparing the two Pluronic ratios (16:4 vs 17:3) with 5 w/v% of microparticles, the obtained T_{lag} for Pluronic ratio of 17:3 was higher than the obtained T_{lag} for Pluronic 16:4, in both models. This indicates a slower release profile at the first hours (thus less released amounts of MB), even though it was not significant in the overall release. The pH did not affect the release profile of the microparticles/hydrogel systems. Regarding the KP T_{lag} model, the k values for the microparticles alone are higher than the ones obtained with the microparticles embedded in the hydrogels. This is attributed to the initial burst release since the hydrogels diminish this effect.

Overall, the obtained release profiles are similar to the microparticles alone, exhibiting a predominant Fickian release profile. Pluronic gels dissolved significantly within a matter of hours, under the conditions tested, with this being attributed to the loss of the micellized structure. However, Pluronic can be used as a transportation agent for the microparticles loaded with drugs/bioactive agents and has referred in other studies, in *in vivo* conditions pluronic degradation is slower [7]. Also, new Pluronic systems can be improved by combination with other polymers such as Pluronic with hyaluronic acid hydrogels [16], [38], or alginate [32] or even capped with carboxylic acid [44] in order to improve the structure of the system for a more prolonged residency time *in vitro* and *in vivo* without dissolving. Thus, more Pluronic' structure optimization and release profiles need to be done to understand if the Pluronic gel can be used as a retardation agent for drug release or just as a transportation agent of the microparticles.

Table 5.*3* Parameters obtained from the drug-release fittings for Pluronic systems with 2 and 5 w/v% of GG:Alg microparticles in pH 6.5 and 7.4 and of microparticles alone in pH 6.5. (Adapted with permission from [2]. Copyright (2021) (Multidisciplinary Digital Publishing Institute).

Batches (g)/pH	16:4 5 w/v%		17:3 5 w/v%		17:3 2 w/v%		Microparticles
	pH 6.5	pH 7.4	pH 6.5	pH 7.4	pH 6.5	pH 7.4	pH 6.5

KP	K	13.877	12.394	9.599	9.222	9.390	11.638	17.627
	n	0.442	0.438	0.498	0.472	0.510	0.460	0.347
	R^2adj	0.891	0.906	0.917	0.894	0.877	0.904	0.901
KP T_{lag}	k	21.150	22.533	20.995	20.710	23.236	21.849	30.191
	n	0.349	0.309	0.331	0.298	0.312	0.325	0.240
	T_{lag}	1.938	2.923	3.868	3.896	3.959	2.957	2.957
	R^2adj	0.929	0.956	0.965	0.956	0.955	0.961	0.955
PS	k_1	7.791	7.281	4.602	4.562	4.244	6.577	10.751
	k_2	-0.136	-0.133	-0.050	-0.058	-0.042	-0.104	-0.268
	m	0.760	0.714	0.817	0.794	0.884	0.742	0.611
	R^2adj	0.991	0.985	0.993	0.988	0.979	0.979	0.983
PS T_{lag}	k_1	10.316	12.253	9.105	7.820	8.011	11.780	13.744
	k_2	–0.245	–0.389	–0.205	–0.178	–0.158	–0.345	–0.446
	m	0.691	0.593	0.658	0.670	0.730	0.606	0.557
	T_{lag}	0.835	1.746	2.330	1.791	1.872	1.894	0.893
	R^2adj	0.995	0.994	0.997	0.996	0.989	0.991	0.990

5.2.3. Cytotoxicity

Figure 5.11 (a) the cytotoxicity results of the GG:Alg within Pluronic gels. Different concentrations of Pluronic were analysed. Only the concentrations with 20% and 15% were able to be at the gel state, since the gel formation is also dependent on the Pluronic concentration [5]. The GG:Alg microparticles are not cytotoxic, as previously observed in the previous chapter, thus this cytotoxicity comes from Pluronic. Pluronic hydrogel was extremely cytotoxic for the VERO cells. However, Pluronic F127 is approved by the Food and Drugs Administration (FDA) of the United States of America [18]. For example, for dental pump stem cells, Pluronic F127 was found to be non-cytotoxic [3]. To understand if the cytotoxicity might be due to Pluronic F68, both gels were studied separetly with the same cells (Figure 5.11 (b)). With lower Pluronic concentrations the cytotoxicity levels lowered, but F68 had significantly higher cytotoxicity levels than F127, with even Plyuronic F127 being non cytotoxic at lower concentrations (3%), indicating that a the F127 is less cytotoxic than F68. However, both hydrogels were found to be cytotoxic at the used concentrations (F127: 17% and F68: 3%). The cytotoxicity might be attributed to the dilution of the gel structure to the medium, turning it cytotoxic. Also, in the direct method, the gel state of the Pluronic might impede the seeded cells from receiving oxygen and nutrients. In order to prevent the dissolution of Pluronic might be the combination with other polymers in the future. For example, regarding breast cancer cells, in the triple-negative epithelial breast cancer adenocarcinoma MDA-MB-231 cell line, a Pluronic based hydrogel combined with hyaluronic acid was found to be not cytotoxic [16], only with the introduction of nanoparticles made the cytotoxicity increase. Another possibility is the mixture between Pluronic F127 and chitosan, with tripolyphosphate crosslinking, as done by García-Couce *et al.* [48]. The addition of the chitosan increased the gel time compared to the gel alone. Cytotoxicity tests done to human chondrocytes C28/I2 cells indicate that the developed hydrogel did not reveal cytotoxicity to these cells. Also, further studies need to be carried out with different types of cells [49].

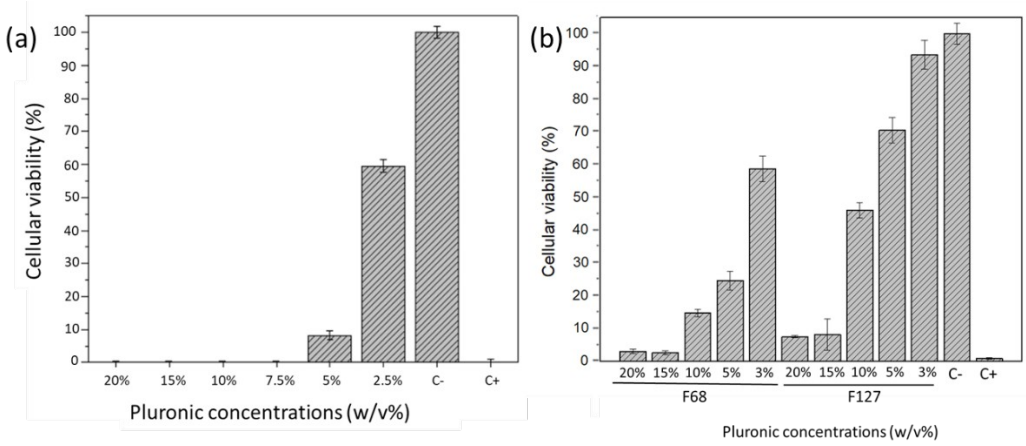

Figure 5.11 (a) VERO cell viability (%) after 48h of indirect exposure to the developed microparticles within Pluronic with different concentrations (F127:F68 ratio 17:3). Different concentrations of Pluronic aqueous solutions were used (20, 15, 10, 7.5, 5 and 2.5 w/v%). (b) VERO cell viability (%) after 48h of indirect exposure to Pluronic F127 and F68 gels. Different concentrations of Pluronic aqueous solutions were used (20, 15, 10, 5 and 3 w/v%). Data were expressed as mean ± standard deviation for at least four experiments. C- is the negative control (no medium alterations) and C+ is the positive control (medium with 10 µL of DMSO).

5.2.4. Magnetically sensitive thermoresponsive injectable DDS microparticle/hydrogel

In this last part, the GG:Alg microparticles with SPIONs and SPIAPTs will be embedded within the hydrogel. In this part, only the Pluronic hydrogel was used. In future studies, Ch/β-GP hydrogels should be conjugated with these types of microparticles.

As previously stated, the proposed system aims to serve as a DDS that is able to deliver drugs/bioactive agents and serve as a magnetic hyperthermia agent, due to the presence of mNPs, for cancer treatments. Thus, in order to deliver both mNPs and drugs, 50 w/w% of the GG:Alg microparticles were loaded with the drug (in this case MB) and the other 50 w/w% were loaded with mNPs (SPIONs or SPIAPTs) (Figure 5.12 S). In this part, rheological properties of these systems will be studied along with drug release and magnetic hyperthermia studies.

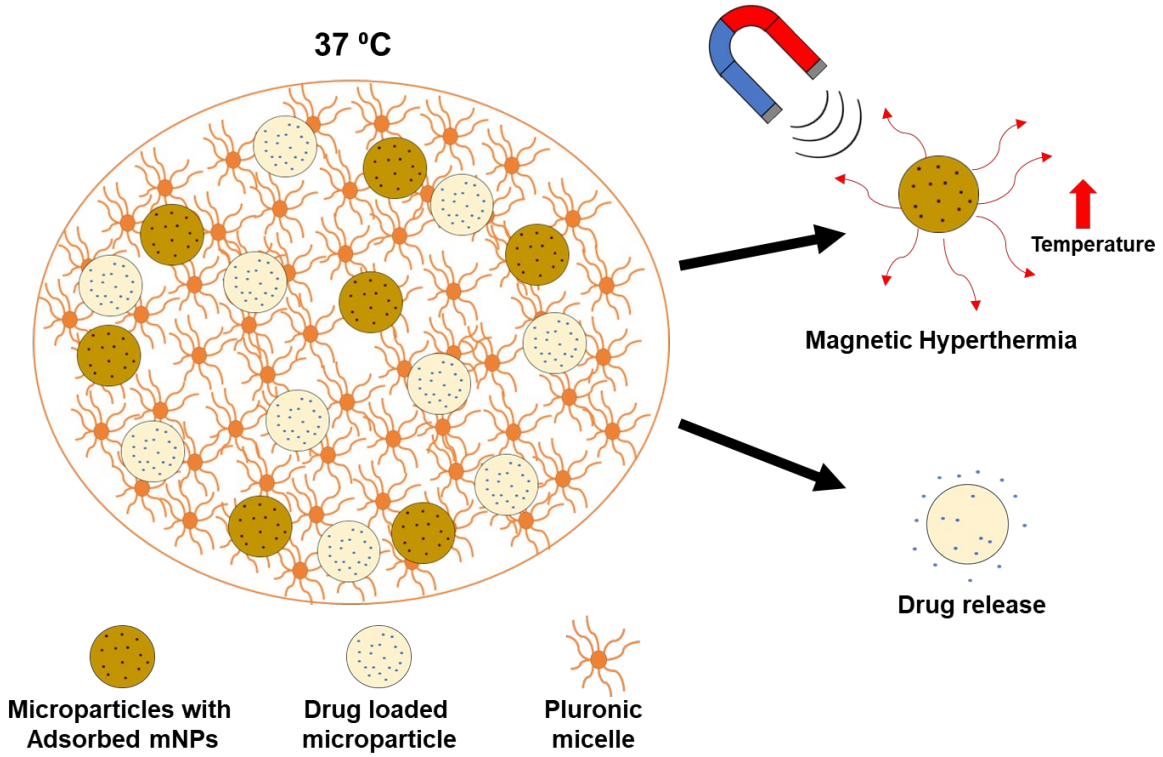

Figure 5.12 Scheme of the Pluronic gel loaded with mNPs loaded microparticles and MB loaded microparticles.

5.2.4.1. Rheological characterization

The introduction of mNPs on microparticles did not alter the transition temperature of the GG:Alg/Pluronic system, as it can be seen by comparison of Figure 5.4 and Figure 5.13 (a), and the systems with of w/w% microparticles with and without mNPs in Figure 5.13 (a).

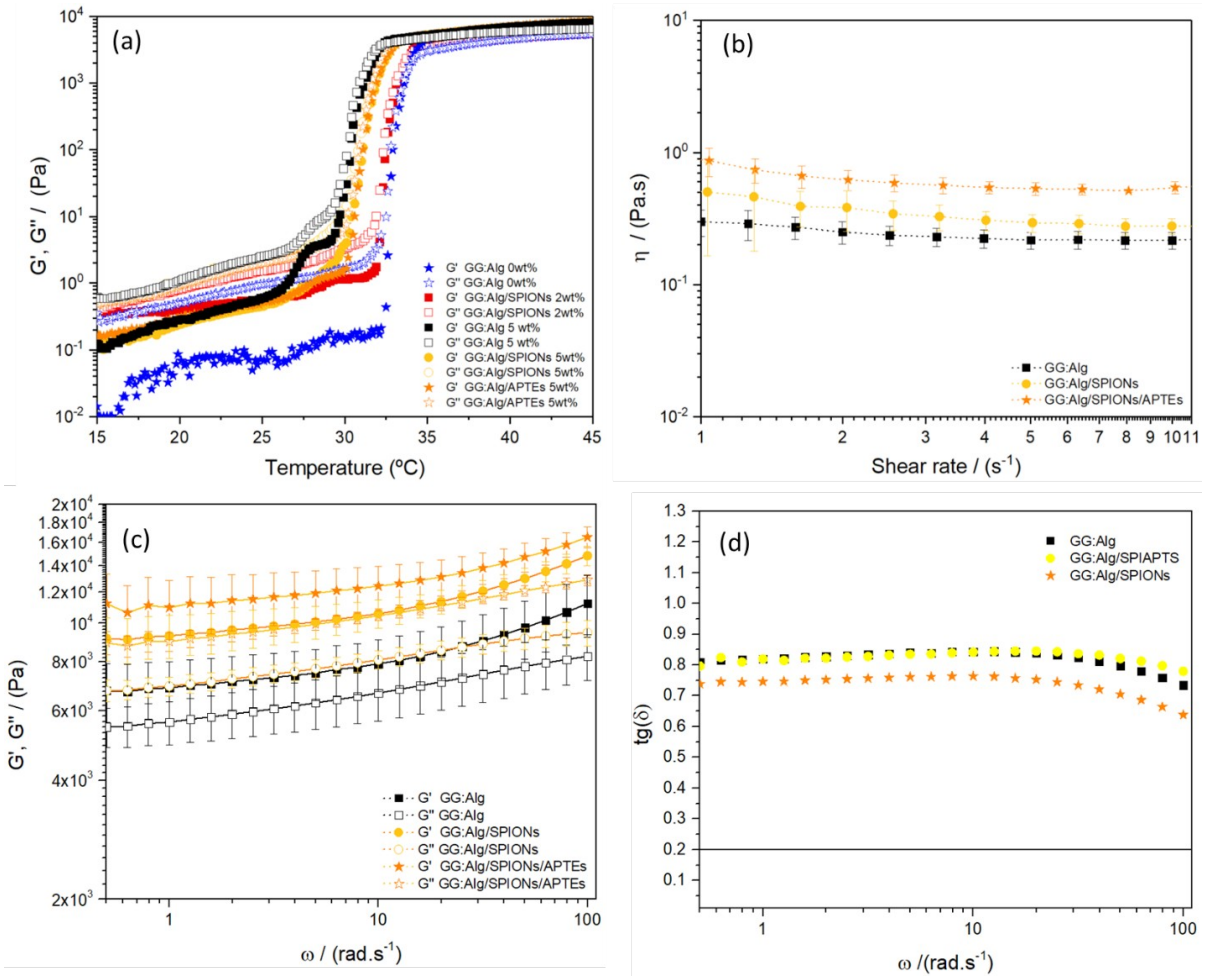

Figure 5.13 (a) Temperature ramp in oscillation for Pluronic systems (F127:F68 – 17:3 ratio) systems with and without microparticles (2 and 5 w/v%). The systems with microparticles were analysed with and without the presence of mNPs; (b) flow curves at 21ºC of a similar system with 5 w/v% of microparticles within the Pluronic; (c) Frequency sweep tests at 37ºC for similar systems in (b); (d) tg(δ) of the analysed systems in (c), a line on 0.2 was put to mark the threshold between soft gel and non-soft gel.

The systems were in the sol state at 21ºC and in the gel state at 37ºC. Flow curves in Figure 5.13 (b) show that the systems have a tendency to shear-thinning behaviour, but close to the Newtonian behaviour previously observed. An increase in viscosity was observed with the introduction of mNPs, especially with SPIAPTs. The mNPs adsorbed at the GG:Alg surface might be interacting with the Pluronic or alter the inter particle relations, might even causing aggregation, and this increasing the viscosity [14]. Other interactions between the mNPs can also have influence. Previous studies used Pluronic F127 to functionalize iron oxide mNPs with oleic acid, where the hydrophobic PPO block interacted with the oleic acid coating of mNPs [50]. For example, Jain *et al.* [51] evaluated systems with SPIONs with and without oleic acid coating, and with Pluronic, showing that without oleic acid, no interaction occurred with Pluronic. Whilst, with the oleic acid layer, bonding was observed in the FTIR spectra. The increased viscosity that was observed with SPIAPTS might be an interaction between Pluronic and SPIAPTS. However, further studies need to be done to understand if there are interactions between SPIAPTS coating and the Pluronic micelles.

Frequency sweeps at 37ºC, presented in Figure 5.13 (c) reveal that the systems were all in the gel state, with the mNPs leading to an increase in moduli. Also, a soft/weak gel structure is still observed, with the moduli close to each other and depending on frequency. Upon analysing the tg(δ) (G''/G') values over the studied angular frequencies at 37ºC (Figure 5.13 (d)), it can be seen that the Pluronic system with microparticles (with and without mNPs) had values ranging from tg(δ) 0.7 to 0.8, using tg(δ) = 0.2 as a threshold to separate the soft gels from non-weak gels [39]. These values indicated that the gel had high G'' values, though G' was still the dominating factor, since the tg(δ) values were close to 1. As a result, the introduction of the mNPs to the microparticles and to the Pluronic at 37ºC did not alter the weak elastic structure [39].

5.2.4.2. MB release studies

Figure 5.14 depicts the release profile of MB from microparticles alone and the system with Pluronic and 1:1 ratio of MB-loaded microparticles and mNPs-loaded microparticles.

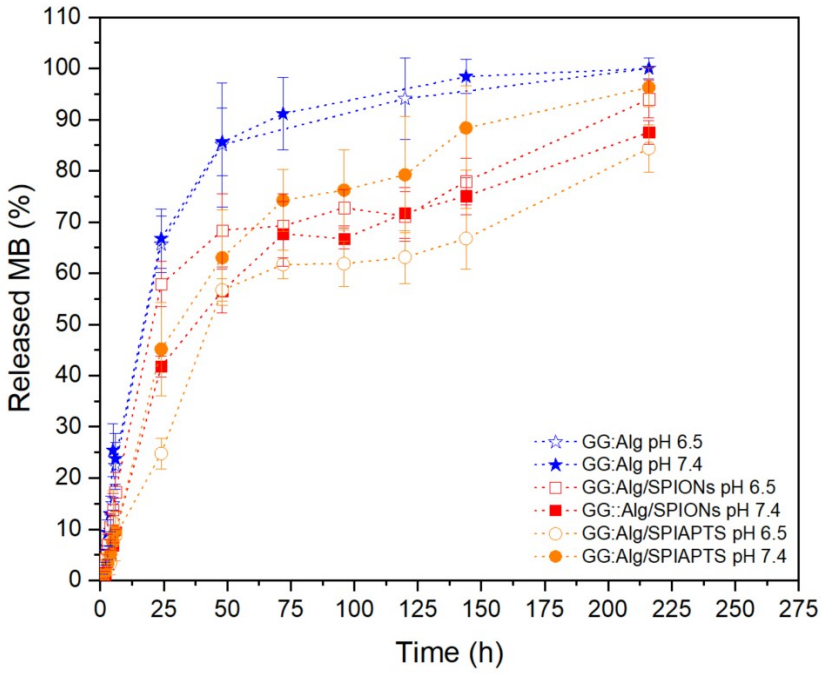

Figure 5.14 Release profiles of GG:Alg microparticles loaded with MB alone, within a Pluronic gel (2 w/w%) and with GG:Alg microparticles loaded with mNPs (2 w/w%) (ratio of microparticles with MB and microparticles with SPIONs of 1:1) at pH 6.5 and 7.4.

Microparticles alone released higher MB quantities, whilst the system with the microparticles with mNPs (ratio 1:1) did not, which might be attributed to the presence of microparticles with mNPs. Upon swelling microparticles with mNPs may absorb part of the MB released and thus delay the release profile of the system. The systems with both types of microparticles had an early burst release profile followed by a stabilization phase, but releasing lower quantities of MB than the systems with just one type of microparticle. Afterwards, the MB release continued to increase until it reached the maximum values.

The maximum amount of released MB in the systems with mNPs was lower than the ones with just one type of microparticle (especially GG:Alg/SPIONs pH 7.4 and GG:Alg/SPIAPTS pH 6.5). This might be attributed to the previously mentioned absorption of MB to the microparticles with mNPs, or possibly some interaction of the mNPs with Pluronic like previously described [50], [51]. Also, since the obtained rheological moduli were higher for the systems with mNPs, indicating a more rigid structure, that could also have affect the release. However, future studies of the relation between Pluronic and mNPs need to be done. Between the studied systems, no significant differences were found between the two studied pH.

5.2.4.2.1. Mathematical fittings

Table 5.4 Parameters obtained from the drug-release mathematical fittings of the MB-loaded microparticles alone and within the Pluronic system at pH 6.5 and pH 7.4. The R2adj that compares the experimental and theoretical values are also presented. the parameters that were obtained from the mathematical fittings of the previous release data. The modified KP and PS were again used. Both models had again good fittings with R^2_{adj} > 0.95. All systems maintained their Fickian release profiles.

Table 5.4 Parameters obtained from the drug-release mathematical fittings of the MB-loaded microparticles alone and within the Pluronic system at pH 6.5 and pH 7.4. The R^2_{adj} that compares the experimental and theoretical values are also presented.

		GG:Alg		GG:Alg/SPIONs		GG:Alg/SPIAPTS	
		pH 6.5	pH 7.4	pH 6.5	pH 7.4	pH 6.4	pH 7.4
KP-T_{lag}	k	33.76	36.39	15.78	15.89	8.81	27.78
	n	0.21	0.20	0.34	0.33	0.43	0.25
	T_{lag}	4.98	4.89	3.72	5.31	3.44	5.73
	R^2adj	0.97	0.96	0.98	0.99	0.97	0.99
PS-T_{lag}	k_1	14.50	13.71	14.16	11.22	7.51	9.68
	k_2	-0.51	-0.45	-0.46	-0.26	-0.05	-0.24
	m	0.53	0.54	0.42	0.45	0.49	0.57
	T_{lag}	2.91	1.95	2.75	4.12	3.14	3.62
	R^2adj	0.99	0.99	0.98	0.99	0.97	0.99

The effect of the mNPs on the release profile was assessed, although the release profile of the microparticles/gel system with the application of an AMF (Alternating Magnetic Field) was not tested. However, in previous works, the application of an AMF led to a faster release of loaded drugs of particles with mNPs. Finotelli *et al.* [52] developed alginate/chitosan beads containing magnetite nanoparticles for insulin release. The application of the magnetic field increased three-fold the release profile. In another study, Xue *et al.* [53] produced DOX-loaded magnetic alginate-chitosan microspheres with SPIONs. The application of an alternating magnetic field also promoted a more pronounced release of DOX. With this, we suppose that a similar effect might occur in the systems studied here. However, this hypothesis needs to be study in future works.

5.2.4.3. Magnetic hyperthermia tests

These tests are in continuation with the magnetic hyperthermia tests in the previous chapter. Unlike the microparticles with SPIONs alone, the introduction of the Pluronic gel, at the gel state, did allow the temperature to increase with the application of an AMF (Figure 5.15). This reduced hyperthermic response has been registered in similar magnetic gels that restrain both Brownian and Néel movements that reduce the temperature increase [54], [55]. The Brownian movements are supressed by the loss of Brownian movements at the microparticles surface and by the Pluronic gel structure. The suppression of the Néel contribution was attributed to the gel structure, where the Pluronic matrix could have dissipated the heat released from the particles, impeding the increase in temperature of the microparticle/gel system [55].

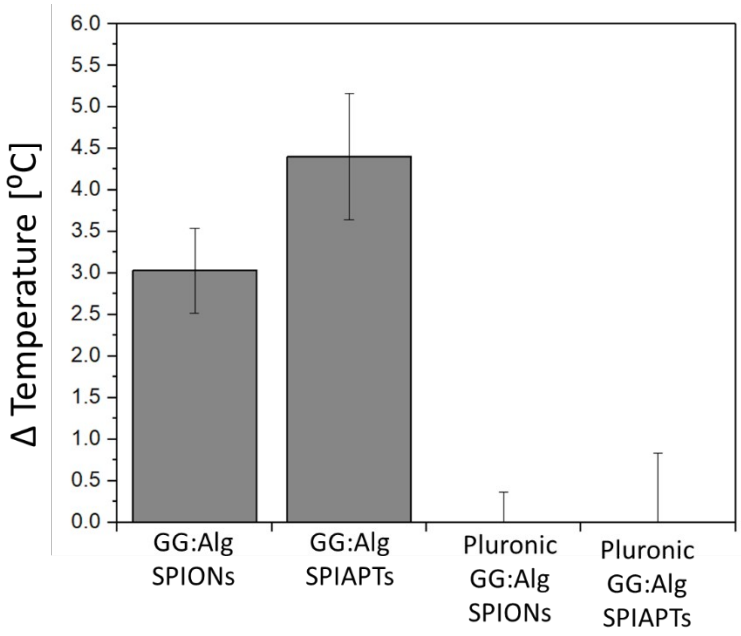

Figure 5.15 Magnetic hyperthermia study: Temperature variation with the application of an alternating magnetic field (300 Gauss and 388.5 kHz) of the SPIONs and SPIATS of microparticles with SPIONs and SPIAPTs and them embedded in Pluronic (17:3 ratio and 5 w/v% microparticle concentration).

5.3. Conclusions

The use of different ratio of Pluronic F127 and F68 allowed the manipulation of the systems sol-gel transition. The introduction of the microparticles reduced the transition temperature. The ratio of Pluronic F127 and F68 and the microparticle concentration allows the manipulation of the sol-gel transition temperature. Pluronic ratios (F127:F68) of 16:4 and 17:3 were found to be suitable for the desired injectable DDS with the transition temperature within the body temperature.

With the transition to the body temperature, Pluronic transition was almost instantaneous. The Pluronic gel could be considered a "weak gel", and was not able to withstand for long periods of time within PBS solutions, since the gel had almost fully

dissolved after 24 h. The microparticles release profiles with MB suffered some initial delay with the 17:3 ratio, preventing some initial burst release with the Pluronic gel. However, due to the fact that the Pluronic dissolved in a matter of hours in PBS solutions, the release profile was not affected by the Pluronic gel for long period of time. Regarding cytotoxicity, Pluronic was found to be cytotoxic for the Vero cell lines. However further studies need to be made with other types of cells. In this study Pluronic did not serve as a retardation barrier of drug release but as a possible transportation system for the microparticles. Nevertheless, most likely the *in vivo* conditions will promote a slower degradation of the Pluronic, meaning that delayed drug release might be achieved.

The mNPs adsorbed at the microparticles surface did not affect the Pluronic transition temperature and only increased slightly the apparent viscosity of the system at the sol state and the moduli at the gel state. However, within the gel state, the mNPs were not able to increase their temperature with the application of an external AMF, due to the conditioning of the Brownian movements restrained by the microparticles and Pluronic matrix and Néel relaxations by the Pluronic gel structure. The mixing of MB loaded GG:Alg microparticles with mNPs loaded ones with a ratio of 1:1 revealed that the release profile was affected by the microparticles with mNPs, since they absorbed part of the released MB, thus delaying the release profile of the system.

5.4. References

[1] J. Yu, H. Qiu, S. Yin, H. Wang, and Y. Li, "Polymeric drug delivery system based on pluronics for cancer treatment," *Molecules*, vol. 26, no. 12, pp. 1–23, 2021, doi: 10.3390/molecules26123610.

[2] H. Carrêlo, A. R. Escoval, P. I. P. Soares, J. P. Borges, and M. T. Cidade, "Injectable Composite Systems of Gellan Gum : Alginate Microparticles in Pluronic Hydrogels for Bioactive Cargo Controlled Delivery : Optimization of Hydrogel Composition based on Rheological Behavior," *Fluids*, vol. 7, no. 375, 2022, doi: 10.3390/fluids7120375.

[3] I. M. A. Diniz, C. Chen, X. Xu, and S. Ansari, "Pluronic F-127 hydrogel as a promising scaffold for encapsulation of dental-derived mesenchymal stem cells," 2015, doi: 10.1007/s10856-015-5493-4.

[4] A. M. Pragatheeswaran, S. B. Chen, C. F. Chen, and B. H. Chen, "Micellization and gelation of PEO-PPO-PEO binary mixture with non-identical PPO block lengths in aqueous solution," *Polymer (Guildf).*, vol. 55, no. 20, pp. 5284–5291, 2014, doi: 10.1016/j.polymer.2014.08.031.

[5] B. Shriky *et al.*, "Pluronic F127 thermosensitive injectable smart hydrogels for controlled drug delivery system development," *J. Colloid Interface Sci.*, vol. 565, pp. 119–130, 2020, doi: 10.1016/j.jcis.2019.12.096.

[6] F. Redaelli, M. Sorbona, and F. Rossi, "Synthesis and processing of hydrogels for medical applications," *Bioresorbable Polym. Biomed. Appl. From Fundam. to Transl.*

Med., pp. 205–228, 2017, doi: 10.1016/B978-0-08-100262-9.00010-0.

[7] J. Y. Heo *et al.*, "An injectable click-crosslinked hydrogel that prolongs dexamethasone release from dexamethasone-loaded microspheres," *Pharmaceutics*, vol. 11, no. 9, 2019, doi: 10.3390/pharmaceutics11090438.

[8] M. Zhang, M. Djabourov, C. Bourgaux, and K. Bouchemal, "Nanostructured fluids from pluronic® mixtures," *Int. J. Pharm.*, vol. 454, no. 2, pp. 599–610, 2013, doi: 10.1016/j.ijpharm.2013.01.043.

[9] L. G. Rio, P. Diaz-rodriguez, and M. Landin, "New tools to design smart thermosensitive hydrogels for protein rectal delivery in IBD," *Mater. Sci. Eng. C*, vol. 106, no. September 2019, p. 110252, 2020, doi: 10.1016/j.msec.2019.110252.

[10] K. V. Athira, P. Sadanandan, and S. Chakravarty, "Repurposing Vorinostat for the Treatment of Disorders Affecting Brain," *NeuroMolecular Med.*, vol. 23, no. 4, pp. 449–465, 2021, doi: 10.1007/s12017-021-08660-4.

[11] P. Zarrintaj *et al.*, "Poloxamer: A versatile tri-block copolymer for biomedical applications," *Acta Biomater.*, vol. 110, pp. 37–67, 2020, doi: 10.1016/j.actbio.2020.04.028.

[12] A. Pitto-Barry and N. P. E. Barry, "Pluronic® block-copolymers in medicine: From chemical and biological versatility to rationalisation and clinical advances," *Polym. Chem.*, vol. 5, no. 10, pp. 3291–3297, 2014, doi: 10.1039/c4py00039k.

[13] E. Gioffredi *et al.*, "Pluronic F127 hydrogel characterization and biofabrication in cellularized constructs for tissue engineering applications .," *Procedia CIRP*, vol. 49, no. iii, pp. 125–132, 2016, doi: 10.1016/j.procir.2015.11.001.

[14] L. C. Gonçalves, A. B. Seabra, M. T. Pelegrino, D. R. De Araujo, J. S. Bernardes, and P. S. Haddad, "Superparamagnetic iron oxide nanoparticles dispersed in Pluronic F127 hydrogel: potential uses in topical applications," *RSC Adv.*, vol. 7, no. 24, pp. 14496–14503, 2017, doi: 10.1039/c6ra28633j.

[15] D. Rafael *et al.*, "Efficient EFGR mediated siRNA delivery to breast cancer cells by Cetuximab functionalized Pluronic® F127/Gelatin," *Chem. Eng. J.*, vol. 340, pp. 81–93, 2018, doi: 10.1016/j.cej.2017.12.114.

[16] B. D. M. Santana, J. C. Pieretti, R. N. Gomes, and G. Cerchiaro, "Cytotoxicity towards Breast Cancer Cells of Pluronic F-127 / Hyaluronic Acid Hydrogel Containing Nitric Oxide Donor and Silica Nanoparticles Loaded with Cisplatin," 2022.

[17] X. Cheng, X. Lv, J. Xu, Y. Zheng, X. Wang, and R. Tang, "Pluronic micelles with suppressing doxorubicin efflux and detoxification for efficiently reversing breast cancer resistance," *Eur. J. Pharm. Sci.*, vol. 146, p. 105275, 2020, doi: 10.1016/j.ejps.2020.105275.

[18] M. T. Cidade, D. J. Ramos, J. Santos, H. Carrelo, N. Calero, and J. P. Borges, "Injectable hydrogels based on pluronic/water systems filled with alginate microparticles for biomedical applications," *Materials (Basel).*, vol. 12, no. 7, pp. 1–14, 2019, doi: 10.3390/ma12071083.

[19] B. Delgado, H. Carrêlo, M. V. Loureiro, A. C. Marques, J. P. Borges, and M. T. Cidade, "Injectable hydrogels with two different rates of drug release based on pluronic / water system filled with poly (e -caprolactone) microcapsules," *J. Mater. Sci.*, 2021, doi: 10.1007/s10853-021-06156-x.

[20] C. Tipa, M. T. Cidade, T. Vieira, J. C. Silva, P. I. P. Soares, and J. P. Borges, "A new long-term composite drug delivery system based on thermo-responsive hydrogel and nanoclay," *Nanomaterials*, vol. 11, no. 1, pp. 1–22, 2021, doi: 10.3390/nano11010025.

[21] S. Giovagnoli, T. Tsai, and P. P. Deluca, "Formulation and release behavior of doxycycline-alginate hydrogel microparticles embedded into pluronic F127 thermogels as a potential new vehicle for doxycycline intradermal sustained delivery," *AAPS PharmSciTech*, vol. 11, no. 1, pp. 212–220, 2010, doi: 10.1208/s12249-009-9361-8.

[22] T. Li, Q. Bao, J. Shen, R. V Lalla, and D. J. Burgess, "Mucoadhesive in situ forming gel for oral mucositis pain control," *Int. J. Pharm.*, vol. 580, no. February, p. 119238, 2020, doi: 10.1016/j.ijpharm.2020.119238.

[23] K. Suman, S. Sourav, and Y. M. Joshi, "Rheological signatures of gel-glass transition and a revised phase diagram of an aqueous triblock copolymer solution of Pluronic F127," *Phys. Fluids*, vol. 33, no. 7, Jul. 2021, doi: 10.1063/5.0057090.

[24] N. Rapoport, "Physical stimuli-responsive polymeric micelles for anti-cancer drug delivery," *Prog. Polym. Sci.*, vol. 32, no. 8–9, pp. 962–990, 2007, doi: 10.1016/j.progpolymsci.2007.05.009.

[25] S. Costanzo *et al.*, "Rheology and morphology of Pluronic F68 in water," *Phys. Fluids*, vol. 33, no. 4, 2021, doi: 10.1063/5.0049722.

[26] M. H. Lee, G. H. Shin, and H. J. Park, "Solid lipid nanoparticles loaded thermoresponsive pluronic–xanthan gum hydrogel as a transdermal delivery system," *J. Appl. Polym. Sci.*, vol. 135, no. 11, Mar. 2018, doi: 10.1002/app.46004.

[27] I. Nastase, C. Croitoru, A. Vartires, and L. Tataranu, "Indoor Environmental Quality in Operating Rooms: An European Standards Review with Regard to Romanian Guidelines," *Energy Procedia*, vol. 85, no. November 2015, pp. 375–382, 2016, doi: 10.1016/j.egypro.2015.12.264.

[28] K. Al Khateb *et al.*, "In situ gelling systems based on Pluronic F127/Pluronic F68 formulations for ocular drug delivery," *Int. J. Pharm.*, vol. 502, no. 1–2, pp. 70–79, 2016, doi: 10.1016/j.ijpharm.2016.02.027.

[29] G. Wei, H. Xu, P. T. Ding, M. Li, and M. Zheng, "T hermosetting gels with modulated gelation temperature for ophthalmic use: the rheological and gamma scintigraphic studies," 2002. [Online]. Available: www.elsevier.com/locate/jconrel

[30] H. Zhang, J. Cheng, and Q. Ao, "Preparation of Alginate-Based Biomaterials and Their Applications in Biomedicine," pp. 1–24, 2021.

[31] S. Gaisford, A. E. Beezer, and J. C. Mitchell, "Diode-array UV spectrometric evidence for cooperative interactions in binary mixtures of pluronics F77, F87, and F127," *Langmuir*, vol. 13, no. 10, pp. 2606–2607, 1997, doi: 10.1021/la962033r.

[32] H. R. Lin, K. C. Sung, and W. J. Vong, "In situ gelling of alginate/Pluronic solutions for ophthalmic delivery of pilocarpine," *Biomacromolecules*, vol. 5, no. 6, pp. 2358–2365, 2004, doi: 10.1021/bm0496965.

[33] M. Margarita *et al.*, "Rheology and applications of highly filled polymers: A review of current understanding," *Prog. Polym. Sci.*, vol. 66, pp. 22–53, 2017, doi: 10.1016/j.progpolymsci.2016.12.007.

[34] M. Bek, J. Gonzalez-gutierrez, C. Kukla, B. Maroh, and L. S. Perše, "Rheological Behaviour of Highly Filled Materials for Injection Moulding and Additive Manufacturing: Effect of Particle Material and Loading," *Appl. Sci.*, vol. 10, no. 7993, 2020, doi: 10.3390/app10227993.

[35] Y. Zheng *et al.*, "Injectable hydrogel-microsphere construct with sequential degradation for locally synergistic chemotherapy," *ACS Appl. Mater. Interfaces*, vol. 9, no. 4, pp. 3487–3496, 2017, doi: 10.1021/acsami.6b15245.

[36] M. M. Denn and J. F. Morris, "Rheology of non-brownian suspensions," *Annu. Rev. Chem. Biomol. Eng.*, vol. 5, pp. 203–228, 2014, doi: 10.1146/annurev-chembioeng-060713-040221.

[37] A. Talmo and E. Meshkati, "Rheology, Rheometry and Wall Slip," in *Advances in Slurry Technology*, IntechOpen, 2022. doi: 10.5772/intechopen.108048.

[38] S. Chatterjee, P. C. leung Hui, C. wai Kan, and W. Wang, "Dual-responsive (pH/temperature) Pluronic F-127 hydrogel drug delivery system for textile-based transdermal therapy," *Sci. Rep.*, vol. 9, no. 1, pp. 1–13, 2019, doi: 10.1038/s41598-019-48254-6.

[39] P. Sánchez-Cid *et al.*, "Biocompatible and Thermoresistant Hydrogels Based on Collagen and Chitosan," *Polymers (Basel).*, vol. 14, no. 2, pp. 1–14, 2022, doi: 10.3390/polym14020272.

[40] I. Zarandona, C. Bengoechea, E. Álvarez-Castillo, K. de la Caba, A. Guerrero, and P. Guerrero, "3D printed chitosan-pectin hydrogels: From rheological characterization to scaffold development and assessment," *Gels*, vol. 7, no. 4, 2021, doi: 10.3390/gels7040175.

[41] M. Ghanbari, M. Salavati-Niasari, F. Mohandes, B. Dolatyar, and B. Zeynali, "In vitro study of alginate-gelatin scaffolds incorporated with silica NPs as injectable, biodegradable hydrogels," *RSC Adv.*, vol. 11, no. 27, pp. 16688–16697, 2021, doi: 10.1039/d1ra02744a.

[42] Y. Liu, Y. Yu, C. Liu, J. M. Regenstein, X. Liu, and P. Zhou, "Rheological and mechanical behavior of milk protein composite gel for extrusion-based 3D food printing," *Lwt*, vol. 102, pp. 338–346, 2019, doi: 10.1016/j.lwt.2018.12.053.

[43] M. Jalaal, G. Cottrell, N. Balmforth, and B. Stoeber, "On the rheology of Pluronic F127 aqueous solutions," *J. Rheol. (N. Y. N. Y).*, vol. 61, no. 1, pp. 139–146, 2017, doi: 10.1122/1.4971992.

[44] S. Y. Park, Y. Lee, K. H. Bae, C. Ahn, and T. G. Park, "Temperature / pH-Sensitive Hydrogels Prepared from Pluronic Copolymers End-Capped with Carboxylic Acid

Groups via an Oligolactide Spacer," pp. 1172–1176, 2007, doi: 10.1002/marc.200600914.

[45] Y. Lin and P. Alexandridis, "Temperature-dependent adsorption of Pluronic F127 block copolymers onto carbon black particles dispersed in aqueous media," *J. Phys. Chem. B*, vol. 106, no. 42, pp. 10834–10844, 2002, doi: 10.1021/jp014221i.

[46] J. C. Gilbert, J. Hadgraft, A. Bye, and L. G. Brookes, "Drug release from Pluronic F-127 gels," *Int. J. Pharm.*, vol. 32, no. 2–3, pp. 223–228, 1986, doi: 10.1016/0378-5173(86)90182-1.

[47] H. Carrêlo, P. I. P. Soares, J. P. Borges, and M. T. Cidade, "Injectable composite systems based on microparticles in hydrogels for bioactive cargo controlled delivery," *Gels*, vol. 7, no. 3, 2021, doi: 10.3390/gels7030147.

[48] J. García-Couce, M. Tomás, G. Fuentes, L. J. Cruz, I. Que, and A. Almirall, "Chitosan/Pluronic F127 Thermosensitive Hydrogel as an Injectable Dexamethasone Delivery Carrier," *Gels*, vol. 8, p. 44, 2022.

[49] S. Nie and W. L. W. Hsiao, "Thermoreversible Pluronic ® F127-based hydrogel containing liposomes for the controlled delivery of paclitaxel : in vitro drug release , cell cytotoxicity , and uptake studies," pp. 151–166, 2011, doi: 10.2147/IJN.S15057.

[50] H. Vu-Quang *et al.*, "Pluronic F127-folate coated super paramagenic iron oxide nanoparticles as contrast agent for cancer diagnosis in magnetic resonance imaging," *Polymers (Basel).*, vol. 11, no. 4, 2019, doi: 10.3390/polym11040743.

[51] T. K. Jain, M. A. Morales, S. K. Sahoo, D. L. Leslie-Pelecky, and V. Labhasetwar, "Iron oxide nanoparticles for sustained delivery of anticancer agents," *Mol. Pharm.*, vol. 2, no. 3, pp. 194–205, 2005, doi: 10.1021/mp0500014.

[52] P. V. Finotelli *et al.*, "Microcapsules of alginate/chitosan containing magnetic nanoparticles for controlled release of insulin," *Colloids Surfaces B Biointerfaces*, vol. 81, no. 1, pp. 206–211, 2010, doi: 10.1016/j.colsurfb.2010.07.008.

[53] W. Xue *et al.*, "AMF responsive DOX-loaded magnetic microspheres: Transmembrane drug release mechanism and multimodality postsurgical treatment of breast cancer," *J. Mater. Chem. B*, vol. 6, no. 15, pp. 2289–2303, 2018, doi: 10.1039/c7tb03206d.

[54] A. Gonçalves, F. V. Almeida, J. P. Borges, and P. I. P. Soares, "Incorporation of dual-stimuli responsive microgels in nanofibrous membranes for cancer treatment by magnetic hyperthermia," *Gels*, vol. 7, no. 1, pp. 1–17, 2021, doi: 10.3390/GELS7010028.

[55] P. Monks *et al.*, "Spatiotemporally Resolved Heat Dissipation in 3D Patterned Magnetically Responsive Hydrogels," *Small*, vol. 17, no. 5, pp. 1–12, 2021, doi: 10.1002/smll.202004452.

6. THE GG:ALG/CH/Β-GP SYSTEM

6.1. Introduction

In this chapter, the development of the GG:Alg/Ch/β-GP system will be addressed. Firstly, a Ch/β-GP hydrogel was developed without GG:Alg microparticles. Then, the optimized Ch/β-GP hydrogel was combined with GG:Alg microparticles to develop a thermoresponsive system. The main goal was to optimize the sol-gel transition temperature so that the system is in the sol state at 21ºC (operating room temperature) and in the gel state at 37ºC (human body temperature).

This chapter will be based on the following article:

H. Carrêlo; M. Jiménez-Rosado; Victor Perez-Puyana; A. Romero; J. P. Borges; P.I.P. Soares; "A Thermoresponsive Injectable Drug Delivery System of Chitosan/β-Glycerophosphate with Gellan Gum/Alginate Microparticles" (2023) (in preparation)

6.1.1. Chitosan

Chitosan (Ch) is a natural biopolymer derived from chitin. Chitin is found in the exoskeletons of crustaceans such as shrimp and crabs, as well as in the cell walls of fungi. Chitosan is obtained by deacetylation of chitin using an alkaline treatment, having at least a degree of deacetylation higher than 50% [1]. Chitosan is a linear polysaccharide composed of β(1→4) linked D-glucosamine (GlcN) and N-acetyl-D-glucosamine (GlcNAc) units [2] (Figure 6.1 (a), (b) and (c)). Chitosan is a cationic polymer due to the presence of amino groups in its chains, resulting in a positively charged polymer. Consequently, it only dissolves in acidic solvents. Also, higher protonation increases electrostatic repulsion between polymeric chains. Chitosan has useful properties for biomedical purposes, such as [3]–[10]:

- Non-toxic: It does not induce inflammation or cause an immune response from the human body;
- Antimicrobial: Because it is a cationic polymer, it exhibits bactericidal and bacteriological properties. Polymers with positive charges adhere to bacterial surfaces and alter the permeability of bacteria's membranes that prevent bacteria growth. A low degree of deacetylation and low pH chitosan have better antibacterial properties;
- Mucoadhesive: Chitosan has shown to adhere to the mucus layer that covers the mucosal surfaces within the body. Mucoadhesive materials can prolong the residence time of drugs or devices on mucosal surfaces;
- Hemocompatibility: The amino groups of chitosan can interact with the platelets in the blood and promote wound healing;

- Antioxidant: chitosan can scavenge the active oxygen free radicals *in vitro*. This prevents the destruction of membrane lipids, proteins and DNA;
- Biodegradability: chitosan is known to be degraded by enzymes, like lysozyme;
- Antitumour activity: chitosan and its derivatives have shown anticancer properties. It can selectively permeate through cancer cell membranes for anticancer activities with cellular enzymatic, antiangiogenic, and immunoenhancing activities [11].

6.1.2. Chitosan thermoresponsive hydrogels

Chitosan solutions and hydrogels are not thermoresponsive hydrogels; however, the mixing with β-GP (β-Glycerophosphate) (Figure 6.1 (d)) has resulted in the creation of thermoresponsive chitosan/β-GP hydrogels (Ch/β-GP) [12]. The addition of the β-GP to an acidic chitosan solution will have three major impacts on the solution [12], [13]:

- Increase of the pH to physiological pH (around 6.8 to 7.4);
- Inhibition of chitosan precipitation;
- Grant a thermoresponsive behaviour to the solution.

The thermoresponsive behaviour can be explained by multiple factors such as electrostatic interactions (with the interaction of phosphate and amino groups), hydrophobic interactions (via glycerol of β-GP) and hydrogen bonding [14]. At low temperatures, in Ch solutions in an acidic medium, the aggregation of the Ch chains is prevented by the inter-chain electrostatic repulsions, with water molecules between the Ch chains that form a regular arrangement [13]. The added β-GP interacts electrostatically with chitosan (Figure 6.1 (e)), maintaining the water molecules arrangements around the chitosan chains. However, with temperature increase, the instability of the water molecules around Ch (solvent-polymer interactions) increases and the polymer-polymer interactions of Ch are promoted by the glycerol moieties, resulting in the formation of a 3D structure [13]. Also, at low temperatures, Ch adopts a coiled conformation due to the presence of hydrogen bonds. With higher temperatures, these bonds might decrease in number, favouring Ch interchain interactions to form a hydrogel [13], [15].

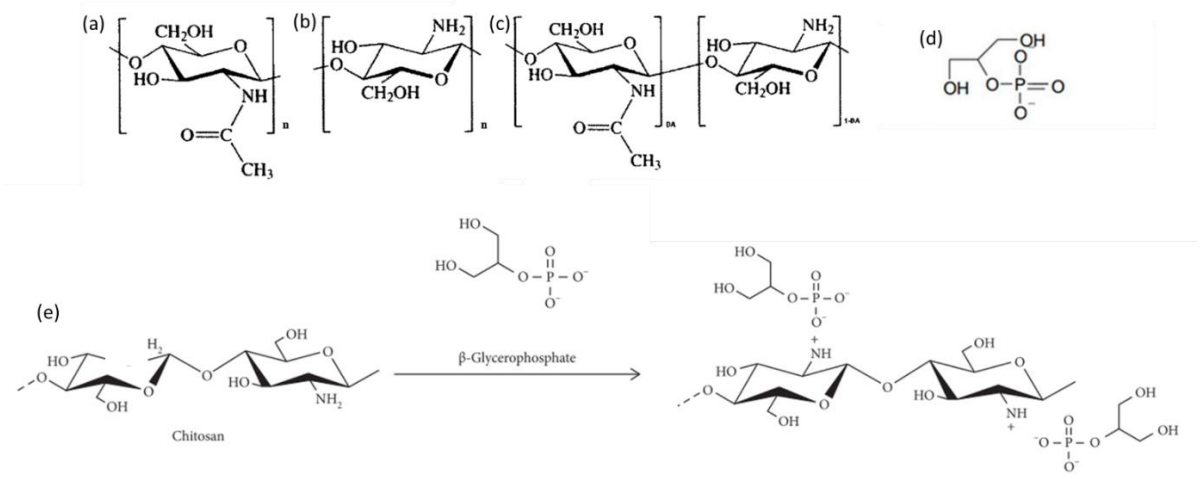

Figure 6.1 Chemical structures of (a) chitin poly(*N*-acetyl-b-D glucosamine) repeat units; (b) chitosan (poly(D-glucosamine) repeat units; (c) Structure of partially deacetylated chitosan, a copolymer characterized by its average degree of deacetylation DD. (Adapted with permission from [1]. Copyright (2006) Elsevier). (d) Structure of β-Glycerophosphate (Adapted with permission from [16]. Copyright (2021) Multidisciplinary Digital Publishing Institute). (e) Interaction between Ch and β-GP, with the positively charged amino groups of Ch interact with the negatively charged phosphate groups of β-GP (Adapted with permission from [17]. Copyright (2021) Hindawi).

6.1.3. Properties of the Ch/β-GP

The sol-gel transition of Ch/β-GP hydrogel is not reversible, thus by decreasing the temperature the system will not reverse to the sol state [12], [15]. Also, the transition is time-dependent, thus, it means that the transition is not instantaneous when compared to other thermoresponsive polymers, such as Pluronic, that have the sol gel transition occurring almost instantaneously [18]. However, the transition time, and also the transition temperature are dependent on different factors. Higher concentrations of β-GP accelerates the hydrogel gelation time and decreases the transition temperature [13]. Higher concentrations of chitosan decrease the gelation time, but shifts the sol-gel transition to higher temperatures [17]. By decreasing the molecular weight of Ch the gelation time is increased, however, gelation can be faster by increasing chitosan deacetylation degree [12], [15], [17].

The molecular weight and degree of deacetylation of chitosan affects the mechanical properties of the hydrogel and the rheological properties of the solution and sol-gel transition. High molecular weight chitosan provides superior gel strength [19]. Also, higher concentrations of β-GP increase the mechanical properties of the hydrogel [13].

Regarding the type of salt, other glycerophosphates that do not use sodium have also been studied, even though this study only used disodium salt glycerophosphate (β-GP). In a study done by Owczarz *et al.* [20], calcium glycerophosphate (Ca-GP) and magnesium glycerophosphate (Mg-GP) salts were used and compared with the (β-GP) . The use of Ca-GP promoted a faster gelation whilst the Mg-GP delayed the transition.

6.1.4. Ch/β-GP applications

Ch/β-GP as a thermoresponsive hydrogel has been used in different studies for biomedical applications [12], [14], [21]. Zhao *et al.* [22] used this hydrogel for wound dressing to promote a faster healing. The hydrogel was loaded with β-cyclodextrin-curcumin for its antioxidant, anti-inflammatory, immunomodulatory, and antimicrobial properties. The hydrogel had a porous structure after gelation and was able to release the cargo with a sustained profile. At the end of 14 days, the *in vitro* cumulative release was around 39.95 ± 6.90%, without a burst release effect and with a degradation of 53.26 ± 5.41% within a PBS solution of pH 7.35. Also, in *in vitro* studies, the hydrogel displayed anti-oxidative and antimicrobial capacities. In *in vivo* wound infection models, faster wound closure was observed on rats with hydrogel with improved histological outcomes.

The Ch/β-GP can also be conjugated with other polymers. Schan *et al.* [23] developed a chitosan/glycerophosphate hydrogel mixed with collagen for the treatment of ulcers caused by endoscopic submucosal dissection. Collagen did not alter the physicochemical properties of the systems, maintaining the thermoresponsive characteristics of the Ch/β-GP hydrogels, with fluidity at lower temperatures (low viscosities). The addition of collagen provided better biocompatibility, promoted growth factor delivery to cells and coagulation. Roehm *et al.* [24] conjugated Ch with gelatin to produce bioprinting inks and then mixed β-GP. Results showed that viable cells were well distributed within the printed fibres, showing that the Ch/ β-GP was a viable candidate as an ink for bioprinting. For DOX (Doxorubicin) controlled delivery to treat breast cancer, Fathi *et al.* [25] blended poly(N-isopropyl acrylamide-co-itaconic acid) (PNIPAAm-co-IA) with Ch and glycerophosphate solution to produce a thermoresponsive and pH-sensitive hydrogel. The swelling capacities of the hydrogel were pH and temperature dependant. DOX release was revealed to be faster at acidic conditions (pH 5.5) at 37ºC than at neutral pH (pH 7.4) at 40ºC. The hydrogel proved to be non-cytotoxic to MCF-7 (Michigan Cancer Foundation-7) cells with anti-proliferative capacity. Saeednia *et al.* [26] developed a Ch/β-GP hydrogel loaded with carbon nanotubes and methotrexate. *in vitro* degradation with enzymes, showed that the nanotubes lowered the degradation rate of the hydrogel. However, higher concentrations of nanotubes led to faster degradation rates when compared to lower concentrations. The addition of the nanotubes decreased the release rate of the drug. *In vitro* studies with MCF-7 breast cancer cells showed that the presence of the nanotubes enhanced the drug antitumor activity due to the slower drug release when compared to samples without nanotubes. Also, the sharp edges of the carbon nanotubes may have caused cancerous cell membrane damage, thus shrinking the tumour size. Previously, the same author also did a similar study [27] but with graphene oxide, where its addition also decreased the release rate of the same drug, showing a potential as breast cancer therapy system for the delivery of methotrexate .

6.1.5. Microparticles within Ch/β-GP hydrogels

Ch/β-GP has also been combined with microparticles. Mahmoudian *et al.* [28] developed hydroxypropylmethylcellulose (HPMC) microparticles to deliver vancomycin to prevent bacterial infections. These microparticles were then loaded in thermoresponsive Ch/β-GP hydrogels for local treatment of osteomyelitis. Microparticles with a diameter range of 1.5–6.4 μm were successfully produced, with drug encapsulation of around 73%. *In vitro* release of vancomycin was delayed by the presence of the Ch hydrogel serving as a barrier. Zan *et al.* [29] used poly-3-hydroxybutyrate microparticles with 5-fluorouracil (5-FU) and embedded them in a Ch/β-GP hydrogel. The initial released drug amounts were significantly reduced (from 85% down to 29% in the first 8 h of released 5-FU), and the release was extended for longer times. Also, using HPMC microparticles with the antibiotic vancomycin within Ch/β-GP hydrogels. Similarly, to the previous study, the release time was prolonged. Karimi *et al.* [30] developed a Ch/β-GP with cellulose acetate butyrate nanoparticles for *in vivo* intratumoral administration in mice bearing breast cancer and *in vitro* with 4T1 breast cancer cell lines. Nanoparticles produced by the solvent evaporation process and optimized via a two-level fractional factorial design were developed and loaded onto the hydrogel. Drug release from the nanoparticles was delayed by the presence of the hydrogel. The composite system proved higher efficiency in the *in vitro* and *in vivo* trials than the free drug and drug loaded hydrogel.

The combination of Ch/β-GP hydrogels and GG:Alg microparticles studied in this thesis has never, as far as the research showed, been studied. Hence, this chapter will focus on the study and characterization of GG:Alg microparticles with thermoresponsive hydrogels. Materials and methods (production and characterization) are described in Chapter 3.

6.2. Results and Discussion

6.2.1. Pre-tests

At a pre-tests phase, the β-GP was dissolved in ultrapure water solutions and mixed with the chitosan solution. No hydrogel was formed with the temperature increase. However, when the β-GP was dissolved within an acetic acid solution and then mixed with the chitosan solution, a hydrogel formed with a temperature increase from 10ºC to 37ºC. This was attributed to the different pH of the precursor solutions. In the solution with only ultrapure water, the pH was higher than the solution with acetic acid. At more acidic pH, Ch remains soluble; however, at higher pH the chitosan precipitates and no interaction with β-GP occurred [15]. As previously stated in Chapter 3, different concentrations of β-GP were used and mixed with a chitosan solution (3 w/v%): 0 (Ch/0%β-GP), 2 (Ch/2%β-GP), 3 (Ch/3%β-GP), 4 (Ch4%β-GP) and 5 (Ch/5%β-GP) w/v%.

The addition of β-GP to chitosan solutions led to a pH increase, at 10ºC and after 1 hour of mixing, as can be observed in Table 6.1. The introduction of this salt stabilized the

solutions' pH around the neutral pH. This stabilization occurs when the molar concentration of β-GP exceeded the molar concentration of the amine groups in chitosan [31]. The transition temperature is also related to the pH increase. With higher pH, the chitosan chains decrease their charge density, leading to more interchain electrostatic interaction, resulting in faster gelation [32].

Table 6.1 Variation of the pH of the solutions after 1h mixing at 10ºC in the different systems (batch) with 0, 2, 3, 4 and w/v% of β-GP within the Ch solution.

Batch	pH
Ch/0%β-GP	6.41 ± 0.07
Ch/2%β-GP	7.09 ± 0.06
Ch/3%β-GP	7.24 ± 0.03
Ch/4%β-GP	7.40 ± 0.07
Ch/5%β-GP	7.45 ± 0.04

Afterwards, it was observed that the thermoresponsiveness of the hydrogel was dependent on time, and temperature ramps (as used to study Pluronic gels) could not be used to fully characterize the Ch/β-GP hydrogel. Thus, a rheological protocol was prepared that accounted for time at three temperatures: 10ºC was the temperature at which the mixture was prepared; 20ºC was chosen since it is an intermediary temperature and close to the operating room temperature; and 37ºC was used since it is the body temperature. Different periods of time during each temperature were used, to understand how the moduli varied with time at each phase: 10 minutes were given to the 10ºC phase (it is important to notice that the solutions had been mixed at 10ºC for 1 hour before the test); 30 minutes were given to the 20ºC phase (no gelation occurred for this period); at 37ºC, 2 hours were given. The thermoresponsive behaviour was not reversible. The decrease of a temperature of 37ºC to 10ºC did not revert the hydrogel to the sol system, similar to previous works [12], [15], [26].

6.2.2. Ch/β-GP hydrogel and the β-GP effect

Figure 6.2 represents the behaviour of different concentrations of β-GP within chitosan solutions with the customized rheological test.

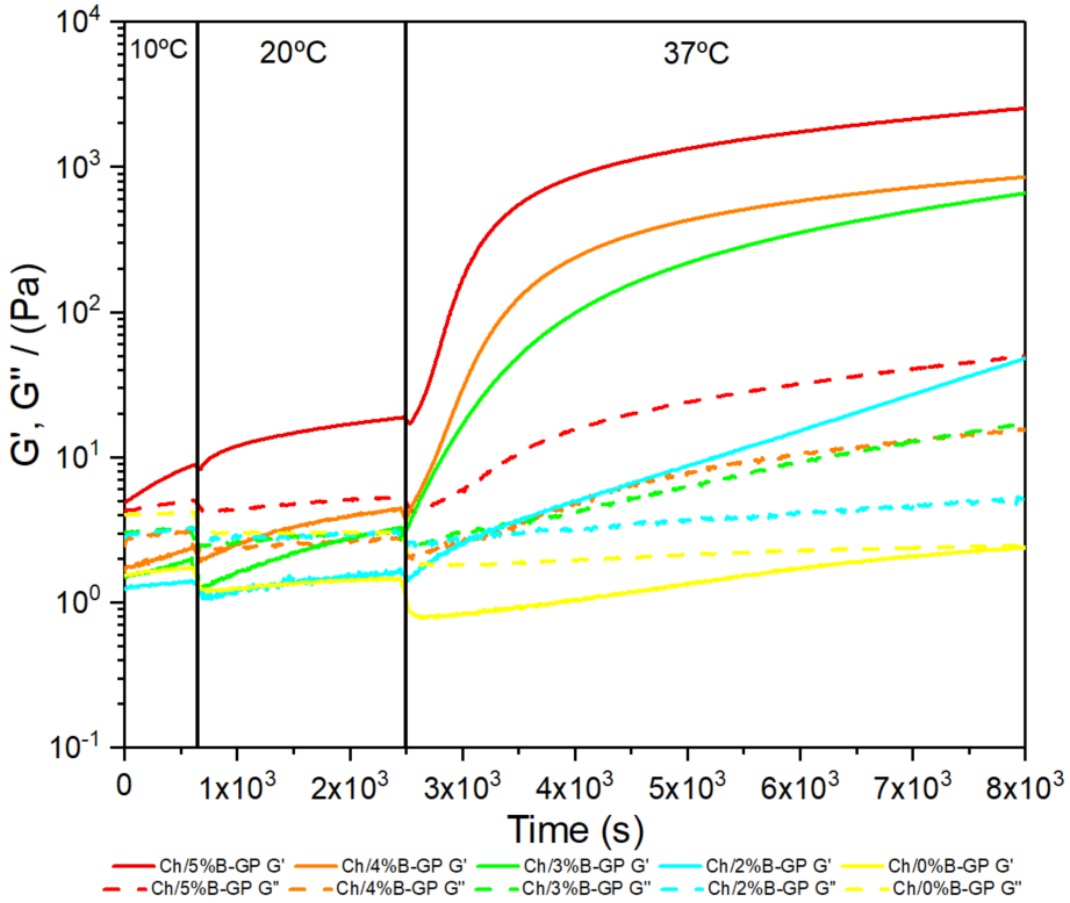

Figure 6.2 Transient test at different temperatures in oscillation at a frequency of 1Hz. Temperatures of 10ºC during 10 minutes, 20ºC for 30 minutes and 37ºC for up to 1.5 hours. Different concentrations of B-GP were evaluated (0, 2, 3, 4 and 5 w/v%).

At 10 °C, all systems presented a viscous state with G''>G', except for Ch/5%β-GP. All systems had the moduli within 1 and 10 Pa. Higher amounts of β-GP showed a significant increase in G' with time, whereas G'' remained stable. The Ch/5%β-GP had a significant increase of both moduli, with G'>G'', depicting an elastic behaviour. The lower concentrations retained G''>G' with a positive slope of G' with time and G'' with a null slope.

At 20 °C, G' continued to increase with time, whereas G'' remained constant. However, in the systems with no salt and in Ch/2%β-GP, the viscous behaviour was maintained with G''>G'. In the other samples, the G' increased to a point that the values shifted to G'>G'' for Ch/3%β-GP, Ch/4%β-GP, but with the values of G' and G'' still close. Ch/5%β-GP presented a great increase in G', with a greater difference to G''. The loss modulus remained almost constant, with similar values to those presented at the 10ºC phase.

The temperature increase from 20ºC to 37ºC resulted in an abrupt increase in moduli values of almost 3 decades, for Ch/3%β-GP, Ch/4%β-GP, and Ch/5%β-GP, indicating hydrogel gelation. The Ch/2%β-GP system exhibited an almost linear increase. For Ch/3%β-GP, Ch/4%β-GP, and Ch/5%β-GP, after a determined amount of time at 37ºC, the moduli decreased their slope and stabilized in a plateau with a slightly positive slope, indicating that the gel phase

was achieved, and some structure was still being formed with time, but at a far slower rate. This is attributed to the slower diffusion of molecules through the hydrogel structure in the gel state [15]. Higher concentrations of β-GP led to faster gelation. Ch/5%β-GP reached the plateau around after 13 minutes from the switch to 37ºC. Ch/4%β-GP reached it at around after 19 minutes and Ch/3%β-GP at around 23 minutes. Also, higher concentrations of β-GP led to higher moduli values with Ch/5%β-GP having the higher moduli and Ch/2%β-GP and Ch/0%β-GP the lower values. Thus, the speed of gelation and the gel's strength is dependent on the concentration of β-GP.

All obtained results are in agreement with the literature, with higher salt concentrations leading to higher moduli and faster gelation [12], [15], [32]. For the following tests, the Ch/4%β-GP system was chosen since it was viscous at 10ºC and 20ºC, allowing blending with the microparticles, and exhibited an elastic structure at 37ºC.

Figure 6.3 shows the Ch/0%β-GP and Ch/4%β-GP systems at the 3 studied temperatures and at different times. Without β-GP, no sol gel transition was registered. The test is in accordance with Figure 6.2, when comparing the system physical state, temperatures, and times. After 1 hour at 10ºC, the system is viscous (G'<G'' and with low values). At 20ºC after 20 minutes the system remains at the sol state. At 37ºC, after 20 minutes the Ch/4%β-GP is at the gel state. In Figure 6.2 the transition to the gelation plateau was registered around 20 minutes for the Ch/4%β-GP system after the transition to 37ºC.

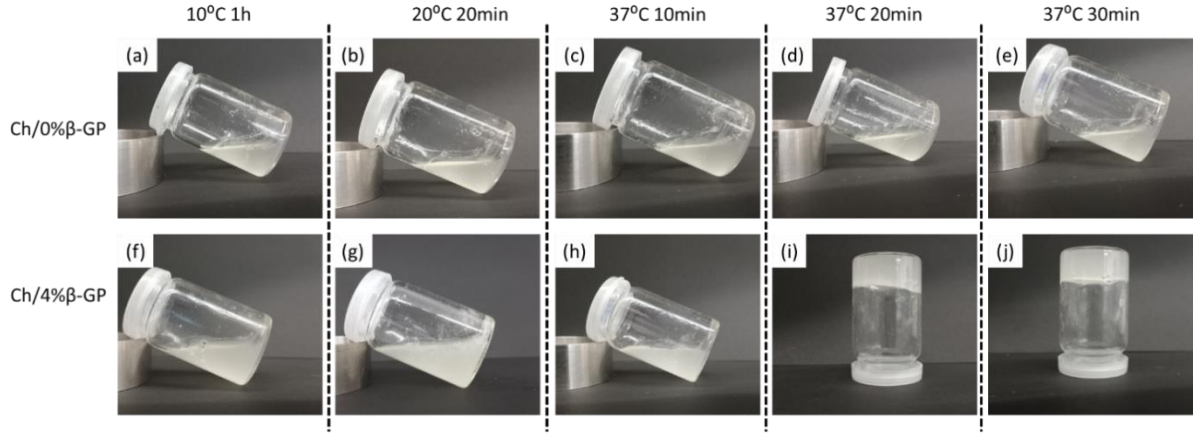

Figure 6.3 Images of the hydrogel without ((a), (b), (c), (d) and (e)) and with ((f), (g), (h), (i) and (j)) β-GP (4 w/v%), at 10ºC, 20ºC and 37ºC at different times: 10ºC after 1 h of mixing; 20ºC after 20 min; 37ºC after 10, 20 and 30 min.

6.2.2.1. Scanning electron microscope (SEM) and Fourier-transform infrared spectroscopy (FTIR)

Freeze-dried hydrogels were analysed via SEM to understand the hydrogel's morphology. Even though all freeze-dried hydrogels appeared to be similar, at the surface of the Ch/3%β-GP sample (Figure 6.4 (a)), a more porous appearance was noted with larger pores when compared with the samples with higher concentrations β-GP (Figure 6.4 (b) Ch/4%β-GP; (c) Ch/5%β-GP). This might indicate a less rigid structure, that is in accordance with the

previous results (Figure 6.2) and with previous studies [28]. Similar structures were also analysed by Mahmoudian and Ganji [28], where similar lyophilized porous structures of Ch/ β-GP hydrogels were also obtained.

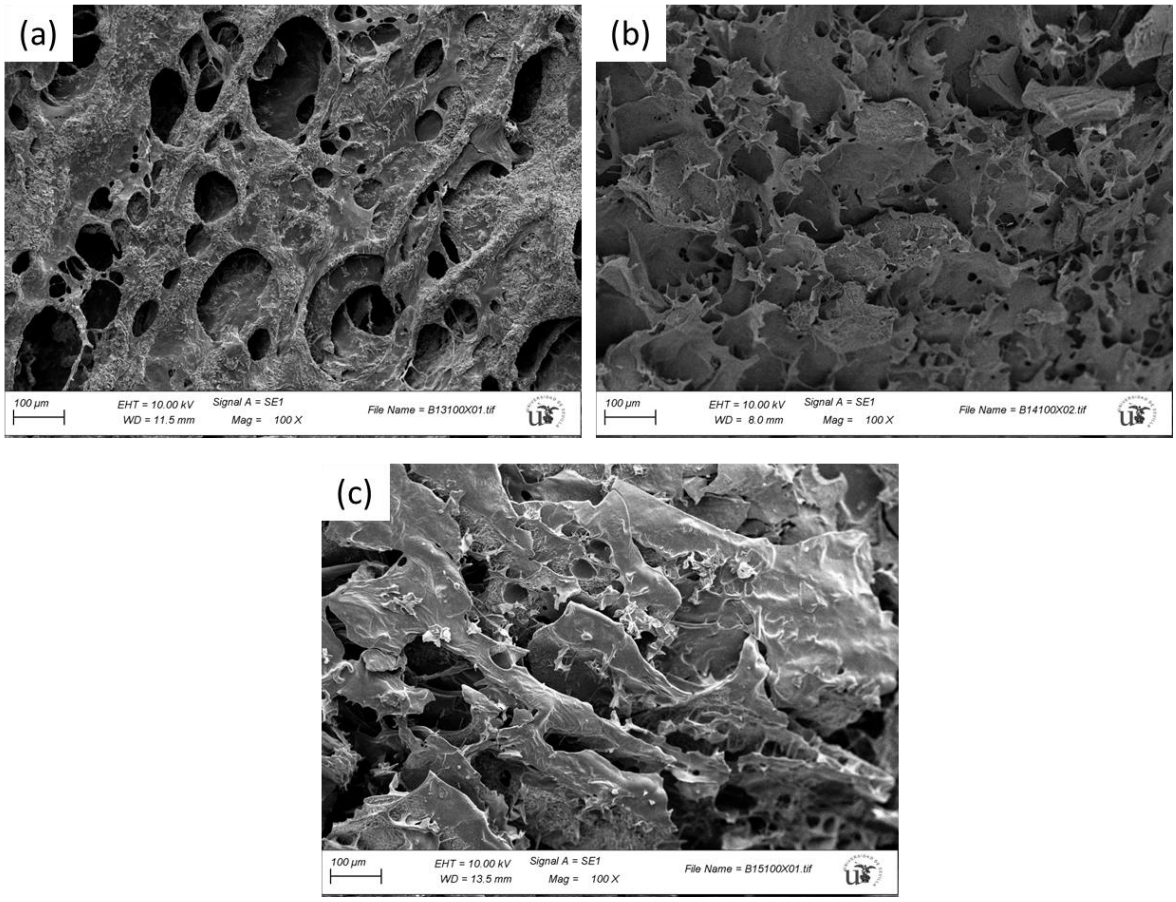

Figure 6.4 SEM analysis of freeze-dried (a) Ch/3%β-GP, (b) Ch/4%β-GP and (c) Ch/5%β-GP surfaces.

FTIR analysis was done to characterize the obtained hydrogel. The Ch powder (Figure 6.5) revealed O-H and N-H stretching vibrations at 3500-3200 cm^{-1} and C-H stretching at 2920-2878 cm^{-1} [12], [14], [21]. The band at 1650 cm^{-1} was attributed to the stretching of C=O of amide I, while the band at 1590 cm^{-1} was associated with the amide group [12], [14]. Bands were observed between 1200 and 1500 cm^{-1}, corresponding to the stretching of C-N of the amide, the O-H deformation of CH_2-OH and C-H bending of CH_2 groups at 1377 cm^{-1}, and the O-H deformation of CH-OH coupled with CH_3 deformation and wagging of CH_2 at 1320 cm^{-1} [21]. In the presence of β -GP, a characteristic band appeared at 1000 cm^{-1} related to the aliphatic P-O-C stretching, with a main band at 1050 cm^{-1} attributed to PO_4^{-3-} and a small shoulder at 940 cm^{-1} related to $-HPO^{-4}$ groups [21]. The Ch/β-GP hydrogel exhibited combined bands attributed to Ch and β-GP, including strong bands at 1650 cm^{-1} and 3200-2500 cm^{-1}, indicating the presence of both Ch and β-GP in the hydrogel. The band at 1650 cm^{-1} was related to the amide I band of Ch, while the bands at 3200-2500 cm^{-1} were attributed to the N-H and O-H stretching vibrations of β-GP.

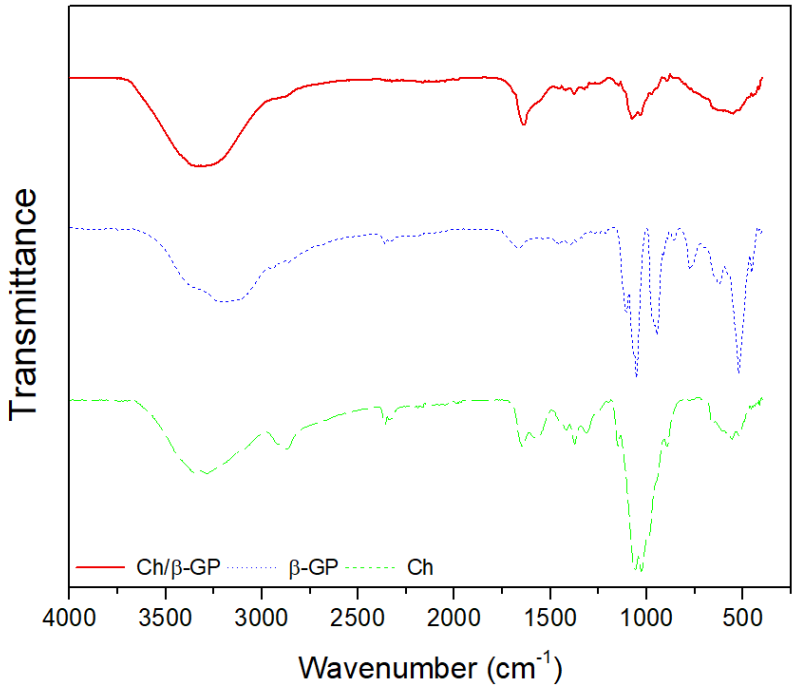

Figure 6.5 FTIR analysis in transmittance of Ch/4%β-GP, chitosan powder (Ch) and β-GP powder.

6.2.3. Introduction of GG:Alg microparticles into the chitosan/β-glycerophosphate hydrogel

Figure 6.6 (a) shows a rheological transient test similar to the one in Figure 6.2. However, in this test, Ch/4%β-GP was combined with 0, 2 and 5 w/v% of GG:Alg microparticles, after 1 h mixing at 10ºC. The microparticles introduction led to an increase in moduli values at all temperatures.

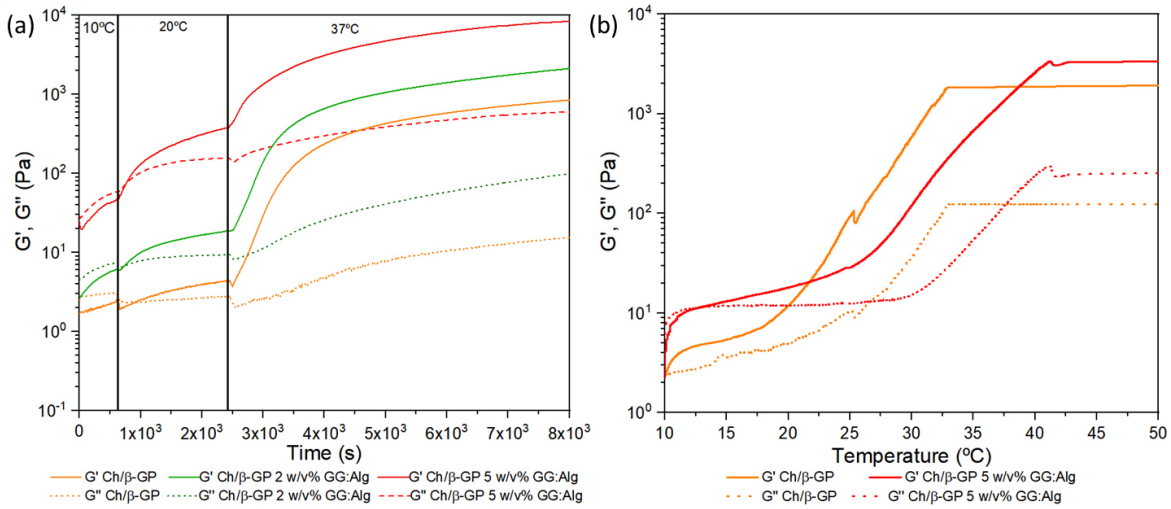

Figure 6.6 (a) Transient analyses of Ch/β-GP hydrogel with different concentrations of GG:Alg microparticles (0, 2 and 5 w/v%) at 3 different temperatures: 10ºC (10 min); 20ºC (30 min) and 37ºC (1.5h); (b) Temperature ramp in oscillation of Ch/β-GP hydrogel with 0 and 5 w/v% GG:Alg microparticles.

At 10ºC, within the studied time, the viscous regime was maintained (G''>G'); however, an increase of the moduli was registered with the presence of microparticles and with the increase of their concentration. With 5 w/v% of microparticles, the moduli values increased by a decade. Both moduli and slope of the curve increased with the GG:Alg presence.

At 20ºC the transition of G'> G'' was registered in all systems, with an apparent stabilization in a plateau better observed for the systems with GG:Alg, and especially for the loss modulus. However, G' still presented a positive slope with time, thus increasing. Between the systems with 0 and 2 w/v%, the moduli values were within the same decade (1 to 10 Pa). With 5 w/v% the moduli were higher than the moduli with 2 and 0 w/v% of microparticles almost by a decade, indicating a more elastic structure.

With the passing to the 37ºC stage, the moduli increased significantly for the systems with 0 and 2 w/v%, with the previously portrayed behaviour. An abrupt increase of the moduli, followed by a stabilization at a plateau with a positive slope was observed. The moduli of the system with 5 w/v% also increased but not so significantly, since at the 20ºC the moduli were already at higher values, closer to the ones at the 37ºC. All systems converged in a plateau at 37ºC, with the beginning of the plateau being anticipated by the presence of the microparticles and higher moduli values being obtained in their presence. The system without microparticles reached the plateau at 19 minutes, as previously stated. With the introduction of the microparticles, the transition was faster: with 2 w/v% plateau was reached after 15 minutes and with 5 w/v% the plateau was reached after 11 minutes.

In Figure 6.6 (b) a temperature ramp (now similar to that used for Pluronic in the previous chapter) was done. Since the viscoelastic properties of the hydrogel depend on time, a significant time had to be given to each degree to let the hydrogel reach a quasi-equilibrium state, similar to the plateau observed in the previous figures. Thus, a temperature increase rate of 0.05 ºC/min was chosen, allowing the hydrogel to be at each degree for around 20 minutes. Since, at 37ºC, the Ch/4%β-GP with 0 w/v% of GG:Alg stabilized at the plateau after 19 minutes, the selected time was appropriate. Only the systems without and with 5 w/v% of microparticles were analysed.

At lower temperatures, the Ch/β-GP hydrogel displayed a positive slope of the moduli, with G' surpassing G'' in the first region. However, in Figure 6.6 (a) at 10ºC the loss modulus is superior to the elastic one. This was attributed to insufficient time for the transition to an elastic-dominated structure that was done in the previous test. A significant increase in the slope of the moduli was observed at around 20ºC, followed by a plateau around 32ºC, indicating full gelation of the hydrogel. The addition of microparticles, with a concentration of 5 w/v% resulted in higher moduli at lower temperatures but delayed the significant increase in moduli to higher temperatures, with a plateau being achieved at around 41ºC with higher moduli values than the hydrogel without microparticles. The decrease of the transition temperature was not expected, and further tests need to be done since the tests only accounted for 20 min at each temperature.

The addition of the microparticles accelerated the sol-gel transition. Similar Ch/β-GP hydrogels had faster gelation but with different microparticles [28], [29]. Ganji *et al.* [28] detected a reduction in the time needed for the moduli to increase (gelation time) from 13 minutes to 8 minutes with the introduction of HPMCs microparticles into similar Ch hydrogel systems. Also, the microparticles increased the moduli, giving the hydrogel a more elastic structure, since they serve as reinforcements within the hydrogel structure.

6.2.3.1. Microparticle/hydrogel system characterization

Figure 6.7 shows frequency sweeps done at different temperatures and times to the Ch/4%β-GP system with 0, 2 and 5 w/v% of GG:Alg microparticles.

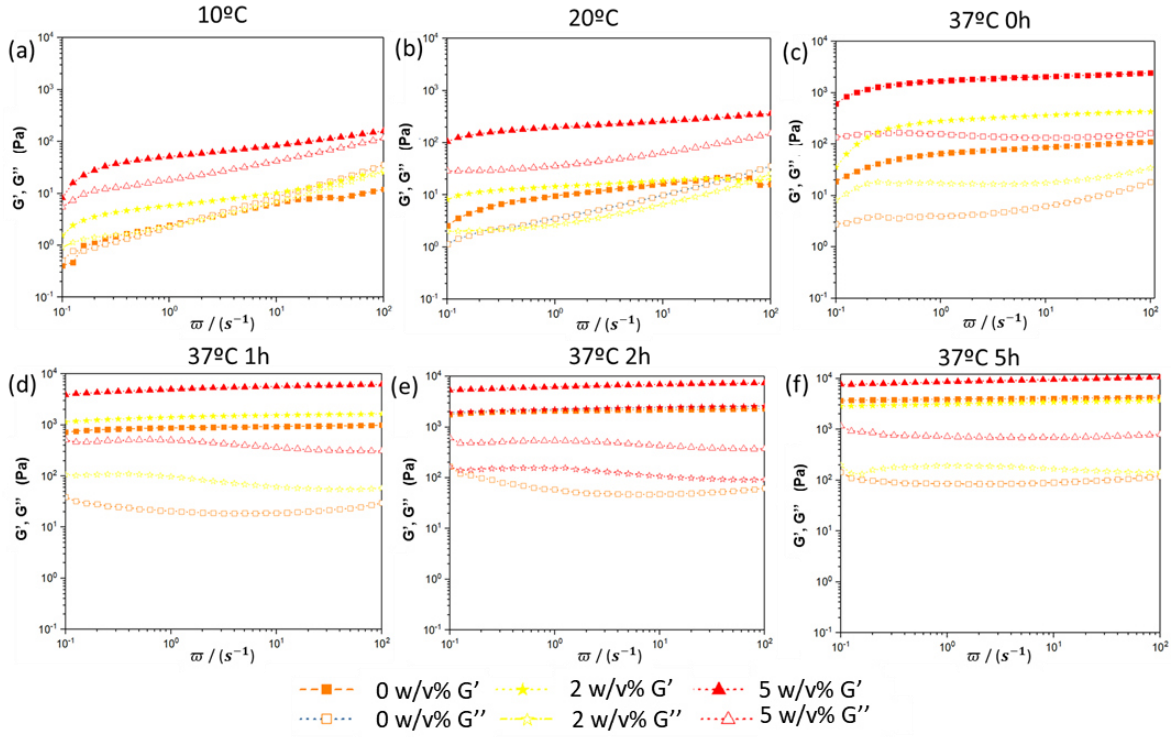

Figure 6.7 Frequency sweeps of Ch/4%β-GP hydrogel with 0, 2 and 5 w/v% of microparticles at different temperatures and times. For 10ºC the samples were immediately analysed after the end of 1h of mixing, for the 20ºC the samples were analysed after 20 min at 20ºC. For 37ºC the samples were immediately analysed (0 h) and then again analysed after 1, 2 and 5 h.

At 10ºC (Figure 6.7 (a)), all systems without microparticles had a viscous behaviour with an increasing slope. The system with 0 w/v% had very similar moduli values at lower frequencies and a viscous regime at higher frequencies. With the addition of the microparticles, the G' surpassed the G'' at lower frequencies followed by a convergence at higher ones. The addition of microparticles with 2 w/v% led to an increase in moduli values, especially at lower frequencies. With higher frequencies, at 10ºC, the effect of the microparticles (with 2 w/v%) diminished, converging to the values without microparticles. With 5 w/v%, the moduli increased, over one decade, with G'>G'', but with a positive slope, indicating a system with a stronger elastic characteristic [33].

With the transition to 20 ºC (Figure 6.7 (b)), the G′ in all systems surpassed G′′. A decrease in the slopes was observed, with a less pronounced dependence on frequency. This indicates the formation of a more elastic system [33]. The moduli values increased in all systems, especially at the lower frequencies when compared with Figure 6.7 (a). Convergence of moduli for higher frequencies was also observed for the systems with 0 and 2 w/v% of microparticles.

At 37ºC 0 hours (Figure 6.7 (c)), the system exhibited a transition to a more elastic structure, with higher moduli, and reduced dependence on frequency and G′>G′′. At this temperature, the systems with 0 and 2 w/v% no longer converged the moduli at the higher frequencies range, with 2 w/v% having higher G′ than the system with 0 w/v%. After 1 hour (Figure 6.7 (d)) the moduli had further increased and the dependence on frequency ceased, thus confirming the formation of a gel state. After 2 and 5 hours (Figure 6.7 (e) and (f)) the moduli increased slightly when compared with the 1-hour test.

Noticeably, after 2 and 5 hours, the systems with 0 and 2 w/v% had similar moduli values, thus the microparticles at this concentration had no significant effect on the gel's final rheological structure, only affecting the gelation. In Figure 6.6 (a) the moduli values of the systems with these concentrations are in accordance with the ones obtained in this test. With 5 w/v%, the microparticles affected the moduli of the Ch hydrogel, with higher moduli in all ranges of analysed frequencies. Between Figure 6.6 (d) to (e) (1, 2 and 5 hours), a slight increase in moduli can be observed. Thus, an increase of the moduli continues to occur with time, as it was recorded in a plateau with a positive slope in Figure 6.2 and Figure 6.6.

Figure 6.8 represents the obtained flow curves for the Ch/4%B-GP system with 0, 2 and 5 w/v% of microparticles at 10ºC and 20ºC. This was done to understand the viscosity and possible injectability of the system. The tests were done after 20 minutes of stabilization within the rheometer gap. All samples revealed a shear thinning behaviour. An increase in viscosity was registered with a temperature increase and microparticle presence. The effect of microparticle concentration was not affected by shear flow. However, the effect of temperature diminished with the shear flow. This can be seen by the approximation of the viscosities of the samples at 10ºC and at 20ºC. This is attributed to the destruction of the structure created by the effect of the temperature increase. Further rheological studies need to be performed to understand if the proposed thermoresponsive hydrogel is viable for injectability purposes [34].

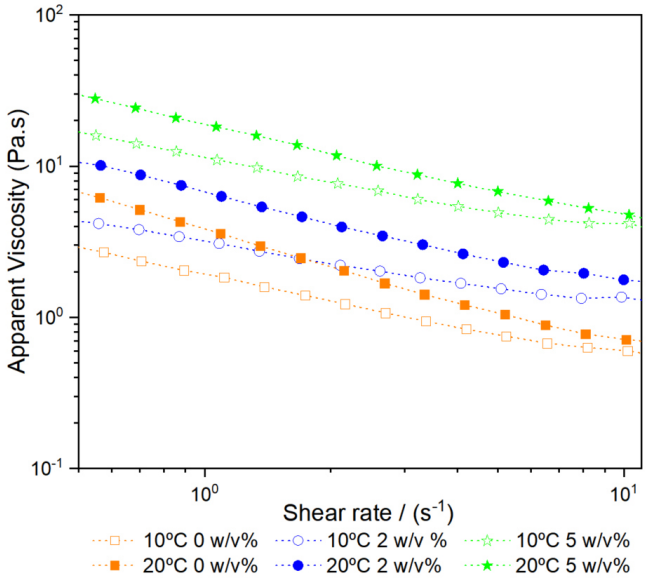

Figure 6.8 Flow curves of Ch/4%B-GP with 0 (orange), 2 (blue) and 5 w/v% (green) of microparticles at 10ºC (hollow marks) and 20ºC (full marks). The samples were left to stable at each temperature for 20 min.

Figure 6.9 shows images of the proposed microparticle/hydrogel system using Ch/4%B-GP with 2 and 5 w/v% of microparticles. These can be compared with those of Figure 6.3, which show the hydrogel without microparticles. The system maintained its viscous behaviour at temperatures of 10ºC and 20ºC, even after 20 minutes at 20ºC. A viscosity increase between 2 and 5 w/v% was noticeable, particularly after 10 minutes at 37ºC. After 20 minutes, both systems had fully gelled. These images are in accordance with the previous results.

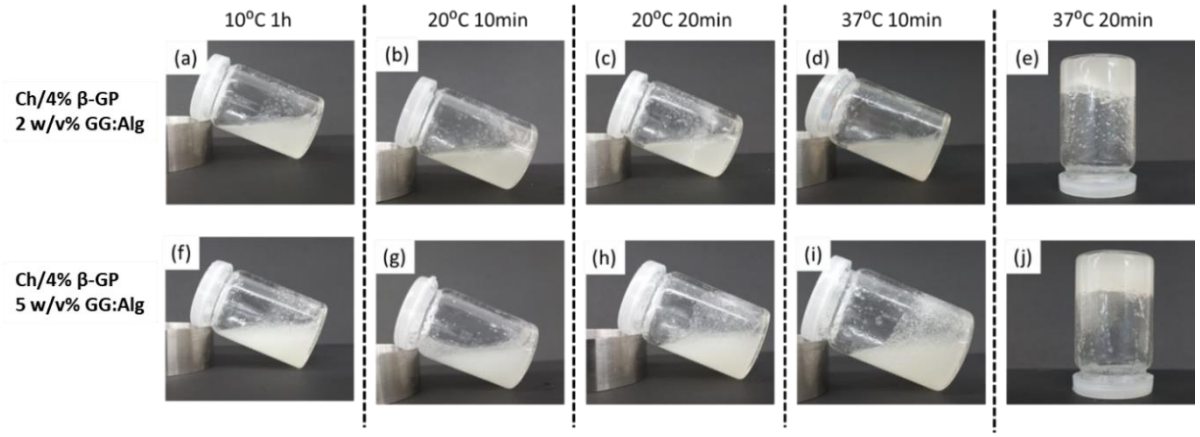

Figure 6.9 Ch/4%β-GP hydrogels with different concentrations of GG:Alg microparticles: 2 ((a), (b), (c), (d) and (e)) and 5 ((f), (g), (h), (i) and (j)) w/v%) at different temperatures (10ºC, 20ºC and 37ºC) at different times: 10ºC after 1 h of mixing; 20ºC after 20 min; 37ºC after 10, 20 and 30 min.

With the previous results, it is possible to say that the Ch/β-GP sol state is a viscoelastic fluid dependent on time and temperature. To further characterize this fluid, the comparison of the complex and apparent viscosities is presented in Figure 6.10, to evaluate the Cox-Merz rule. This rule states that the apparent viscosity (from rotational measurements - Figure 6.8) is equal to the complex viscosity (obtained from oscillatory tests Figure 6.7) for the same

deformation value, shear rate, and angular frequency. This rule finds a theoretical explanation for linear polymers and their solutions [35]. Suspensions behave differently from homogenous solutions and dilutions when applied to shear deformations and to oscillatory frequency deformations [36]. Within a flow field, particles alter the flow, and the rheological characteristics of the fluid will change with the presence of this cargo [37], [38]. Chitosan solutions have been shown to demonstrate the Cox-Merx phenomenon [39]. Also, using Ch/4%β-GP solutions and comparing systems without microparticles, Ryl *et al.* [35] also applied the same rule on similar thermoresponsive hydrogels with different temperatures. This rule only worked for lower temperatures and at higher deformations. With higher deformations, the disparities between the two viscosities were larger and were also attributed to the destruction of the structure. However, the chitosan concentrations used in that study were lower than in this thesis and no particles were used. Thus, to compare with these previous studies this rule was applied in this thesis.

Figure 6.10 depicts the application of this rule for 10ºC (a) and 20ºC (b). For η*, all samples decrease their η* with the applied angular frequency, similar to the shear-thinning behaviour of the η. At 10ºC, for the solution 0 w/v%, the η and η* are close but not fully similar. However, with increasing shear rate/angular frequency, the two viscosities tended to converge, similarly to previous studies [35]. With 2 and 5 w/v% the same phenomenon occurred but with a higher difference between the two viscosities, especially at lower deformations. The converging tendency at higher deformations was still maintained. The convergence can be observed in Figure 6.10 (c), that is the ratio between the two viscosities, where there is a tendency to 1 at the higher shear rates. For 20ºC, the differences between the two viscosities increased, especially for the case with 5 w/v%. However, both viscosities are still approximated at higher deformations, as it can be seen in Figure 6.10 (d).

With these results, the Cox-Merx rule was closer to be applicable for the systems with no microparticles and at higher deformation rates Figure 6.10 (c) and (d), very similarly to the obtained results by Ryl *et al.* [35]. However, the rule failed to be fully applied in the systems with microparticles, since they induced some heterogeneity to the systems, and further contributed to the separation of the two viscosities. This is accordance with literature where most suspensions do not follow this rule [36].

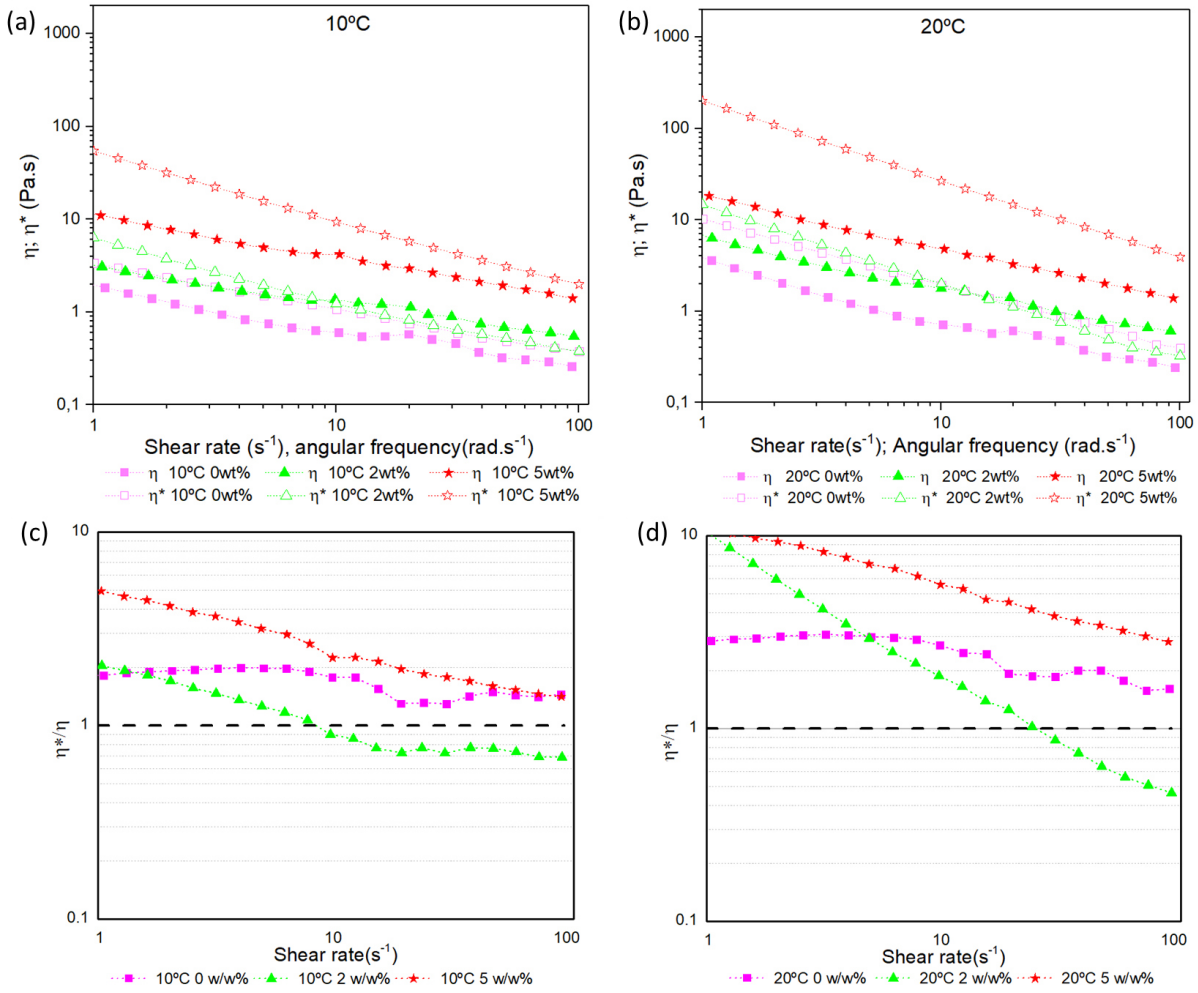

Figure 6.10 Comparison of the Cox-Merz rule for the of Ch/4%B-GP with 0, 2 and 5 w/v% of GG:Alg microparticles at 10ºC (a) and 20ºC (b). Apparent viscosity (η) is in full marks and Complex viscosity (η*) is in open marks. Ratio between the η* and η (η*/ η) for (c) 10ºC and (d) 20ºC.

6.2.4. *In vitro* MB release

Figure 6.11 represents the release profile of the loaded GG:Alg microparticles within the Ch/4%β-GP hydrogel within PBS pH 6.5 and 7.4 (with 2 w/v% of microparticle concentration). The Ch/β-GP significantly delayed the MB release profile, with the microparticles having almost all their content released at the end of 96 hours and the microparticles/hydrogel system not.

After the first 24 hours, the microparticles within the hydrogel had released more than half of the MB content; however, they ceased to release more afterwards. The release profile of the GG:Alg within the Ch/β-GP hydrogel reached a plateau. This was attributed to the MB that was retained within the GG:alg microparticles and within the Ch/β-GP hydrogel structure that would be released with their disintegration. It is important to notice that the Ch/β-GP hydrogel does not have an immediate gelation, taking some time to reach the gel state. With Ch/4%β-GP and 2 w/v% of GG:Alg the system reached the gel plateau after 15 minutes. During

those 15 minutes, a significant amount of MB might have been released from the microparticles and contributed to the release profile.

The pH appeared to have an effect on the release profile of the system, with the average release of the system within PBS pH 7.4 being higher than the one within PBS pH 6.5. However, a T-test showed that no statistically significant differences were found in the last 4 measured times. For example, at 96 h pH 7.4: 76.40 ± 8.29 %; pH 6.5: 69.00 ± 3.47 % with t(8)=2.31, p=0.12. Hence, the hydrogel served as a barrier for the release profile from the microparticles.

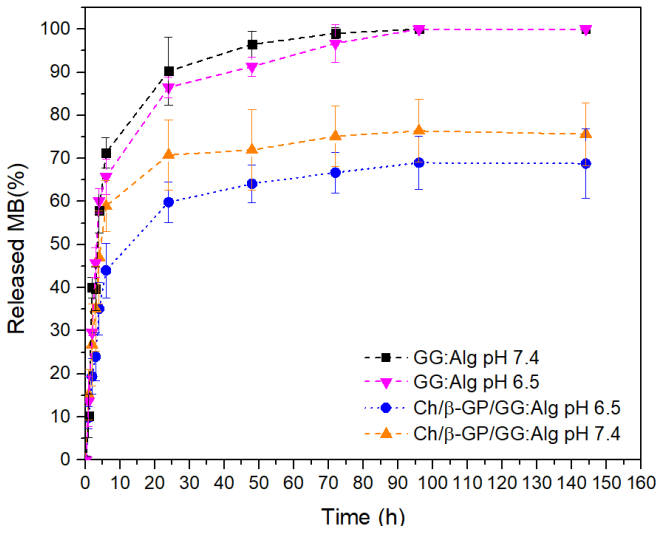

Figure 6.11 Release profiles of GG:Alg microparticles, and GG:Alg within the Ch/β-GP hydrogel with GG:Alg microparticles (2 w/v%) at pH 6.5 and 7.4.

6.2.4.1. Mathematical fittings

Table 6.2 presents the parameters obtained from the mathematical fittings using the modified KP (Korsmeyer-Peppas) and PS (Peppas-Sahlin) models, the KP T_{lag} and PS T_{lag}. Both models had a good fitting with the R^2_{adj} being always higher than 0.95. In both models, the Fickian release profile was obtained, since *n* and *m* were lower than 0.43. Even with the introduction of the microparticles within this hydrogel this release profile was still maintained.

Table 6.2 Release mathematical modelling of MB loaded GG:Alg microparticles within a Ch/4% β-GP hydrogel (2 w/v%) at pH 7.4 and pH 6.5 and release profile of GG:Alg alone at pH 7.4.

		GG:Alg pH 7.4	GG:Alg/Ch/B-Gp pH 7.4	GG:Alg/Ch/B-Gp pH 6.5
KP T_{lag}	k	55.206	38.132	27.072
	n	0.133	0.140	0.207
	T_{lag}	1.991	1.987	0.993
	R^2_{adj}	0.972	0.955	0.958
PS T_{lag}	k_1	44.810	30.787	24.922
	k_2	-4.953	-3.281	-2.236
	m	0.340	0.347	0.378

	T_{lag}	0.971	0.941	0.923
	R^2_{adj}	0.980	0.971	0.985

6.2.5. Cytotoxicity of GG:Alg/ Ch/β-GP

Figure 6.12 depicts the cytotoxicity of the Ch/β-GP hydrogel system with and without the GG:Alg microparticles. To evaluate the possible cytotoxic effects of chitosan powder and the different hydrogels (2% β-GP, 4% β-GP, 5% β-GP, 4% β-GP GG:Alg), *in vitro* cytotoxicity tests using Vero cells were performed. The cytotoxicity was evaluated using direct contact and indirect extract method, whose results are depicted in Figure 6.12 (a) and Figure 6.12 (b), respectively.

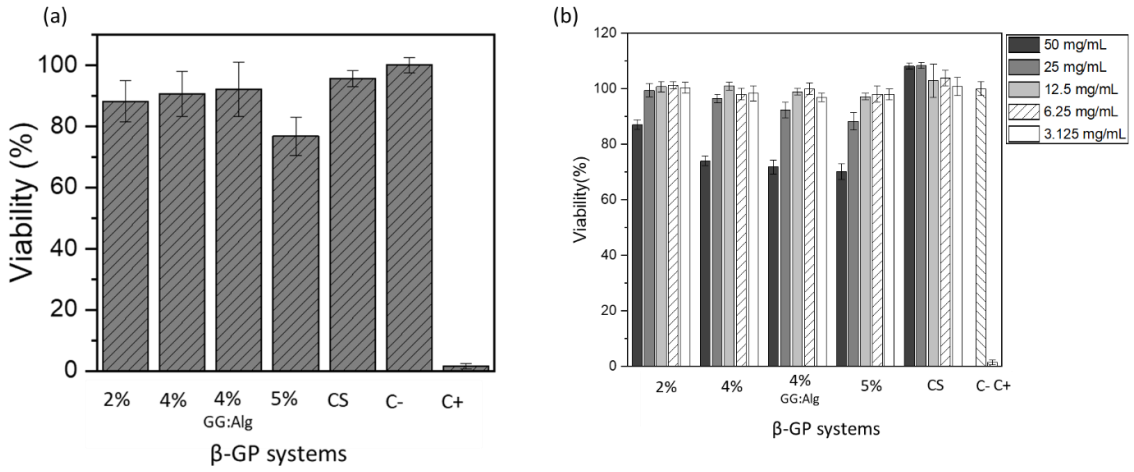

Figure 6.12 VERO cell viability (%) after 48h of direct contact (a) or exposure to the extract (b) of chitosan (powder) and Ch/β-GP hydrogel system with and without GG:Alg microparticles. Without microparticles different β-GP concentrations were used (2, 3, 4 and 5%) With microparticles only the system with 4% of β-GP was studied with 5 w/v% of GG:Alg microparticles (4% Alg:GG). Different dilutions of the extract were tested (50, 25, 12.5, 6.25 and 3.125 mg/mL). Data were expressed as mean of the corrected absorbance normalized to C- ± combined standard uncertainty for at least four replicas. C- is the negative control (cells in compete culture media) and C+ is the positive control (medium with 10 %of DMSO).

Both the assays agree with each other, since the 0.8 cm^2 of hydrogel used in direct contact assay had approximately 20 mg and was put in contact with cells in a volume of 0.5 mL of culture media. Through the direct contact assay, the viability of Vero cells in all samples was higher than 80% except for the 5% formulation. The powder form of chitosan was found to be non-cytotoxic as well as their extract products. However, the Ch/β-GP hydrogel showed a decrease in cellular viability when higher quantities of the extract (50 mg/mL) were placed in contact with cells. This could be due to an excess of acid, water, and β-GP salt that reduced cellular viability. Nonetheless, even at the higher concentration of 50 mg/mL, the cellular viability was approximately 80%, which is considered non-cytotoxicity according to the ISO 10993-5 standard [40]. Therefore, the pure extracts of 50 mg/mL of hydrogel lies at the

threshold between non-cytotoxic and weak cytotoxicity, which is still acceptable. On the other hand, the lower extract concentrations exhibited no cytotoxicity.

The various concentrations of β-GP used did not show significant differences in cytotoxicity. Previous studies reported that high amounts of this salt could be cytotoxic [12], [14], [23], but within the tested concentrations no cytotoxicity was observed. Although, a tendency for lower cellular viability was also observed with higher quantities of salt. Furthermore, the addition of microparticles did not affect the cytotoxicity levels of the Ch/β-GP hydrogel. Previous studies have also demonstrated no cytotoxicity in different cell lines like bone cells and L929 fibroblast cells [12], [21], [41]. Thus, the proposed thermoresponsive system with GG:Alg microparticles were found to be non-cytotoxic to used cell lines, showing potential to be used as future DDS.

6.3. Conclusions

The Ch/β-GP hydrogel was developed using a combination of chitosan and glycerophosphate salt. The combination of these two molecules in an acetic acid solution at 10ºC allows the production of a crosslinked thermoresponsive system. The sol-gel transition was dependent on temperature and time. The amount of β-GP that was used allowed for the optimization of the sol-gel transition, leading to faster gelation and higher moduli, thus more rigid hydrogel. Hydrogels with a concentration of 4 w/v% of β-GP presented a sol-gel temperature transition suitable for application in injectable formulations. The addition of microparticles also led to faster gelation and more elastic structures.

The Ch/β-GP hydrogel was able to be in the sol state at 20ºC and in the gel state at 37ºC, revealing that might be useful for future injectable applicability. The Ch/β-GP hydrogel did regulate the release profile of the MB loaded GG:Alg microparticles in the long run, with the pH of the release medium (this case PBS) having no effect, (within the studies pH's of 7.4 and 6.5). No cytotoxicity was found for the Ch/β-GP hydrogel, regardless of the quantity of salt used, and by the direct and the indirect method. The addition of the microparticles was found to not alter the non-cytotoxicity of the hydrogel.

6.4. References

[1] M. Rinaudo, "Chitin and chitosan: Properties and applications," *Prog. Polym. Sci.*, vol. 31, no. 7, pp. 603–632, 2006, doi: 10.1016/j.progpolymsci.2006.06.001.

[2] L. Gasperini, J. F. Mano, and R. L. Reis, "Natural polymers for the microencapsulation of cells," *J. R. Soc. Interface*, vol. 11, no. 100, 2014, doi: 10.1098/rsif.2014.0817.

[3] S. A. Agnihotri, N. N. Mallikarjuna, and T. M. Aminabhavi, "Recent advances on chitosan-based micro- and nanoparticles in drug delivery," *J. Control. Release*, vol. 100, no. 1, pp. 5–28, 2004, doi: 10.1016/j.jconrel.2004.08.010.

[4] P. H. Yassue-Cordeiro *et al.*, "Chitosan-based nanocomposites for drug delivery," *Appl.*

Nanocomposite Mater. Drug Deliv., pp. 1–26, 2018, doi: 10.1016/b978-0-12-813741-3.00001-7.

[5] F. Ebru, K. Tuba, and G. Altıncekic, "Investigation of gelatin / chitosan as potential biodegradable polymer films on swelling behavior and methylene blue release kinetics," *Polym. Bull.*, no. 0123456789, 2020, doi: 10.1007/s00289-020-03280-7.

[6] H. Hyun, Y. B. Yoo, S. Y. Kim, H. S. Ko, and H. J. Chun, "Hydrogel-Mediated DOX · HCl / PTX Delivery System for Breast Cancer Therapy".

[7] C. Tsao, F. M. Kievit, K. Wang, A. E. Erickson, and R. G. Ellenbogen, "Chitosan-Based Thermoreversible Hydrogel as an in Vitro Tumor Microenvironment for Testing Breast Cancer Therapies," 2014.

[8] M. Fathi, M. Alami-milani, M. H. Geranmayeh, J. Barar, H. Erfan-niya, and Y. Omidi, "Dual thermo- and pH-sensitive injectable hydrogels of chitosan/(poly(N-isopropylacrylamide-co-itaconic acid)) for doxorubicin delivery in breast cancer," *Int. J. Biol. Macromol.*, p. #pagerange#, 2019, doi: 10.1016/j.ijbiomac.2019.01.122.

[9] F. Chang, C. Tsao, A. Lin, M. Zhang, and S. L. Levengood, "PEG-Chitosan Hydrogel with Tunable Stiffness for Study of Drug Response of Breast Cancer Cells," 2016, doi: 10.3390/polym8040112.

[10] D. Zhao, S. Yu, B. Sun, S. Gao, S. Guo, and K. Zhao, "Biomedical applications of chitosan and its derivative nanoparticles," *Polymers (Basel).*, vol. 10, no. 4, 2018, doi: 10.3390/polym10040462.

[11] H. S. Adhikari and P. N. Yadav, "Anticancer Activity of Chitosan, Chitosan Derivatives, and Their Mechanism of Action," *Int. J. Biomater.*, vol. 2018, pp. 27–38, 2018, doi: 10.1155/2018/2952085.

[12] E. Assaad, M. Maire, and S. Lerouge, "Injectable thermosensitive chitosan hydrogels with controlled gelation kinetics and enhanced mechanical resistance," *Carbohydr. Polym.*, vol. 130, pp. 87–96, 2015, doi: 10.1016/j.carbpol.2015.04.063.

[13] S. Saravanan, S. Vimalraj, P. Thanikaivelan, S. Banudevi, and G. Manivasagam, "A review on injectable chitosan/beta glycerophosphate hydrogels for bone tissue regeneration," *Int. J. Biol. Macromol.*, vol. 121, pp. 38–54, 2019, doi: 10.1016/j.ijbiomac.2018.10.014.

[14] H. Qin, J. Wang, T. Wang, X. Gao, Q. Wan, and X. Pei, "Preparation and characterization of chitosan/β-glycerophosphate thermal-sensitive hydrogel reinforced by graphene oxide," *Front. Chem.*, vol. 6, no. NOV, 2018, doi: 10.3389/fchem.2018.00565.

[15] J. Cho, M. C. Heuzey, A. Bégin, and P. J. Carreau, "Physical gelation of chitosan in the presence of β-glycerophosphate: The effect of temperature," *Biomacromolecules*, vol. 6, no. 6, pp. 3267–3275, 2005, doi: 10.1021/bm050313s.

[16] T. Irimia *et al.*, "Chitosan-based in situ gels for ocular delivery of therapeutics: A state-of-the-art review," *Mar. Drugs*, vol. 16, no. 10, 2018, doi: 10.3390/md16100373.

[17] P. Rahmanian-devin, V. B. Rahimi, and V. R. Askari, "Thermosensitive Chitosan-β-Glycerophosphate Hydrogels as Targeted Drug Delivery Systems: An Overviewon Preparation and Their Applications," *Adv. Pharmacol. Pharm. Sci.*, 2021, doi: 10.1155/2021/6640893.

[18] M. T. Cidade, D. J. Ramos, J. Santos, H. Carrelo, N. Calero, and J. P. Borges, "Injectable hydrogels based on pluronic/water systems filled with alginate microparticles for biomedical applications," *Materials (Basel).*, vol. 12, no. 7, pp. 1–14, 2019, doi: 10.3390/ma12071083.

[19] A. R. Taherian, P. Lacasse, B. Bisakowski, M. Pelletier, S. Lanctôt, and P. Fustier, "Rheological and thermogelling properties of commercials chitosan/β-glycerophosphate: Retention of hydrogel in water, milk and UF-milk," *Food Hydrocoll.*, vol. 63, pp. 635–645, 2017, doi: 10.1016/j.foodhyd.2016.09.031.

[20] P. Owczarz, A. Rył, and J. Sowiński, "Influence of glycerophosphate salt solubility on the gelation mechanism of colloidal chitosan systems," *Int. J. Mol. Sci.*, vol. 22, no. 8, 2021, doi: 10.3390/ijms22084043.

[21] A. Skwarczynska, M. Kaminska, P. Owczarz, N. Bartoszek, B. Walkowiak, and Z. Modrzejewska, "The structural (FTIR, XRD, and XPS) and biological studies of thermosensitive chitosan chloride gels with β-glycerophosphate disodium," *J. Appl. Polym. Sci.*, vol. 135, no. 27, pp. 1–8, 2018, doi: 10.1002/app.46459.

[22] Y. Zhao, J. G. Liu, W. M. Chen, and A. X. Yu, "Efficacy of thermosensitive chitosan/β-glycerophosphate hydrogel loaded with β-cyclodextrin-curcumin for the treatment of cutaneous wound infection in rats," *Exp. Ther. Med.*, vol. 15, no. 2, pp. 1304–1313, 2018, doi: 10.3892/etm.2017.5552.

[23] J. Shan *et al.*, "Development of chitosan/glycerophosphate/collagen thermo-sensitive hydrogel for endoscopic treatment of mucosectomy-induced ulcer," *Mater. Sci. Eng. C*, vol. 103, no. November 2017, p. 109870, 2019, doi: 10.1016/j.msec.2019.109870.

[24] K. D. Roehm and S. V. Madihally, "Bioprinted chitosan-gelatin thermosensitive hydrogels using an inexpensive 3D printer," pp. 0–11, 2011.

[25] M. Fathi, M. Alami-Milani, M. H. Geranmayeh, J. Barar, H. Erfan-Niya, and Y. Omidi, "Dual thermo- and pH-sensitive injectable hydrogels of chitosan/(poly(N-isopropylacrylamide-co-itaconic acid)) for doxorubicin delivery in breast cancer," *Int. J. Biol. Macromol.*, vol. 128, pp. 957–964, 2019, doi: 10.1016/j.ijbiomac.2019.01.122.

[26] L. Saeednia, L. Yao, K. Cluff, and R. Asmatulu, "Sustained Releasing of Methotrexate from Injectable and Thermosensitive Chitosan-Carbon Nanotube Hybrid Hydrogels Effectively Controls Tumor Cell Growth," *ACS Omega*, vol. 4, no. 2, pp. 4040–4048, 2019, doi: 10.1021/acsomega.8b03212.

[27] L. Saeednia, L. Yao, M. Berndt, K. Cluff, and R. Asmatulu, "Structural and Biological Properties of Thermosensitive Chitosan-Graphene Hybrid Hydrogels for Sustained Drug Delivery Applications," pp. 1–27, 2017.

[28] M. Mahmoudian and F. Ganji, "Vancomycin-loaded HPMC microparticles embedded within injectable thermosensitive chitosan hydrogels," *Prog. Biomater.*, vol. 6, no. 1, pp. 49–56, 2017, doi: 10.1007/s40204-017-0066-x.

[29] Z. Jia, Z. H. U. Dequan, and T. A. N. Fenwing, "Preparation of Thermosensitive Chitosan Formulations Containing Microparticles Used as Injectable Drug Delivery System *," vol. 14, no. 20376038, pp. 235–241, 2006.

[30] Z. Karimi, T. Somayeh, M. Mohsen, and M. Mirian, "Evaluation of thermosensitive chitosan hydrogel containing gefitinib loaded cellulose acetate butyrate nanoparticles in a subcutaneous breast cancer model," *Int. J. Pharm.*, vol. 624, p. 122036, 2022, doi: 10.1016/j.ijpharm.2022.122036.

[31] D. H. Hee, E. N. Da, H. S. Dong, W. K. Tae, C. S. Byung, and S. C. Ho, "Preparation and biodegradation of thermosensitive chitosan hydrogel as a function of pH and temperature," *Macromol. Res.*, vol. 12, no. 5, pp. 507–511, 2004, doi: 10.1007/bf03218435.

[32] L. Wang and J. P. Stegemann, "Thermogelling chitosan and collagen composite hydrogels initiated with β-glycerophosphate for bone tissue engineering," *Biomaterials*, vol. 31, no. 14, pp. 3976–3985, 2010, doi: 10.1016/j.biomaterials.2010.01.131.

[33] R. G. Larson, *The structure and rheology of complex fluids*. New York: Oxford University Press,

1999.

[34] C. Tipa, M. T. Cidade, T. Vieira, J. C. Silva, P. I. P. Soares, and J. P. Borges, "A new long-term composite drug delivery system based on thermo-responsive hydrogel and nanoclay," *Nanomaterials*, vol. 11, no. 1, pp. 1–22, 2021, doi: 10.3390/nano11010025.

[35] A. Rył and P. Owczarz, "Injectability of thermosensitive, low-concentrated chitosan colloids as flow phenomenon through the capillary under high shear rate conditions," *Polymers (Basel).*, vol. 12, no. 10, pp. 1–17, 2020, doi: 10.3390/polym12102260.

[36] C. Carotenuto, G. Rexha, R. Martone, and M. Minale, "The microstructural change causing the failure of the Cox-Merz rule in Newtonian suspensions: experiments and simulations," *Rheol. Acta*, vol. 60, no. 6–7, pp. 309–325, 2021, doi: 10.1007/s00397-021-01270-8.

[37] G. Street, L. Wce, and U. Kingdom, "Constitutive Model for Time-Dependent Flows of Shear-Thickening Suspensions," *Phys. Rev. Lett.*, vol. 123, no. 21, p. 214504, 2019, doi: 10.1103/PhysRevLett.123.214504.

[38] M. Wyart and M. E. Cates, "Discontinuous Shear Thickening without Inertia in Dense Non-Brownian Suspensions," *Phys. Rev. Lett.*, vol. 112, 2014, doi: 10.1103/PhysRevLett.112.098302.

[39] A. Martínez-Ruvalcaba, E. Chornet, and D. Rodrigue, "Dynamic rheological properties of concentrated chitosan soltions," *Appl. Rheol.*, vol. 14, no. 3, pp. 140–147, 2004, doi: 10.1515/arh-2004-0009.

[40] J. López-García, M. Lehocký, P. Humpolíček, and P. Sáha, "HaCaT Keratinocytes Response on Antimicrobial Atelocollagen Substrates: Extent of Cytotoxicity, Cell Viability and Proliferation," *J. Funct. Biomater.*, vol. 5, no. 2, pp. 43–57, 2014, doi: 10.3390/jfb5020043.

[41] H. T. Ta, C. R. Dass, and D. E. Dunstan, "Injectable chitosan hydrogels for localised cancer therapy," *J. Control. Release*, vol. 126, no. 3, pp. 205–216, 2008, doi: 10.1016/j.jconrel.2007.11.018.

7. CONCLUSIONS AND FUTURE PERSPECTIVES

This chapter presents the main findings of this PhD thesis, followed by possible future works.

7.1. Thesis findings

This PhD thesis had the main objective of developing an injectable magnetic thermoresponsive DDS for possible cancer treatment, namely breast cancer. Thus, the system was expected to be injectable, i.e., being in a liquid/viscous state at operating room temperature and at a gel/elastic state at the body temperature of 37ºC. Then the system should be able to release a loaded cargo and be capable of doing hyperthermic treatment.

To achieve the proposed goal, 5 objectives were established. Here, we present the main results achieved in pursuing these objectives:

- Polymeric microspheres and mNPs produced and fully characterized

Microparticles were produced via coaxial air-flow and optimized via a DOE. Then the microparticles were loaded with SPIONs (Superparamagnetic Iron Oxide Nanoparticles) with and without an APTES ((3-Aminopropyl)Triethoxysilane) coating.

Regarding the optimization of the microparticles production via coaxial air-flow, among the selected factors, air-flow was the most statistically significant in determining the size and size dispersibility of the microparticles. The higher value of air-flow diminished the microparticle diameter but increased the diameters' dispersibility (COV and SPAN). However, this factor's effect on the diameter was more significant than its effect on dispersibility. Pump flow positively affected the microparticles size, and the GG:Alg ratio positively affected the dispersibility. The gap bath-nozzle did not affect the selected responses. With this study, it was possible to define the best parameters to produce microparticles with the smallest possible diameter and the lowest dispersibility. Table 7.1 represents the optimal levels and observed effects.

The produced microparticles had an average wet diameter of around 400 to 450 μm (414.3 ±36.4 μm). When dried, they had a diameter between 150 to 220 μm (171.0 ± 36.0 μm). The pH affected the swelling, the encapsulation of methylene blue, and the microparticles degradation with time. The microparticles exhibited a burst release effect with most MB release occurring in 5 days, with a Fickian release profile. The modified KP and PS models with T_{lag} were the models that best fit the release profiles. The produced microparticles could be loaded with MB and used as a DDS.

Table 7.1 Optimal levels of the coaxial air-flow on GG:Alg microparticles and their effect on the microparticles size and size dispersibility.

Factor	Name	Optimal level	Effects
A	GG:Alg ratio (in 2w/v%)	50%:50%	Decreasing dispersibility attributed to higher viscosity.
B	Gap bath nozzle	15 cm	Not significant.
C	Air-Flow	5 L/min	Decreases particles diameter, but increases dispersibility of diameters.
D	Plump Flow	5 mL/h	Increases the particles diameter.

SPIONs with a diameter of 13.9 ± 5.0 nm were successfully synthesized. The coating with APTES did not alter the core diameter of the obtained mNPs. mNPs were adsorbed at the surface of polymeric microparticles. mNPs suspensions with higher concentration led to higher adsorption efficiency (around 50%) and adsorption capacity (around 15%). APTES coating did not affect the adsorption of mNPs onto the microparticles' surface. After drying the microparticles, mNPs were observed at the microparticles surface in agglomerates, with X-ray Diffraction analysis confirming their presence.

The produced GG:Alg microparticles proved that they could be used to transport drugs and could be used to transport mNPs.

- **Themoresponsive hydrogels (TRH) /gels produced and fully characterized** and **Composite systems (TRH with microspheres, mNPs and drugs incorporated) produced and characterized**

These milestones were achieved by producing two hydrogels with a viscous state at 21ºC and at the gel state at 37ºC. Two thermoresponsive polymers were studied: a mixture of Pluronic F127 and F68 and a chitosan/β-glycerophosphate mixture.

  - **Pluronic system**

Regarding Pluronic, an optimal ratio of F127:F68 (17:3) was determined. An increase in F127 concentration, and a decrease of F68 concentration, decreased the transition temperature of the mixture. Pluronic F127 was the main component of the system that conferred the gel state at physiological temperature, since the F68 did not transition to gel state at the studied concentrations. Also, the sol-gel state transition with a temperature increase was almost instantaneous, with the gel state having a more elastic structure with higher concentrations of Pluronic F127.

The addition of the microparticles led to a decrease of the sol-gel transition temperature. By controlling the concentration of microparticles it is possible to change the transition temperature to operating conditions. It was possible to fully characterize the relation of the sol gel transition temperature with theF127:F68 ratio and the concentration of GG:Alg microparticles. It was even possible to mathematically correlate the concentration of the microparticles and the transition temperatures of the systems for each F127:F68 ratio, using linear correlations. For the selected ratio of 17:3 the mathematical linear regressions were as

follows, with Tp being the Plateau temperature, Ti the initial temperature and c the microparticles concentration, as explained in Chapter 4:

$$Tp = -0.4668c + 35.38 \quad \text{Equation 7.1}$$

$$Ti = -0.4900c + 31.72 \quad \text{Equation 7.2}$$

The rheological characterization of this system was extensive, and as far as we know, never done for a microparticle/gel system. At 21ºC the microparticles presence within the Pluronic did not alter the system from the sol state, with the flow curves being quasi-Newtonian. With higher microparticles concentration, higher viscosities were obtained, but maintained the general Newtonian behaviour.

At 37ºC Pluronic 17:3 ratio was fully at the gel state, as was observed by the frequency sweeps done to the systems. The addition of microparticles did not compromise the gel state at this temperature, maintaining G'>G'', but preserving the weak gel structure of Pluronic. Regarding the durability at 37ºC of the microparticle/Pluronic system, the micelle structure of the Pluronic lead to the dissolution of the system to be within almost a day. At 6 hours the Pluronic had lost over 75% of its original mass. However, the used volumes and *in vitro* conditions are not similar to the *in vivo* environment.

Microparticles with mNPs were only tested with the Pluronic gel. They had no significant impact on the rheological characteristics of the Pluronic gel, only slightly increasing the apparent viscosity and the moduli when SPIONs coated with APTES were used. However, in the overall the introduction of the mNPs did not alter the systems rheological parameters.

Also, the profound rheological characterization that was done in combination with these GG:Alg microparticles was never done, as far as the research done in the literature.

- Chitosan system

The production of the Ch/β-GP (Chitosan/ β-Glycerophosphate) hydrogel was found to be dependant of the concentration of β-GP. Higher amounts of this salt led to faster transitions and higher moduli. This hydrogel was thermoresponsive but also dependant on time. Thus, the time since production and the time at each temperature needs to be equated. An optimal concentration of this salt was found (4 w/v%), with a fully gel state reached after around 19 minutes at 37ºC.

The GG:Alg microparticles introduction altered the rheological characteristics of the chitosan hydrogel (Ch/4%β-GP). At 10ºC the systems with microparticles had higher moduli but remained within the sol state. At 37ºC the sol gel transition was accelerated by the microparticles presence. With 2 w/v% of microparticles the sol-gel transition occurred within 15 min and with 5 w/v% within 11 minutes at 37ºC.

At 10 and 20ºC the microparticles presence increased the systems viscosity but maintained the shear-thinning behaviour of the system, allowing for possible future injectable purposes. The effect of time is evident on this hydrogel, since it takes up to 20 minutes to reach the gel state. The time between the mixture of the salt with Ch, and the time after the temperature switch must be accounted to not impair the administration of the system.

- **The composite system is fully optimized in terms of controlled drug release and magnetic hyperthermia**
    - **Drug release**

With Pluronic gel the initial amount of released drug was delayed with the 17:3 ratio, but for the longer period of time, the release profile was solely dependent on the microparticles. This was attributed to the Pluronic micelle structure that diluted in the studied PBS solutions. Using the mixture with a 1:1 ratio of MB loaded microparticles and mNPs loaded microparticles led to a slowing of the release profile. This was attributed not to Pluronic, but to the presence of the microparticles with adsorbed mNPs (the SPIONs and the SPIATs), that absorbed part of the released MB.

Regarding the chitosan hydrogel with microparticles, the hydrogel significantly controlled the release profile of MB. In both hydrogels the release profile was Fickian, similar to the microparticles alone, thus dependant on simple diffusion of the model drug.

- **Magnetic hyperthermia**

The mNPs adsorbed at the GG:Alg microparticles surface allowed for temperature variations up to 4 ºC with the application of an alternating magnetic field, allowing possible future uses for hyperthermia treatments. The temperature increase was attributed to the Néel relaxations since the Brownian movements are restricted by the entrapment of mNPs on the microparticles surface. Overall, no significant differences between the microparticles with SPIONs and SPIAPTs were observed regarding temperature variations.

The magnetic microparticles were only combined with Pluronic gels, like previously mentioned. Within the Pluronic gel, no temperature increases were detected with the application of an AMF, thus both Brownian and Néel contributions were restrained by the gel structure, thus preventing any temperature increase.

- **The composite system fully validated by *in vitro* studies.**

The microparticles, hydrogels/gels and composite systems cytotoxicity were evaluated using Vero cell line. GG:Alg microparticles alone were non-cytotoxic. The adsorption of mNPs onto the microparticles' surface did not alter their non-cytotoxicity, although when SPIONs coated with APTES were used, a slightly less cell viability was observed, but without any significant cytotoxic effects to the VERO cells. Pluronic was found to be cytotoxic to this cell line. This was attributed to the dilution of the system onto the medium culture solution, that may have caused cytotoxicity or the Pluronic F68.

Ch/β-GP hydrogel with and without microparticles was found to be non-cytotoxic to the Vero cell line. An increase of the β-GP decreased the cellular viability, but remained within non cytotoxic levels. Thus, this system proved to be a viable alternative for future DDS.

7.2. GG:Alg/Pluronic gel vs. GG:Alg/Ch/ β-GP hydrogel: a comparison

Both Pluronic and Ch/β-GP systems were developed and characterized, followed by their mixing with the GG:Alg microparticles. Both systems were developed differently and characterized with different techniques to adjust their rheological properties. However, in the context of this thesis, some comparisons can be made.

The chitosan hydrogel is far more elastic than the Pluronic gel, with this last one being a weak gel, and the former having higher values of G' and G''. This means that the chitosan structure is far more rigid than the Pluronic gel, something attributed to the different types of bonding of each type of system. Also, it is expected for chitosan to be far more durable than Pluronic in PBS solutions, although further studies need to be done.

On the other hand, the thermotransition from sol to gel state in Pluronic is almost instantaneous, whilst with chitosan it is not, and heavily depends on time. Also, the sol state of Pluronic has a far lower viscosity than the chitosan hydrogel, which might affect the injectability of the systems, although future injectability studies need to be done.

Similarly, to both systems, the microparticles affected the temperature transition of the hydrogel, decreasing the transition temperature, increasing the moduli and promoting a faster gelation. This might be related to the microparticles absorption through swelling that promoted the faster gelation.

Pluronic system revealed to have a minor delaying effect on the microparticles release, and only at the initial release times. In a prolonged release, Pluronic had no effect, due to the fact that quickly dissolved into the PBS solution. Thus, the MB release profile was commanded by the microparticles alone. However, the Chitosan/GP system was able to have a prolonged effect on the microparticle release, due to its more rigid structure, since it prolonged the GG:Alg microparticles release profile significantly longer than the Pluronic system, for at least 6 days.

Regarding cytotoxicity assays on Vero cell line, Pluronic was highly cytotoxic, whilst the Ch/β-GP was not. However, Pluronic gel has been found to be non-cytotoxic in previous studies [1], [2]. The cytotoxicity in this study was attributed to the rapid dilution under the used conditions. Therefore, additional studies are needed to improve Pluronic system stability under physiologic conditions. For example, the mixture of Pluronic with other hydrogels is a possible alternative to improve the stability of the system [3]. Also, the quick release and degradation can be useful in therapies that need a first rapid release, which can be made by the Pluronic gel, followed by a second release, that can be done by the microparticles. However, for more prolonged release profiles the Ch/β-GP hydrogel surpassed the Pluronic gel.

In sum, Pluronic gel is a weak gel that might be easily injectable, quickly forms a gel, it rapidly dissolves in aqueous solutions and, in the tested conditions, did not significantly delay the release profiles of microparticles. Ch/β-GP has higher viscosity than Pluronic at the sol state,

it takes some minutes to form the hydrogel, it is a more elastic hydrogel, significantly delays the release profile from the microparticles and is non-cytotoxic for Vero cell lines.

7.3. Future work

Regarding the obtained results, a microparticle/thermoresponsive hydrogel system could be a possible DDS system for cancer treatment. In this thesis, the system with Ch/β-GP proved to be a more adequate system for a DDS with a prolonged release. However, further work and optimization is necessary.

- Microparticles production

In future works the DOE could be redone with equipment with a wider range of parameter levels. For example, higher air-flows and higher pump flows could be explored, with more levels. It is possible to obtain lower microparticle sizes. Other production techniques could also be done to reach even lower microparticles diameters, but maintaining the GG:Alg composition.

Also, the size of the needle should also be addressed in future works. Needle diameter affects the solutions viscosity and thus might affect the GG:Alg diameter. Reducing the needle diameter and increasing its length increases the injection forces, thus altering the extruded solution viscosity [4]. This might also alter the size, and even shape, of the microparticles.

- Pluronic optimization

Pluronic gels in aqueous solutions did not resist for long periods of time in *in vitro* trials done in this thesis. This was due to the micellized structure of the Pluronic gel that was diluted within the PBS solutions. Also, it is noted that Pluronic gels disappears faster with applied forces and with higher volumes of solutions, that promote its dissolution. However, the used *in vitro* conditions are not similar to those find *in vivo*. Although the system almost diluted within 24 h in PBS in these trials, the dilution rate might be longer in more *in vivo* mimicking environments. The real dilution/degradation time in breast cancer mimicking *in vitro* trials should be done to understand if this system is adequate or not to this purpose.

Also, in order to improve the systems, future studies could use crosslinking methods [5] or even combining Pluronic with other polymers to confer a higher resistance to the structure, for example with hyaluronic acid and even chitosan [6], [7]. The more elastic the structure is, in general, the more resistant the system will be to the degradation.

- Other drugs

MB was used as a model drug, to validate the developed systems. However, MB is not a cytotoxic drug used in cancer treatments. Further studies should be done with cytotoxic drugs, like doxorubicin, 5-fluorouracil, eribulin and capecitabine [8]. The loading into the GG:Alg microparticles and the drugs release from the microparticle/hydrogel system needs to be further studied and characterized. Also, possible interactions between the used hydrogels/gels systems and the selected drugs may also need to be evaluated.

- Different concentrations of GG:Alg microparticles in Ch/β-GP system

The amount of released drug can be altered by the concentration of loaded microparticles; however, this affects the transition temperatures of the Ch/β-GP. Other concentrations of β-GP could be explored, and a more profound study, similar to the one done to the Pluronic gel, that correlates the β-GP and the GG:Alg microparticles concentration might be done. This study could be done to allow a wider range of microparticles concentrations within the Ch/β-GP hydrogel without affecting the sol and gel state.

- Injectability studies

Although the rheological studies done ensure that the systems are in liquid/viscous state at operating room temperature and at a gel/elastic state at the body temperature, injectability studies need to be done to understand how the injection procedure might be affected the rheological properties of the systems [9].

Also, the release of the drugs/bioactive agents might also be affected by the Injection of the system. Thus, release studies and also degradation studies also need to be performed after a reproduction of the injection procedure.

- GG:Alg microparticles with mNPs within Ch/β-GP hydrogels

In this thesis, the GG:Alg with MB and mNPs combination was only studied for the Pluronic hydrogels. A study to understand if mNPs have any interaction with the Ch/β-GP may be carried out to see if they affect the rheological behaviour of the system. Also, the characterization of the release profile of the system with a ratio of 1:1 (microparticles with and without mNPs), and other ratios, can also be accessed. The hyperthermic study similar to the Pluronic systems can also be done to understand if in this system there is, or not, temperature variation with the application of an alternating magnetic field (AMF).

- Drug release trials with the application of an AMF.

To understand the effect of the AMF on the release of the GG:Alg alone and the microparticle/hydrogel system, release tests should be done with the application of AMF. It is known that the application of AMF alters drugs' release profile from systems with SPIONs [10], thus it is important to understand how it will affect the GG:Alg/Pluronic systems, and eventually the GG:Alg/Ch/β-GP system with mNPs.

- Degradability of the systems

The degradability of the proposed systems was studied, but the full degradation within PBS was not achieved. However, degradation *in vitro* with more *in vivo* mimicking conditions should be done in the future [11], [12].

- *In vitro* evaluation

The *in vitro* studies in this thesis were performed as a preliminary study, and further studies need to be done. The system needs to be loaded with chemotherapeutic drugs and *in vitro* tests cancer cell lines should be performed. For example with. When full *in vitro* characterization is completed, *in vivo* studies could be considered [13].

7.4. Summary

The development of new DDS for cancer, including breast cancer, has been a growing research topic due to the possibility to deliver cytotoxic drugs *in loco*, and to have cancer treatments that do not induce highly toxic side effects to the patients. The research developed during this Ph.D. thesis aimed to contribute to a step forward in this field. The developed microparticle/hydrogel systems developed in this thesis may provide the basis for the development of a final DDS for breast cancer treatments. Although the main goal of this thesis was focused on breast cancer, the developed systems can be used in other types of solid tumors (e.g.: ovary, endometrial and prostate cancer).

7.5. References

[1] S. Nie and W. L. W. Hsiao, "Thermoreversible Pluronic ® F127-based hydrogel containing liposomes for the controlled delivery of paclitaxel : in vitro drug release , cell cytotoxicity , and uptake studies," pp. 151–166, 2011, doi: 10.2147/IJN.S15057.

[2] I. M. A. Diniz, C. Chen, X. Xu, and S. Ansari, "Pluronic F-127 hydrogel as a promising scaffold for encapsulation of dental-derived mesenchymal stem cells," 2015, doi: 10.1007/s10856-015-5493-4.

[3] S. Chatterjee, P. C. leung Hui, E. Wat, C. wai Kan, P. C. Leung, and W. Wang, "Drug delivery system of dual-responsive PF127 hydrogel with polysaccharide-based nano-conjugate for textile-based transdermal therapy," *Carbohydr. Polym.*, vol. 236, p. 116074, 2020, doi: 10.1016/j.carbpol.2020.116074.

[4] A. Rył and P. Owczarz, "Injectability of thermosensitive, low-concentrated chitosan colloids as flow phenomenon through the capillary under high shear rate conditions," *Polymers (Basel).*, vol. 12, no. 10, pp. 1–17, 2020, doi: 10.3390/polym12102260.

[5] C. Wu, A. K. Gaharwar, B. K. Chan, and G. Schmidt, "Mechanically Tough Pluronic F127 / Laponite Nanocomposite Hydrogels from Covalently and Physically Cross-Linked Networks," pp. 8215–8224, 2011.

[6] J. García-Couce, M. Tomás, G. Fuentes, L. J. Cruz, I. Que, and A. Almirall, "Chitosan/Pluronic F127 Thermosensitive Hydrogel as an Injectable Dexamethasone Delivery Carrier," *Gels*, vol. 8, p. 44, 2022.

[7] B. D. M. Santana, J. C. Pieretti, R. N. Gomes, and G. Cerchiaro, "Cytotoxicity towards Breast Cancer Cells of Pluronic F-127 / Hyaluronic Acid Hydrogel Containing Nitric Oxide Donor and Silica Nanoparticles Loaded with Cisplatin," 2022.

[8] J. Goldberg *et al.*, "The Immunology of Hormone Receptor Positive Breast Cancer," vol. 12, no. May, pp. 1–22, 2021, doi: 10.3389/fimmu.2021.674192.

[9] C. Tipa, M. T. Cidade, T. Vieira, J. C. Silva, P. I. P. Soares, and J. P. Borges, "A new long-term composite drug delivery system based on thermo-responsive hydrogel and nanoclay," *Nanomaterials*, vol. 11, no. 1, pp. 1–22, 2021, doi: 10.3390/nano11010025.

[10] W. Xue *et al.*, "AMF responsive DOX-loaded magnetic microspheres: Transmembrane drug release mechanism and multimodality postsurgical treatment of breast cancer," *J. Mater. Chem. B*, vol. 6, no. 15, pp. 2289–2303, 2018, doi: 10.1039/c7tb03206d.

[11] F. Leonard and B. Godin, "3D in vitro model for breast cancer research using magnetic levitation and bioprinting method," *Methods Mol Biol.*, vol. 1406, pp. 239–251, 2016, doi: 10.1007/978-1-4939-3444-7.

[12] B. J. Ethan, K. Ji, S. Shah, R. R. Mattingly, and B. F. Sloane, "In Vitro Models for Studying Invasive Transitions of Ductal Carcinoma," *J Mammary Gland Biol Neoplasia*, vol. 24, no. 1, pp. 1–15, 2019, doi: 10.1007/s10911-018-9405-3.

[13] J. Yao, C. Zhu, T. Peng, Q. Ma, and S. Gao, "Injectable and Temperature-Sensitive Titanium Carbide-Loaded Hydrogel System for Photothermal Therapy of Breast Cancer," vol. 9, no. December, pp. 1–11, 2021, doi: 10.3389/fbioe.2021.791891.

2023

Henrique Nuno Curado Carrêlo

SMART HYDROGEL-BASED INJECTABLE SYSTEMS FOR